University of Leicester

Deactivation gating and pharmacology of hERG potassium channel

Steven James Thomson BSc(Hons), (Glasgow)

Department of Cell Physiology and Pharmacology

University of Leicester

Thesis submitted in partial fulfilment of the degree of Doctor of Philosophy

Abstract

Deactivation gating and pharmacology of hERG potassium channel

Steven J Thomson, Leicester, July 2012

hERG (Kv11.1) encodes the α-subunit of the potassium (K^+) channel that carries I_{Kr}, an important current for repolarisation of the cardiac action potential. Alterations of hERG current, either through inherited mutations that alter gating or through drugs that block the pore, are associated with Long QT syndrome, cardiac arrhythmias and sudden death.

The N-terminus has an important role in regulating deactivation, a gating process that is important for timing of the hERG current during cardiac action potentials. Removing the entire N-terminus accelerates deactivation. A crystal structure of part of the N-terminus (residues 26-135) was solved in 1998 and showed it contained a PAS domain, but it did not resolve the structure of the functionally important first 26 residues (NT 1-26). Here we present an NMR structure of residues 1-135. The structure reveals that residues 1-10 are unordered and residues 11-24 form an amphipathic helix one face of which is positively charged. Neutralising the positive charge accelerates deactivation to similar rates as if the whole of the N-terminus has been removed. Neutralising negative charge in the C-terminus also accelerates deactivation. We propose a model where the N and C-termini interact to stabilise the open state of the channel and slow deactivation.

Exactly how changes in membrane voltage are transduced into movement of the activation gate is not fully understood. In hERG, the mutation V659A dramatically slows deactivation. Val659 is located in a region where hERG's activation gate is believed to lie. From the structure of Kv2.1 it can be seen the S4-S5 linker forms a cuff around S6 where the activation gate is thought to be. Using cysteine cross-linking experiments we show that V659C interacts with E544C and Y545C in the S4-S5 linker to lock the channel in the open state.

Trapping of drugs in the inner cavity of hERG has been an important model used to help explain why hERG is blocked by so many drugs and with high potency. A series of derivatives of E-4031, a well characterised high-affinity hERG blocker, were made that progressively increased the length of the molecule. Results in this thesis showed these compounds had binding kinetics completely different from E-4031 and none were trapped in the inner cavity. An alternative model of strongly state-dependent drug binding rather than drug-trapping is proposed.

Together, the results in this thesis present new insights on the structural basis for deactivation gating and drug binding in hERG channels.

Acknowledgements

I would like to acknowledge and thank the following people for help and advice;

John Mitcheson for allowing me the opportunity to undertake this work in his lab.

All the past members of the Mitcheson lab; Sarah Nelson, Sarah Dalibalta, George Shehatou, Rachel Hardman and particularly Mike Chang for teaching me to patch ooctyes among other things.

I would like to thank and acknowledge Dr Fred Musket and Samrat Thouta in Biochemistry for their hard work on solving the structure of the N-terminal.

Thanks to all my friends in the Dept of Cell Physiology that I've made over the last few years, Chad, Marie, Sarah, Alex, Conor, Gavin. I've had a great time in Leicester and it's mostly due to you lot.

To my girlfriend Gemma. You truly are the better half of me and I'd be lost without you. I'll never understand how you can have such patience with me but I'm grateful that you do.

I would like to thank the BBSRC and Novartis for providing the funding for this project.

Publications

Papers

Mechanistic insights into hERG K^+ channel deactivation gating from the solution structure of the EAG domain. ***J Biol Chem***, 2011, Vol 286, No8, pp6184 – 6191.
Frederick Muskett, Samrat Thouta, **Steven Thomson**, Alexander Bowen, Phillip Stansfeld and John Mitcheson

Posters

Physiology 2011 – Oxford, UK

Coupling of the Voltage Sensing Domain to the Pore Domain in hERG K^+ Channel
Steven Thomson, Sarah Dalibalta & John Mitcheson

Mechanistic insights into hERG K^+ channel deactivation gating from the solution structure of the EAG domain.
Steven Thomson, Frederick Muskett, Phillip Stansfeld and John Mitcheson

Biophysics 2011, Baltimore, USA

Mechanistic insights into hERG K^+ channel deactivation gating from the solution structure of the EAG domain.
Frederick Muskett, **Steven Thomson,** Samrat Thouta, Alexander Bowen, Phillip Stansfeld and John Mitcheson

Contents

Chapter 1

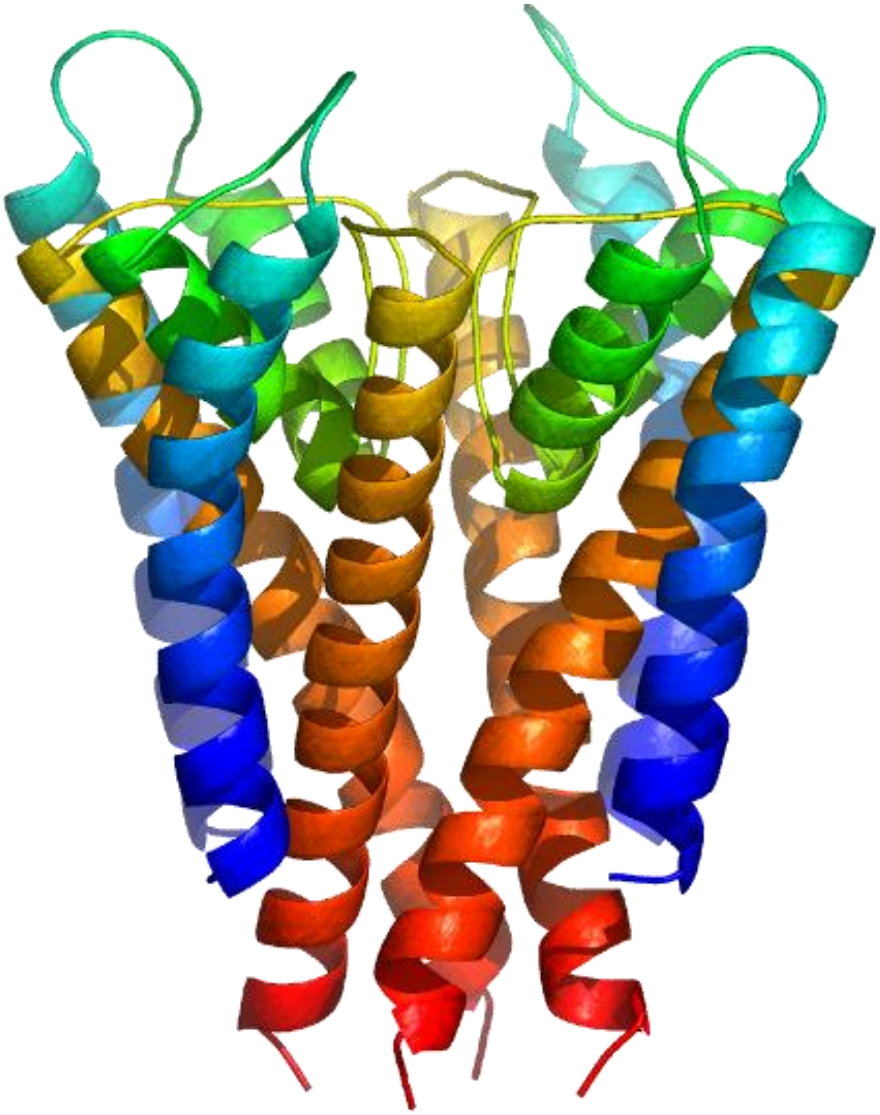

Introduction

Introduction

The cardiac action potential

The ventricular cardiac action potential is formed by a dynamic and intricate combination of several ionic currents. Upon depolarisation of the plasma membrane voltage gated sodium (Na^+) channels (Na_v 1.5) open, allowing a large, rapid Na^+ influx that gives rise to the action potential upstroke seen as phase 0 in figure 1.1. During phase 1 there is a rapid and partial repolarisation as the Na^+ current rapidly inactivates and the transient outward potassium (K^+) currents (I_{to}) pass an outward repolarising current. There are two components of I_{to}. $I_{to,fast}$ is carried by heterotetrameric channels and formed from Kv 4.2, 4.3 subunits. $I_{to,slow}$ is carried by homotetrameric channels formed by Kv 1.4 subunits.

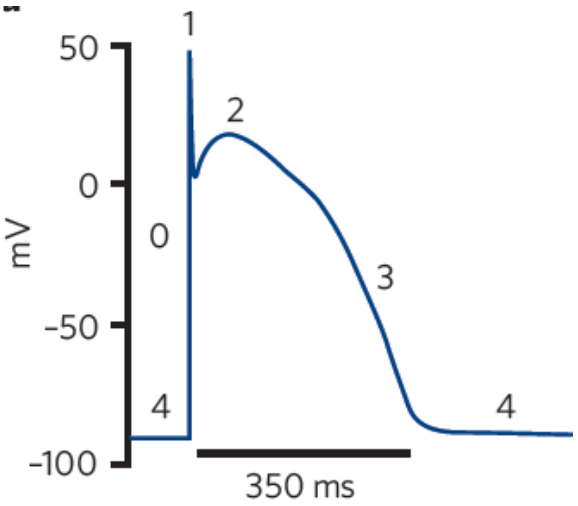

Figure 1.1 Action potential from a human ventricular myocyte. Phase zero is the rapid inward Na^+ current. Phase 1 is the initial repolarisation of the transient outward potassium current. At phase 2 inward Ca^{2+} currents as roughly in balance with outward K^+ currents resulting in the characteristic calcium plateau. Phase 3 is repolarisation by K^+ currents including hERG which returns the membrane to its resting potential (phase 4) (Taken from Sanguinetti & Tristani-Firouzi, 2006).

The transient currents ($I_{to,slow}$ and $I_{to,fast}$) activate very quickly on depolarisation and are named according to their relative kinetics for onset and recovery from inactivation (see table 1.1). They underlie the initial phase of repolarisation (figure 1.1). The ultra-rapidly activating delayed rectifier K^+ current (I_{Kur}) activates quickly and also contributes to the initial repolarisation. Phase 2, the long plateau phase characteristic of ventricular action potentials, reflects the delicate balance between inward and outward currents. The inward current is mostly L-type calcium (Ca^{2+}) current ($I_{Ca,L}$) and

the outward current is made up of the slow, rapid and ultra rapid ($I_{Ks,}$ $I_{Kr,}$ $I_{Kur,}$) potassium currents through delayed rectifier K^+ channels.

Repolarisation occurs during phase 3 when the outward movement of K^+ through delayed rectifier and inward rectifier K^+ channels begins to dominate and $I_{Ca,L}$ inactivates. Several K^+ currents contribute to the outward current that repolarises the membrane during phase 3.

Two broad classes of repolarising K^+ currents have been distinguished based primarily on differences in time and voltage dependent kinetics and pharmacological sensitivities; transient outward K^+ currents (I_{to}), delayed rectifying K^+ currents (I_K) (Sanguinetti & Jurkiewicz, 1990; Barry & Nerbonne, 1996).

The transient K^+ currents activate very fast but in inactivate at different speeds. The fast component inactivates quickly while the slow component is slower to inactivate. The delayed rectifier current I_{Kur} activates much faster than I_{Ks} and I_{Kr} and the current does not inactivate. I_{Kur} is carried by Kv 1.5 channel and is sensitive to block by 4–AP. The delayed rectifiers I_{Ks} and I_{Kr} activate at more depolarised membrane potentials to the transient outward K^+ currents but with slower kinetics and these currents determine the latter (phase 3) of repolarisation and together with the inward rectifier K^+ current (I_{K1}) return the membrane to resting potentials. The delayed rectifiers I_{Ks} and I_{Kr} also differ in their pharmacology. I_{Ks} is blocked by chromanol 293 and I_{Kr} is blocked by a large number of structurally diverse compounds (see later section).

As the membrane potential begins to return towards resting voltages I_{Kr} carried through hERG (Kv 11.1) channels initially increase due to the channels recovering from inactivation but then the current decreases as the channels deactivate and as the K^+ ion

driving force decrease. As the membrane reaches resting its resting potential there is an increase in I_{K1} through $K_{ir}2.1$ channels as it recovers from block by positively charged cytosolic constituents, including Mg^{2+} and polyamines such as spermine and spermidine (Bers, 2002). I_{K1} maintains a background conductance and is responsible for setting the resting membrane potential.

Table 1.1. Cardiac ion channels and currents

Current	Channel	Activation Kinetics	Inactivation Kinetics	Role in action potential
I_{Na}	Nav 1.5	VVF	VF	Rapid Depol
$I_{Ca,L}$	Cav 1.2	VF	M	Depol & Plat
$I_{to,fast}$	Kv4.2,4.3	VF	F	Early Repol
$I_{to,slow}$	Kv1.4	VF	M	Early Repol
I_{Kr}	Kv11.1 (hERG)	M	VF	Plat & Repol
I_{Ks}	Kv 7.1 (+ MinK)	VS	x	Plat & Repol
I_{Kur}	Kv1.5	F	x	Plat & Repol
I_{K1}	Kir 2.1	VF	x	Resting E_m

Abbreviations: F = fast, S = slow, M = moderate, V = very and x = none. Depol = depolarisation, Repol = repolarisation, Plat = plateau. (Adapted from Bers, 2001)

The precise length and waveform of the cardiac action potential varies between cell types (e.g. from ventricular to atrial to Purkinje cells), which reflects variations in ion channel properties and levels of expression in a particular region (Roden et al, 2002). Changes to normal ionic currents through altered ion channel expression by, for example, ischemic heart disease, inherited mutations or through drug block of channels is a common mechanism for arrhythmias (Delisle et al, 2004). K^+ channels have been intensively studied in recent arrhythmia research. One K^+ channel that has received a great deal of attention is the hERG K^+ channel.

The Molecular Basis of the I_{Kr} Current

I_{Kr} is carried by hERG channels.

The molecular basis of I_{Kr} was elucidated when the gene *KCNH2* (hERG) was cloned, functionally characterised and shown to express a K^+ current with similar properties to I_{Kr} (Sanguinetti et al, 1995; Trudeau et al 1995). The name hERG has a similar origin to that of Shaker potassium channel. A drosophila mutant was identified that, when anaesthetised with ether, exhibited a phenotype in which their legs would kick like go-go dancers. The mutation turned out to be a K^+ channel gene and was named ether-a-go-go (EAG). A gene with homology to EAG was cloned from a human hippocampus library and called **H**uman **E**ther-a-go-go **R**elated **G**ene (hERG) (Warmke & Ganetzky, 1994). The channel encoded by hERG recapitulated the major voltage dependant and pharmacological properties of I_{Kr}, including inward rectification, fast onset and recovery from inactivation and specific block by methanesulphonanilide anti-arrhythmic compounds such as E4031 and dofetilide. However, there are differences in the gating properties between native I_{Kr} and hERG currents in heterologous expression systems. For instance hERG deactivates slower than I_{Kr} and it took several years to explain these differences.

hERG exists in three isoforms; hERG 1, 2 and 3. hERG1 is the cardiac isoform whereas hERG2 and hERG3 are found predominantly in neurons (Shi et al, 1997). hERG1 has some splice variants, hERG1a and hERG1b. hERG1a is the full length version and is the one which all the experiments in this thesis have been performed on. hERG1b has a shorter N-terminus than 1a but is otherwise identical (Robertson et al, 2005). There is also a variant of hERG1 with a truncated C-terminus, $hERG1_{USO}$ and also $hERG1b_{USO}$ which has both the N and C-termini truncated.

The truncated N-terminus (in hERG1b) results in faster deactivation (discussed below and the role of the N-terminus in deactivation is the subject of the first results chapter). In native tissue hERG1a is the most abundant form and 1b less so. They can co-assemble to form a heteromeric channel that has faster deactivation and more closely resembles I_{kr}. As well as co-assembly of 1a and 1b altering the gating properties of hERG there is also the possibility that hERG can co-assemble with an auxiliary subunit.

It is well established that in order to recapitulate I_{Ks}, Kv 7.1 has to associate with MinK (KCNE1) (Barhanin et al, 1996; Sanguinetti et al, 1996). MinK is a β-subunit with a single transmembrane spanning domain that co-assembles with Kv7.1 to alter its function. MinK shifts the voltage dependence of activation in a positive direction, slows down the activation gating, increases the channels conductance 10 fold and removes inactivation gating. Whether hERG co-assembles with β-subunits including MinK, MinK Related Protein 1 (MiRP1 (KCNE2)) or some other auxiliary subunit has been the subject of considerable debate (Abbott et al, 1999: Weerapura et al, 2002). Some papers report that MiRP1 accelerates deactivation and some say it slows it. While other groups report there is a shift in the voltage dependence of activation others do not. Co-immunoprecipitation experiments in myocytes yield varying results depending on the age and species of animal and the area of the heart under investigation (Abbott et al, 1999: Weerapura et al, 2002). What is clear is that if hERG does have an auxiliary subunit any alterations in behaviour it confers to hERG are minor and that hERG does not require a β-subunit in the same way that Kv 7.1 does. While β-subunits may modulate potassium channel function it is the α-subunits that form the pore and confer the voltage sensitivity.

Long QT syndrome

Long QT syndrome (LQTS) is an increase in the time between the Q and T complexes as seen on the electrocardiograph (ECG). It is described as a syndrome because LQTS can manifest itself to have relatively minor effects like fainting or it can cause a condition known as Torsades de points (Tdp) which can lead to ventricular fibrillation and sudden death and also because there is more than one underlying cause of LQTS. There are over 700 mutations in 12 genes associated with congenital LQTS with mutations in hERG, KCNQ1 and SCN5A being the most common (Hedley et al, 2009). LQT1 stems from altered I_{Ks} current, LQT3 from altered I_{Na} and LQT2 from altered hERG current. LQTS can also be acquired, usually due to inhibition of hERG currents.

The congenital form of LQT2 results from inherited mutations. These mutations can be divided into two categories, those that result in a non-functional channel and those with altered channel gating. There are a number of naturally occurring mutations that result a hERG channels misfolding and being retained within the endoplasmic reticulum (ER) and these account for the majority of mutations (Delisle et al, 2004). These mutations are not restricted to one area of the channel but can be found throughout e.g. T65P in the N-terminus, N470D in S2, A561V in S5, L615V near the selectivity filter and N861I in the C-terminus (Delisle et al, 2004).

Other mutations that alter gating can also result in LQTS, such as R56Q. Arg56 is located in the eag domain of the N-terminus and when it is mutated to Gln the channel deactivates much faster than WT (Chen et al, 1999). Faster deactivation means there is less I_{Kr} current at the later stage of the action potential to repolarise the myocyte which can lead to a longer QT interval.

The acquired form of LQTS arises most commonly through drug block of the channel, which therefore reduces the amount of I_{Kr} available to repolarise the myocyte. A large number of drugs can block hERG and the acquired form of LQTS is far more common than the congenital form. Since the identification of hERG as carrying I_{Kr} in the mid 1990's several drugs have been withdrawn from the market due to them interacting with hERG and causing an increased risk of arrhythmias. The tightening of regulations by drug-licensing authorities has led to pharmaceutical companies testing all their new compounds for any hERG activity at a very early stage of the drug discovery process. In order to gain a better understanding of why so many compounds block hERG it is necessary to understand its structure.

The Structure of hERG channels

Overview of Structure

Kv channel α-subunits form tetramers, with each subunit containing six transmembrane spanning α-helices (S1–S6) (Hille, 2001). S1–S4 forms the voltage sensing domain (VSD) with S5 and S6 forming the pore domain. hERG is the one of the largest Kv channels, comprising 1159 amino acids. hERG has large intracellular amino (NH_2) and carboxy (COOH) termini (fig 1.2). The N-terminus is ~355 residues long, the transmembrane spanning S1 to S6 domains are approximately ~315 amino acids long and the C-terminus is about ~495 residues long. In percentage terms, 30% of the channel forms the intracellular N-terminus, 27% forms S1-S6 and 43% is in the C-terminus. 27% of the channel is in the membrane and 73% intracellular. The functional roles of the intracellular termini are not entirely clear. In the N-terminus the first 135 residues of hERG are known as the 'eag' domain. The eag domain is highly conserved within the EAG family of K^+ channels (Kv10, Kv11 & Kv12). The structure for most of hERG has yet

to be solved, but there are now several structures for the eag domain. Within the EAG domain, residues 26-135 form a PAS domain (Morais Cabral et al, 1998). The PAS domain takes its name from the proteins **P**er (period circadian protein), **A**rnt (aryl hydrocarbon receptor nuclear translocator protein) and **S**im (single-minded protein). PAS domains are structural folds without a conserved amino acid sequence and so are hard to detect by searching a proteins sequence (Morais Cabral et al, 1998). Proteins with PAS domains are known to be involved in signalling cascades such as those regulating circadian rhythms and signalling through detection of diatomic gases, O_2, NO and CO and metabolic substrates such as flavins and NADPH. They often bind haem and redox sensitive molecules. hERG does not have a haem group associated with it and the function of the PAS domain in hERG is not fully resolved, although it is known to have a role in regulating channel deactivation (discussed below and in chapter 3).

The C-terminus contains a cyclic Nucleotide Binding Domain (cNBD). cNBD's are found in hyperpolarisation-activated cyclic nucleotide-gated (HCN) channels, where cAMP binds to modulate the channel. Cyclic nucleotides bind in a pocket formed by the β-roll and C-helix and its binding shifts the voltage dependence of activation to more positive potentials, accelerates activation kinetics and stabilises the open state of the channel (Zagotta et al, 2003). The key residues involved in cAMP binding are not conserved in hERG's cNBD and direct application of cAMP to the intracellular side of hERG and EAG channels in excised patches does not affect channel activity so cAMP does not modulate the function of hERG through binding to the cNBD (Brelidze et al, 2009). Like the PAS domain in the N-terminus the role of the cNBD in the C-terminus of hERG is not clear. While the cNBD in hERG shares a lot of sequence homology with other cNBD's it is not strictly accurate to refer to it as such as in does not bind cyclic nucleotides at

physiologically relevant concentrations. It is only in the past year that new evidence from Dr Mitcheson's laboratory and others has demonstrated the mechanistic importance of the cNBD in hERG and this is discussed in chapter 3.

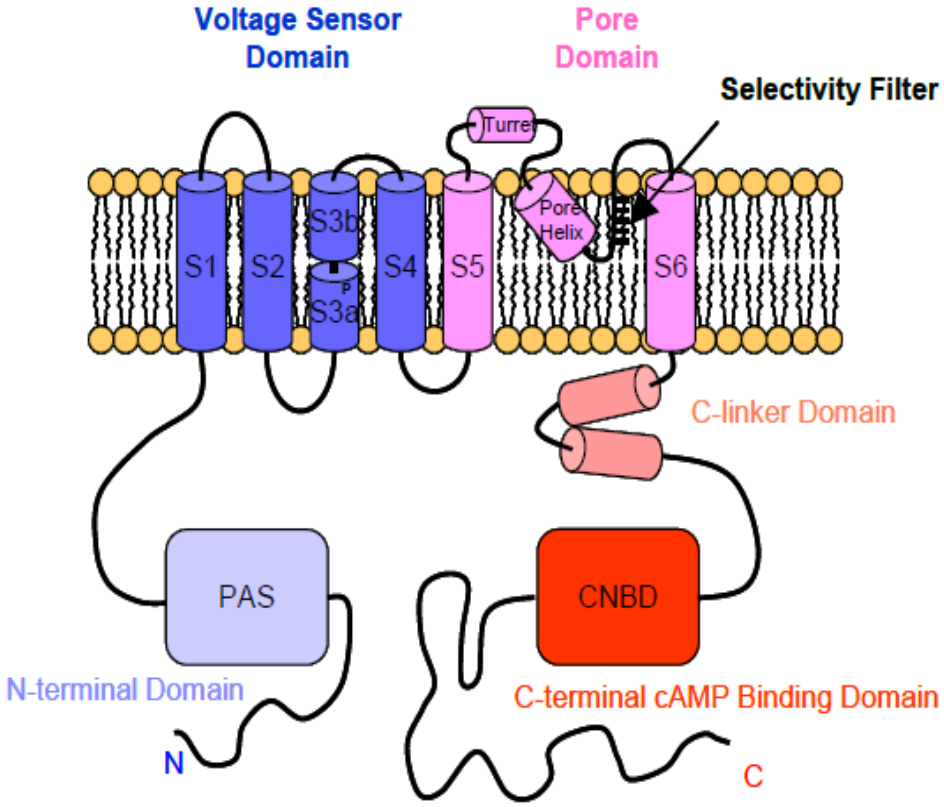

Figure 1.2. Secondary structure of hERG. S1 to S4 form the voltage sensing domain (VSD). S5 and S6 comprise the pore domain. hERG has large intracellular N and C-termini. Residues 1-135 of hERG are known as the 'EAG' domain. Within the EAG domain residues 26-135 form a PAS domain. The C-linker connects the end of S6 to the C-terminus. The C-terminus contains a domain with homology to a cyclic Nucleotide Binding Domain (cNBD).

Structure of the pore and ion conduction

There are two ways that ion channels differ from simple aqueous pores. One is the ability to selectively discriminate between different ions and only allow the passage of one species of ion. The second is the ability to open and close (gate) in response to stimuli such as intracellular Ca^{2+} or cyclic nucleotides or, in the case of Kv channels, changes in voltage across the membrane.

How potassium channels allowed K^+ ions to flow through them but not Na^+ ions was puzzling. K^+ ions have a bigger radius (1.33Å) than Na^+ ions (0.95Å) so presumably any pore in the channel that was wide enough to permit the passage of K^+ must also be wide enough to permit the passage of Na^+ but this was not the case (Doyle et al, 1998).

The first crystal structure of a K^+ channel, KcsA, was solved by Rod MacKinnon's laboratory in 1998. KcsA is a simple bacterial K^+ channel from *Streptomyces lividans* and it has two transmembrane spanning α-helices M1 and M2 (Doyle et al, 1998). M1 is the outer helix and M2 is the inner helix that lines the inner cavity of the channel (fig 1.3). M1 and M2 are analogous to S5 and S6 in hERG respectively. The channel has 4 identical subunits with 4-fold symmetry around the central pore. The helices are not perpendicular to the membrane but are tilted at 25^0. The M2 helices cross at the inner face of the membrane creating a bundle crossing that occludes the ion conduction pathway thus this structure of KcsA is thought to represent the closed state of the channel (fig 1.3). Because the helices are tilted they cross at the bundle on the inner membrane but then widen out to create a large aqueous cavity. This cavity protrudes roughly two-thirds of the distance across the membrane. A re-entrant pore-loop on the extracellular side of the membrane between the two transmembrane helices contains the K^+ channel "signature sequence" TXGYG (Doyle et al, 1998). The TXGYG residues

combine from all four α-subunits to line a region at the extracellular end of the channel pore known as the selectivity filter. It is this filter which confers a preference for the passage of K^+ ions, over other ions, to the channel (Doyle et al, 1998). In each subunit the carbonyl oxygen atoms of the selectivity filter face towards the potassium conduction pathway. Together these oxygen atoms form octahedral binding sites that mimic the K^+ ion hydration shell and coordinate the dehydrated K^+ ions in single file, separated by a single water molecule (fig 1.4). In hERG, however, the selectivity filter sequence is slightly different; SVGFG instead of TXGYG for most K^+ channels. The threonine is changed to a serine and the tyrosine for a phenylalanine but it is thought that the structure of the selectivity filter is similar (Sanguinetti & Tristani-Firouzi, 2006). When in the aqueous cavity, potassium and sodium ions are coordinated with water molecules. When K^+ moves into the selectivity filter, the filter mimics the hydration shell of K^+ ions. The smaller radius of Na^+ ions mean the selectivity filter cannot efficiently mimic the hydration shell of Na^+ ions, thus making it very hard for Na^+ ions to pass though (fig 1.4).

Ion conduction is facilitated by two features of the pore. One, the pore helix has an intrinsic dipole with the negative end pointed towards the inner cavity at the base of the selectivity filter. The negative charge stabilise the positive K^+ ion in the membrane and draws it towards the selectively filter. Two, because the aqueous cavity protrudes roughly two-thirds of the way across the membrane it effectively reduces by two-thirds the distance a K^+ ion must travel in order to move out of the cell. The length of the selectivity filter is relatively short (12Å) compared to the distance across the membrane (~35Å).

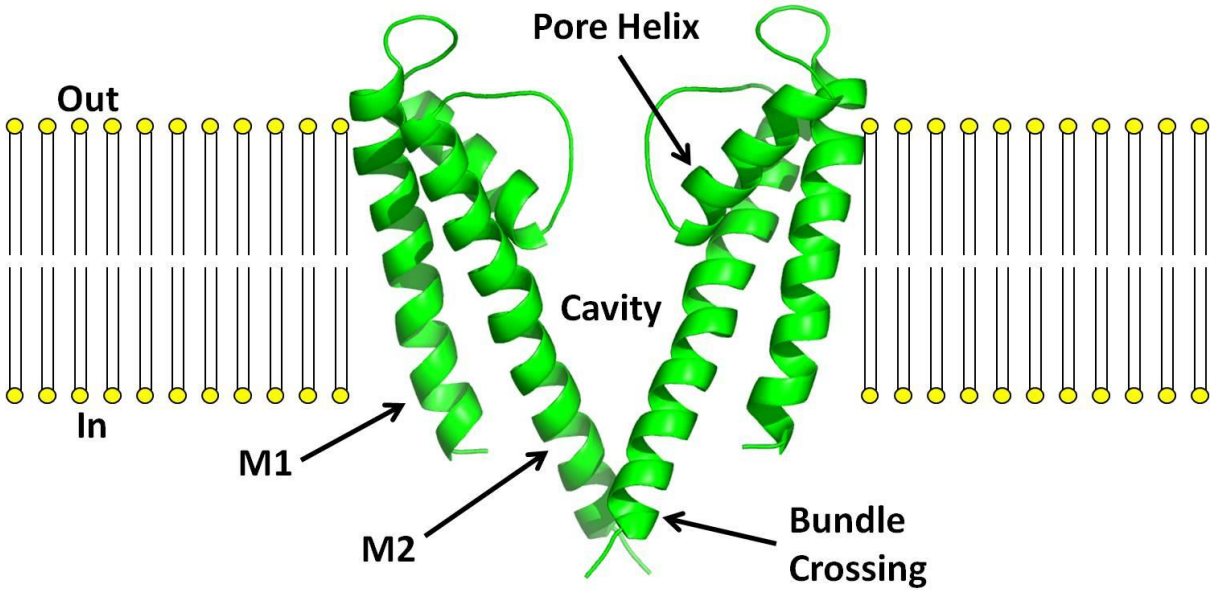

Figure 1.3. Structure of KcsA potassium channel. M1 is the outer helix and M2 is the inner helix that lines the inner cavity of the channel. The channel has 4 identical subunits but for clarity only 2 of the 4 subunits are shown. The channel has 4-fold symmetry around the central pore. The helices are tilted with respect to the membrane by 25^0 thus forming a cross bundle near the inner membrane surface and widening into a central cavity. The M2 helices cross at the inner face of the membrane creating a bundle crossing that occludes the ion conduction pathway thus this structure of KcsA is thought to represent the closed state of the channel.

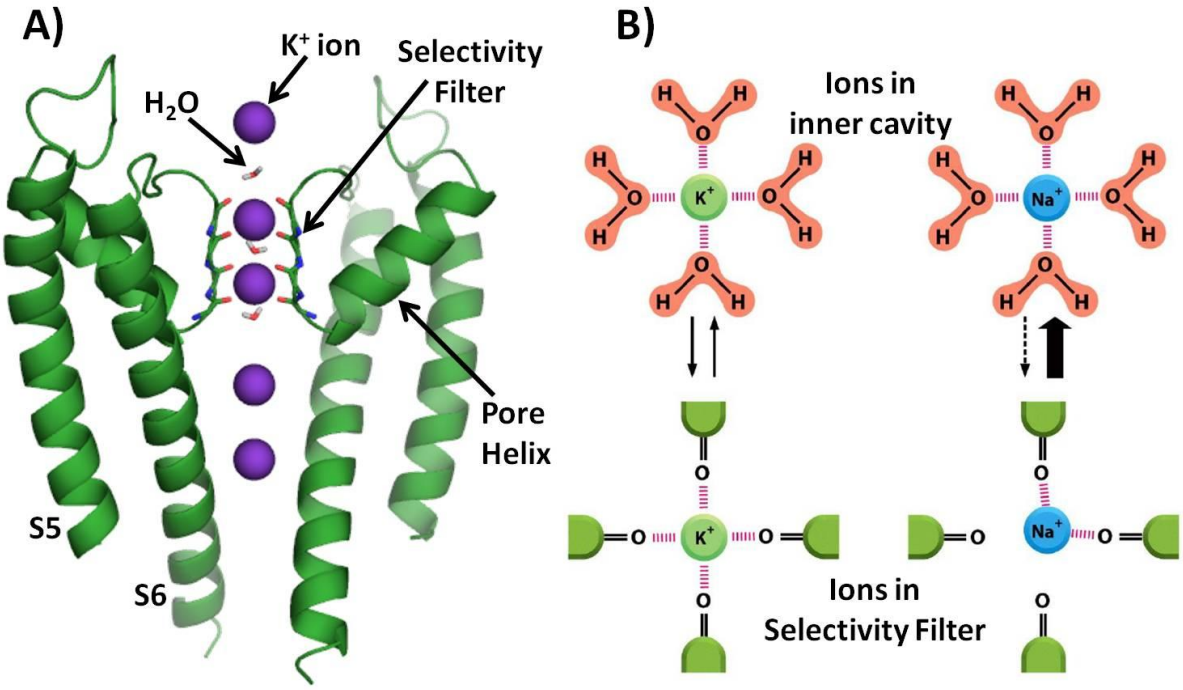

Figure 1.4. Potassium ions passing through the selectivity filter.

A) The α-helices of the pore domain are shown in ribbon form, and the side chains of the residues that make up the selectivity filter are shown in stick form. Dehydrated potassium ions are shown in purple and are separated in the selectivity filter by water molecules. For clarity the voltage sensing domain (S1 – S4) has been removed and only 2 of the 4 subunits are shown. The figure is a homology model of hERG, based on the crystal structure of KcsA in the closed state. Figure adapted from PhD thesis of Dr Phil Stansfeld.

B) Potassium and sodium ions in the inner cavity are coordinated with water (top). The selectivity filter mimics the hydration shell of K^+ ions (bottom). The radius of Na^+ ions is smaller than K^+ ions therefore the selectivity filter cannot efficiently mimic the hydration shell of Na^+ ions as the distances are too great to form interactions. (Figure adapted from Alberts et al, 2008)

Structural insights into gating

Summary of hERG gating

The transmembrane electric field provides the force that drives the gating of Kv channels. At membrane potentials negative to -80mV hERG channels are in a non-conducting, closed state. Depolarisation of the membrane to potentials more positive than -60mV causes channels to open via the S6 activation gate and allows the outward flow of K^+ ions. With membrane depolarisation the channel also begins to enter the non-conducting inactivated state, which involves conformational changes at the selectively filter. hERG gating differs from other Kv channels in two ways. Firstly, entry into and recovery from C-type inactivation is much faster than other Kv channels and the kinetics of inactivation are also faster than the kinetics of channel activation and deactivation (Smith et al, 1996). This limits outward conductance at depolarised potentials and is why hERG currents are small in the early plateau phase of the cardiac action potential. Secondly, activation and deactivation are slower than most other Kv channels. Together this means hERG passes little current upon strong depolarisations as the channel rapidly enters a non-conducting, inactivated state before opening of the activation gate. Instead, hERG conducts most of its current as the membrane potential starts to return to the resting potential. During the cardiac action potential, other currents start to repolarise the membrane potential and when this happens hERG rapidly recovers from inactivation into a conducting state and then deactivates relatively slowly. The unusual gating kinetics are very important to the physiological role of hERG. Reduced inactivation could result in more outward current at the plateau phase which could repolarise the cell early and not allow enough time for proper contraction of the

myocyte. Also, if deactivation is sped up then this would result in longer action potentials and less hERG current to oppose early afterdepolarisations.

Overview of activation gating

Clay Armstrong originally proposed the existence of an intracellular gate that opens to allow entry of ions or drugs into the inner cavity (Armstrong 1969, 1971). The existence of an intracellular activation gate in hERG is supported by studies of channel block by hERG specific blockers like E-4031. hERG channels are not blocked when the cell membrane is held at potentials below the activation threshold (Spector et al, 1996a). High affinity block only occurs after depolarisation to potentials where the channel is open, indicating that a gate must be opened in order for drugs to access the binding sites in the inner cavity (Spector et al, 1996a).

Insights into the structural basis of the activation gate were offered when the first crystal structure of a K^+ channel, KcsA, was solved (Doyle et al, 1998). The bundle crossing formed by the inner helices was proposed to be the activation gate. While the structure of KcsA revolutionised our understanding of ion conduction in K^+ channels, it alone did not provide a structural basis for the movement of the gate as the structure of KcsA was solved in the closed state. It was only with subsequent structures of other K^+ channels that the structural basis for activation gating became apparent.

The first structure of a K^+ channel in an open state was the Ca^{2+} gated MthK channel from the archeon *Methanobacterium thermoautotrophicum* (Jiang et al, 2002a; Jiang et al, 2002b). The structure of MthK channels revealed an overall architecture very similar to KcsA. MthK had two membrane spanning α-helices, M1 and M2, join by a re-entrant pore loop that forms the selectivity filter. However, there was a difference in the area

around the bundle crossing thought to be the activation gate. The inner helices were splayed near the inner membrane creating an opening 12Å in diameter. MthK was crystallised in the presence of calcium and as it is a calcium gated channel the crystal structure is believed to represent the open state of the channel. The splaying of the inner helices was facilitated by the bending of the M2 helix by about 30^0 at Gly83. This bending at glycine gave rise to glycine hinge hypothesis of channel activation gating.

Gly83 in MthK is located just below the base of the selectivity filter and a glycine at this position is almost universally conserved among potassium channels, including hERG. Glycines confer a degree of flexibility to helices which may allow the inner helix to pivot at this point to facilitate splaying open of the bundle crossing. Mutation of the Gly466 in Shaker (analogous to Gly83 in MthK) resulted in a non-functional channel. Most amino acids substituted at this position resulted in non-functional channels but when the glycine was mutated to a proline the channel was still functional. Proline, like glycine, allows a helix to bend at that position supporting the idea that the channel needs to hinge at that position in order to function. Moreover, the shaker mutant G466A was non-functional, however, the gating was restored by placing a glycine at the adjacent position (G466A:V467G) (Labro et al, 2003; Ding et al, 2005).

hERG has a glycine at position 648, equivalent to Gly83 in MthK and Gly466 in Shaker. Mutations of this residue do not have the dramatic effects seen in other channels. Mutation to small residues has no impact on gating whereas mutation to larger amino acids biases the channel towards the open state (Hardman et al, 2007). Most mutations of the putative glycine hinge in hERG are generally well tolerated and the glycines are probably required for the tight packing of the inner helix and residues at the base of the pore helix rather than to act as a hinge. Molecular dynamic simulations suggest that the

S6 of hERG is inherently flexible and doesn't require either glycine to act as a hinge in order to open (Hardman et al, 2007).

The structure of the first voltage gated K^+ channel was KvAP from *Aeropyrum pernix* (Jiang et al, 2003). The structure was similar to the previous published structures, the channel is a tetramer with four-fold symmetry around the pore and the S6 inner helix is kinked at the proposed glycine hinge. The bundle crossing was splayed creating an opening almost the same width as the opening in MthK so the KvAP structure is thought to represent the open state of the channel.

However, the crystal structure of Kv 1.2, the first eukaryotic K^+ channel structure, showed that the inner helix was not bent at the proposed glycine hinge but the S6 helix was kinked further down the helix at the Pro-X-Pro motif (Long et al, 2005a). This motif is conserved in the eukaryotic Kv 1-4 family but the bacterial channels that provided the early crystal structures do not have the Pro-X-Pro motif. In Kv channels that don't have a Pro-X-Pro motif the position equivalent to the second Pro residue there is a conserved glycine, in addition to the one proposed to be the glycine hinge, which could act as an alternative hinging point. Mutation of either the Pro-X-Pro motif or the glycine at the position equivalent to the second proline result in a non-functional channel or one with severely retarded gating and often shifts the voltage dependence of activation to more negative potentials (Shealy et al, 2003). hERG does not have a Pro-X-Pro motif but does have a glycine at the position equivalent to the second proline (Gly657). Mutations at this position are well tolerated, just like mutations at Gly648, and have a minimal impact on hERG activation gating (Mitchseson et al 2000a; Hardman et al, 2007). Given the lack of a Pro-X-Pro motif and that mutation of the proposed glycine hinges had little impact

on activation gating, it is not clear how the S6 of hERG moves to open and close the cross bundle to allow the conduction of ions.

Overview of voltage sensing

When the first voltage gated ion channel, a voltage gated Na^+ channel from *Electrophorus electricus*, was cloned it revealed that each of the 4^{th} transmembrane domains contained 4 to 7 positively charged arginines or lysines separated by 2 hydrophobic residue (Noda et al, 1984). When the first voltage gated potassium channel, Shaker, was cloned by Lily Jan's group it also revealed that the S4 helix had positively charges arginines separated by 2 hydrophobic residues and it was immediately put forward as a candidate for the voltage sensing region of the channel (Tempel et al, 1987; Papazian et al, 1987). The S4 transmembrane helix in Shaker contains six positively charged amino acids (5 arginines and 1 lysine) with the 4 arginine residues in the most N-terminal (extracellular) portion of S4 being the ones more important for voltage sensing. Neutralising the positive residues in S4 reduced the gain (e.g. the activation curve was shallower, reflecting less voltage sensitivity) and the midpoint of activation was shifted (Papazian et al, 1991; Logothetis et al, 1992). The movement of the positively charged arginines in S4 across the membrane results in a current called the gating current which is distinct from the ionic current from ions passing through the pore of the channel. When the arginines in S4 were neutralised this resulted in less gating current (Aggarwal & MacKinnon 1996; Seoh et al, 1996).

The structure of Kv1.2 revealed that the S4 helix is a 3_{10} helix rather than an α-helix (Long et al, 2005a). A 3_{10} helices differs from α-helices in the arrangements of their hydrogen bond networks. In an α-helix the carbonyl oxygen of amino acid (*i*) interacts with the nitrogen of the amide group of i+4 whereas in a a 3_{10} helix the carbonyl oxygen

of residue i interacts with the third residue along the helix (i+3) (Vieira-Pires & Morais-Cabral, 2010). 3_{10} helixes have been described in the S4 helix of mammalian voltage gated potassium channels Kv1.2, Kv2.1 (Long et al, 2005a; Long et al, 2005b; Long et al, 2007), in the bacterial cyclic nucleotide-regulated potassium channel MlotiK1 (Clayton et al, 2008) and also in the bacterial sodium channel NavAb from *Arcobacter butzleri* (Payandeh et al, 2011). In an α-helix one residue is spaced at 100^{o} round the helix relative to the next residue resulting in 3.6 residues per turn of the helix. In a 3_{10} helix residues are spaced 120^{o} round the helix relative to the next residue resulting in 3 residues per turn of the helix. This means that for 2 helixes containing the same number of amino acids the 3_{10} helix will be more tightly wound, longer and thinner than the corresponding α-helix. 3_{10} helices having 3 residues per turn mean that every third residue will be on the same face of the helix. As the arginines in S4 are spaced at every third position they lie on the same face of the S4 helix.

How the voltage sensor moves through the membrane in response to changes in voltage is still not fully resolved. The 'helical screw' model proposed that S4 moves out and rotates on depolarisation with the positive arginines pairing with negatively charged in S1, S2 and S3 as they move through the membrane. However, this model was put forward before the realisation that the voltage sensing arginines lay on the same face of the S4 helix in a groove made by S1, 2 and 3. This shields the arginines from the apolar lipid environment and allows for the vertical movement of S4 rather than twisting in the helical screw model.

The paddle model was proposed by Rod MacKinnon on the basis of the KvAP voltage sensor. The KvAP voltage sensing domain was lying parallel, rather than perpendicular, to the inner membrane and it was proposed that S4 together with the C-terminal end of

S3 (S3b), which form a paddle 'helix-turn-helix' motif, move completely across the membrane on depolarisation. The paddle motion of KvAP was controversial. The voltage sensor was in the resting state but the channel pore was open. The position of the S4-S3b paddle at the inner membrane at rest was inconsistent with experimental evidence that hanatoxin could access that region from the extracellular side of the membrane at rest. It has now been established that the structure of the voltage sensing domain of KvAP was not representative of the native channel (Lee et al, 2005). The motion of the voltage sensor is probably somewhere between the two different models outlined above.

The activation of hERG is slow. This is probably due to two factors. One, Shaker has six positively charged residues in S4 whereas hERG has one less positively charged residue. The number of charged residues that move across the electric field and contribute to the gating current is less in hERG than in Shaker (Piper et al, 2003). Shaker activates quickly and the gating current associated with activation is also quick. However, when the gating current was measured in hERG there was a small, fast component but the majority of the gating current was slow and corresponded well with the time course of activation (Piper et al, 2003). In another experiment, three residues on the N-terminal portion of S4 were tagged with a fluorescent probe and changes in fluorescence correlate well with the voltage and time dependent properties of hERG gating. The fluorimetry experiments reported two components, a slow one which had the same voltage range and kinetics of hERG activation and a fast one which corresponded roughly but not exactly with the fast inactivation. The mutation G628C:S631C in hERG

which removes inactivation gating and application of extracellular TEA which slow C-type inactivation did not affect the fluorescence signal.

The second factor that accounts for the slow activation of hERG is that the arginines in S4 can form salt bridges with acidic residues in S1, S2 and S3 and these interactions help stabilise the closed state of the channel (Papazian et al, 1991; Seoh et al, 1996). hERG has more acidic residues than other Kv channel resulting in more interactions which further stabilise the closed state of the channel (Subbiah et al, 2004). These two factors help explain the slow voltage sensor movements seen in gating current and voltage clamp fluorimetry experiments.

On membrane depolarisation there is a conformational change that results in the splaying open of the inner helices, thereby increasing the diameter of the aperture and allowing the passage of ions through the pore. How changes in transmembrane voltage are transduced into opening and closing of the activation gate is the subject of chapter 4 so is discussed there.

Overview of Inactivation gating

Inactivation is a process by which a channel enters a non-conducting state with depolarisation and is distinct from the non-conducting, deactivated state. Inactivation is an umbrella term which encompasses more than one type of inactivation mechanism. Classical experiments involving the squid giant axon required a mixture of proteolytic enzymes to be briefly applied to soften the stiff axoplasm to allow the easy perfusion of internal solutions. However, leaving the enzyme mixture on for too long altered the currents that were subsequently seen. Depolarisation of the squid giant axon elicits a

rapid inward sodium current which then declines as channels inactivate. After prolonged enzymatic treatment the rapid inward current was unaltered but the decline in current associated with inactivation was no longer observed (Armstrong 1973). The decline in Na current after activation was similar to the decline in K^+ current that Clay Armstrong had observed in other earlier experiments involving open K channel block by TEA and derivatives (Armstrong 1969, 1971). This led Clay Armstrong to conclude that the inactivation gate must be a peptide on the intracellular mouth of the channel that blocks the pore after activation of the channel (Armstrong & Bezanilla, 1977). Subsequent work has shown the Na channel inactivation gate to be formed by the IFM (Ile-Phe-Met) motif in the intracellular linker between domains III and IV which binds to a receptor site at the intracellular mouth of the pore to block conduction (Vassilev et al, 1988; Vassilev et al, 1989; West et al, 1991). This type of inactivation is known as 'ball and chain' inactivation.

Shaker potassium channels inactivate in a manner analogous to sodium channels (Hoshi et al, 1990; Zagotta et al, 1990). The inactivation process is sensitive to cytoplasmic application of proteolytic enzymes again suggesting some kind of peptide gate at the intracellular mouth of the channel. Attention was drawn to the N-terminus as the candidate for the ball and chain that was responsible for inactivation. There are at least 5 different splice variants of the N-terminus all with varying inactivation kinetics (Hoshi et al, 1990; Zagotta et al, 1990). Deletion of the N-terminus dramatically slows inactivation. Experiments involving inside-out patch recordings in the N-truncated channel showed that reperfusion of the missing N-terminus restored inactivation gating (Hoshi et al, 1990; Zagotta et al, 1990). Furthermore, increasing the length of the chain decreased the speed of inactivation while shortening it increased the rate of inactivation

(MacKinnon et al, 1993). This ball and chain inactivation is termed N-type inactivation and is rapid in its onset. When the N-terminus, and thus N-type inactivation, was removed in Shaker it revealed a second, slower type of inactivation, C-type inactivation (Hoshi et al, 1990).

C-type inactivation is a constriction or collapse of the selectivity filter at the extracellular mouth of the channel. Evidence for C-type inactivation occurring around the outer mouth of the channel comes from experiments in Shaker where externally, but not internally, applied TEA slows inactivation (Choi et al, 1991) and mutation of Thr449, on the outer mouth of the selectivity filter, significantly accelerates C-type inactivation (Lopez-Barneo et al, 1993).

Some of the first experiments conducted on hERG after its discovery were to establish if the rapid inactivation which limited outward current at positive membrane potentials was due to N-type inactivation (Smith et al, 1996; Spector et al, 1996b). Deletion of the N-terminus did not remove inactivation or change its kinetics thus ruling out N-type inactivation. It was also speculated that the channel was being blocked in a voltage dependant manner by positively charged cytosolic constituents such as Mg^{2+} or polyamines – the mechanism that accounts for the rectification of K_{ir} channels. However, this was not the case as removal of Mg^{2+} and polyamines did not affect inactivation (Smith et al, 1996; Spector et al, 1996b). One of the hallmarks of C-type inactivation is slowing by extracellular TEA and this was observed in hERG channels. In addition, mutations at position Ser631 on the outer mouth of the channel (analogous to Thr449 in Shaker) also disrupted inactivation. This meant that the inactivation in hERG had to be an unusually fast form of C-type inactivation. C-type inactivation in hERG differs from C-type inactivation in Shaker in two ways; one, the onset and recovery from

inactivation is much faster in hERG than in Shaker and two, inactivation in hERG appears to be intrinsically voltage dependent unlike C-type inactivation in Shaker.

In Shaker the slow inactivation is caused by a Glu residue that is well conserved among Kv channels. This Glu (E418) forms a hydrogen bond network with other residues around the pore helix and stabilises the open state of the selectivity filter (Larsson & Elinder 2000). Mutations at this position (E418C) resulted in much faster inactivation kinetics. The residues lining the selectivity filter in almost all K^+ channels are Gly-Tyr-Gly. The Tyr78 is proposed to form part of a hydrogen bond network with two Trp68 and Trp67 in KcsA and this again stabilises the open state of the selectivity filter (Dolye et al, 1998). hERG is thought to enter into and recover from inactivation faster than other channels due to a disrupted hydrogen bonding network around the selectivity filter. In hERG, at the position equivalent to the E418 Shaker, there is not a conserved Glu but an Ile residue which partly explains the faster inactivation gating. Also, the residues lining the selectivity filter in hERG the Tyr is replaced by a Phe (Gly-Phe-Gly). Mutating the Tyr in Shaker to a Phe increases the rate of inactivation due to disrupting the hydrogen bond network around the selectivity filter (Ranganathan et al, 1996). The inward-rectifying potassium channels Kir 6.1 and 6.2 also have a Phe residue in the selectivity filter, however these channels do not undergo inactivation gating.

hERG channel inactivation gating appears to be intrinsically voltage dependent and separate from voltage dependent activation gating. The $V_{0.5}$ of inactivation is around -90mV compared to around -20mV for the $V_{0.5}$ of activation and the slope of inactivation is much shallower than the slope of activation (see first results chapter). Mutations such as S631A and Y542A shift the voltage dependence of inactivation to more positive potentials by as much as 100mV without affecting the voltage

dependence of activation (Smith et al, 1996; Fan et al, 1999; Sanguinetti & Xu 1999). Moreover, the mutation W563A hERG shifts the voltage dependence of activation by -60mV while leaving inactivation gating unaltered (Subbiah et al, 2004).

Deactivation

Deactivation is the process whereby the channel closes at the intracellular activation gate. Deactivation in hERG is slow when compared to other Kv channels like Shaker. Removing the N-terminus dramatically alters deactivation, increasing its rate by about 10 fold. Deleting just the eag domain has the same effect. In fact, removal of only the first 16 residues also results in a channel with much faster deactivation. If the N-truncated channel is expressed and then the eag domain is introduced to the cytoplasm of the cell the EAG domain will restore the slow deactivation gating. Moreover, if the N-truncated channel is expressed and a peptide fragment corresponding to the first 16 residues is introduced into the cytoplasm of the cell it can rescue the slow deactivation. When a patch of membrane is excised containing channel(s) that have had the slow deactivation restored the affect of the 16 residues was not washed off which suggested the peptide fragment was tightly bound to a receptor site somewhere on the channel and had a critical functional role in deactivation gating.

Mutations in the N-terminus are associated with long Q-T syndrome (LQTS). hERG passes the majority of its current when the membrane starts to repolarise as the channels quickly recover from inactivation but slowly deactivate so that they are in an open conducting state. Several naturally occurring mutations in the N-terminus speed up deactivation and as a result the channel spends less time in a conducting state after the recovery form inactivation. The resulting reduction in hERG current means there is

less current to oppose early after depolarisations and leads to increase likelihood of arrhythmia.

The molecular basis for the N-terminus regulation of deactivation is the subject of the first results chapter so deactivation gating is discussed more fully in chapter 3.

The Structural Basis of hERG Current Inhibition

In addition to congenital LQTS caused by inherited mutations individuals can also suffer from acquired LQTS in which drug block of hERG reduces I_{Kr} current and can predispose an individual to arrhythmia. The drug induced form of LQTS is an unwanted side effect of many unrelated classes of medicines (Roden, 2008). The number and structural diversity of drugs that can induce LQTS through block of hERG is large. Several distinct classes of drugs have been withdrawn from the market or had their use severely restricted because of long QT liability including, terfenadine and astemizole (antihistamines), cisapride (5HT agonoist) and sparfloxacin (an antibiotic). hERG block and long QT liability of drugs is also a major problem for the pharmaceutical industry when trying to get new medicines to market. Sertindole (antipsychotic) was refused a licence by the FDA because it increased the risk of atrial fibrillation (Stansfeld et al, 2006).

There are two main differences between hERG and other Kv channels which help explain the unusual susceptibility of hERG to block. One difference is the inner cavity may be larger than other channels and the other difference is the presence of two aromatic residues in the middle of S6 that are not present in other Kv channels.

Structure of the inner cavity

The first difference between hERG and other Kv channels that explains why hERG is more susceptible to block by so many drugs is that the majority of Kv channels have a Pro-X-Pro motif in S6 between the base of the selectivity filter and the activation gate whereas hERG does not (fig 1.5). The presence of proline residues in an α-helix will break or kink the helix by disrupting the hydrogen bond network of the helix. The Pro-X-Pro motif is proposed to kink S6 resulting in a smaller than otherwise inner cavity. hERG has Ile-Phe-Gly in place of Pro-X-Pro. The absence of prolines, and therefore lack of disruption to S6, is thought to create an inner cavity that has a larger volume than other Kv channels. The larger inner cavity of hERG allows a wide variety of drugs to access and bind within the inner cavity. Drug trapping occurs when the intracellular activation gate closes behind drugs that have entered the inner cavity when the channel was in the open state after depolarisation. Drug trapping is not unique to hERG channel block. Experiments by Clay Armstrong showed that the delayed rectifier currents in the squid giant axon could be blocked by compounds that were being trapped (Armstrong 1966, 1969, 1971). Internally applied tetraethylammonium (TEA) only blocked after the membrane potential was depolarised, suggesting that the binding site was behind the activation gate in the channel pore. TEA blocked outward current much better that inward current and increasing the concentration of external K^+ ions reduced the level of block. The only location that external K^+ ions and intracellularly applied TEA could interact was in the pore of the channel. By comparing block by TEA and other quaternary ammonium ions (QA) of different sizes, Armstrong showed that large QA compounds caused a slowing of deactivation that he termed “foot in the door” block as the QA molecule acted as a wedge that prevented the deactivation gate from closing.

However, smaller QA compounds could block without slowing deactivation. In a subsequent elegant series of experiments by Gary Yellen's group, they were able to show that mutated Shaker channels, quite large, high affinity compounds were being trapped within the inner cavity upon channel closure (Holmgren et al, 1997; Liu et al, 1997).

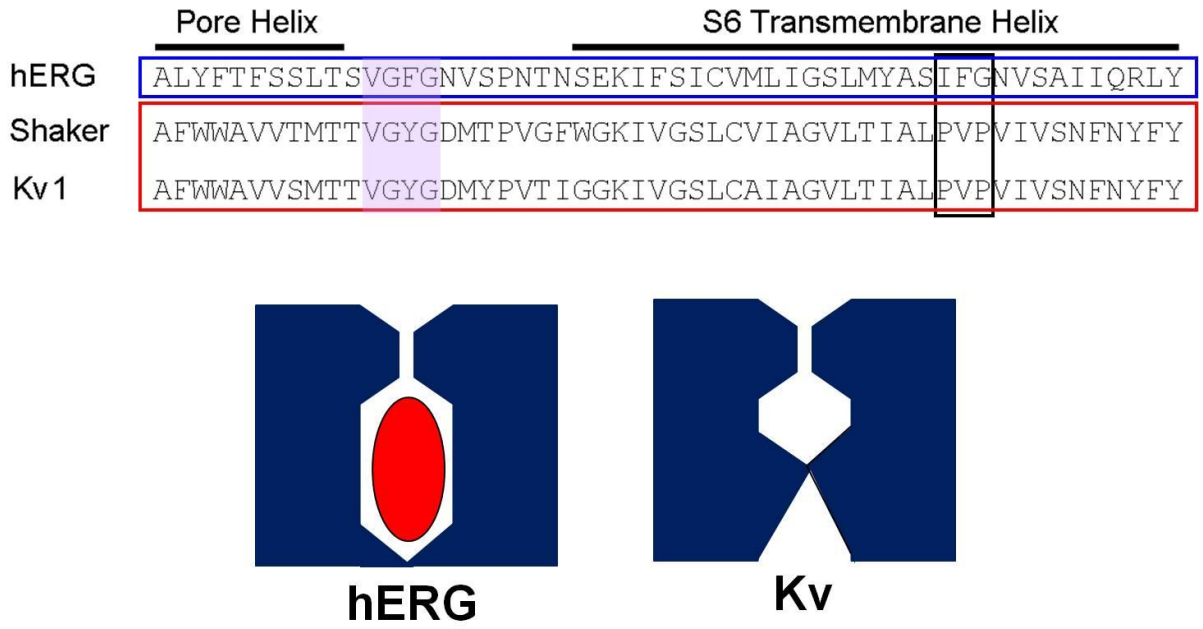

Figure 1.5. hERG lack the Pro-X-Pro sequence in S6 which results in a larger inner cavity than other Kv channels.

Top) Sequence alignement of pore helix and selectivity filter through S6 of hERG, Shaker and Kv1 channels. hERG has an Ile-Phe-Gly in place of the Pro-X-Pro motif of most other K^+ channels.

Bottom) The lack of a Pro-X-Pro motif is thought to create a larger inner cavity because there is no kinking in the middle of S6. The red oval represents a trapped drug molecule.

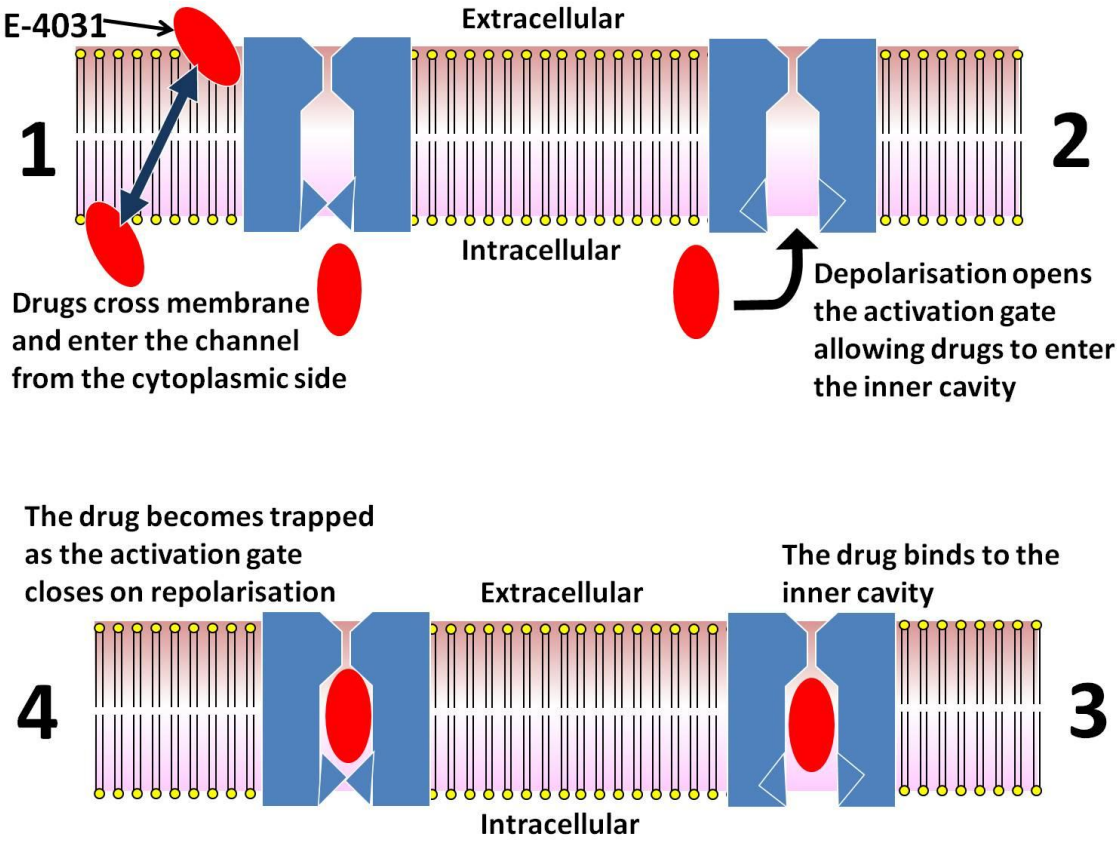

Figure 1.6. Drugs bind to the inner cavity and are trapped on closure of the activation gate. 1) Drugs need to cross the cell membrane in order to reach the binding site in the inner cavity. 2) When the cell is depolarised the activation gate opens. 3) The drug enters into the inner cavity. 4) When the membrane potential repolarises the channel deactivates and the drugs are trapped behind the activation gate.

The drug trapping hypothesis has been used to explain why so many drugs can block hERG with high affinity and with slow time course for recovery from block. Further evidence of drug trapping came from a mutant with very unusual activation properties. The activation gate normally opens on depolarisation of the membrane. However, the mutant D540K hERG has the unusual property of also opening upon hyperpolarisation of membrane potential (Sanguinetti, & Xu, 1999). Using the methanesulfonanilide MK-499, a high affinity hERG channel blocker, WT hERG currents were blocked by repetitively applying a 5 second voltage step to 0mV in the presence of 2µM MK-499. After the current was inhibited repetitive pulses to -160mV for 20 seconds were then applied with the membrane potential held at -90mV between pulses. After ~15 minutes the membrane potential was then stepped back to 0mV and the level of current was measured and compared to the level of current at 0mV after current inhibition by MK-499. There was a 5% recovery in current after repetitive pulsing to -160mV (Mitcheson et al, 2000b). The same protocol was used to assess D540K hERG currents recovery from inhibition. After current inhibition and repetitive pulsing to -160mV the D540K hERG current had recovery to 85% of the current amplitude before block (Mitcheson et al, 2000b). Both WT and D540K hERG were blocked by MK-499 but D540K currents recovered after pulsing to -160mV whereas WT currents did not. D540K hERG channels open at hyperpolarised potentials and this allows the drug to exit the inner cavity but because WT hERG channels remain closed at hyperpolarised potentials drug molecules that had bound at 0mV were trapped in the inner cavity.

Drug binding residues

The second difference between hERG and other Kv channels that explains why hERG binds lots of drugs with high affinity are the two aromatic residues, Tyr652 and Phe656, on S6 that face into the channel vestibule and allow for high affinity binding (fig 1.7). These aromatic residues are not conserved in other Kv channels which typically have an Ile and Val in homologous positions (Mitcheson et al, 2000a).

Experiments by Mitcheson et al 2000a, introduced an alanine scan at the base of the pore helix and along the S6 helix of hERG in a series of experiments designed to identify the residues that were important for drug binding. Applying 300nM of MK-499 reduces WT hERG currents by 85%. However, Y652A and F656A hERG current were unaffected by the application of 300nM MK-499. Further work by Fernandez et al 2004, showed that the physicochemical interaction of Tyr652 and Phe656 with compounds differ from one another. The tyrosine at position 652 is believed to form cation-π interactions between the positively charged nitrogen of the drug and the π electrons of the phenol group of Tyr652. Substitutions of a variety of different residues at position 656 show that block by MK-499, cisapride and terfenadine is well correlated with the hydrophobic volume of the substituted residue, indicating that hydrophobicity and not aromaticity is the more important physicochemical feature of binding for these compounds at this position. It is likely that compounds bind to hERG in a number of different ways. However, what is important is that the presence of eight aromatic residues in hERG allows for a great diversity of hydrophobic and electrostatic interactions with compounds that are not as energetically favoured in other Kv channels that have an Ile and Val residues in analogous positions. Another residue on S6 that was virtually unaffected by MK-499 during the alanine scan experiments was Gly648. This glycine

may not be directly involved in drug binding, but rather the lack of reduction in G648A hERG current on application of MK-499 may be through an allosteric effect. As discussed below residues Thr623, Ser624 and Val625 at the base of the pore helix are involved in drug binding. Although Gly648 is positioned twenty-five residues away from Thr623 in the primary structure, they are very closely packed together in the tertiary structure, see figure 1.7 (Hardman et al, 2007). Mutations at position 648 to residues with larger side groups, e.g. glycine to alanine, may result in a repositioning of the residues at the base of the pore helix so that it is less accessible for drug binding or the substitution of Gly648 for an amino acid with a bulkier side group may also physically impede drug binding to the residues at the base of the pore helix.

As well as having allosteric effects on the drug binding site, mutations can also influence sensitivity to block by affecting channel gating. V659A hERG currents were far less susceptible to block than WT hERG currents even though Val659 is not thought to be directly involved in binding. V659A resulted in very slow deactivation (see chapter 4). Slow closure of the activation gate allows drugs to escape from the inner cavity upon repolarisation, reducing trapping of blockers within the inner cavity.

Other residues identified as being involved in drug binding were Thr623, Ser624 and Val625 located at the base of the pore helix, (Mitcheson et al, 2000a; Perry et al, 2004; Perry et al, 2006). V625A hERG currents were the least effected by MK-499 of these three mutants with only a 15% reduction in current followed by T623A and then S624A hERG which had a 60% reduction in current. These residues are not unique to hERG and are reasonably well conserved in Kv channels so by themselves don't explain why so many compounds preferentially block hERG.

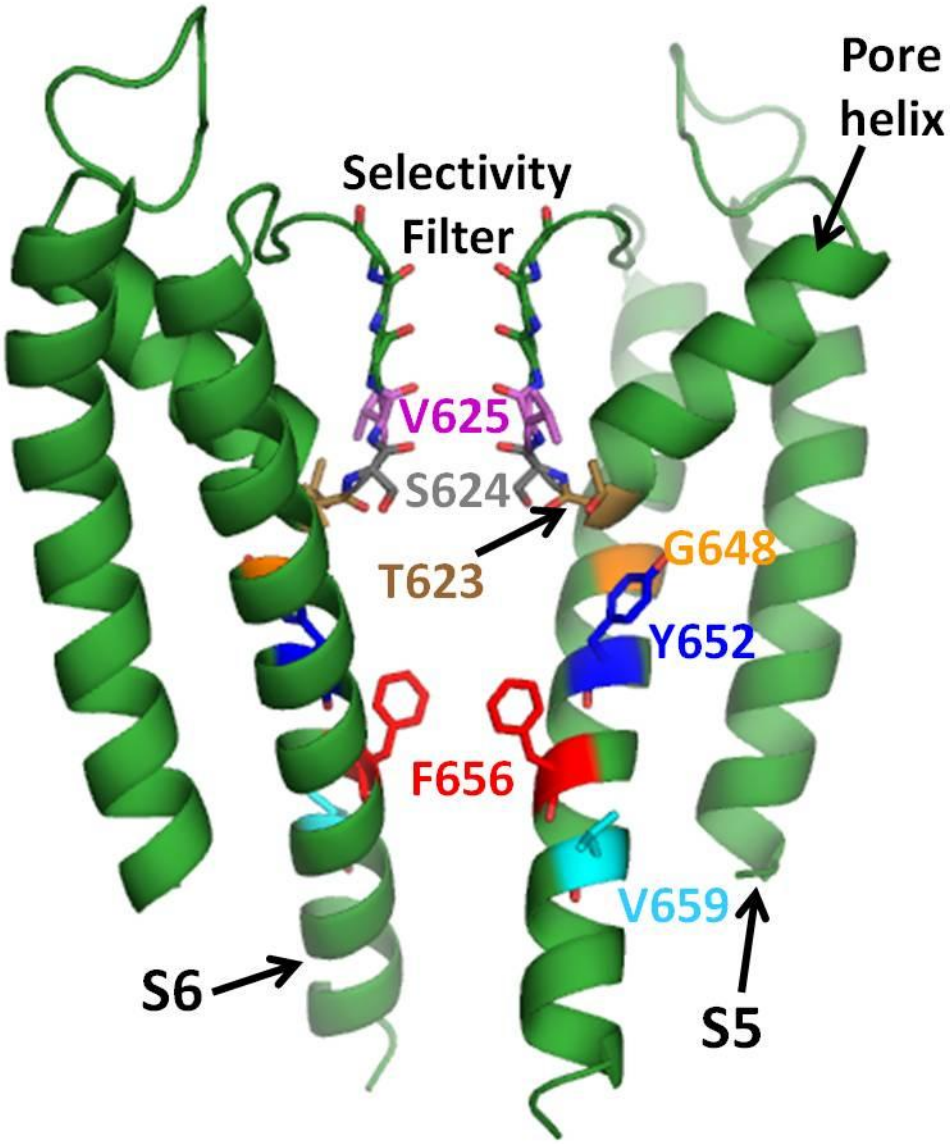

Figure 1.7. Drug binding residues in the inner cavity of hERG. The inner cavity amino acids suggested to form the drug binding site are illustrated in different colours. (Val625 – purple, Ser624 – gray, Thr623 – brown, Gly648 – orange, Tyr652 – dark blue, Phe656 – red, Val659 – pale blue). Figure adapted from PhD thesis of Dr Phil Stansfeld. Homology model of hERG based on KcsA.

Inactivation gating and drug binding

hERG channels share the same inner cavity aromatic and polar residues as EAG channels and yet EAG channels are far less sensitive to block than hERG (fig 1.8). A crucial difference may be the lack of inactivation in EAG channels. hERG channels exhibit C-type inactivation. Mutations around the outer mouth of EAG channels that introduce C-type inactivation increase sensitivity to drug block (Ficker et al, 2001). Conversely, mutation of residues around the outer mouth of the channel that effect C-type inactivation in hERG, e.g. S620T and S631A, reduce sensitivity to drug block (Ficker et al, 1998). One hypothesis that may explain these findings is that inactivation in hERG causes a repositioning of inner cavity residues from a position where they are not optimally arranged to bind drug to one where there are (Chen et al, 2002).

Experiments by Chen et al 2002, showed that if the two aromatic residues on S6 of EAG are mutated to be placed one residues lower (towards the carboxy terminus) this increases the sensitivity of EAG to block. They also showed that if the two aromatic residues on the S6 of hERG are mutated to be one position lower (again towards the carboxy terminus) this decreases the sensitivity of hERG to block. Moving the aromatic residues to the adjacent position means that they are now orientated 100^{o} round the S6 helix and the side chains of the aromatic residues are not facing in the same directions as they were in the WT channel. It therefore appears that simply having the aromatic residues present on S6 is not enough for high affinity drug binding but these residues must be in the correct orientation to be able to interact with the drug molecules. It is thought that inactivation in hERG causes a repositioning of inner cavity residues from a position where they are not optimally arranged to bind drug to one where there are (Chen et al, 2002).

Work on Shaker has shown that during inactivation not only is there a rearrangement of amino acids around the outer mouth of the channel but there is also a rearrangement of residues in the inner cavity (Panyi & Deutsch 2006).

Further work on Shaker has shown that mutating the isoleucine at position 470, which is analogous to Tyr652 in hERG, to tyrosine (I470Y) slows activation and increases the rate of C-type inactivation; similar to hERGs gating kinetics (Klement et al 2008). The residues that line the inner cavity and those around the pore that are involved in inactivation gating, although clearly not close in the primary structure, are closely interdependent in the functional channel and more work is needed to understand the precise nature of this relationship.

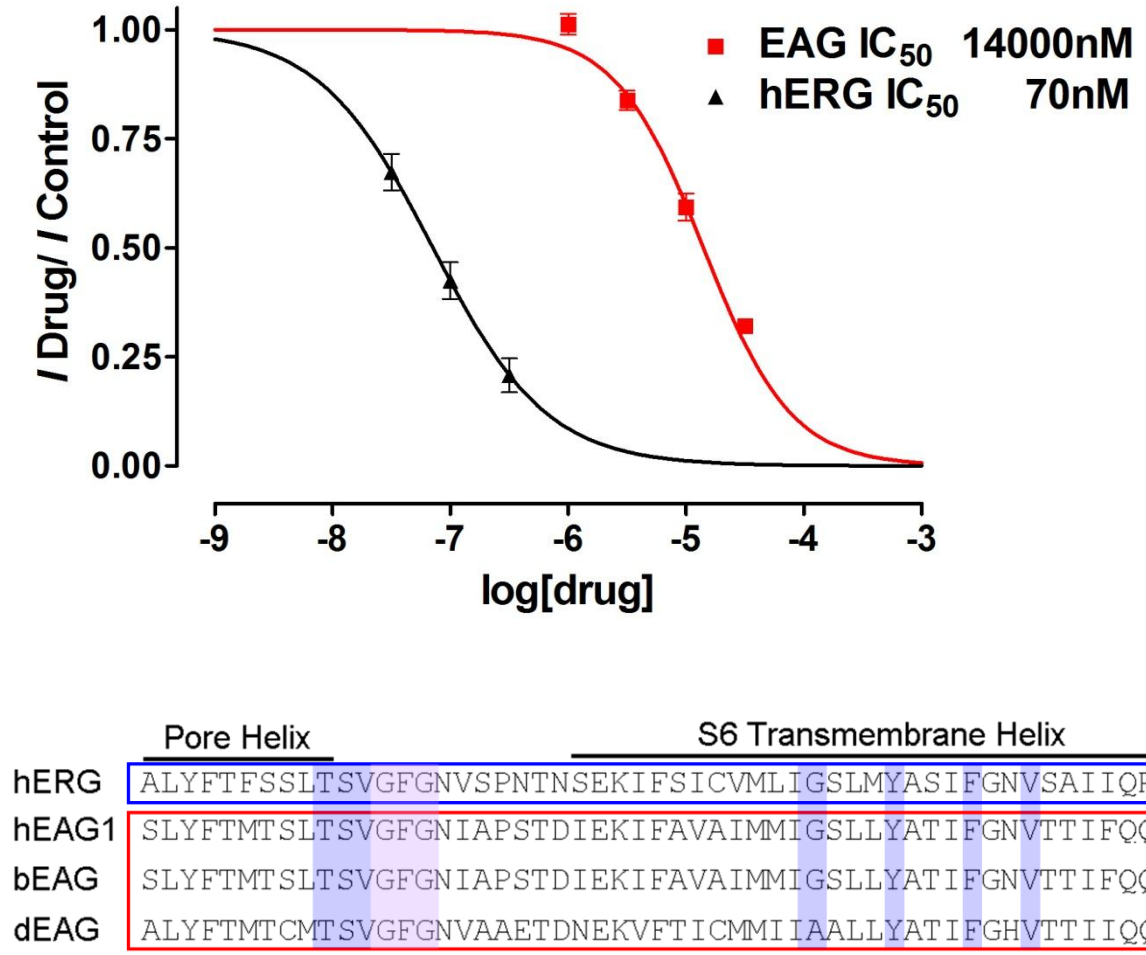

Figure 1.8. EAG is far less sensitive to block than hERG even though the key drug binding residues are conserved.

The top panel shows the IC_{50} of Cisapride (a well known hERG blocker) on WT hERG and WT EAG. Cisapride is far less potent on EAG than hERG.

The bottom panel is a sequence alignment of the selectively filter and S6 of hERG and EAG channels. The key aromatic residues Tyr and Phe in the middle of S6 are conserved. Also conserved are the residues at the base of the pore helix that are important in drug binding. (See chapter 8 for more detail).

Aims of this thesis

The aims of this thesis were;

1) To solve the structure of the whole eag domain including the first 26 amino acids that are critical for deactivation gating and were not solved in the previous crystal structure of the eag domain. And guided by the structure, investigate the molecular basis of the slow deactivation that the NT 1-26 region confers to hERG.

2) Explore the molecular basis for the slow deactivation of V659A hERG. Val659 hERG was mutated to glycine, alanine, cysteine, isoleucine and phenylalanine and the effect on deactivation gating was compared to WT hERG. The possibility that Val659 couples the activation gate to the voltage sensor via an interaction with the S4-S5 linker was probed by cysteine cross-linking experiments.

3) Test the drug trapping hypothesis using derivatives of the hERG blocker E-4031. E-4031 is a well characterised, potent hERG channel blocker. E-4031 binds to the inner cavity residues and exhibits slow recovery from block when the activation gate closes. In order to investigate the importance of trapping for drug potency we had two series of derivatives of E-4031 made that got progressively longer. The aim of developing the derivatives of E-4031 was twofold. One was to use them as a "molecular ruler" to measure the size of the inner cavity. This could then be used to produce information about the size of the inner cavity. Secondly, to investigate if making drugs longer could be a means to reduce potency.

Chapter 2

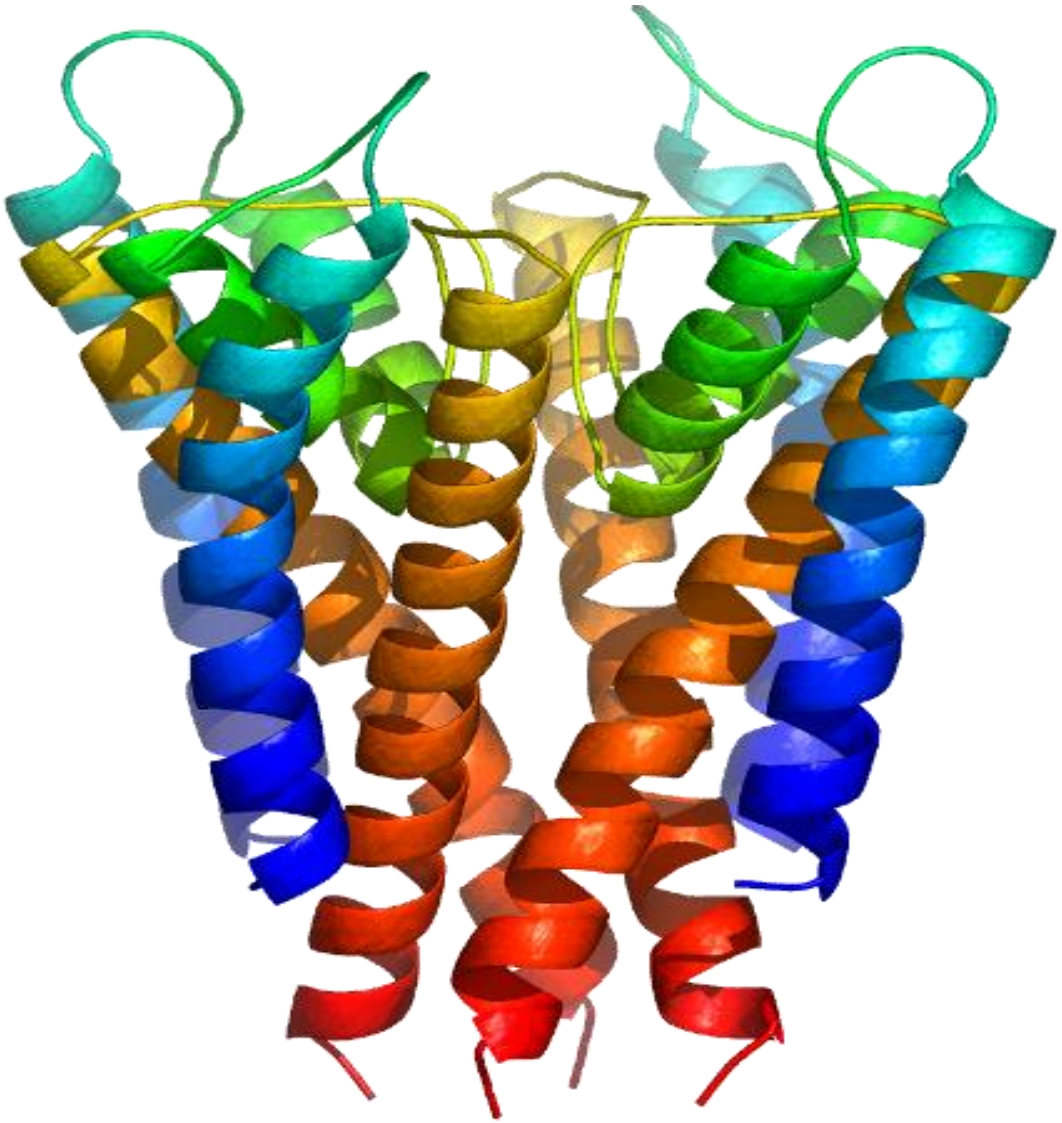

Materials and Methods

Molecular Biology

The structure-function studies presented here required various molecular biology techniques in order to create the many mutants required to undertake this project. The polymerase chain reaction (PCR) technique was used for the site-directed mutagenesis of hERG DNA. The mutated plasmid DNA was transformed into bacterial cells for DNA amplification. This plasmid DNA was removed from the host bacterial cells and commercially available kits were used to remove impurities, as described below. The purified DNA was linearised with a restriction enzyme and *in vitro* transcribed into RNA, again using a commercially available kit as described below. The RNA was injected into *Xenopus* oocytes and hERG currents were recorded by two electrode voltage clamp.

A number of different expression vectors were used in this study. The majority of mutants including the NT 1-26 & cyclic Nucleotide Binding Domain mutants were made in the pXoom vector (Jespersen et al, 2002). Mutants designed to investigate coupling between S6 and the S4-S5 linker used the pSP64 vector. Both vectors have 3' & 5' untranslated regions and a polyadenylation sequence at the 3' end which stabilise the RNA and boost expression levels. pXoom has a T7 RNA polymerase promoter and neomycin/kanamycin resistance whereas pSP64 has a SP6 promoter and ampicillin resistance. The restriction enzymes used to linearised the plasmid DNA prior to *in vitro* transcription with RNA polymerase were Xba I & EcoRI for pXoom and pSP64 respectively. Wild-type (WT) hERG in the pXoom vector was gratefully received from Dr Paul Groot-Kormelink (Novartis Institutes for Biomedical Research, Horsham, Sussex).

Mutagenesis

Oligonucleotide primers were engineered to contain the desired mutation using Vector NTI software (Invitrogen) and were ordered from Euro Fins MWG (Ebersberg, Germany). The primers were 30 to 40 bases in length, had a melting temperature ≥ 78^{o}C and had a GC content of 40 to 60 percent. These primers were used to introduce mutations into hERG cDNA using the QuikChange technique (Agilent Technologies, Waldbronn, Germany) a polymerase chain reaction (PCR) based approach. Each cycle of the PCR involved denaturing the double stranded DNA at 95^{o}C then lowering to the primer annealing temperature of 55^{o}C and then stepping to 72^{o}C to allow DNA extension by the polymerase. Using an automated thermal cycler machine, the reaction was repeated a further 24 times and led to the exponential increase in DNA. The PCR reaction contained; 19.5 µl nuclease free H_2O, 1.25 µl primer #1 (100ng/µl), 1.25 µl primer #2 (100ng/µl), 2 µl plasmid DNA (25ng/µl), 1 µl Dimethylsulfoxide (DMSO) and 25µl 2x*PfuUltra* Master Mix (Agilent Technologies, Waldbronn, Germany), total reaction volume 50µl. On completion of the PCR the product was incubated at 37^{o}C with the restriction enzyme DpnI (New England Biolabs, Hitchin, UK) for 1 hour which selectively digests methylated, non-mutated (template) DNA. The mutated, non-methylated PCR product was then transformed into competent bacteria.

Transformation of competent cells

Transformation, the process of inserting new genetic information into a cell, allows for the potentially massive amplification of the inserted plasmid DNA as the bacteria divide, to yield hundreds of micrograms of DNA depending on the volume and density of the bacterial cell culture. This DNA can then be harvested and directly used for transfection of mammalian cells such as CHO cells or transcribed into RNA for expression in *Xenopus*

oocytes. Transformations of plasmid DNA were carried out using DH5α competent cells. The cells were slowly thawed on ice and placed into flacon 2059 tubes which had been pre-chilled on ice for 30 minutes. 3µl of PCR product was added and the cells were left to incubate on ice for 30 minutes. The cells were then heat shocked in a water bath at 42^{o}C for 45 seconds and returned immediately to ice. 900µl of super optimal broth with catabolite repression (SOC) media was added to the flacon tube and it was placed in a shaking incubator for 1 hour at 37^{o}C and 240 rpm. 200 µl of the cells were plated onto Lysogeny broth (LB) agar with ampicilin (100µg/ml) or kanamycin (30µg/ml) (depending upon the antibiotic resistance gene carried by the vector), and incubated overnight at 37^{o}C. A single colony was picked the next morning and grown in 5ml LB Broth with the appropriate antibiotic (37^{o}C, 240 rpm) for 8 hours. 0.5ml of the broth was mixed with 0.5ml of glycerol and this glycerol stock was stored at -80^{o}C. The remaining cells where lysed (see below) so the DNA could be extracted and sequenced to confirm the insertion of the desired mutation.

Preparation of DNA

There are many different products from various different biotechnology companies for the purification of plasmid DNA from bacterial cells. Generally they work by alkaline lysis of the cell to release the plasmid DNA. The lysate is centrifuged and the supernatant containing the plasmid DNA is passed through a silica-gel column which binds DNA. The column is washed to remove excess salt or cell debris and the plasmid DNA is eluted. The kits used in this project were the mini/midi/maxi prep kits from Qiagen, CA, USA and the preparations were carried out as per the manufactures handbook. To quantify the DNA it was run on a 1% agarose gel, stained with ethidium bromide (0.6µg/ml), alongside the standard DNA ladder (hyperladder 1, Bioline) as a comparison.

Linearization of DNA

The DNA was linearised with a restriction enzyme appropriate for the vector (e.g. XbaI for pXoom, 3hrs at 37^{o}C) that cuts at a single specific site 3' to the stop codon and polyadenylation sequence. After linearization, 100 µg/ml of Proteinase K and 0.5 % SDS was added to the DNA and incubated for 30 minutes at 50°C to denature any contaminating proteins and in particular RNAases. The linearised DNA was purified by passing through a silica-gel column from the the Qiaquick gel extraction kit (Qiagen, USA). DNA was eluted using Tris-EDTA buffer and quantified on a gel the same as for DNA described above.

Preparation of RNA

Linearised DNA was *in-vitro* transcribed into cRNA using the commercially available kit mMESSAGE mMACHINE© (Ambion, Austin, TX,USA). All bench surfaces were washed with ethanol and to avoid contamination by RNAases, all pipetting was done using filter pipette tips. The reaction mixture contained; 1 µl of nuclease-free water, 10 µl of NTP/CAP mix, 2 µl of 10x reaction buffer, 2 µl of RNA polymerase enzyme mix, and 5 µl of DNA template (0.2 µg/µl) The reaction was incubated at 37^{o}C for 2 hours. After 2 hours, 1 µl of DNAase1 was added to the reaction and incubated for a further 15 minutes at 37 °C. This removed any template DNA present. RNA was quantified by taking a small sample (0.5 to 1 µl) and heating to 85 °C for 3 minutes then run on a 1 % denaturing formaldehyde agarose gel. The gel was made of 10x MOPS EDTA sodium acetate (MESA) buffer made up of MOPS (3-(N-Morpholino)propanesulfonic acid, 2 M), sodium acetate (50 mM), EDTA (10 mM), pH 7. RNA was quantified on the gel against a known RNA control sample, then diluted to a concentration of 500 ng/µl and aliquots were stored at -80 °C until needed for injection into *Xenopus* oocytes.

Electrophysiological Recordings

Oocyte isolation

Xenopus laevis frogs were humanely killed by immersion in anaesthetic (3-Aminobenzoic acid ethyl ester, Sigma, UK) and pithing. The ovarian lobes were removed via an incision into the lower abdominal wall. The lobes were placed into oocyte Ringer (OR2) solution containing (in mM); NaCl 82.5, KCl 2.5, Na_2HPO_4 1, $MgCl_2$ 1, HEPES 5 (pH 7.5). The ovarian lobules were cut into clumps of 10 – 20 oocytes and digested in 30 ml of collagenase (1 mg/ml, Sigma, UK) until the follicular layer could be easily removed with forceps (approximately 25 – 30 minutes). The oocytes were then washed in Barth's solution to wash out the collagenase. Barth's solution contains (in mM); 88 NaCl, 1 KCl, 0.41 $CaCl_2$, 0.33 $Ca(NO_3)_2$, 1 $MgSO_4$, 2.4 $NaHCO_3$, 10 HEPES, pH 7.4. The oocytes were mechanically defolliculated with forceps and transferred to petri dishes containing Super Barth's solution (Barth's solution supplemented with 1mM sodium pyruvate and 50 µg/ml gentamicin). Oocytes were injected the following day using a Nanolitre 2000 micro-injector (World Precision Instruments, Hitchin, UK).

Oocyte injection

Glass pipettes were pulled on a programmable horizontal puller (Sutter Instruments, Novato, CA, USA) and the tips broken to be approximately 30 µm wide and with a sharp or jagged tip that pierces the oocyte with the least damage. The pipettes were filled with mineral oil (Sigma, UK), placed on the injector and the RNA was sucked into the pipette. The pipette tip was placed into each oocyte and they were injected with 10 – 60 nl cRNA per oocyte. The amount of cRNA injected depended on how well the mutant construct was known to express. To allow for differing expression levels in the oocytes

from week to week, two different amounts of RNA were injected. Oocytes were studied 1 – 6 days after injection. The oocytes were cultured in Super Barth's solution at 16^{o}C and the solution was changed daily.

Two electrode voltage clamp recordings

The two electrode voltage clamp (TEVC) technique uses two electrodes; one electrode measures the membrane potential relative to the bath (ground) electrode and the other passes the current required to clamp the membrane potential at the command potential. The TEVC technique was employed to record whole-cell currents in *Xenopus* oocytes. TEVC allows the recording of comparatively large amplitude currents (10 nA to 10µA) compared to 1pA to 1nA using the patch clamp technique. The single-electrode voltage clamp (SEVC), also known as the switch clamp technique, is often used to record currents in the range of 100pA to 10nA, e.g too large for patch clamp but too small for TEVC. TEVC offers other practical advantages for studying ion channels over patch clamp recording. The same sharp electrodes may be used repeatedly, the electrodes can be mounted on course movement manipulators and because of the relativity large size of the oocytes low magnification 'bench top' microscopes can be utilised.

When a test voltage is set, the voltage electrode measures the difference of the inside of the oocyte relative to the bath (membrane potential) and through a feedback amplifier it deducts the membrane voltage from the command potential set by the experimenter and sends an output to the current electrode which injects the current required to clamp the membrane potential to the command potential.

The oocytes were placed in a recording chamber and bathed at room temperature (19-21^{o}C) in 2 mM K^{+}, low Cl^{-} recording solution. The solution had the following

composition (mM); 96 Na 2-(*N*-morpholino)ethanesulfonic acid (MES), 2 K MES, 2 $Ca(MES)_2$, 5 HEPES, 1 MgCl2, pH 7.6. The flow rate was ~4 ml/min. The microelectrodes were made from 1mm diameter filamented borosilicate thin walled glass (TW150F-4, World Precision Instruments) and pulled using a horizontal puller (Sutter Instruments). They were filled with 3 M KCl and the tips were broken to a resistance of 1 - 2 MΩ.

Solutions and Compounds

Compounds were added daily to recording solutions from a 10 mM stock solution in which the compounds has been dissolved in DMSO and stored at -20^{o}C. DMSO concentration was < 0.1% of the final drug solution concentration. Cisapride, tert-butylhydroperoxide ($tbHO_2$) and dithiothreitol (DTT) were purchased from Sigma, UK, E4031 was purchased from Calbiochem, UK and E-4031 derivatives were custom synthesised by Chemical Synthesis Services Ltd and provided courtesy of Novartis Institute for Biomedical Research (Horsham, UK).

Data acquisition & analysis

Voltage protocols were generated and currents recorded using pCLAMP (v8.2) software on a PC communicating via a Digidata 1322A digital to analogue converter with a voltage clamp amplifier (GeneClamp 500B). All of these devices are supplied by Molecular Devices, Sunnyvale, CA, USA. Data was analysed in Clampfit software (Molecular Devices), Excel 2007 (Microsoft) and Prism 5.0 (GraphPad). Most currents were recorded with a sampling frequency of 2 - 5 kHz. However for capturing very fast kinetic events such as the rapid onset and recovery from hERG current inactivation the sampling frequency was increased to 20 kHz. The signal was filtered at half of the sampling frequency.

Concentration-response relationship

Currents were allowed to stabilise in control solution or after reaching steady state inhibition at each drug concentration. Tail current amplitudes were leak subtracted and normalised to control. The normalised data were fitted with a Hill function

$$(I\mathrm{Drug}/I\mathrm{Control}) = \frac{1}{(1 + (\frac{[D]}{IC_{50}})^{h})}$$

where IC_{50} is the concentration at which the drug inhibits the current by 50%, [D] is the drug concentration and *h* is the Hill coefficient. Concentration-response relationships from single cells were fit with the Hill function and then IC_{50} and Hill slopes were averaged to get the mean and SEM values.

Time constants of deactivation

hERG currents were fully activated with a 1 second pulse to +40mV and deactivation measured during test pulses to varying potentials (see chapters 3 & 4). The decaying phase of hERG tail currents were fit with an exponential function to obtain the time constants (τ) for deactivation. Current traces were fit with the function

$$f(t) = \sum_{i=1}^{n} A_i \, e^{-t/\tau_i} + \mathrm{C}$$

where A is the amplitude, τ is the time constant, C is steady state current and i refers to each component.

Analysis of voltage dependence of hERG activation + inactivation

For the voltage dependence of activation, peak tail currents were normalised against maximal peak tail current and plotted as a function of the test potential. Leak currents

were measured with a 50ms pulse to the same membrane potential as the tail currents (normally -70mV) prior to the test pulses and were subtracted from the tail currents. Tail current-voltage relationships were fit with a Boltzmann function

$$G\ (V) = \frac{1}{1 + \exp(\frac{V_{0.5} - Vm}{K})}$$

to find the half point for the voltage dependence of activation ($V_{0.5}$) and the slope factor (k), a measure of the relative voltage sensitivity of the channels. G (V) is the normalised conductance and Vm is the membrane potential. This Boltzmann function was also used for analysis of the voltage dependence of inactivation. The protocol and analysis are described in more detail in chapter 3.

Statistical Analysis of the data

The data are presented as mean ± standard error of the mean (S.E.M). Statistical comparisons were made using an unpaired t-test unless otherwise stated in the text of the results sections. Differences were considered statistically significant for $p \leq 0.05$. Excel (Microsoft) and Prism (GraphPad) were used to analyse and plot the results. Abbreviations used to denote statistical significance are; * = $p \leq 0.05$, ** = $p \leq 0.01$ and *** = $p \leq 0.001$.

Chapter 3

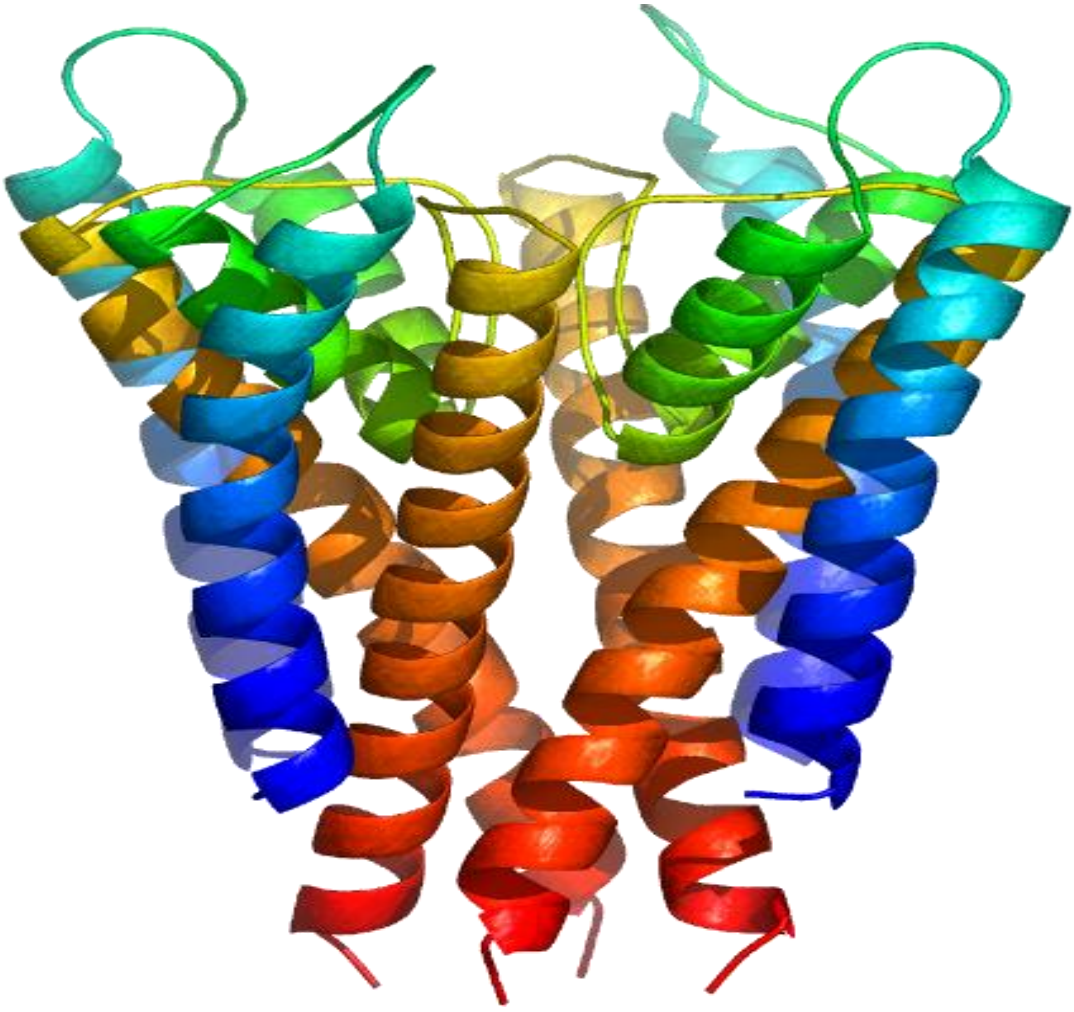

The role of the N-terminus resides 1 – 26 & the C-terminal cNBD in deactivation gating

Introduction

The speed of hERG's three gating processes, activation, inactivation and deactivation are crucial for its normal role in the cardiac action potential. The slow activation and rapid onset of inactivation limits the outward current during the plateau phase of the action potential. When the membrane begins to repolarise channels rapidly recover from inactivation back into a conducting state, where the channels pass most of their current, before then slowly closing. Some naturally occurring mutations, such as R56Q located in the N-terminus, increase the rate of deactivation which reduces the amount of current available to repolarise the membrane and opposes early depolarisations (fig 3.1) (Chen et al, 1999).

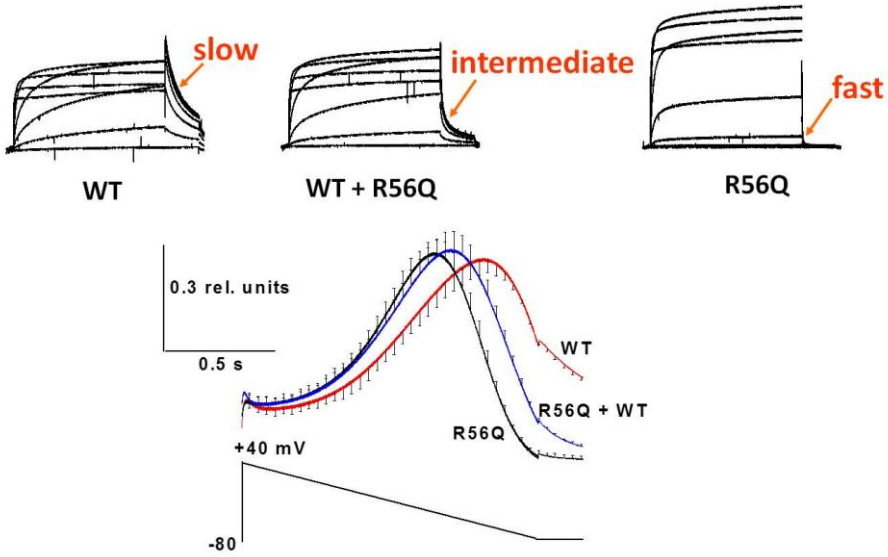

Figure 3.1. Naturally occurring mutation R56Q deactivates faster than WT hERG.
The top 3 current traces were elicited using a standard I-V protocol; from a holding potential of -90mV the cell was stepped in 20mV increments to +30mV before stepping down to -70mV to elicit tail currents. In the WT channel (top left) the tail currents decay slowly. The tail currents in the N-terminus mutant R56Q (top right) decay very quickly. When WT and R56Q are co-expressed the rate of the decay of the tail current was intermediate between the slow decay of WT and the rapid decay of R56Q.
The bottom current trace shows the hERG currents elicited from WT, WT + R56Q and R56Q using the ramping voltage protocol (shown underneath the current traces) that simulates the cardiac action potential. R56Q peak current occurs earlier that WT hERG and there is much less current late in the simulated action potential. (Adapted from Chen et al, 1999).

The N-terminus of hERG is intracellular and is approximately 355 resides long. The N-terminus has an important role in regulating the deactivating gating of hERG. Many naturally occurring mutations, such as F29L, N33T, G53G, R56Q, C66G, H70R, A78P, L86R are found in the N-terminus and specifically in the 'eag' domain at the beginning of the N-terminus (Chen et al, 1999). When the N-terminus is removed (N-truncated hERG, abbreviated as NTK hERG) deactivation is dramatically accelerated, figure 3.2 (Spector et al, 1996b; Schonherr & Heinemann 1996). Figure 3.2 shows the fully-activated I-V protocol used throughout this chapter to measure the rate of deactivation. The protocol is described in detail in the results section but briefly, the membrane potential is held at -90mV and then stepped to +40mV for 1 second to fully activate and inactivate the current. The membrane potential is then stepped down to a range of potentials to measure the rate of deactivation. The current traces underneath the voltage protocol show the last 100ms of the step to +40mV and the first two seconds of the step to the deactivation test potentials. The wild type hERG channel deactivates slowly whereas NTK hERG deactivates rapidly. The bottom panel shows WT and NTK tail currents normalised to the same amplitude so that gating can be compared and shows that NTK is clearly deactivating much faster than WT hERG. The cartoons of the channel on the right hand side illustrate what part of the channel has been removed.

Experiments by Morais-Cabral et al, 1998 showed that slow deactivation could be restored to the N-truncated channel by injecting purified 'eag' domain (residues 1-135) protein into the oocyte. EAG domain protein was grown in *E.coli* and purified. This purified protein was acutely applied to excised inside-out patches of membrane containing N-truncated hERG channels and this had no effect on the rate of deactivation gating.

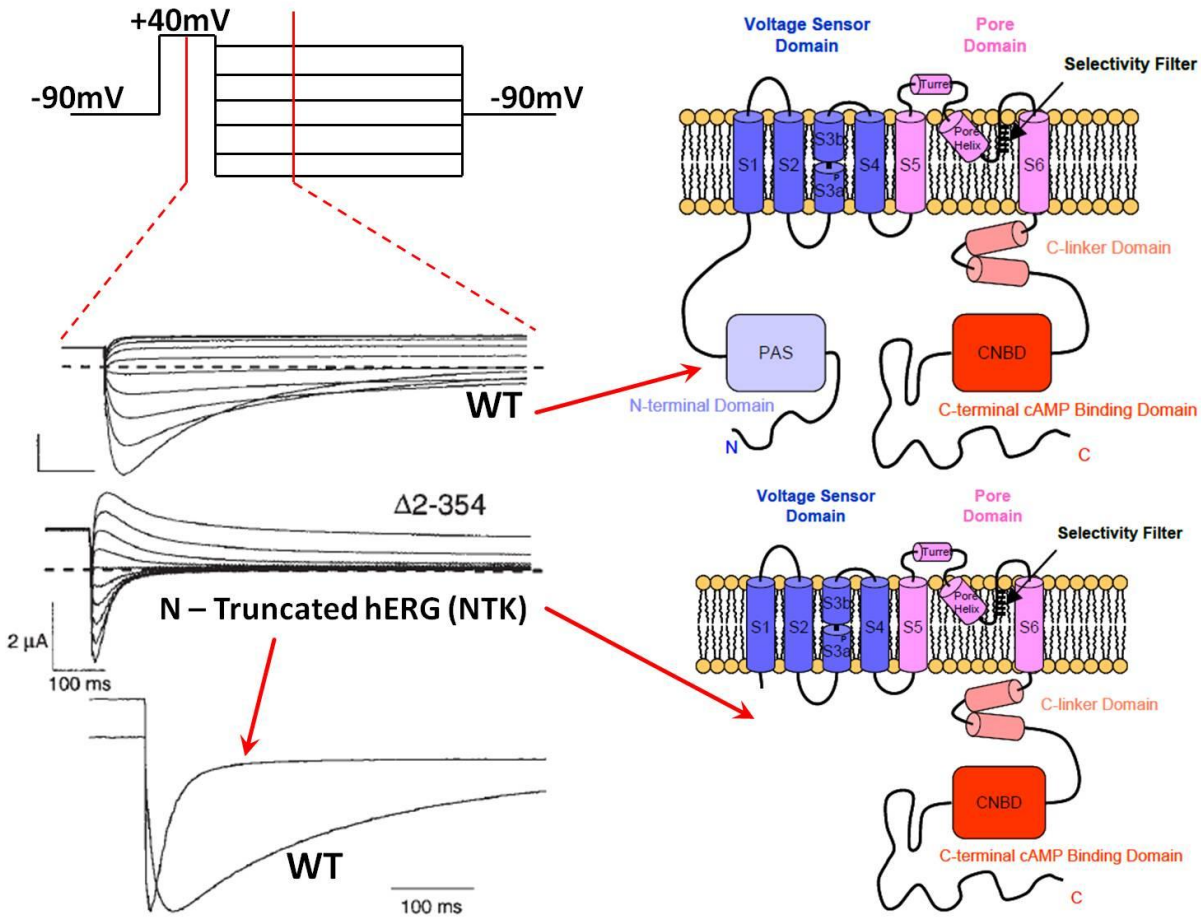

Figure 3.2. Removing the intracellular N-terminus in hERG dramatically increases the speed of deactivation.

The fully activated I-V (FA I-V) protocol (top left) is properly described in figure 3.9 and this FA I-V is used to elicit currents that are shown below it. The top current trace shows the slow deactivation of WT hERG over a range of membrane potentials. The cartoon of hERG (top right) had its N-terminus intact.

The middle current trace is N-truncated hERG as represented by the lower of the two cartoons of hERG with the N-terminus missing. The tail currents of the channel with the N-terminus removed decayed much faster than the WT channel above it.

Current traces at the bottom left are normalised tail currents of WT and NTK hERG at -110mV. NTK deactivates faster than WT hERG (Current traces from Wang *et al,* 1998)

However, when the purified eag domain was injected into the cell the slow deactivation gating was gradually restored over 24 hours. The restoration of normal, slow deactivation was not lost when patches were excised from the membrane. This suggested that the eag domain slowed deactivation by forming a stable interaction with some part of the channel and not by a rapid association and disassociation.

It is not entirely surprising that removing about a third of the channel alters the gating of the channel, but intriguingly the same rapid deactivation was also observed if only the first 16 residues of the 355 residues in the N-terminus are removed. Wang *et al*, 1998, showed that it was not necessary to remove the whole of the N-terminus to observe accelerated deactivation gating, the same affect could be seen by deleting the first 16 amino acids. Moreover, it has been shown that if the N-truncated hERG channel is expressed and a peptide fragment corresponding to the first 16 residues of the N-terminus is dialysed into the cell this restores the slow deactivation gating seen in the wild type channel. Furthermore, if the same experiment is performed on excised inside-out patches the slow deactivation is restored by application of peptide and can be washed-off suggesting that the peptide fragment is quickly binding and unbinding to a receptor site somewhere on the channel (Wang et al, 2000). This is quite different to the stable interaction formed when the entire eag domain was applied to NTK hERG (Morais-Cabral et al, 1998) and this point is pickup in the discussion.

The N-terminus contains a motif running from residue 1 to 135 called an 'eag' domain so called because it is well conserved within the EAG family of K^+ channels. Within the 'eag' domain residues 26 to 135 form a structural motif called the PAS domain. The structure of the PAS domain of hERG was solved in 1998 by MacKinnon's group in New York

(Morais-Cabral et al, 1998). However, the region that is critical for the slow deactivation, the first 26 residues which are referred to as NT 1-26 for N-terminus 1-26, was not resolved in the crystal structure and the authors stated that this was probably due to that region being too flexible and dynamic to form a stable crystal.

The aims of this results chapter were to solve the structure of the NT 1-26 region by NMR spectroscopy and, guided by the structure, investigate the molecular basis of the slow deactivation that the NT 1-26 region confers to hERG. The NMR experiments were performed by Dr Fred Muskett, Senior Experimental Officer and Structural Biology Facility Manager and Samrat Thouta an MSc student. I carried out the electrophysiological recordings and mutagenesis studies.

Results

NMR solution structure of the N-terminal of hERG

As mentioned in the introduction to this chapter the structure for the first 26 residues of hERG, which are critical in regulating slow deactivation, was not resolved in MacKinnons crystallographic study, probably because NT1 -26 is too flexible. In this study, a solution, rather than a solid state, NMR approach was used in order to elucidate the structure of the entire eag domain, including this flexible part of the channel.

Twenty overlaid NMR structures are shown in figure 3.3. The structures have been aligned from Ser26 through Val132 in the PAS domain. Because the twenty structures have been aligned against residues 26 to 132 they superimpose well as the PAS domain forms a regular, reproducible fold. Residues 26 to 135 form a PAS domain that is very well defined in the NMR data. However, NT 1-26 is less ordered, hence the 'spaghetti-like' appearance in figure 3.3. NT 1-26 forms an independent domain from the PAS domain and NT 1-26 appears to hinge from the PAS domain at residue 25/26. This explains why it was not resolvable in the crystal structure. In fact, there is a regular structure in part of NT 1-26 (discussed below) but it is not part of, and is independent from, the PAS domain so does not superimpose well in figure 3.3. In figure 3.4 the protein backbone of the PAS domain from the 20 solution structures (in blue) are superimposed with the previously solved crystal structure (in red) of the PAS domain they were in excellent agreement (fig 3.4).

The NMR data reveals that NT 1-26 has two distinct regions. NT 1-26 contains an amphipathic α-helix running from Glu11 to Gly24 while Met1 to Pro10 are unordered (figure 3.5). Again there are 20 overlaid structures aligned against residues 11 to 24.

These residues overlay very well because this region forms an amphipathic α-helix. One side of the helix is composed of hydrophobic residues (Phe14, Leu15, Ile18, Ile19 and Phe22) and the other side formed from either charged or polar residues (Thr13, Asp16, Thr17, Arg20, Lys21 and Glu23). The helix is represented by a ribbon with the hydrophobic residues in magenta and the charged or polar residues in cyan. For clarity only the side-chains of residues in the helix are shown. A helical wheel diagram of the helix residues is shown in figure 3.6 which again shows that one face of the helix is charged and one face is neutral.

A surface charge rendering of the eag domain is shown in figure 3.7. Figures A and B show the EAG domain in the same *y* and *z* orientation but B has been rotated 180^{o} around the *x* axis compared to A. Positive charge is blue, negative charge is red and white indicates neutral/hydrophobic. Only one of the four subunits that comprise a potassium channel is shown. It was very striking from the rendering of the surface charge just how positive (blue) one face of the NT 1-26 region was and it was important to establish if this charge had a role in deactivation gating. The stable α-helix was also a striking feature of the NMR data and again it was important to determine its role in deactivation.

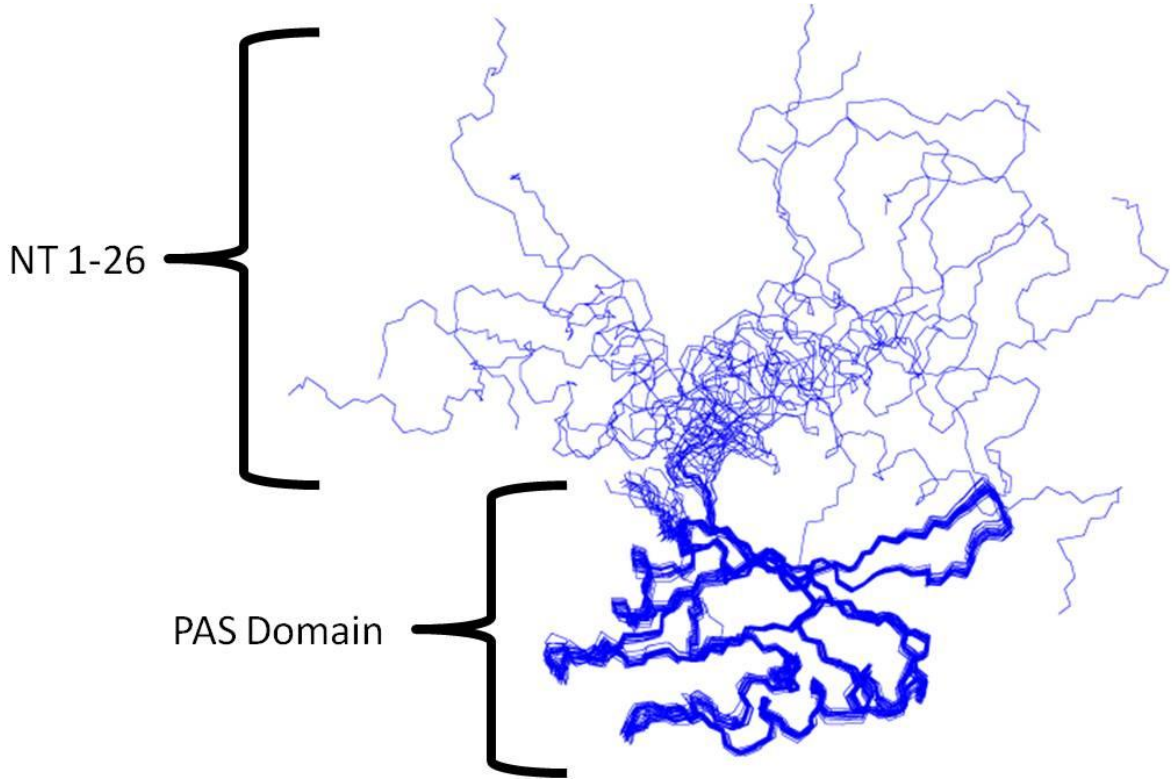

Figure 3.3. Superposition of the protein backbone of the EAG domain (residues 1 – 135).

20 NMR structures have been aligned against residues Ser26 through Val132 in the PAS domain. The 20 structures for the region 26 to 132 overlay well because the PAS domain is a constrained structure. The 20 structures in the NT 1-26 do not overlay well. Although NT 1-26 do not over lay well, there is more agreement in structure in the region adjoining the PAS domain (residues 11 – 26) than in residues 1 – 10 which appear unordered.

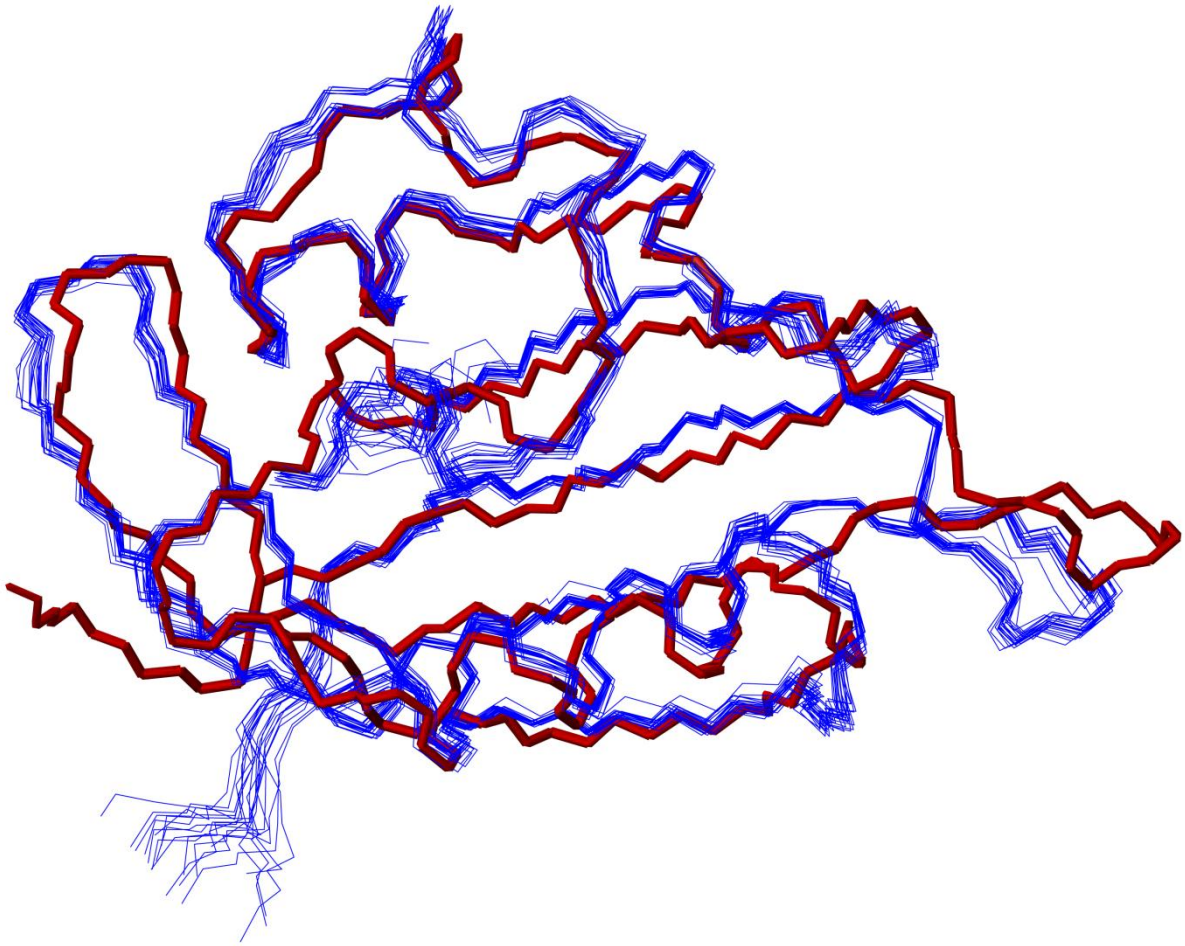

Figure 3.4. Superposition of NMR and crystal structures.

20 NMR solution structures (blue) have been overlaid with MacKinnon's lab previously published crystal structure of the PAS domain (red). The new NMR structure aligns well with the previously resolved crystal structure.

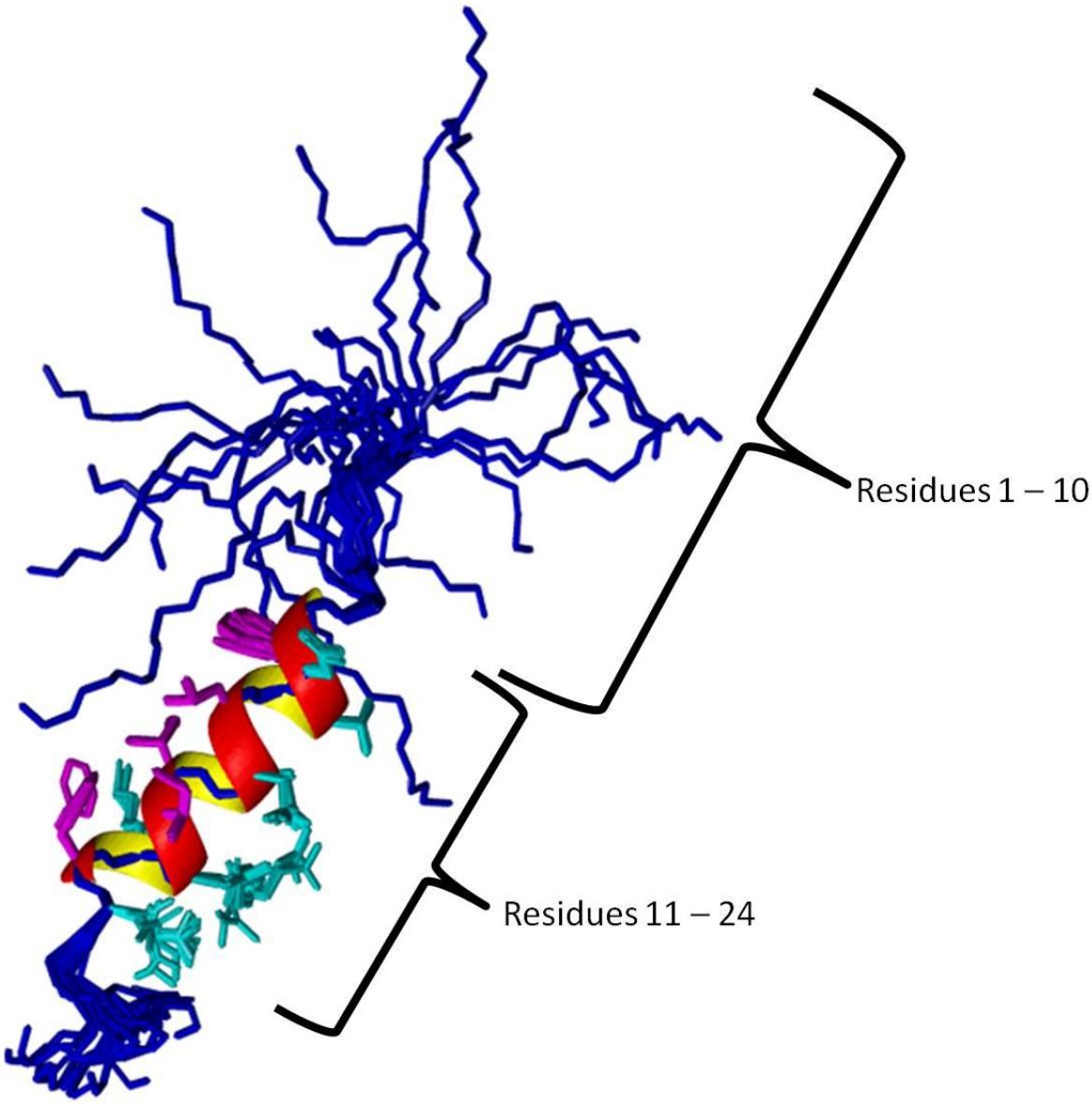

Figure 3.5. Structure of NT 1 – 26 domain of hERG.

The peptide backbone (blue) of Met1 to Glu25 from the 20 structures in fig 3.2 superimposed to illustrate amphipathic helix extending from Glu11 to Gly24. The helix is represented by a ribbon with the hydrophobic residues in magenta and the charged or polar residues in cyan. For clarity only the side-chains of residues in the helix are shown.

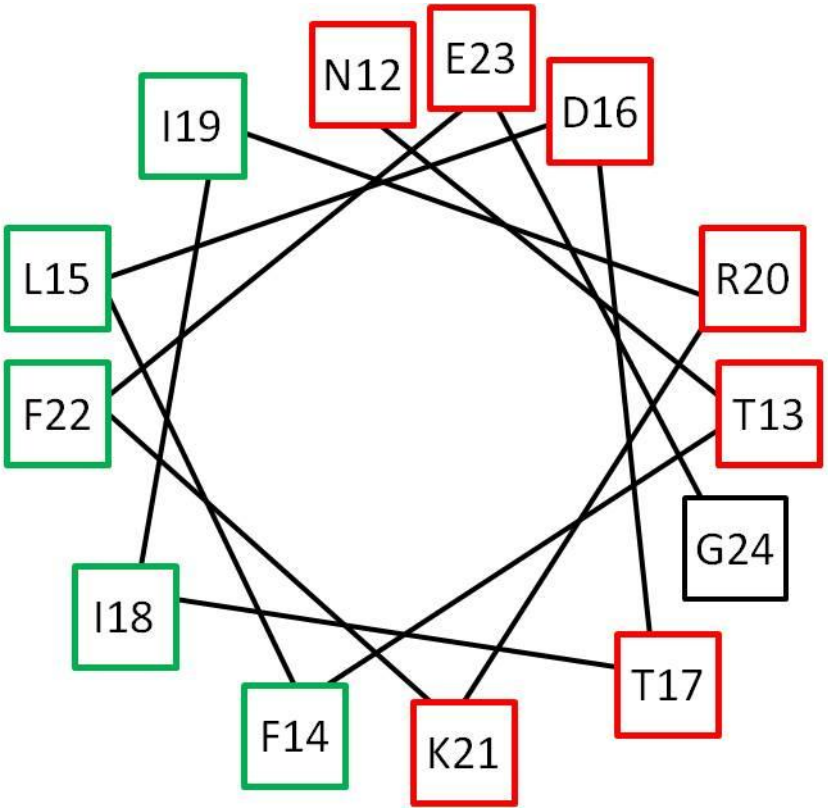

Figure 3.6. Helical wheel representation of the amphipathic helix from fig 3.4.

Charged residues are in red boxes, hydrophobic residues are in green boxes and neutral residues are in black boxes. The wheel runs from residue 12 to 24.

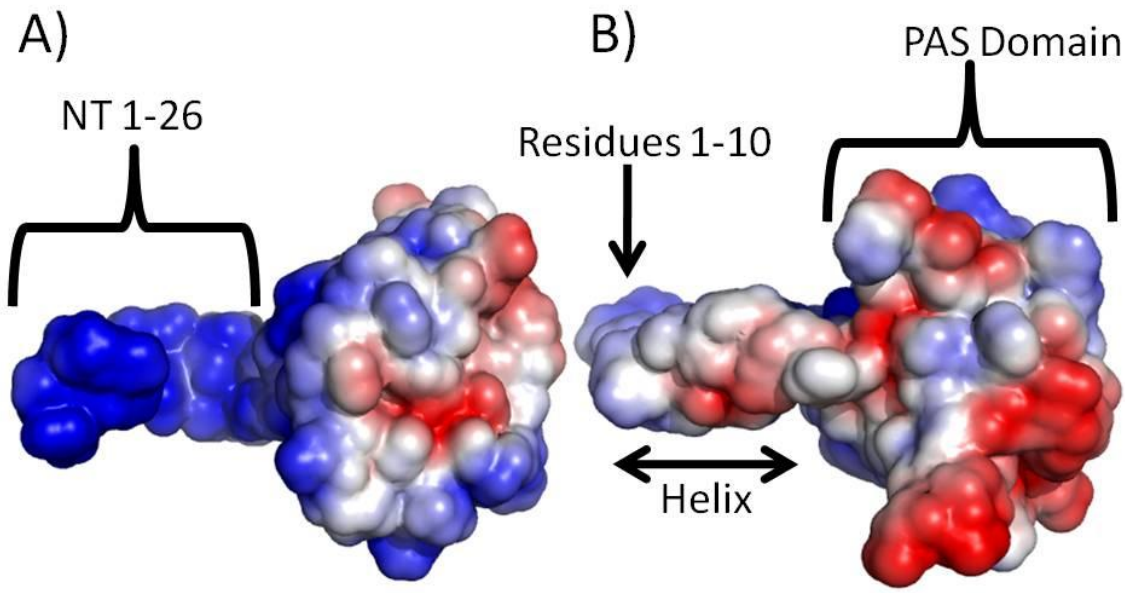

Figure 3.7. Rendering of surface charge on the EAG domain.

Figures A and B show the EAG domain in the same *y* and *z* orientation but B has been rotated 180^{o} around the *x* axis compared to A. Positive charge is blue, negative charge is red and white indicates neutral/hydrophobic. Only one of the four subunits that comprise a potassium channel are shown. A) One face of NT 1-26 is very positive in charge. In the figure NT 1-26 is kinked where the disordered residues 1-10 meet the helix and residues 1-10 project towards the reader. B) The other face of NT 1-26 is hydrophobic with a one negatively charged residue (Asp16). In B NT 1-26 is also kinked where the disordered residues 1-10 meet the helix and residues 1-10 but now project away from the reader.

Is the positively charged face of NT 1 – 26 important for deactivation gating?

It has been known for some time that removing the N-terminus increases the rate of deactivation and that this effect can be localised to the first 16 residues. The NMR data revealed that one face of NT 1 – 26 was positively charged. There are five basic residues in NT 1-26, three are in the disordered first ten residues, Arg4, Arg5, His7 and two are in the amphipathic helix, Arg20 and Lys21 (fig 3.8). In order to investigate the importance of this charge for deactivation gating the charge was removed by mutating to alanine. The following mutants were made R4A:R5A, H7A, R20A, K21A & R20A:K21A.

Figure 3.8. **Residues 1 to 34 of WT hERG.**
Amino acids sequence of NT 1-26 and the start of the PAS domain. Basic residues are highlighted in red.

The 'fully activated' I-V voltage protocol (FA I-V) used to investigate the rate of deactivation is shown in figure 3.9 along with the currents elicited using the protocol in WT hERG. The membrane potential was held at -90mV and then stepped to +40mV for 1 second to fully activate the channel and also inactivate the channel and hence there is not much current at this potential. The membrane potential was then stepped down, in 20mV increments, from -50mV to -130mV for 5 seconds and then stepped back to the holding potential. Time constants for deactivation were obtained by fitting with a single exponential curve. A double exponential fit would give a better description of the time course, but a single fit was chosen as it allows for direct comparison between mutants and with WT hERG.

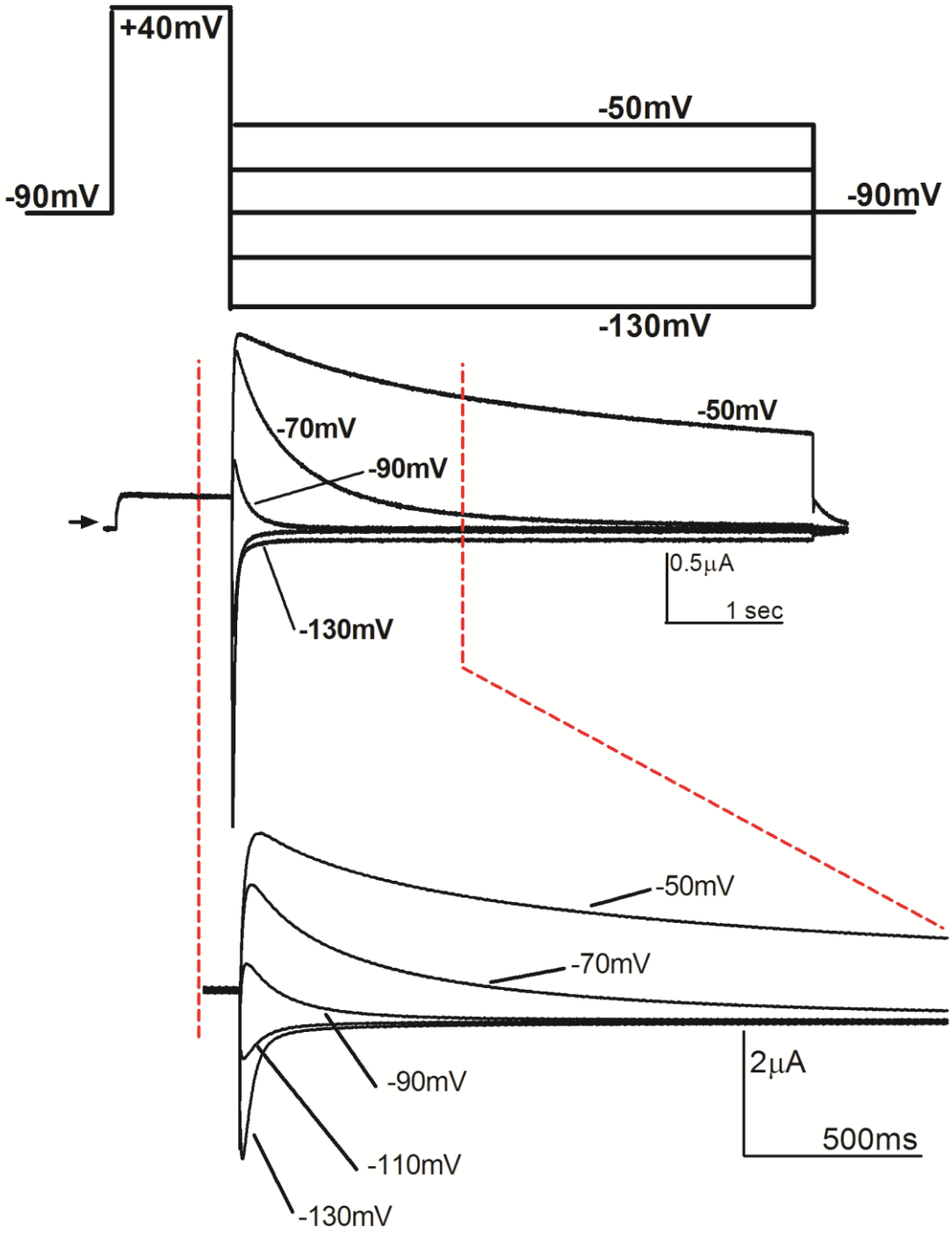

Figure 3.9. Fully activated I-V (FA I-V) protocol used to measure deactivation kinetics. From the holding potential (-90mV) the membrane potential was depolarised to +40mV for one second to fully activate the channel. The membrane potential was then stepped down to -50mV and then in 20mV increments to -130mV for five seconds before returning to the holding potential. Shown directly underneath the voltage protocol are the currents elicited from the FA I-V for WT hERG. Shown in the bottom panel is an expanded view of the last 50ms of the +40mV step and the first 2 seconds of the repolarising step.

Before showing the results of the alanine mutants that remove the basic residues it is prudent to begin with a characterisation of WT and NTK hERG. Figure 3.10 shows a portion of the tail currents from the FA I-V. NTK hERG clearly deactivates much faster than WT hERG, time constants at -70mV were 564.1 ± 20 ms for WT hERG and 15.7 ± 0.9 ms for NTK hERG. Removing the N-terminus increases the rate of deactivation which is consistent with previous findings (Spector et al, 1996b; Schonherr & Heinemann 1996). As well as examining if there was any change in the rate of deactivation the voltage dependence of activation was also studied using the following protocol; from a holding potential of -90mV the membrane potential was stepped from -80mV to +50mV for 5 seconds in 10mV increments and then stepped down to -70mV for 2.5 seconds to elicit tail currents before returning to the holding potential (fig 3.11). At the start of the protocol there was a short (50ms) pulse to -70mV to measure the leak and this value was subtracted from the peak tail current. There was 15 seconds between sweeps. The mean normalised tail currents were then plotted against voltage and fitted with a Boltzmann function to give the half maximal voltage of activation ($V_{0.5}$) and the slope. The threshold for activation of WT hERG was -60mV and the channel reaches maximal activation around +10mV. For NTK hERG the activation threshold is positively shifted to -40mV and the channel also reaches maximal activation around +10mV (fig 3.12). The slope of NTK hERG was steeper than WT hERG. There was a significant difference in the $V_{0.5}$ of activation and the slope between WT and NTK hERG, again this is consistent with existing literature (Spector et al, 1996; Wang et al, 1998) (fig 3.12). It has also been shown that removing the N-terminus does not alter the time constant of activation (Spector et al, 1996; Wang et al, 1998) so this parameter was not investigated in this study.

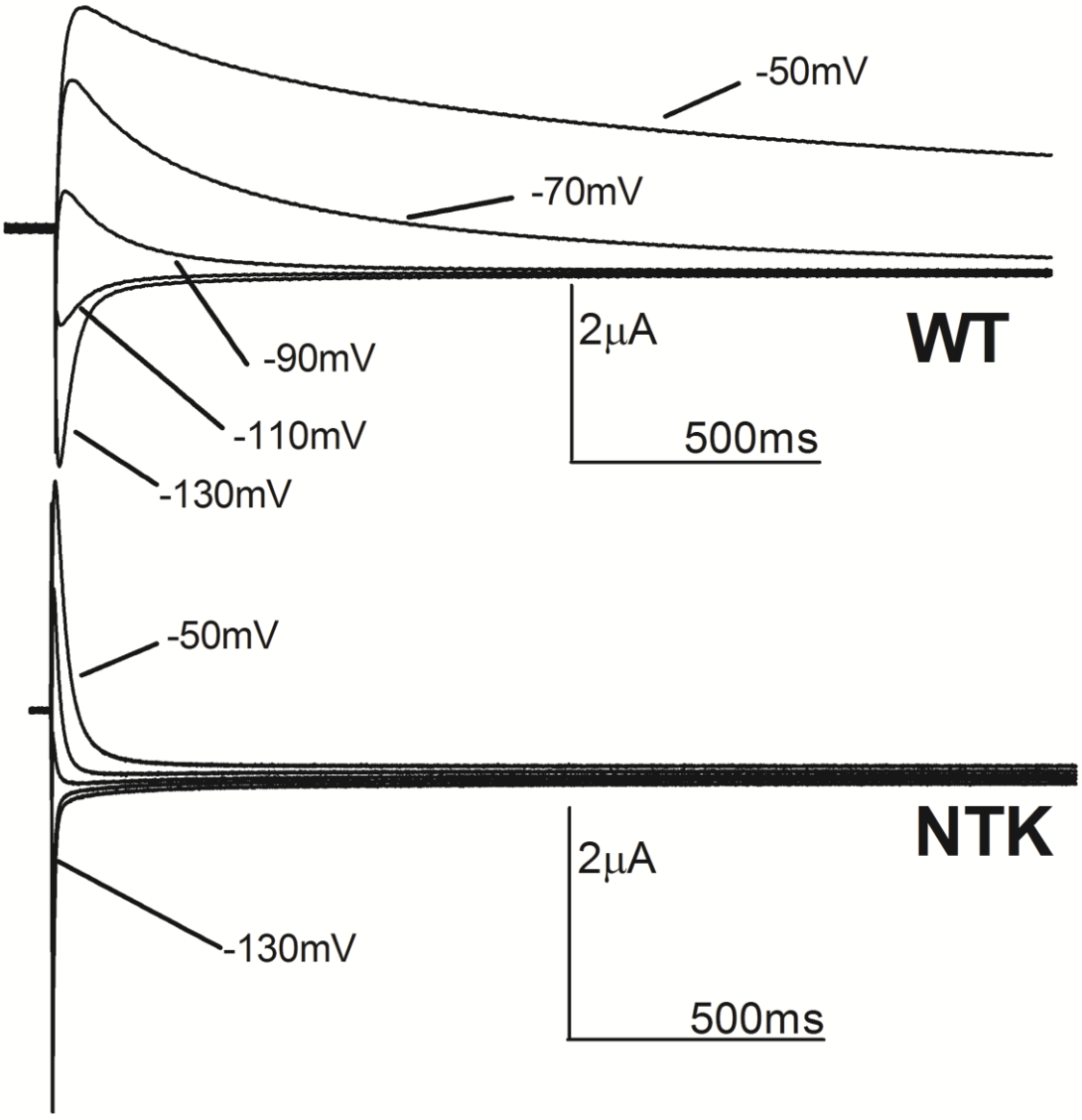

	Deactivation τ (ms) at -70mV	Deactivation τ (ms) at -130mV	n
Wild Type	564.1 ± 20.0	40.9 ± 7.1	8
NTK hERG	15.7 ± 0.9 ***	4.2 ± 0.2 ***	6

Figure 3.10. NTK hERG deactivates faster than WT hERG.

Representative tail currents of WT and NTK hERG elicited using the FA I-V. The time constants of deactivation were derived by fitting the decaying phase of the tail currents with a single exponential function.

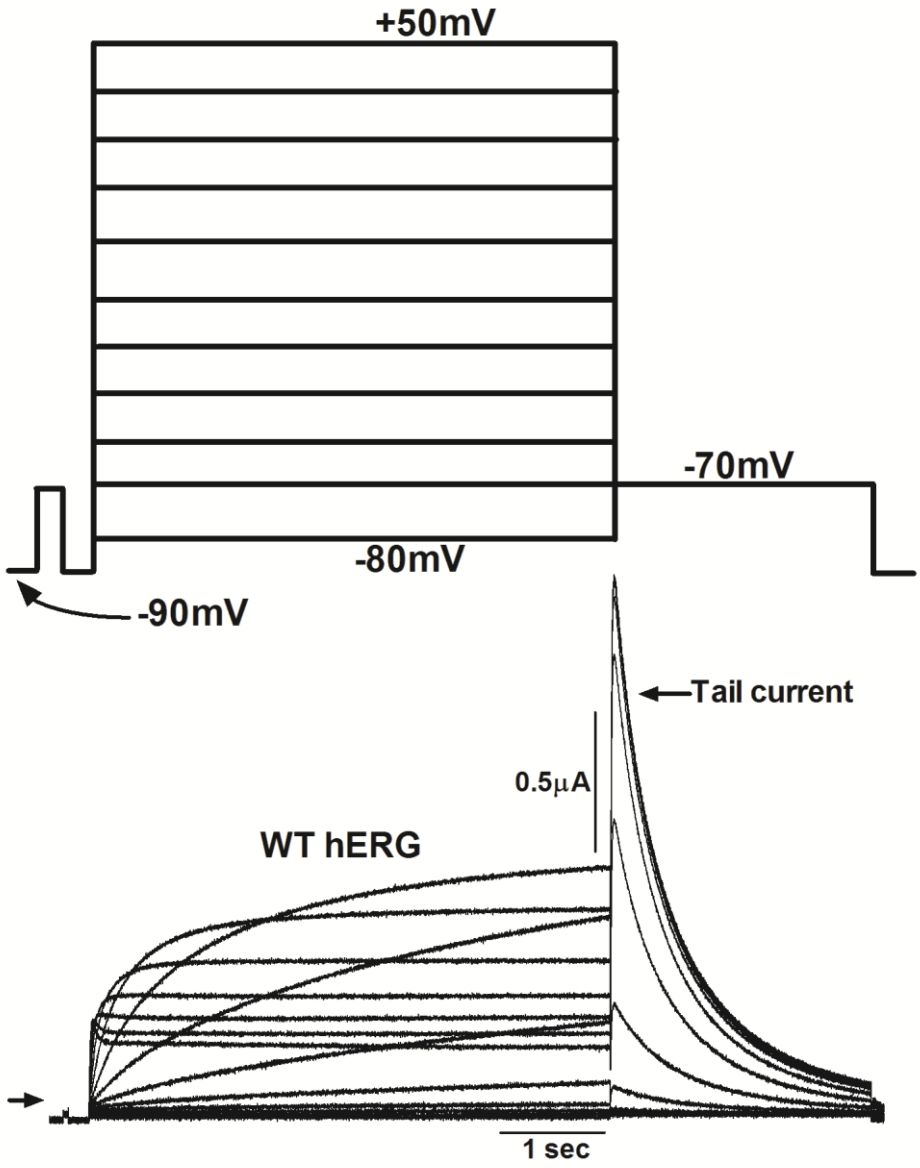

Figure 3.11. Current-voltage protocol used to determination the voltage dependence of activation.

The membrane potential was held at -90mV and stepped in 10mV increments from -80mV to +50mV for 5 seconds. Then membrane potential was then stepped down to -70mV for 2.5 seconds to elicit tail currents before returning to the holding potential. At the start of the protocol there was a short (50ms) pulse to -70mV to measure the leak and this value was subtracted from the peak tail current. The currents elicited using the voltage protocol are shown below it.

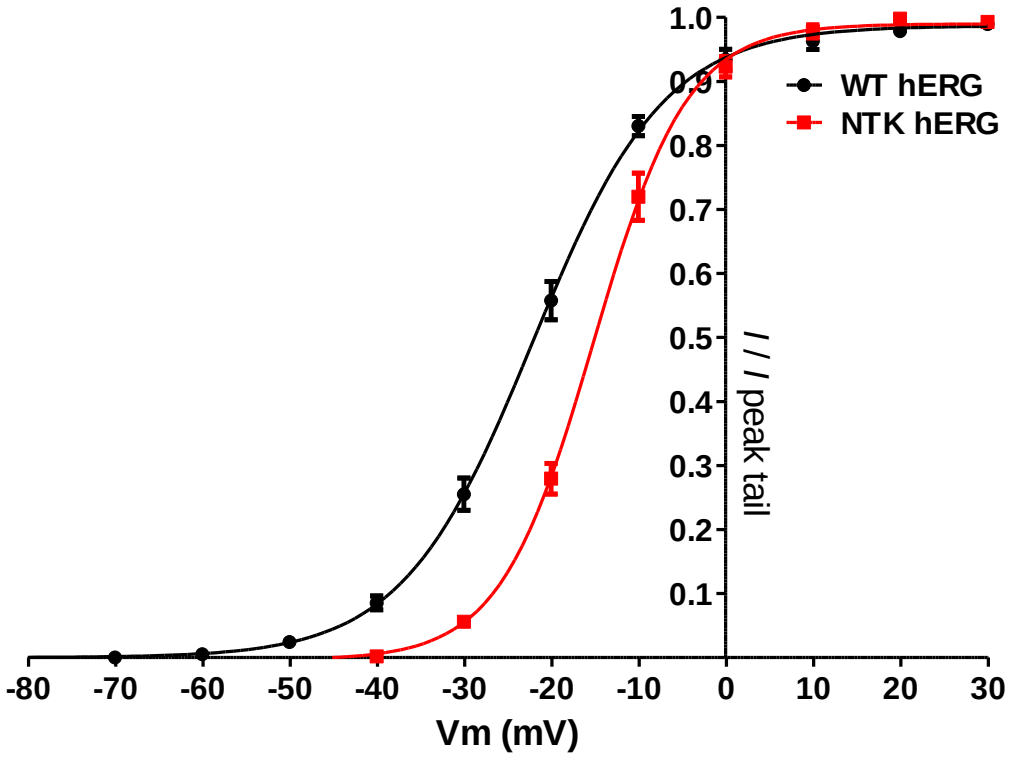

	$V_{0.5}$ of activation (mV)	Slope (mV)	n
Wild Type	-21.7 ± 0.8	7.7 ± 0.6	8
NTK hERG	-14.9 ± 0.8 ***	5.4 ± 0.3*	6

** $p < 0.01$

Figure 3.12. Activation curves for WT and NTK hERG.

Mean normalised peak tail currents plotted as a function of test potential then fitted with a Boltzmann function to give the voltage dependence of activation.

All of the mutations that removed the positive charge increased the rate of hERG channel deactivation (fig 3.13). The double mutant R4A:R5A had the fastest deactivation of all of the mutants (30.7 ± 1.7 ms at -70mV) and deactivated at a rate very close to NTK hERG (15.7 ± 0.9 ms at -70mV) compared to WT which deactivates at 564.1 ± 20.0 ms at -70mV (fig 3.13 & 3.14).

The other double alanine mutant R20A:K21A also deactivated quickly (86.7±9.7 ms at -70mV). The next fastest deactivating mutant was the single mutant H7A (153.2±10.0 ms at -70mV) followed by the other two single mutants R20A and K21A (236.5 ± 40 & 256.9 ± 5.3 ms at -70mV respectively) (fig 3.13 & 3.14).

Figure 3.15 shows the voltage dependence of activation of the above mutants. R4A:R5A has a threshold of activation around -40mV and it reaches maximum activation about +20mV. H7A has a threshold of activation around -50mV and reaches maximum activation about 0mV. R20A has an activation threshold about -60mV and reaches maximum activation about 20mV. K21A has a threshold of activation about -50mV and it reaches maximum activation about 20mV. The double mutant R20A:K21A has an activation threshold about -60mV and it reaches maximum activation about 30mV. The $V_{0.5}$ of activation of K21A and R20A:K21A is not significantly different from WT hERG. H7A and R20A have slight but statistically significant shifts in their $V_{0.5}$ of activation in a negative direction, whereas the $V_{0.5}$ of R4A:R5A is significantly shifted by 10mV to -11.7 ± 1.7mV from 21.7 ± 0.8mV in WT hERG.

As some mutants shift activation in a positive direction and some shift it in a negative direction while others have no effect, the increased rate of deactivation seen in these mutants cannot be explained by a shift in voltage dependence.

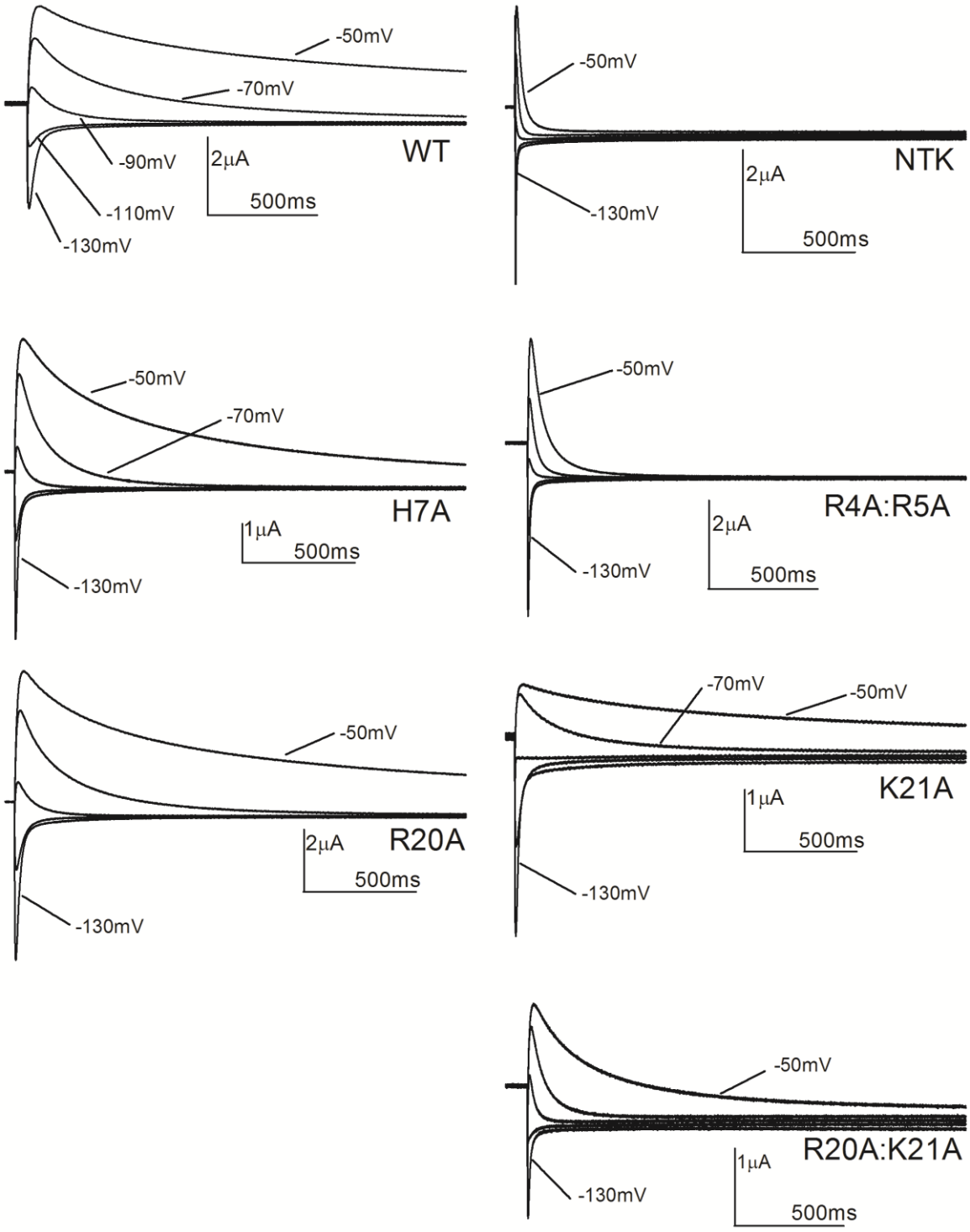

Figure 3.13. Family of current traces showing the rate of deactivation in charge neutralising mutants in NT 1-26. Currents were elicited using the FA I-V. NTK hERG deactivates very quickly, as do the double mutants R4A:R5A and R20A:K21A. H7A, R20A and K21A deactivate at a rate a half to a third of WT.

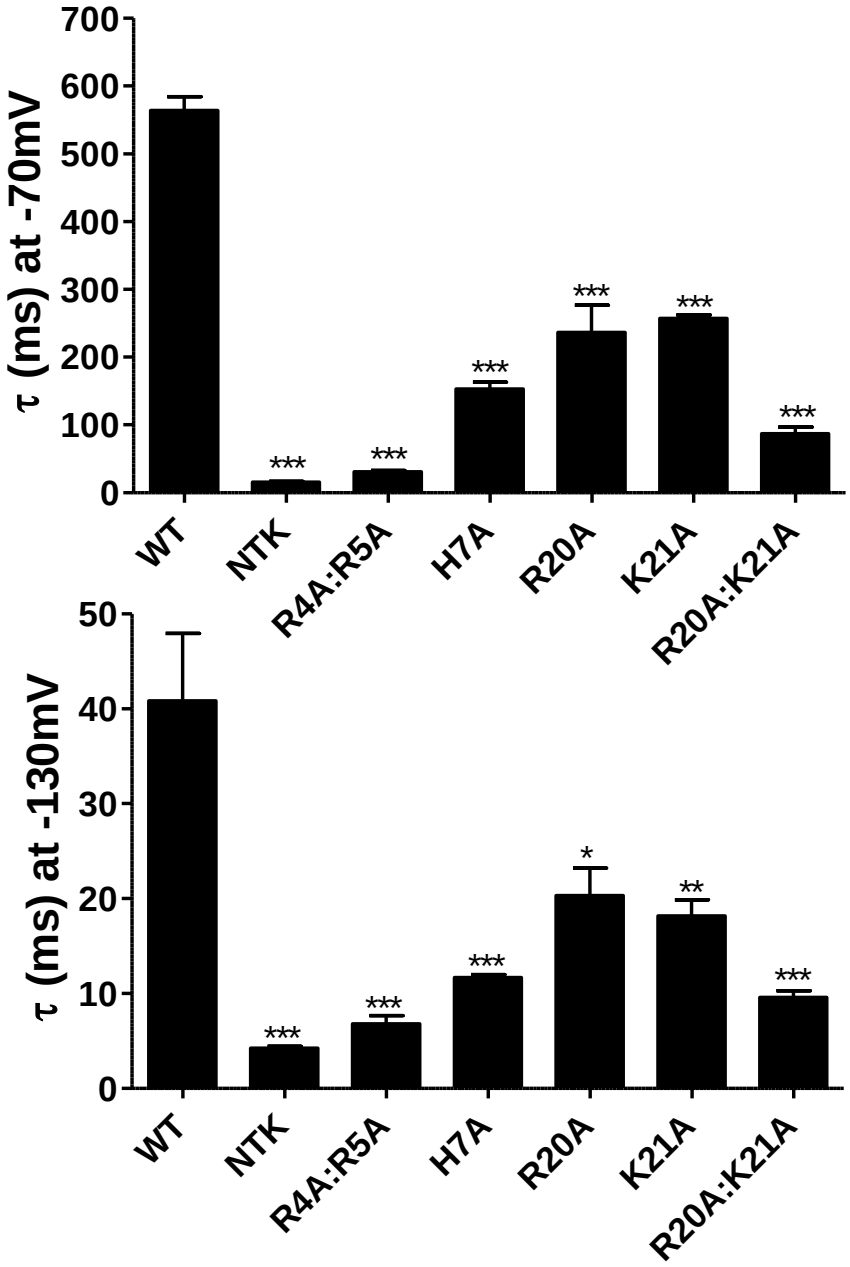

	τ (ms) -70mV	τ (ms) -130mV	n
WT hERG	564.1 ± 20.0	40.9 ± 7.1	8
NTK hERG	15.7 ± 0.9	4.2 ± 0.2	6
R4A:R5A	30.7 ± 1.7	6.7 ± 0.8	6
H7A	153.2 ± 10.0	11.7 ± 0.2	5
R20A	236.5 ± 40	20.3 ± 2.1	5
K21A	256.9 ± 5.3	18.1 ± 1.7	5
R20A:K21A	86.7 ± 9.7	9.6 ± 0.7	6

Figure 3.14. **Bar graph of time constants for charge neutralising mutants deactivation at -70mV and -130mV.** Time constants were derived from a single exponential fit of the decaying phase of the tail currents in fig 3.13.

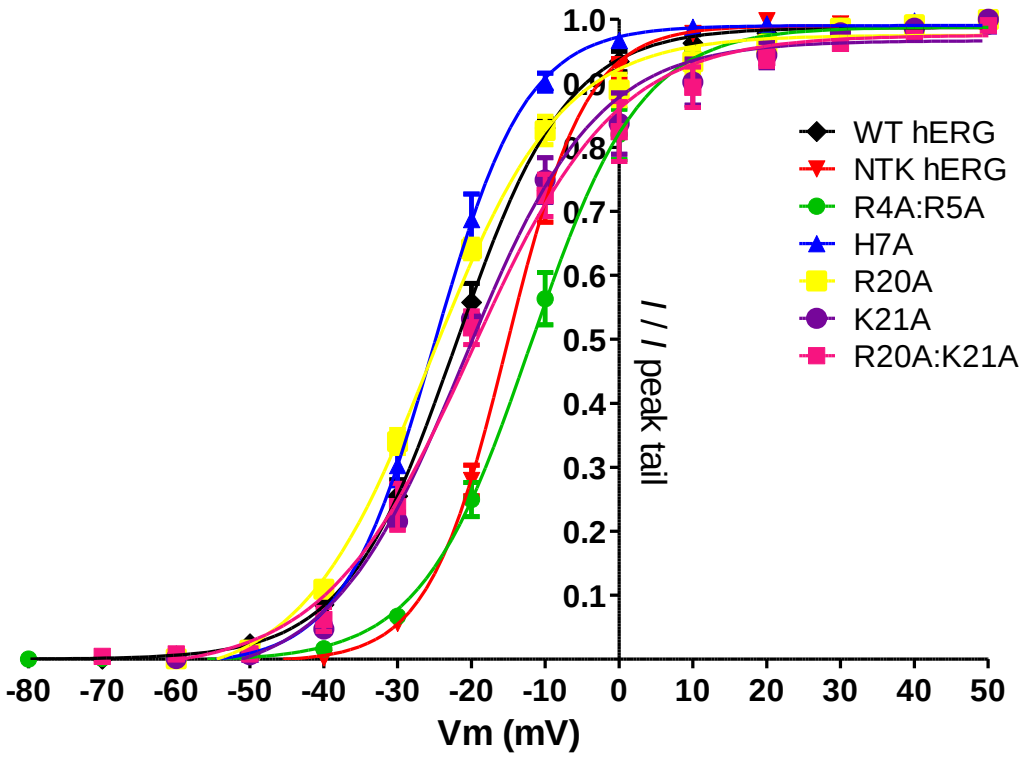

	$V_{0.5}$ of activation (mV)	Slope (mV)	n
Wild Type	-21.7 ± 0.8	7.7 ± 0.6	8
NTK hERG	-14.9 ± 0.8 ***	5.4 ± 0.3*	6
R4A:R5A	-11.7 ± 1.3***	7.5 ± 0.5	6
H7A	-26.5 ± 1.7*	5.9 ± 0.2*	5
R20A	-25.7 ± 0.7**	9.3 ± 1.1	5
K21A	-20.9 ± 0.3	10.0 ± 1.6	5
R20A:K21A	-20.0 ± 0.7	10.1 ± 1.6	6

Figure 3.15. Voltage dependence of activation charge neutralising mutants.

Activation curves for charge neutralising mutants in NT 1-26. Peak tail currents normalised to maximal tail current were plotted against membrane voltage and fitted with a Boltzmann function.

In order to confirm that the fast deactivation observed when the basic residues were mutated to alanine was as a result of the loss of the positive charge and not due to another property of the alanine side chain (e.g. smaller in size than arginine) residues 4 & 5 were mutated to leucine which is similar in size and branched like arginine but not charged. The double mutant R4L:R5L still deactivates much faster than WT hERG, with a time constant of 64.6±1.2 ms compared to 564.1±20.0 ms at -70mV (fig 3.17), confirming that it is the loss of the positive charge that is causing the increased rate of channel closure and not another property within the side chain of the residues at positions 4 and 5. The $V_{0.5}$ of activation for R4L:R5L was the same as R4A:R5A and significantly shifted compared to WT hERG (fig 3.19).

As well as the five basic residues in NT 1-26 there are two basic residues (Arg27 & Lys28) just outside NT 1-26 in the start of the PAS domain, figure 3.16. In order to ascertain if the influence of positive charge on slowing deactivation was limited to NT 1-26 or extended in to the PAS domain the two basic residues Arg27 and Lys28 were mutated to leucine, figure 3.18. Unlike removing the positive charge in NT 1-26, there was no affect of removing the positive charge in the start of the PAS domain and the mutant R27L:K28L deactivates at a similar rate to the wild type channel (fig 3.18).

Figure 3.16. Residues 1 to 34 of hERG. Amino acid sequence of NT 1-26 and the start of the PAS domain. Basic residues at the start of the PAS domain are highlighted in red.

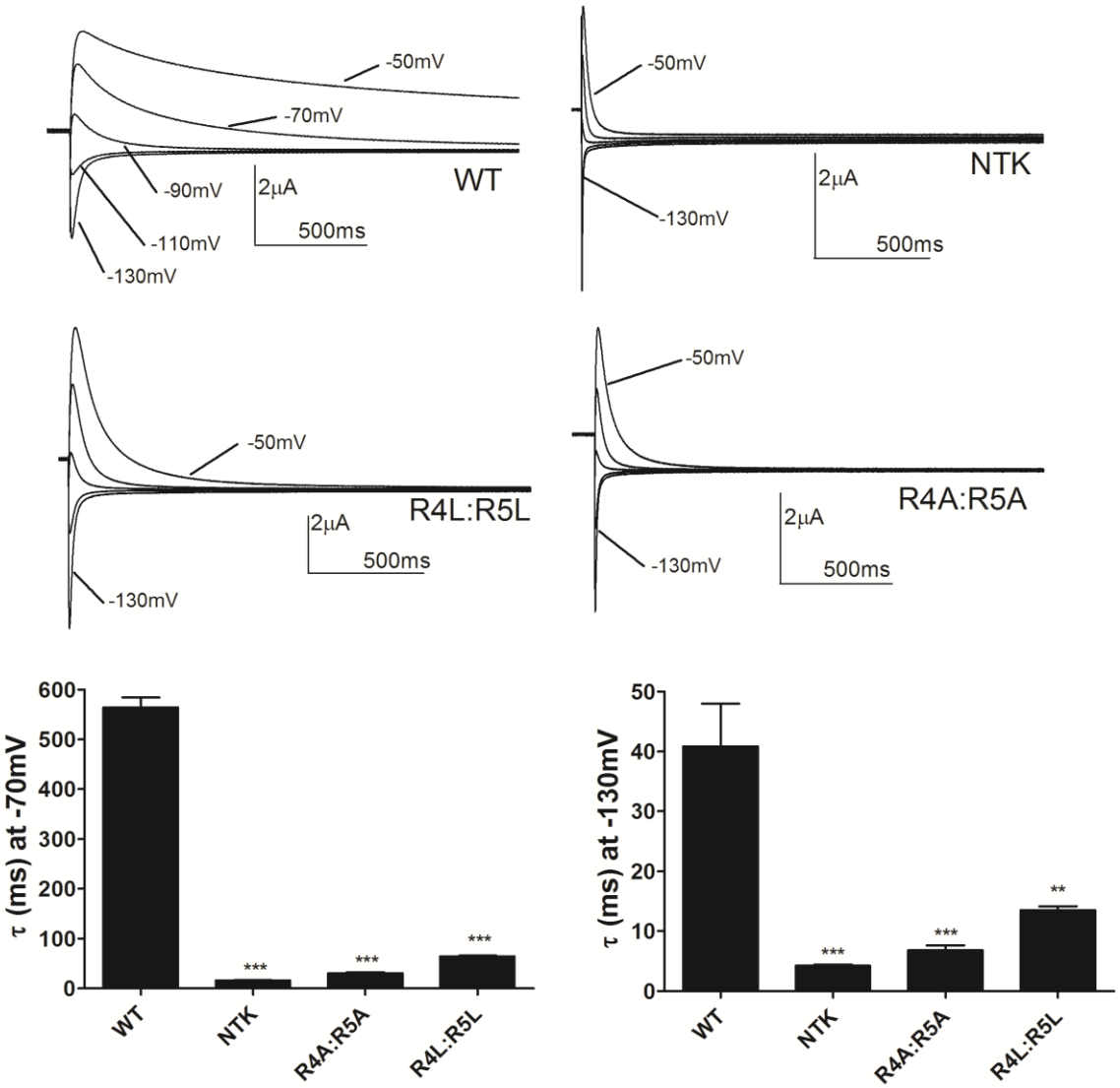

	τ (ms) -70mV	τ (ms) -130mV	n
WT hERG	564.1 ± 20.0	40.9 ± 7.1	8
NTK hERG	15.7 ± 0.9	4.2 ± 0.2	6
R4A:R5A	30.7 ± 1.7	6.7 ± 0.8	6
R4L:R5L	64.6 ± 1.2	13.5 ± 0.6	7

Figure 3.17. Family of current traces showing the rate of deactivation in charge neutralising mutants at positions 4 and 5.

Currents were elicited using the FA I-V. NTK hERG deactivates very quickly, as do the double mutants R4A:R5A and R4L:R5L.

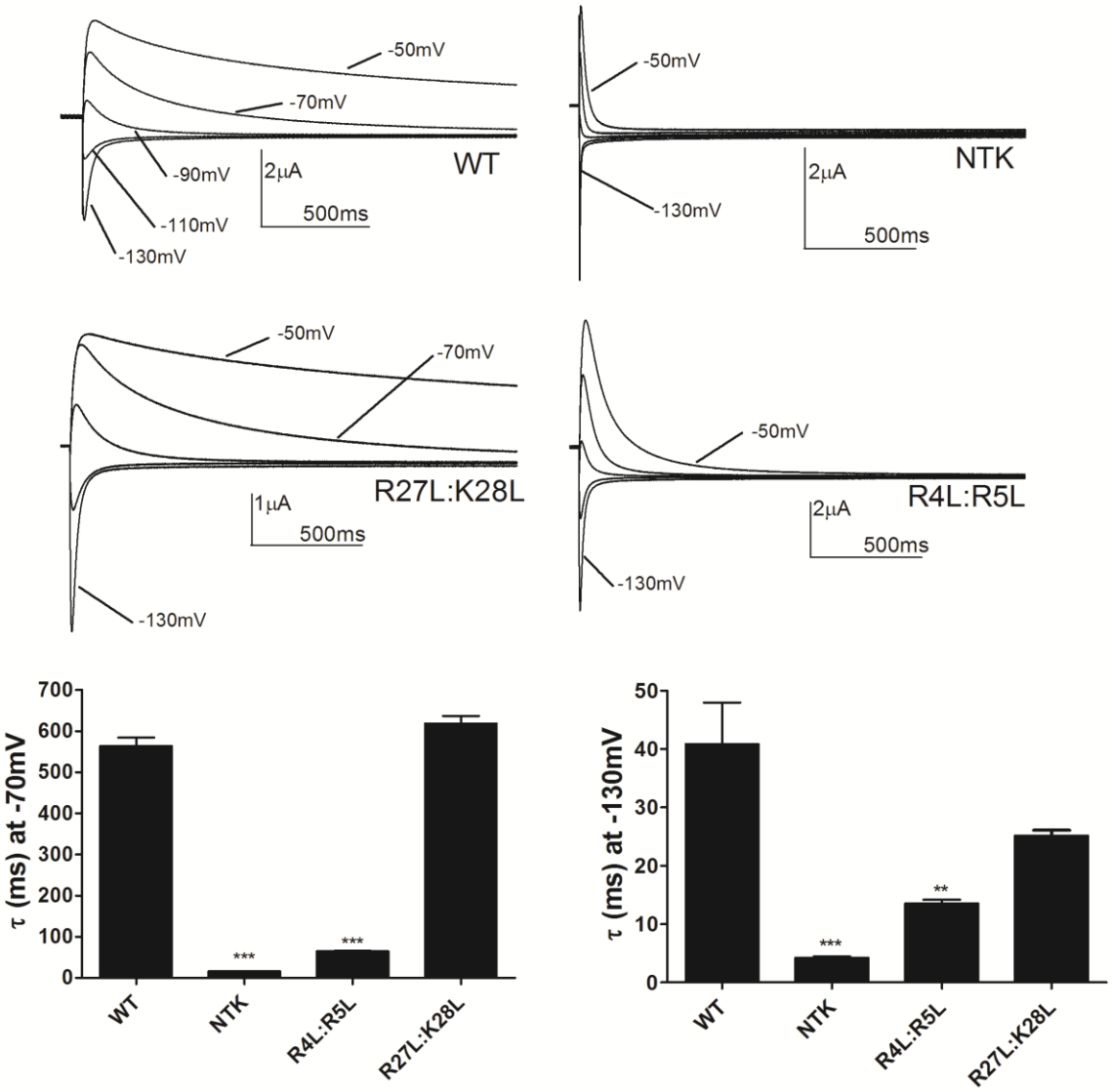

	τ (ms) -70mV	τ (ms) -130mV	n
WT hERG	564.1 ± 20.0	40.9 ± 7.1	8
NTK hERG	15.7 ± 0.9	4.2 ± 0.2	6
R4L:R5L	64.6 ± 1.2	13.5 ± 0.6	7
R27L:K28L	615.7 ± 20.6	26.2 ± 1.2	7

Figure 3.18. Family of current traces showing the rate of deactivation in charge neutralising mutants at positions 27 and 28. Currents were elicited using the FA I-V.R27L:K28L deactivates at a rate similar to WT hERG whereas R4L:R5L deactivates much faster than WT hERG.

The voltage dependence of activation of R4L:R5L and R27L:K28L was measured using the I-V protocol described above. Figure 3.19 shows the voltage dependence of activation for the mutants that removed the positive charge at positions 4 & 5 and at 27 & 28 by introducing a leucine. The $V_{0.5}$ of R27L:K28L is the same as WT hERG whereas R4L:R5L caused a significant shift in the voltage dependence of activation, moving it in a positive direction, similar to R4A:R5A and NTK hERG.

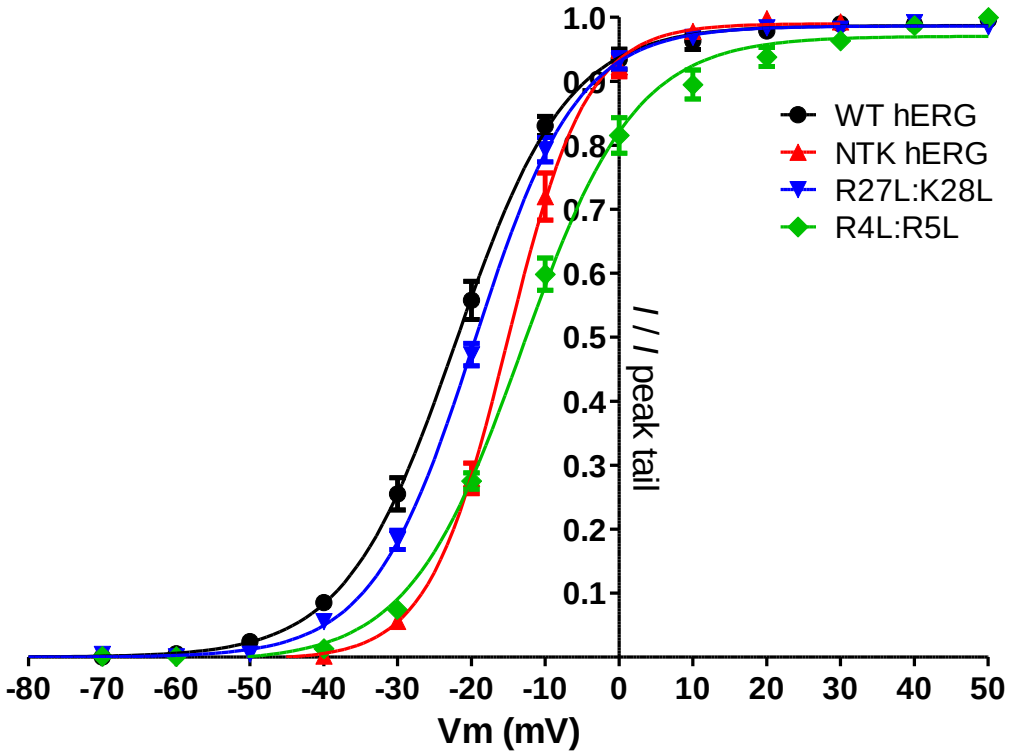

	$V_{0.5}$ of activation (mV)	Slope (mV)	n
Wild Type	-21.7 ± 0.8	7.7 ± 0.6	8
NTK hERG	-14.9 ± 0.8 ***	5.4 ± 0.3*	6
R27L:K28L	-19.6 ± 0.6	7.0 ± 0.2	7
R4L:R5L	-12.9 ± 0.8 ***	7.8 ± 0.6	7

Figure 3.19. Voltage dependence of activation of leucine mutants. Peak tail currents normalised to maximal tail current were plotted against membrane voltage and fitted with a Boltzmann function.

Affects of mutations in the amphipathic helix

Along with the NMR data revealing that one face of NT 1-26 is positively charged the data also revealed that NT 1-26 contains an amphipathic helix running from Glu11 to Gly24. In order to assess the role of the helix in deactivation gating the helix was disrupted by introducing a proline residue in two places on opposite sides of the helix, either at position Asp16 or Ile18, which are towards the middle of the helix. Proline residues are technically imino acids not amino acids. In proline residues the side chain attached to the α-carbon is not 'free' at the other end but joins with the nitrogen atom in what should be the amino group, creating a cyclic side chain. Because the nitrogen atom is bonded with the side chain group it is not able to maintain the hydrogen bond network required to keep the helical structure intact. The bulky nature of the cyclic side chain also sterically hinders the regular periodicity of the helix. Substituting proline at residue 18 accelerated deactivation to a rate similar to as if the whole of the N-terminus had been removed (τ was 42.5 ± 6.1ms compared to 564.1 ± 20ms for WT at -70mV) (fig 3.20). Substituting a proline on the other side of the helix at position 16 had the opposite effect on deactivation and slowed it (1499.7 ± 181.5ms compared to 564.1 ± 20ms for WT at -70mV) (fig 3.20).

Figure 3.21 shows the voltage dependence of activation for the proline mutants that break the helix at positions 16 and 18. Both D16P and I18P hERG caused a significant shift in the voltage dependence of activation moving it in a positive direction. It is worth noting that these two mutations have the opposite effects on deactivation, D16P slowed it while I18P accelerated it, but their voltage dependence of activation and slope were identical. The altered rates of deactivation seen in these mutants cannot be explained by any shift seen in the voltage dependence.

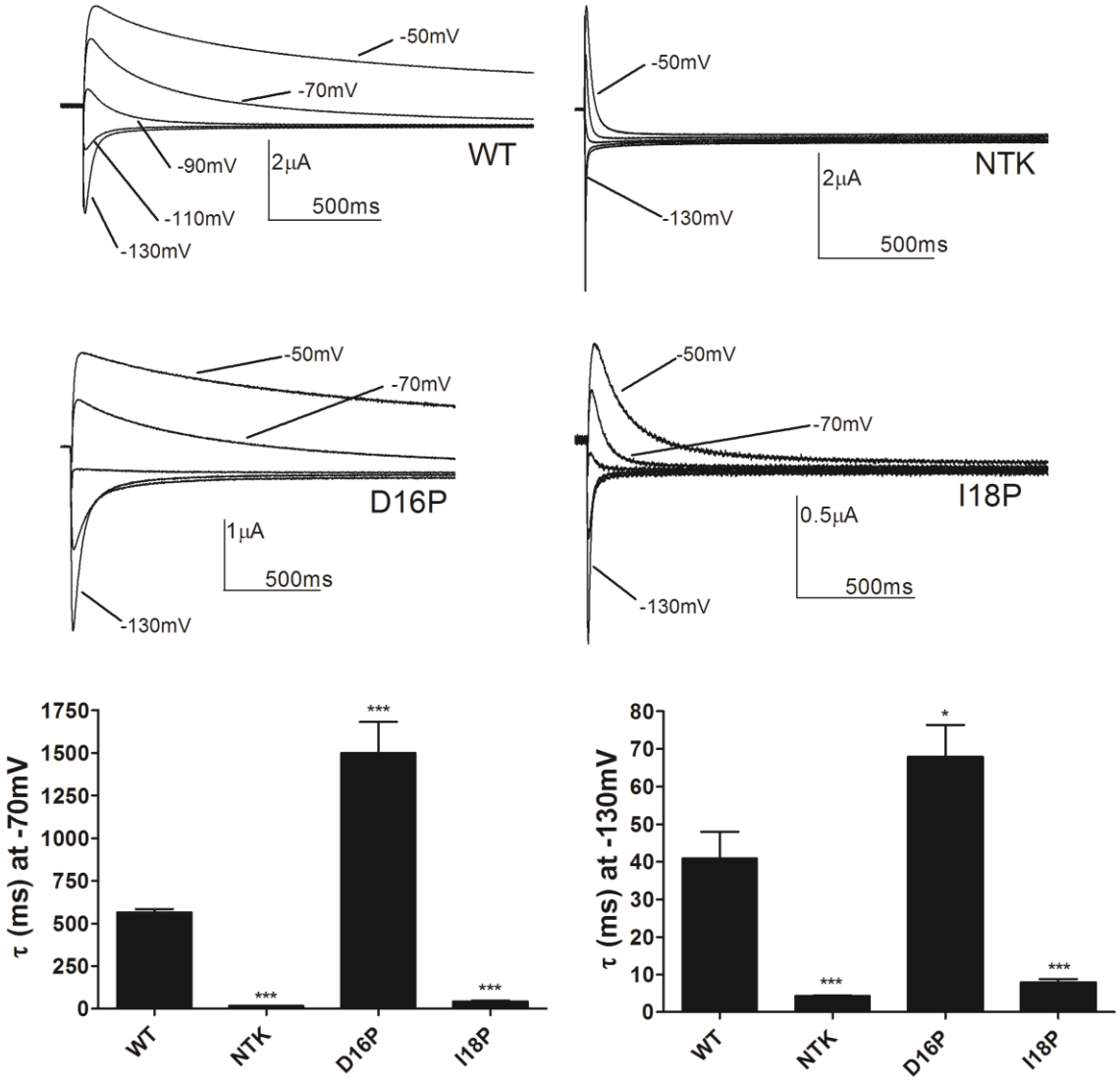

	τ (ms) -70mV	τ (ms) -130mV	n
WT hERG	564.1 ± 20.0	40.9 ± 7.1	8
NTK hERG	15.7 ± 0.9	4.2 ± 0.2	6
D16P	1499.7 ± 181.5	68.8 ± 7.7	5
I18P	42.5 ± 6.1	7.8 ± 0.9	9

Figure 3.20. Family of current traces showing the rate of deactivation in proline mutants that break the amphipathic helix. Currents were elicited using the FA I-V protocol. I18P deactivates very quickly whereas D16P deactivates slower than WT hERG. Bar graphs of time constants for deactivation for D16P and I18P hERG are shown below the current traces. Mean time constants were derived by fitting the decaying phase of tail currents with a single exponential function.

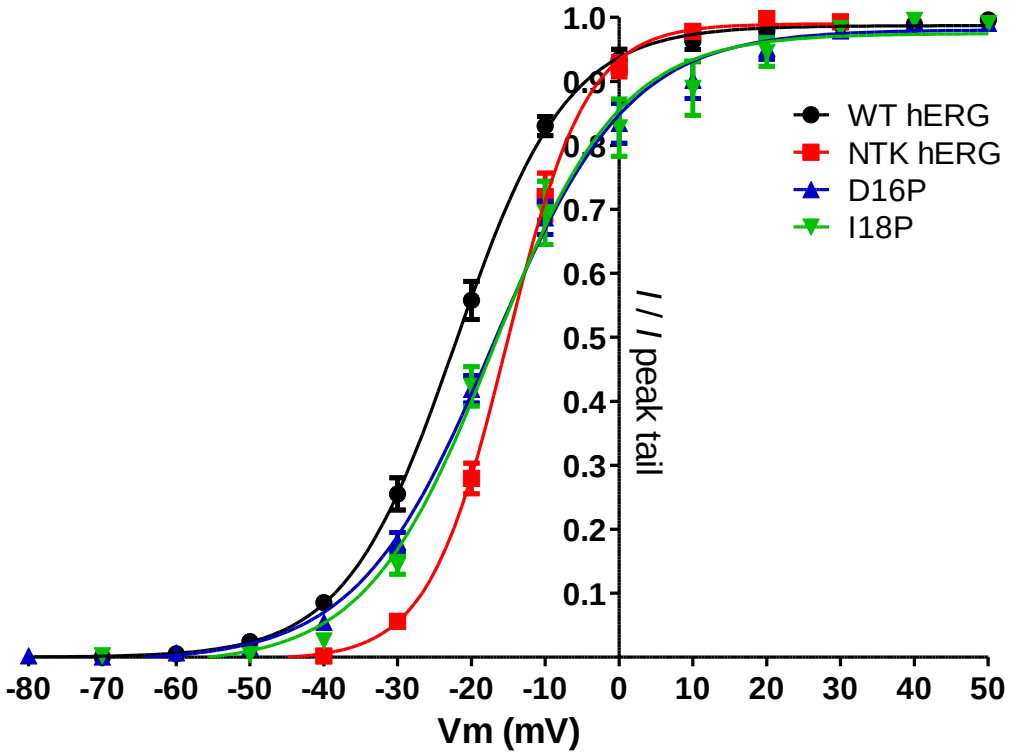

	$V_{0.5}$ of activation (mV)	Slope (mV)	n
Wild Type	-21.7 ± 0.8	7.7 ± 0.6	8
NTK hERG	-14.9 ± 0.8 ***	5.4 ± 0.3*	6
D16P	-16.9 ± 1.0 **	9.3 ± 0.6	5
I18P	-16.3 ± 1.6 **	9.0 ± 1.4	9

Figure 3.21. Voltage dependence of activation of proline mutants that break the helix. Peak tail currents normalised to maximal tail current were plotted against membrane voltage and fitted with a Boltzmann function.

Interaction of NT 1-26 with the C-terminus cNBD to regulate deactivation.

It is clear that the eag domain and NT 1-26 region have a receptor site somewhere on the hERG channel. When purified eag domain protein was injected into a cell expressing NTK hERG it restored slow deactivation and when patches were excised from the membrane the slow deactivation remained suggesting that the eag domain was tightly bound to the channel (Morais-Cabral et al, 1998). Wang et al, 2000 showed that when a peptide fragment of the first 16 residues were applied to the intracellular side of the N-truncated channel that it would restore normal deactivation gating but in contrast this effect was washed off when a patch was excised containing indicating that the peptide fragment was rapidly associating and disassociating with a receptor site somewhere on the channel. One face of NT 1-26 is positively charged and this charge is important for normal deactivation gating. It was hypothesised that the basic residues in NT 1-26 could be interacting with acidic residues somewhere in the channel to stabilise the open state and regulate deactivation. One region of hERG that stands out as being rich in acidic amino acids is the cyclic Nucleotide Binding Domain (cNBD) in the intracellular C-terminus.

Fig.3.22 shows an electrostatic surface of a homology model of the hERG channel cNBD and C-linker based on the crystal structure of HCN2 channel cNBD (Zagotta et al, 2003). The model shows four large acidic patches on or close to the C-helix of the cNBD, in a region symmetrically orientated around the central pore of the cNBD, and on the surface facing away from the membrane and presumed to be largely exposed to the cytoplasm. We hypothesised that these negatively charged regions could form the interaction site for the NT 1-26 domains with a 1:1 stoichimetry.

These acidic patches were due to a high density of Glu and Asp residues at positions 843, 847, 850, 857 and 864, on the cNBD C-helix. Within the central cNBD pore are a further group of acidic residues at positions 840, 836 and 837. Acidic residues were systematically mutated to Lys or Ala and the effects on deactivation was measured as previously described.

Figure 3.23 shows representative current traces of 14 cNBD mutants used to investigate the role of the cNBD in deactivation gating. All of the mutations significantly accelerated deactivation (the only exception was D864K and only at -70mV, which slowed deactivation) with E847K and E857K and the double mutant E847A:E857A having the most pronounced effects on deactivation (figures 3.23, 3.24 and 3.25).

The voltage dependence of activation of the cNBD mutants is shown in figure 3.25. Some cNBD mutants are slightly right shifted, some are left shifted and some are unchanged, see figure 3.25. Changes to the voltage dependence of activation do not correlate with changes to the rate of deactivation and thus any changes to the voltage dependence of activation do not explain the changes to the rate of deactivation.

These result suggest that alterations to the electrostatic surface of the cNBD accelerate deactivation in a manner that is consistent with a charge-charge interaction with the NT 1-26 domain

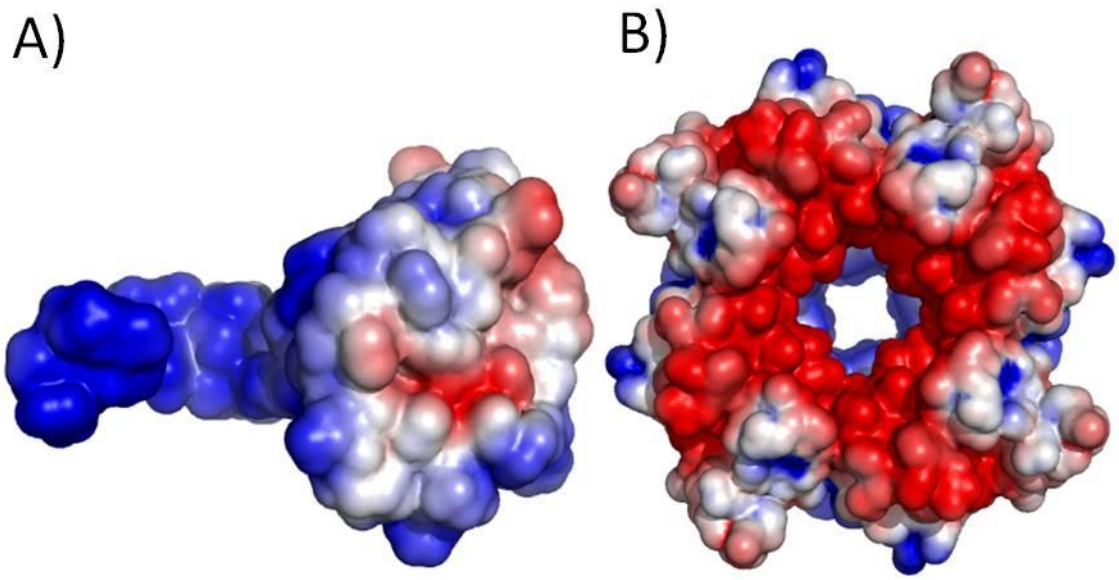

Figure 3.22.Rendering of surface charge on the EAG domain and homology model of cNBD.

A) One side of NT 1-26 in EAG domain is positively charged (blue). Only one of four channel subunits of the N-terminus EAG domain is shown.

B) Homology model of hERG cNBD based on the HCN2 cNBD structure by Zagotta *et al,* 2003. There is a lot of negative charge in the cNBD (red). All four subunits of the cNBD are shown.

Images A & B are not on the same scale.

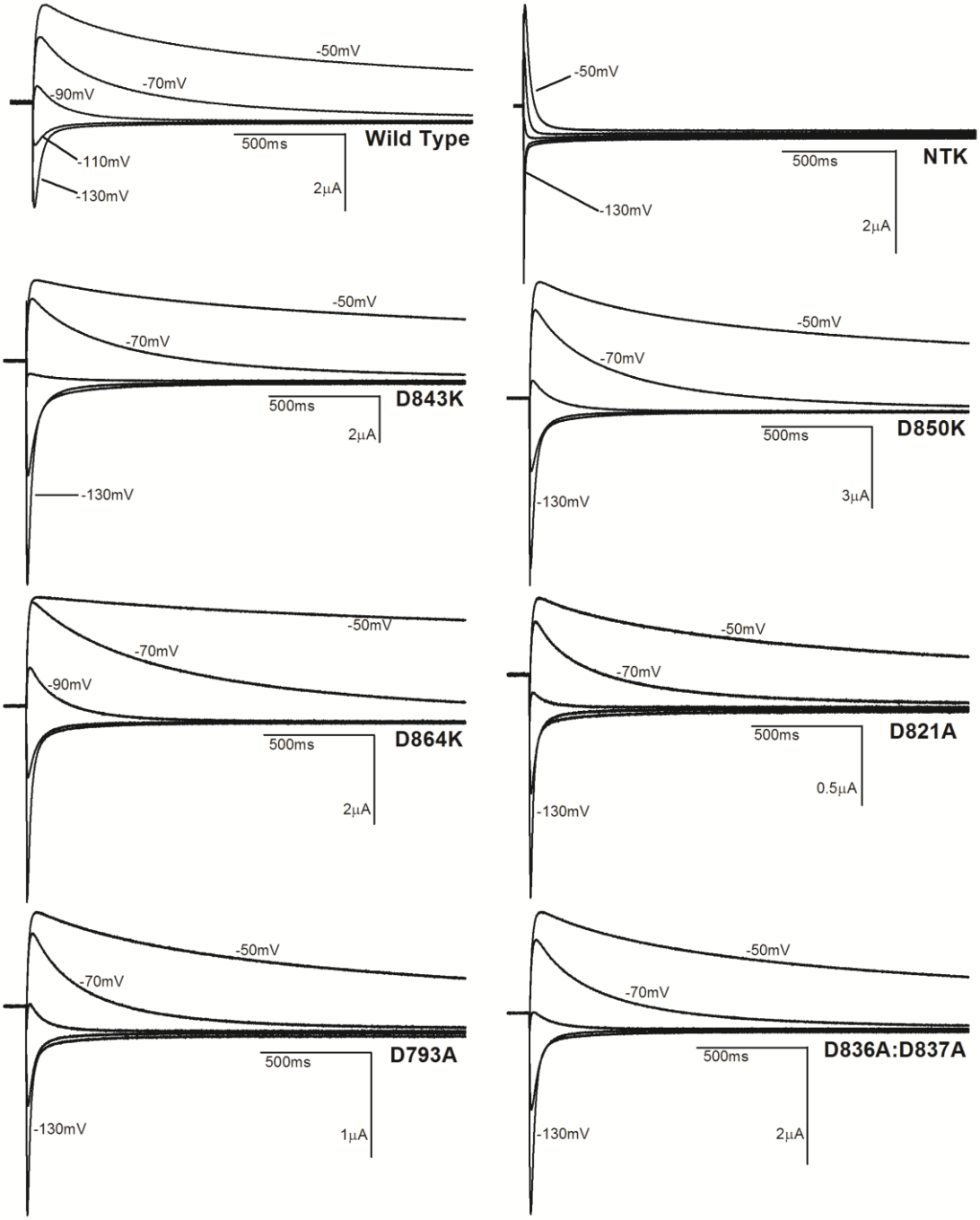

Figure 3.23. Family of current traces showing the deactivation in charge neutralisation or charge reversal mutants in the cNBD in the C-terminal if hERG. All the mutants deactivate faster than wild type hERG apart from D864K and only at -70mV. Currents were elicited using the FA I-V described previously.

Figure continued →

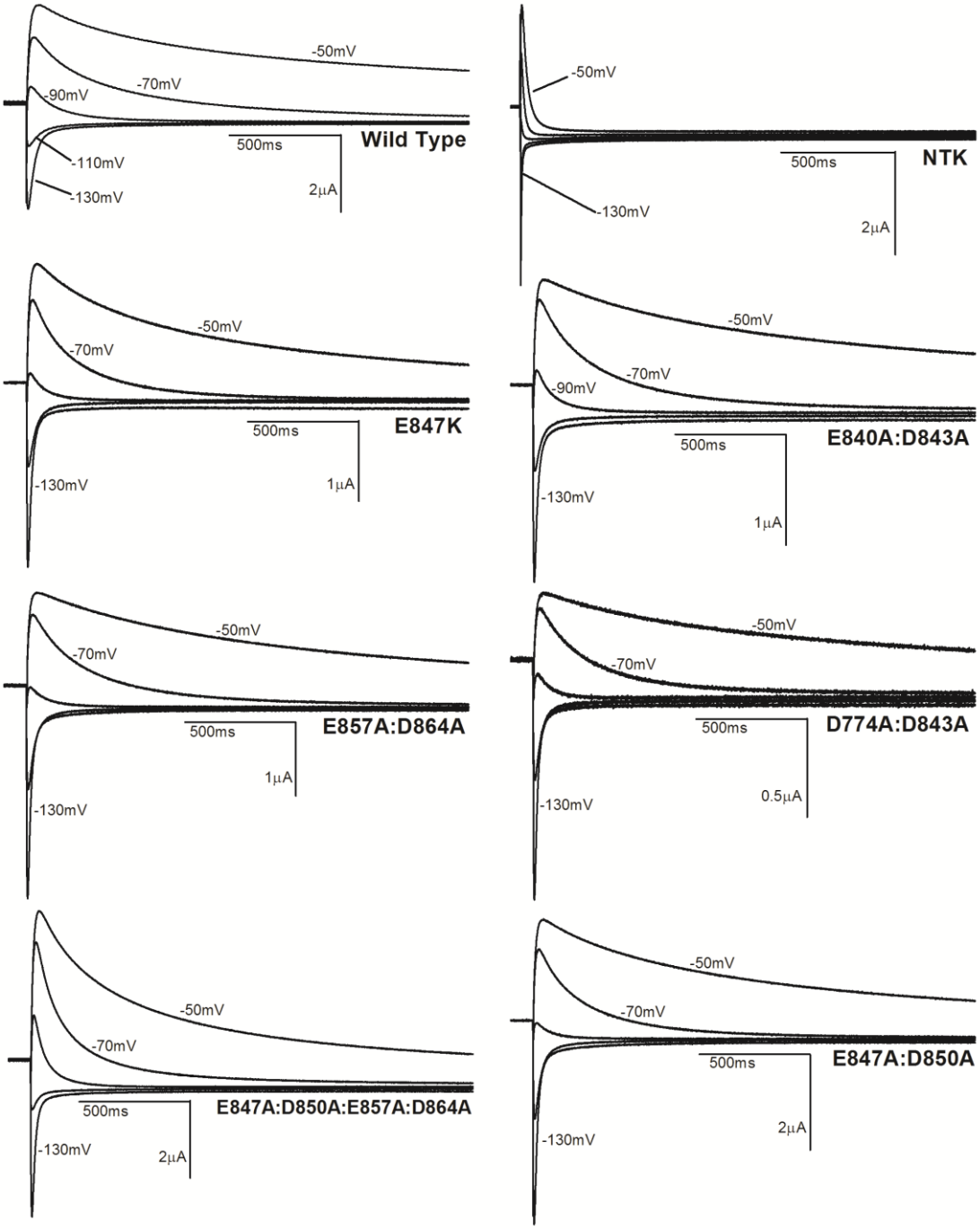

Figure 3.23 (continued). Family of current traces showing the deactivation in charge neutralisation or charge reversal mutants in the cNBD in the C-terminal if hERG.

Figure continued →

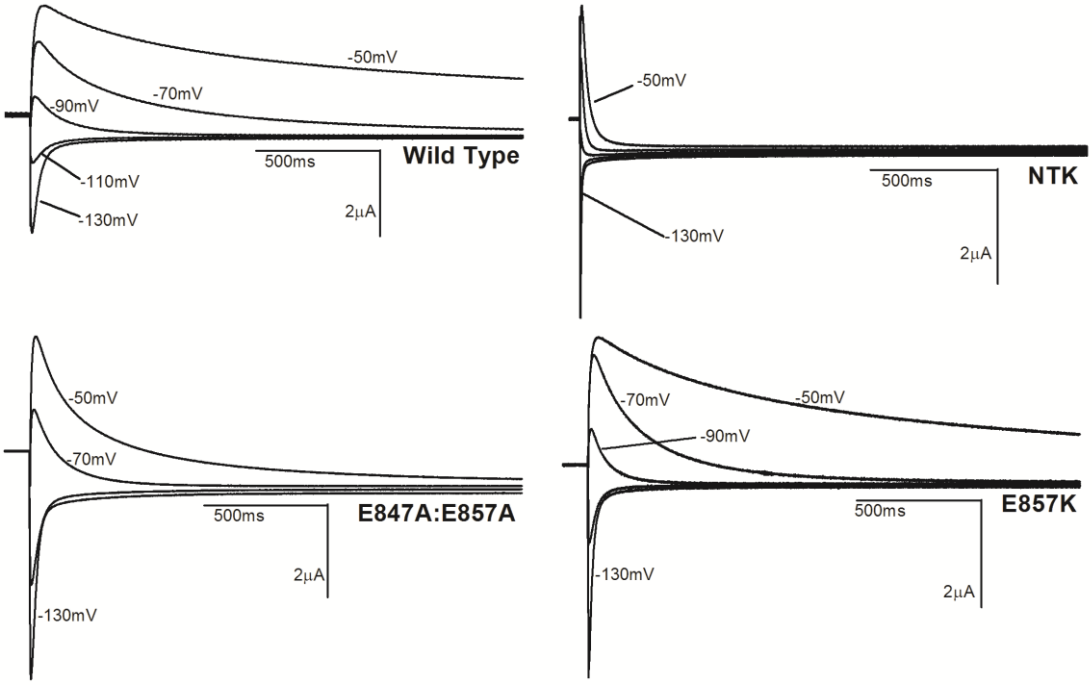

Figure 3.23 (continued). Family of current traces showing the deactivation in charge neutralisation or charge reversal mutants in the cNBD in the C-terminal if hERG.

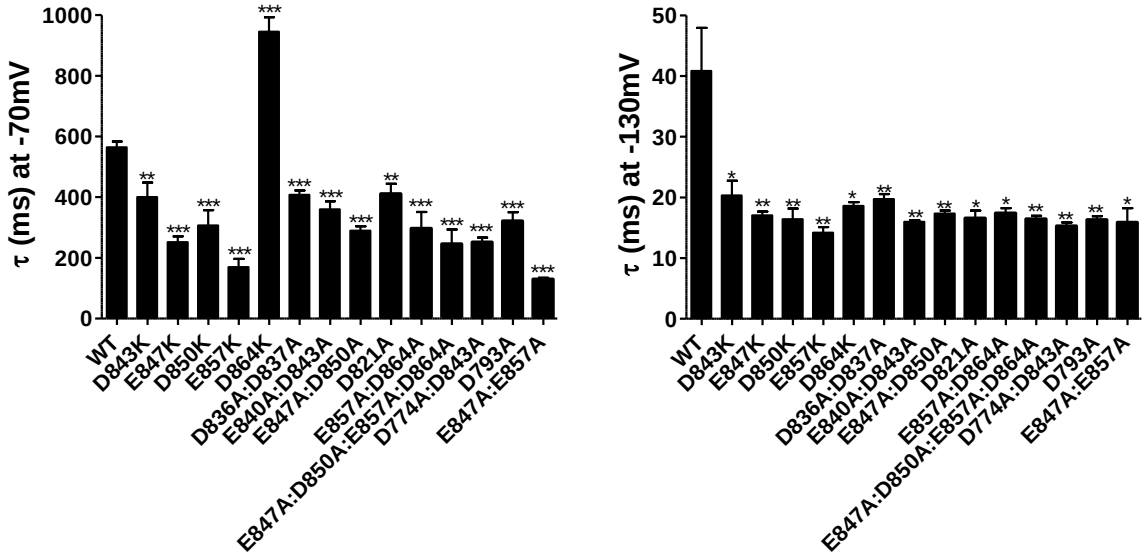

	τ (ms) -70mV	τ (ms) -130mV	n
WT hERG	564.1 ± 20.0	40.9 ± 7.1	8
D843K	400.3 ± 32.1	20.3 ± 2.6	5
E847K	251.8 ± 25.4	17.0 ± 0.6	7
D850K	306.9 ± 33.1	16.4 ±1.7	5
E857K	169.4 ± 27.3	14.1 ± 0.9	6
D864K	945.0 ± 48.2	18.6 ± 0.6	6
D836A:D837A	408.1 ± 18.6	19.7 ± 0.8	9
E840A:D843A	360.4 ± 20.7	15.9 ± 0.4	7
E847A:D850A	289.7 ± 17.6	17.3 ± 0.5	8
D821A	411.0 ± 20.3	16.5 ± 1.0	6
E857A:D864A	296.7 ± 35.6	17.4 ± 1.0	7
E847A:D850A:E857A:D864A	246.0 ± 36.4	15.9 ± 0.6	7
D774A:D843A	252.0 ± 12.1	14.6 ± 0.5	5
D793A	321.8 ± 15.6	15.6 ± 0.4	5
E847A:E857A	129.5 ± 10.3	15.8 ± 2.9	6

Figure 3.24. Bar graph of time constants for deactivation for mutations that remove negative charge in the cNBD. All mutations increase the rate of deactivation apart from D864K and only at -70mV. Mean time constants were derived by fitting the decaying phase of tail currents with a single exponential function.

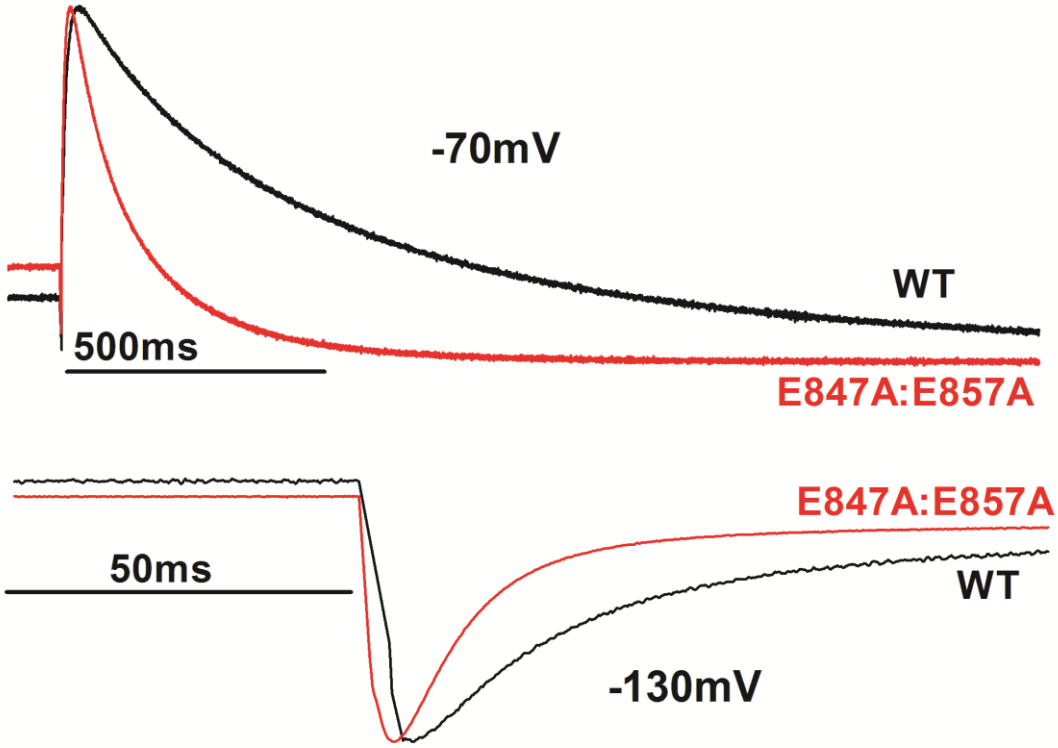

Figure 3.25. Normalised representative current traces of deactivation in WT hERG and E847A:E857A. Of all the mutations in the cNBD the double mutant E847A:E857A deactivated the fastest. Currents have been normalised to the peak tail current at -70mV and -130mV. WT hEGR (black), E847A:E857A (red).

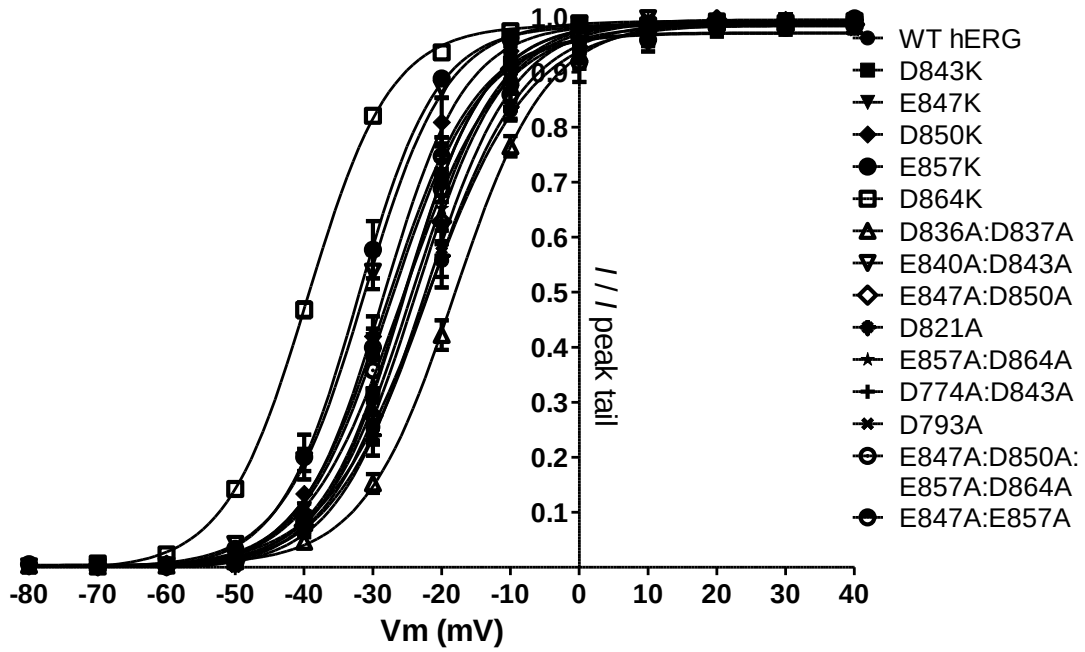

	$V_{0.5}$ of activation (mV)	Slope (mV)	n
WT hERG	-21.7 ± 0.8	7.7 ± 0.6	8
D843K	-25.5 ± 1.4*	6.0 ± 1.0	5
E847K	-27.9 ± 0.9**	6.4 ± 0.6	7
D850K	-28.4 ± 1.3**	5.9 ± 1.3	5
E857K	-32.1 ± 1.0***	5.6 ± 0.5*	6
D864K	-39.5 ± 0.2***	6.0 ± 0.2*	6
D836A:D837A	-18.1 ± 0.9**	6.7 ± 0.7	9
E840A:D843A	-31.2 ± 0.5***	6.0 ± 0.8*	7
E847A:D850A	-23.7 ± 1.2	6.3 ± 0.6*	8
D821A	-22.0 ± 0.5	7.0 ± 0.4	6
E857A:D864A	-24.3 ± 1.4*	6.4 ± 0.4*	7
E847A:D850A:E857A:D864A	-25.7 ± 1.1*	7.0 ± 0.6	7
D774A:D843A	-25.4 ± 1.3*	6.0 ± 0.7*	4
D793A	-22.5 ± 1.2	6.5 ± 0.6	5
E847A:E857A	-27.4 ± 0.9**	6.5 ± 0.6	6

Figure 3.26. Voltage dependence of activation of cNBD mutants. Peak tail currents normalised to maximal tail current were plotted against membrane voltage and fitted with a Boltzmann function.

Effect of removing the N-terminus on inactivation gating

When removing the N-terminus was found to accelerate deactivation gating it was also found to shift the voltage dependence of inactivation in a positive direction (Wang et al, 1998). Having established that replacing the basic residues in NT 1-26 with alanines mimics the effects of fast deactivation seen when the whole of the N-terminus is removed, the effect of the NT 1-26 mutants were investigated on the voltage dependence of inactivation.

To investigate the voltage dependence of inactivation a triple pulse protocol was used. Inactivation gating in hERG is a fast form of C-type inactivation and activation and deactivation gating are slow by comparison. The membrane potential was held at -90mV and stepped to +70mV for 1 second to activate and inactivate the current. The membrane potential was then very briefly stepped to a range of voltages from -150mV to +70mV in 10mV increments for 10ms and then back up to +70mV for 1 second before returning to the holding potential (fig 3.27).

On the first step to +70mV the channel rapidly inactivates before it can fully activate thus there is little current passed at this point. The very short middle pulse to the test potentials allows the current to rapidly recover from inactivation but because this pulse is only 10ms in duration there is little deactivation, so at the end of the 10ms step the channels are in an open, conducting state so when the cell is stepped back up to +70mV the channel passes a robust current because the slow activation has been removed from the equation. The decay in the current after the second step to +70mV is the onset of inactivation. The current was measured 5 to 9 ms after the second step to +70mV depending on individual cell capacitance and current levels.

WT hERG current begins to inactivate at around -130mV to -120mV and reaches 90% inactivation at around -50mV and continues to inactive gradually reaching maximum inactivation at +30mV (fig 3.28). The $V_{0.5}$ of inactivation for WT hERG was -90.5 ± 0.5mV. H7A, R20A:K21A and D16P all have virtually identical voltage dependences of inactivation as WT hERG (fig 3.28). On the other hand NTK hERG current begins to inactive around -50mV and reaches maximum inactivation about +50mV with a $V_{0.5}$ of -27.6 ± 0.6mV. R4A:R5A begins to inactivate between -100mV and -90mV and reaches maximum inactivation about +10mV with a $V_{0.5}$ of -65.3 ± 0.6mV. I18P starts to inactivate between -90mV and -80mV and reaches maximum inactivation about +10mV with a $V_{0.5}$ of -54.6 ± 0.6mV (fig 3.31). Thus, removing the N-terminus results in an approximately 60mV positive shift in $V_{0.5}$ whereas the point mutations R4A:R5A and I18P shift the $V_{0.5}$ about 30mV, about half that of NTK hERG. The other mutants had no effect. These results indicate that specific mutations have differential effects on deactivation and inactivation gating of hERG channel.

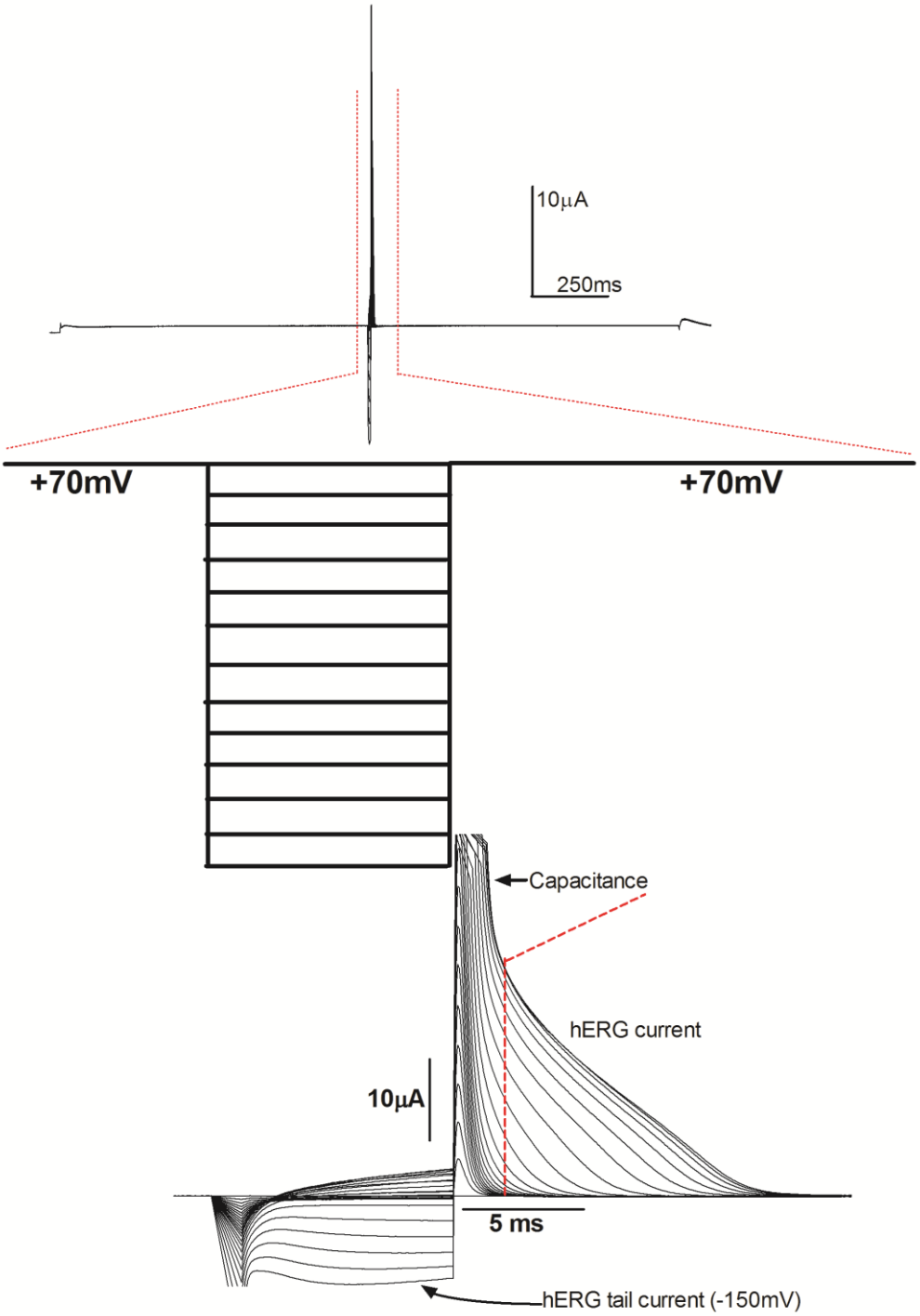

Figure 3.27. Triple pulse voltage protocol used to study the voltage dependence of inactivation. The membrane potential was held at -90mV and then stepped to +70mV for 1 second to fully activate and inactivate the current. The membrane potential was then stepped down to a range of potentials from +70mV to -150mV in 10mV intervals for 10ms. The membrane potential was then stepped back to +70mV for 1 second before stepping back to the -90mV holding potential. The top current trace shows a macro-scale current of WT hERG elicited using the protocol. The bottom current trace is a close-up view of the 10ms step to the test potential and the currents elicited on stepping back to +70mV.

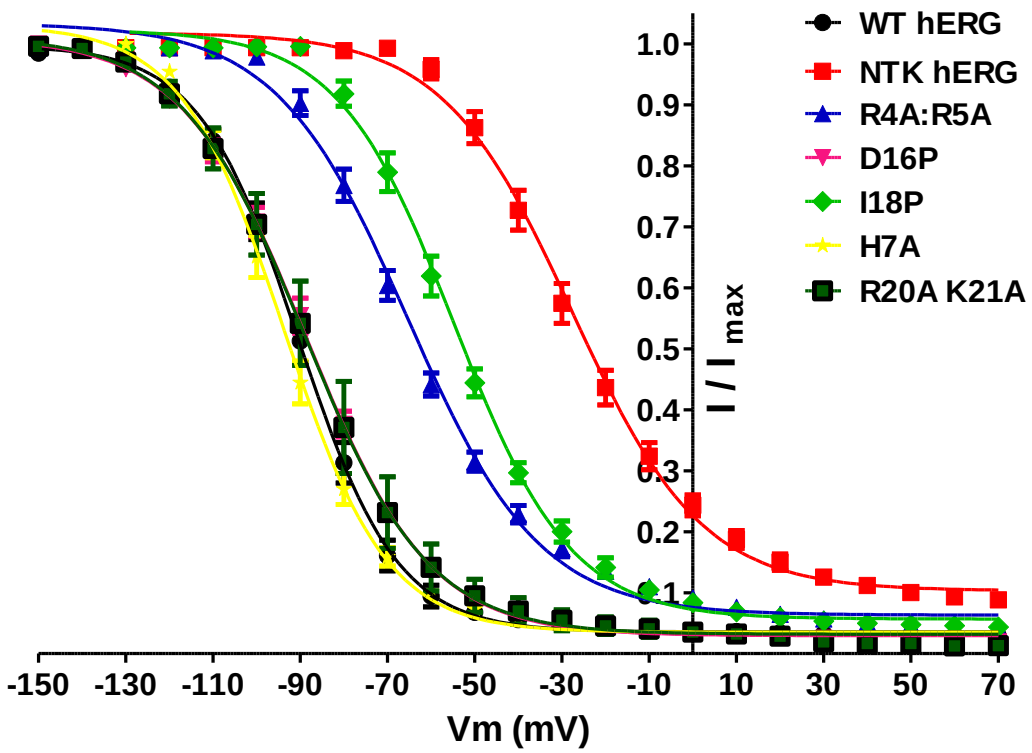

	$V_{0.5}$ of inactivation (mV)	Slope (mV)	n
Wild Type	-90.9 ± 1.7	11.6 ± 0.7	10
NTK	-27.0 ± 1.7 ***	16.3 ± 0.7***	9
R4A:R5A	-66.0 ± 2.6 ***	15.2 ± 1.0*	9
H7A	-93.5 ± 2.6	11.8 ± 0.5	5
D16P	-88.9 ± 1.6	14.1 ± 0.7*	7
I18P	-54.8 ± 1.4 ***	13.5 ± 1.0	5
R20A:K21A	-89.0 ± 4.0	13.1 ± 1.0	6

Figure 3.28. Truncating the N-terminus shifts the voltage dependence of inactivation in a positive direction. Currents at the second step to +70mV were normalised to maximal current at +70mV and were plotted against membrane voltage and fitted with a Boltzmann function (n = 5-9).

Modelling of the NT 1-26 and cNBD complex

Molecular dynamics simulation carried out by Dr Phil Stansfeild, a collaborator at Oxford University, suggested that NT 1-26 may be interacting with a region in the cNBD called the C-helix. Residues Glu847 and Glu857 lie along the C-helix and mutating these residues produces the fastest deactivating channels in this study which supports the modelling data. Also thought to be located on the C-helix are residues 843 and 850. When these residues were mutated there was less of any effect on deactivation than Glu847 and Glu857 but they still deactivated faster than WT hERG. The homology model of the hERG cNBD was based on the crystal structure of the HCN2 cNBD (Zagotta et al, 2003).

Figure 3.29 shows a model of the interaction between NT 1-26 and cNBD. The lables point to the disordered residues 1-10 (a), the helix running from residues 11 to 24 in NT 1-26 (b) and the PAS domain (c). Figure 3.29A shows the eag domain (green) and the cNBD (red). All four of the subunits that make up the channel are shown. The purple patches on the red cNBD are residues 843, 847, 850 and 857.

Pannel B of Fig 3.29 is an expanded view of part of modelled complex showing interactions of one eag domain (green) with two cNBDs (red). The C-linker is not shown. The NT1-26 amphipathic helix (labeled b as above) sits in a cleft at the interface of two adjacent cNBDs. The unstructured Met1-Pro10 region (labled a) interacts with the C-helix of one of the cNBDs.

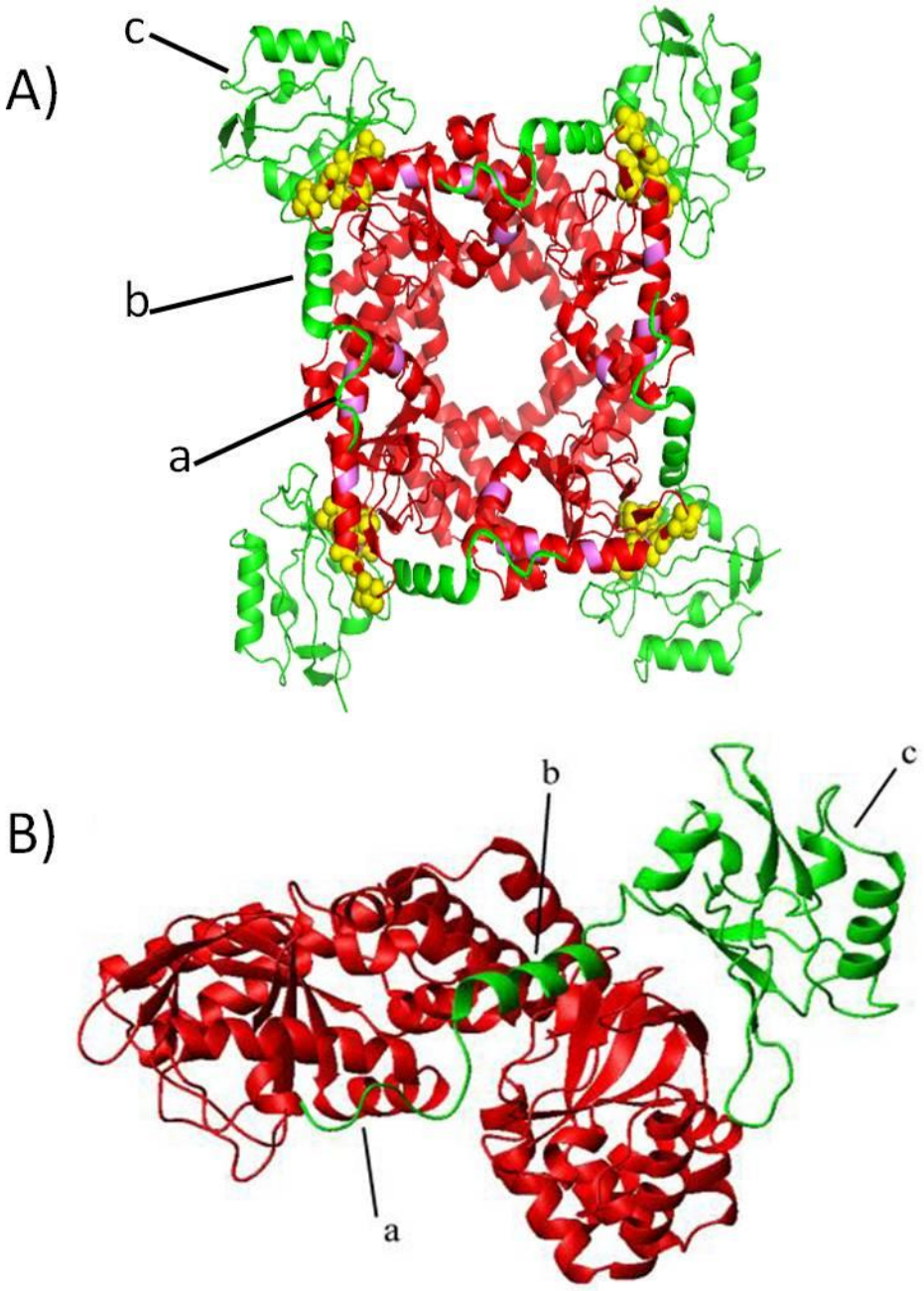

Figure 3.29. Model of the interaction between NT 1-26 and cNBD. A) Modelled complex of the eag domain (green) and the cNBD & C-linker. Four molecules of the eag domain interact with the tetrameric cNBD. Label (a) is the unstructured Met1-Pro10 region, (b) the amphipathic helix (Gln11-Gly24), and (c) the PAS domain.
B) Expanded view of part of modelled complex showing interactions of one eag domain (green) with two cNBDs (red). The C-linker is not shown. The NT1-26 amphipathic helix (b) sits in a cleft at the interface of two adjacent cNBDs. The unstructured Met1-Pro10 region interacts with the C-helix of one of the cNBDs.

Discussion

Structure of the NT 1-26 deactivation domain

Presented here are novel insights into the structure and function of the first 26 residues of the N-terminus which are known to be critical for the slow deactivation gating in hERG. The NMR structure shows that residues 1 – 10 are disordered and residues 11 to 24 form an amphipathic α-helix. The structure of the region of the PAS domain (residues 26 to 135) from our NMR data are in excellent agreement with the previously published crystal structure (Morais Cabral et al, 1998). One face of NT 1-26 is positively charged and the other face is neutral/hydrophobic. Knowledge of this region drove the direction of mutagenesis studies on deactivation gating.

The role of the NT 1-26 amphipathic α-helix in deactivation

The structure of the helix running from residue 11 to 24 is vital to mediate the slow deactivation in WT hERG. Breaking (or kinking) the helix at Ile18 by introducing a proline accelerated deactivation to a rate very similar to the channel that had the whole of the N-terminus removed. However, breaking the helix on the opposite side at Asp16 had the opposite effect on deactivation and slowed it. It appears that by breaking or kinking the helix at Ile18 the NT 1-26 region is no longer orientated to bind to its receptor site and is therefore not able to slow the deactivation process. Breaking or kinking the helix at position Asp16 orientates NT 1-26 to a position that stabilises the binding of NT 1-26 to its receptor site and thus slows deactivation more than in the WT channel.

The basic residues in NT 1-26 are key to the function of this region

Having discovered that one face of NT 1-26 is positively charged we wanted to investigate what the importance of this was. Mutating the basic residues Arg4, Arg5, His7, Arg20 and Lys21 increased the rate of deactivation similar to that seen in NTK hERG. The effect of removing the N-terminus on deactivation gating can be mimicked by charge neutralisation mutations at positions Arg4, Arg5, His7, Arg20 and Lys21 strongly suggesting that NT 1-26 is forming a charge interaction somewhere on the channel.

As mentioned in the introduction to this chapter, when the NTK hERG channel was expressed, and purified eag domain protein was injected into the cell the channel recovered its slow deactivation. When patches of membrane were excised containing NTK hERG channels with the purified eag domain the effect of deactivation was not washed off. However, when the same experiment was done but this time a peptide fragment corresponding to NT 1-16 the recovery of slow deactivation was lost on excising patches of membrane. It would appear that the PAS domain within the eag domain is required for a tight interaction with the channel, whereas the NT 1-26 region does not. It might be the case that the role, or at least one of the roles of the PAS domain, is to hold the NT 1-26 region close to the C-terminus (see later section) so it is able to quickly bind and unbind as the channel opens and closes.

The role of NT 1-26 in inactivation gating

As well as the effect on accelerating deactivation gating, removing the N-terminus also shifts the voltage dependence of inactivation in a positive direction. R4A:R5A and I18P shift the $V_{0.5}$ of inactivation about half (30mV) that of the shift seen in NTK hERG (60mV). The other mutants under investigation here had no discernible effect on the voltage dependence of inactivation. While the effects of removing the whole N-terminus

on the deactivation kinetics can be localised to NT 1-26 and specifically to the 5 basic residues it is not possible to find the sub domain responsible for modulating the voltage dependence of inactivation as none of the mutations reproduced the shift in the voltage dependence of inactivation seen in NTK hERG. This could be partly due to there being more than one domain within the N-terminus responsible for modulating inactivation gating. Clearly another region of the N-terminus must be responsible for the other half of the shift seen in NTK hERG.

The role of the cNBD in regulating deactivation gating.

The NT 1-26 region must be interacting with another region of the channel in order to produce the effects seen on deactivation and inactivation. NT 1-26 is an intracellular domain so it must be interacting with another intracellular part of the channel. There are three possible places that could be the site of interaction; the S2-S3 linker, the S4-S5 linker and the C-terminus. To the best of my knowledge there are no reports of mutations in the S2-S3 linker causing any similar effects on gating to those seen when the N-terminus is removed.

The S4-S5 linker has been the subject of intense investigation and mutating residues here have pronounced effects on gating (Sanguinetti & Xu 1999). The S4-S5 linker is short in hERG, and is thought to run from Asp540 to Tyr545. It has been shown that Asp540 in the S4-S5 linker interacts with Arg665 which is located around the level of the activation gate on the lower portion of S6 (Ferrer et al, 2006). Presented in chapter 4 is evidence of an interaction between Tyr545 in the S4-S5 linker and Val659 also around the activation gate in S6. Given how short the S4-S5 linker is and that Asp540 and Tyr545 form interactions with S6 it leaves little space for Arg4, Arg5, His7, Arg20 and Lys21 to interact with it. Even without the interactions at Asp540 and Tyr545 there is

still not sufficient room for the 5 basic residues in NT 1-26 to interact with the S4-S5 linker given their spacing along this region. Notwithstanding, it is perfectly possible that some part of the intercellular N or C-termini interacts with the S4-S5 linker given how large they are.

Removing the N-terminus accelerates deactivation. An obvious question to ask is what happens when the C-terminus is removed. Aydar & Palmer, 2001 investigated the role of the C-terminus in deactivation gating and found that deleting the whole of the C-terminus results in a non-functional channel. However, it is possible to delete some portions of the C-terminus. Aydar & Palmer, 2001 made a series of C-terminus deletions Δ163, Δ 215, Δ 236, Δ 278, Δ 311 and Δ 344. The Δ163 and Δ 215 deletions had no effect on deactivation gating. Deleting the last 236 and 278 residues of hERG accelerates the rate of deactivation and the Δ 311 and Δ 344 truncations did not express functional channels. This region of the channel contains a cyclic nucleotide binding domain.

HCN (hyperpolarisation-activated cyclic nucleotide-gated channels) channels carry the I_f current responsible for the pacemaker current. This channel has the unusual property of opening with membrane hyperpolarisation, rather than depolarisation, and the channel is also modulated by cyclic nucleotides such as cAMP which bind to a cyclic nucleotide binding domain (cNBD) in the channels intracellular C-terminus. Although hERG contains a domain in its C-terminus which has homology to the HCN channel's cNBD, hERG's gating is not modulated by cyclic nucleotides (Brelidze et al, 2009). Three of the key residues in the HCN channel that interact with cAMP in the binding pocket are Glu582, Arg591 and Ala593 (Zagotta et al, 2003). At the analogous position in hERG there is an Asp, Ser and Gly respectively. Binding of cAMP to the cNBD in HCN channels causes a rearrangement of the domain around the C-helix that is transduced via the C-linker to

the activation gate in S6 and also probably up to the selectivity filter (Zagotta et al, 2003).

Until recently it was not thought possible to truncate large portions of the C-terminus. However, work from Matt Trudeau's laboratory at the University of Maryland in Baltimore has shown it is possible to delete substantial parts of the C-terminus as long as this is done in the S620T mutant background (Gustina & Trudeau, 2011). They show that deletions in the cNBD increase the rate of deactivation to rates similar to NTK hERG. They also repeated the experiment where the NTK channel is expressed and a purified eag domain is injected into the cell to see if it will recover the slow deactivation. However, this time in addition to the channel having the N-terminus deleted the cNBD was also deleted and a purified eag domain was injected into the cell. In this case the eag domain fragment was unable to restore the slow deactivation when the cNBD was missing. They also probed for an interaction between the eag domain and the cNBD by using a co-precipitation experiment. Residues 1-135 were tagged with GST and passed through a column containing beads that bind GST. A Flag-tagged cNBD (residues 666-872) was passed through the column. After leaving overnight and washing the column, the products were analysed by Western blot. The western blot was probed for the Flag-tag. The GST-tagged eag domain produced a clear band whereas the GST alone (control) produced no band on the blot.

All of these experiments were carried out in the S620T background. Ser620 is located on the outer mouth of the selectivity filter on the extracellular side of the channel and is nowhere near the C-terminus. Ser620 is known to be very important for the fast C-type inactivation seen in hERG. The S620T mutant channel abolishes C-type inactivation. How inactivation gating and the selectivity filter are linked to allow the expressions of a

channel that would otherwise be non-functional is not clear but it lends weight to the notion that it is possible for the C-terminus and selectivity filter to communicate with each other as is proposed here with R4A:R5A and I18P interacting with the cNBD and causing a shift in the $V_{0.5}$ of inactivation.

Residues 1-135 in the N-terminus of eag channels are known as the eag domain as they are so well conserved among this family of potassium channels. The N-terminus is known to be important for deactivation gating. The different members of the eag family have different deactivation properties, and yet the N-termini are well conserved. So what is the basis for differences in deactivation gating? All members of the eag family have a domain in the C-terminus with a high degree of homology to the HCN cNBD. However, there is far more variation between the eag family's cNBD's than there is variation between their N-termini so this seems a likely place to account for the differences in deactivation (Brelidze et al, 2009).

Until very recently the structure of the HCN2 channels cNBD was the best approximation of what the hERG cNBD would resemble. However, Bill Zagotta's group, who published the HCN2 cNBD structure in 2003, have just published the structure of the cNBD from a channel in the eag family, the zebrafish eag-like channel (zELK or Kv 12.1) (Brelidze et al, 2012). The structure of the zELK cNBD is very similar to the HCN2 channel but with two notable differences; one, the cNBD forms a pair of dimers rather than a tetramer and two, the C-helix is much shorter. The fact that an ion channels must have four-fold symmetry along the line of the pore to allow for proper ion conduction but can have only two-fold symmetry in the N and C-termini is not without precedent. The crystal structure of the a ligand gated ionotropic glutamate channel (ratGluA2) from

Eric Gouaux's laboratory show that the channel has just this arrangement (Sobolevsky et al, 2009).

The shorter C-helix in the zELK cNBD structure may explain why some of the mutations to it e.g E847K accelerate deactivation more than others e.g D843K.

The new structure of a cNBD in an eag channel family member can now be used to refine the parameters for the molecular dynamic simulations and help direct new mutagenesis studies to identify residues that when mutated accelerate deactivation to rates similar to NTK hERG.

The identification of Arg4 and Arg5 as having an important role in deactivation gating has been aided by past studies that made various deletions in the N-terminus starting with the whole of the N-terminus and focusing-in on the first 16 residues. Only in the past 12 months has it been show to be possible to make large deletions of the C-terminus and then make smaller and smaller deletions in order to focus in on the residues involved in regulating deactivation gating.

The approach of making sequential deletions in the N-terminus to hone in on the residues responsible for mediating slow deactivation gating was possible because of the discrete nature of the basic residues. There are only 2 pairs of basic residues in the NT 1-26 region and a histidine. The approach of making sequential deletions in the C-terminus is likely to be less successful than in the N-terminus because there are many more acidic residues in the C-terminus than there are basic residues in the N-terminus. The basic residues in the N-terminus are side-by-side in the protein primary sequence (e.g. at positions 4 and 5) and therefore also close to each other on the tertiary structure of the folded protein. However, acidic residues that are close together in the

tertiary structure of the folded C-terminus may be separated by 10, 50 or 100 residues in the primary protein sequence. In this case making sequential deletions will only remove one of the residues responsible for slowing deactivation gating.

R20A and K21A hERG deactivate at a rate in-between WT and NTK hERG and the double mutant R20A:K21A had an additive effect on the rate of deactivation is much closer to that of NTK hERG. The effect of the individual mutations R4A and R5A was not studied here but it is know that R5A deactivates at a rate between WT and NTK hERG, suggesting that both Arg 4 and 5 need to be mutated to reproduce the rate of deactivation seen in NTK hERG. It therefore seems likely that a double mutant of C-terminus acidic residues will be required to reproduce the fast deactivation seen in the basic residue double mutants in the N-terminus. There are 51 acidic amino acids in the C-terminus of hERG, meaning that there are 2601 possible combinations of double acidic residue mutants that could be made. If the area is narrowed to the cNBD, there are 18 acidic residues in this region with a possible 324 double mutants that could be made. The modelling data identify acidic residues in the cNBD that might be involved in an interaction with the NT 1-26 region. Two of the residues indentified were Glu847 and Glu857 and the double mutant E847K:E857K deactivates very quickly although not as quickly as NTK hERG.

The mutations that remove the acidic residues in the C-terminus do not accelerate deactivation to the same degree as the mutations that remove the basic residues in the N-terminus. It may be that because there are so many acidic residues in the C-terminus that when the primary acidic residue involved in the interaction with a basic residue is mutated, the basic residue is able to interact with another acid residue due to the abundance of them. With thousands of possible combinations of acid residues to

mutate and however useful modelling data has been the only definitive way to find all of the interactions between the N and C-termini will be to solve the structures of them together.

The C-terminus in hERG is large, almost 500 amino acids long. It is not yet clear if the C-terminus of hERG is modulated by any signalling molecules or if the presence of a cNBD is simply an evolutionary hangover. There is now a picture beginning to emerge of a C-terminus that plays a direct role in channel gating but this picture is far from complete and will no doubt be the focus of intense research over the coming years.

Here we propose a mechanism by which the NT 1-26 region interacts with the C-helix in the cNBD through a charge interaction. This interact causes a reorientation of the cNBD analogous to the binding of cyclic nucleotides that is transduced via the C-linker to the region of the activation gate in the proximal end of the S6 helix and stabilises the open state of the channel and resulting in slow deactivation.

Chapter 4

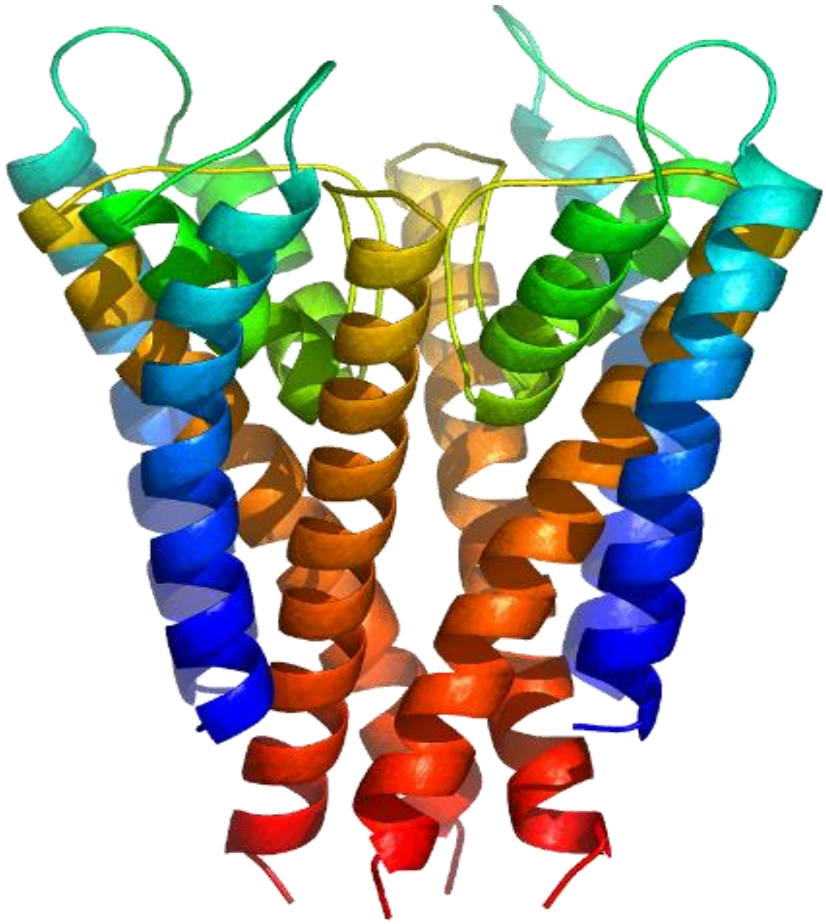

Val659 role in deactivation gating and coupling of the pore to the voltage sensor

Introduction

The ability to gate in response to changes in voltage across the membrane is an essential feature of all voltage gated ion channels. Voltage gated potassium channels can be split into two distinct functional units; a voltage sensing unit (S1-S4) and an ion conducting pore (S5&S6). The molecular identity of the voltage sensor has been intensively studied and is well understood. The fourth transmembrane segment (S4) contains six positively charged arginines (or lysines) in Shaker (5 in hERG) with the 4 arginine residues in the most N-terminal (extracellular) portion of S4 being the ones more important for voltage sensing (Piper et al, 2003; Yellen 1998). Less well understood however, is the process by which sensing the change in voltage across the membrane is translated into movement of the activation gate to allow the passage of ions, a process known as 'electromechanical coupling'.

Channel gating involves the opening and closing of the activation gate. The activation gate is thought to be located at the C-terminal end of the S6 helix and is formed by the crossing of the S6 helices to form the bundle-crossing. Channel gating is thought to involve splaying apart of the S6 helices to allow the passage of ions. From the crystal structures of Kv1.2 and Kv2.1 from MacKinnons laboratory, it can be seen that the S4-S5 linker, a short helix that runs across the inner face of the membrane and links the main voltage sensor S4 to the outer helix of the pore S5, forms a 'cuff' around the area of S6 where the activation gate is thought to be located (Long et al, 2007; Long et al, 2005a; Long et al, 2005b). The cuff of the S4-S5 linker may be a site of interaction that links the voltage sensing domain to the pore domain.

The S4-S5 linker is one region of hERG known to be particularly sensitive to mutations. The charge reversal mutation D540K hERG results in a channel that opens upon hyperpolarisation as well as depolarisation of the plasma membrane (Sanguinetti & Xu 1999). Previous work has also shown that Asp540 couples the voltage sensing domain to the activation gate in the lower portion of S6 at residue Arg665 (Ferrer et al, 2006). The interaction of Asp540 with Arg665 occurs when the channel is in the closed state. When Asp540 is mutated to Lys the channel can open at membrane potentials negative to the resting membrane potential as well as positive to it. It is thought that the presence of a basic residue in the case of D540K results in a charge repulsion of the Arg at 665 and this destabilises the closed state of the channel allowing it to reopen at negative membrane potentials.

Experiments by Mitcheson et al, 2000 to identify the drug binding residues in the inner cavity of hERG introduced an alanine scan along S6. Alanine substitution at Val659 produced a channel with dramatically slower deactivation gating than WT hERG, and yet mutation of the residues either side of Val659 did not slow the deactivation kinetics. Val659 is in the C-terminal part of S6 where the activation gate is thought to be. Drug binding studies suggest the valine is located on the face of the S6 helix that does not face the ion conduction pathway and this is supported by homology modelling. In order to assess the role of Val659 in normal hERG deactivation gating a series of substitutions were made at this position to assess their impact on deactivation gating. The mutant V659G hERG resulted in a channel that did not deactivate even at very negative membrane potentials, with the activation gate constitutively open. This suggested that in the V659G hERG mutant the voltage sensing domain was no longer coupled to the pore domain. From the crystal structures of voltage gated potassium channel from Rod

MacKinnon's laboratory it can be seen that a short helix that links S4 with S5 runs parallel to the membrane and comes in close proximity to the lower part of S6 where the activation gate is believed to be (Long et al, 2005a; Long et al, 2005b; Long et al, 2007). To assess if electromechanical coupling arises from Val659 contacts with the S4-S5 linker a series of cysteine cross-linking experiments were performed. A cysteine residue was engineered into hERG at position 659 in place of valine and a series cysteines were also introduced individually along the S4-S5 linker to probe possible interactions between position 659 and the S4-S5 linker. The hypothesis was 659Cys is in close proximity to specific positions on the S4-S5 linker and would thus form disulphide bonds that would form in a state dependent manner and lock the channel in a specific confirmation.

Results

Effect of substitutions at position 659 on deactivation gating

To investigate the molecular basis for the striking change in deactivation gating of V659A hERG, Val659 was mutated to residues with different hydrophobicity and varying size side chains; phenylalanine, which has a larger van der Waals volume, isoleucine which is also larger than valine, and three residues with progressively smaller side chains, cysteine, alanine and glycine. See table 4.1 for comparison of side chain volumes and hydrophobicity.

Table 4.1. Properties of amino acids substituted at position 659.

Amino Acid	Van der Waals Volume	Hydrophobicity			Side chain
		1	2	3	
Val (WT)	105	4.2	0.86	0.60	$-CH(CH_3)_2$
Phe	135	2.8	0.88	0.50	$-CH_2C_6H_5$
Ile	124	4.5	0.88	0.70	$-CHCH_2CH_3CH_3$
Cys	86	2.5	0.91	0.90	$-CH_2SH$
Ala	67	1.8	0.74	0.30	$-CH_3$
Gly	48	-0.4	0.72	0.30	-H

1) Kyte & Doolittle (1982). 2) Rose & Wolfenden (1993). 3) Janin (1979)

The voltage dependence of activation was measured using the I-V protocol in figure 4.1. Membrane potential was held at -120mV and stepped from the holding potential to +40mV in 10mV increments for 5 seconds. Membrane potential was then stepped to -140mV for 5 seconds to elicit tail currents before returning to the holding potential. There were 60 seconds between pulses to allow for the complete deactivation of the channels. All voltage clamp recordings were performed in 2mM external K^+ recording solution unless otherwise stated. The relatively negative holding potential (-120mV) and tail potential (-140mV) was required because of the very slow deactivation kinetics of some of the mutants under investigation.

For WT hERG the threshold for activation was around -60mV with the current reaching maximal activation by 0mV. V659F and V659I hERG also activated around -60mV but V659C and V659A hERG threshold for activation was slight left shifted at around -70mV. V659C hERG reached maximum activation at the same voltage as WT around 0mV. V659I and V659F hERG both reached maximum activation around 10mV. All of the mutants had shallower activation curves than WT hERG with V659A hERG having the shallowest activation curve of all of the mutants. The activation curves for the substitutions at 659 are shown in figure 4.2 V659A, V659F and V659I were significantly right shifted compared to WT hERG while there was a significant leftward shift in the $V_{0.5}$ of V659C hERG.

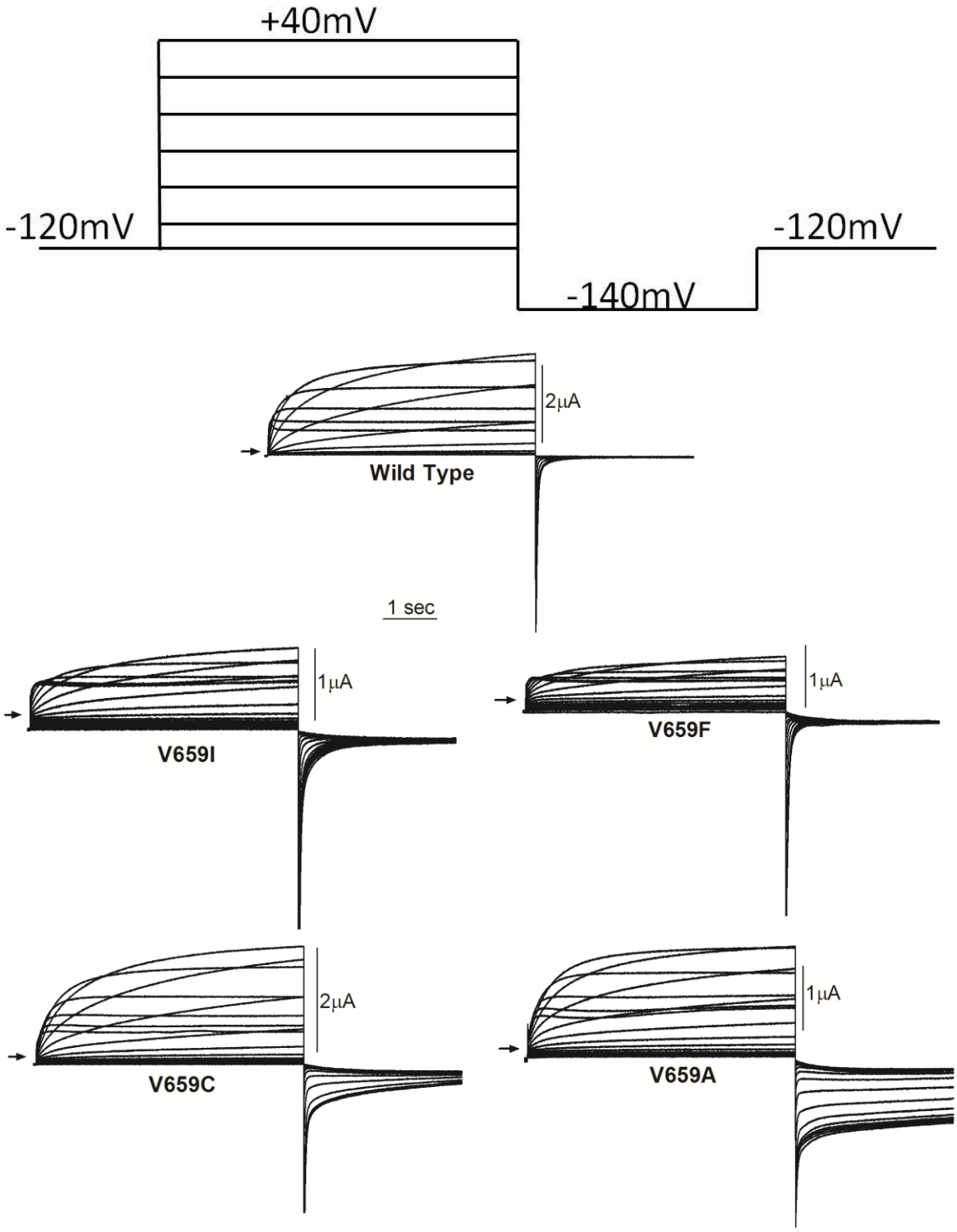

Figure 4.1. Representative I-V current traces for WT hERG and Val659 mutants.
Voltage protocol used to assess the current-voltage (I-V) relationship of Val659 hERG mutants is shown (top). The membrane potential was held at -120mV then stepped to the test potential for 5 seconds before stepping to -140mV for 5 seconds then returning to the holding potential. Repersentative traces of currents electied using the I-V protocol are shown underneath the voltage protocol. Arrows indecate zero current level.

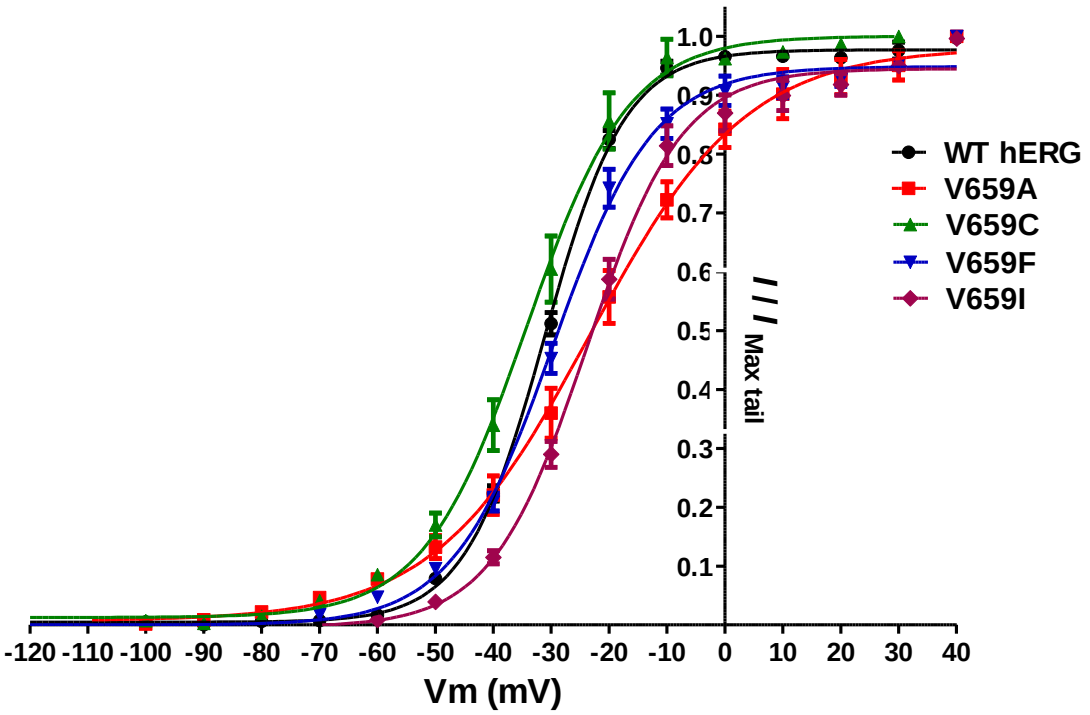

	$V_{0.5}$ of activation (mV)	Slope (mV)	n
WT hERG	-30.7 ± 0.5	7.5 ± 0.3	9
V659A	-22.6 ± 2.3***	14.1 ± 1.5***	4
V659C	-34.4 ± 1.8*	8.9 ± 0.9***	4
V659F	-28.0 ± 1.2*	10.0 ± 0.8**	6
V659I	-21.8 ± 1.5***	9.6 ± 0.9*	8

Figure 4.2. Voltage dependence of activation of WT and Val659 mutants. Activation curves for WT, V659A, V659C, V659F & V659I currents. Peak tail current amplitudes normalised to maximal tail current were plotted against test potential and fitted with a Boltzmann function.

Deactivation of Val659 mutants

A slightly modified version of the fully activated I-V protocol used in the first results chapter was used to study the time course of deactivation. The membrane potential was held at -120mV and stepped to +40mV for 1 second to maximally activate and inactivate the currents and then stepped down to -120mV to measure the time course of deactivation. The time the cells were held at -120mV to measure the rate of deactivation varied from 5 seconds for WT through to 40 seconds for the slowest deactivating mutant V659A. A single voltage (-120mV) was chosen to measure the rate of deactivation because deactivation is so slow in some of the mutants that there is little deactivation over two minutes at membrane potentials positive to -100mV. With a 2mM external K^+ solution E_K is approximately -100mV. A voltage between -100mV and -120mV does not provide sufficient driving force to produce robust currents to measure. From potentials around -140mV an endogenous inward current is sometimes observed particularly if the cell is hypopolarised for several seconds. Therefore -120mV was chosen because it is negative enough to drive deactivation at a reasonable rate and far enough from E_K to produce measurable currents yet not too negative to activate endogenous currents. Mutation to isoleucine, a similar sized, hydrophobic residue resulted in a slight but statistically significant slowing of deactivation (fig 4.3 & 4.4). Mutating the valine to phenylalanine, which has side chain than is slightly larger than valine, also caused a small but statistically significant slowing of deactivation. Substituting the valine to cysteine which has a side chain smaller than valine causes a pronounced slowing of deactivation. Mutation to alanine, which has a side chain smaller than cysteine, slowed deactivation more than the cysteine mutant. Figure 4.3 show normalised deactivation current traces and the tau's are summaries in figure 4.4. The

time constants of deactivation were derived by fitting the decaying phase of the tail currents with a double exponential function.

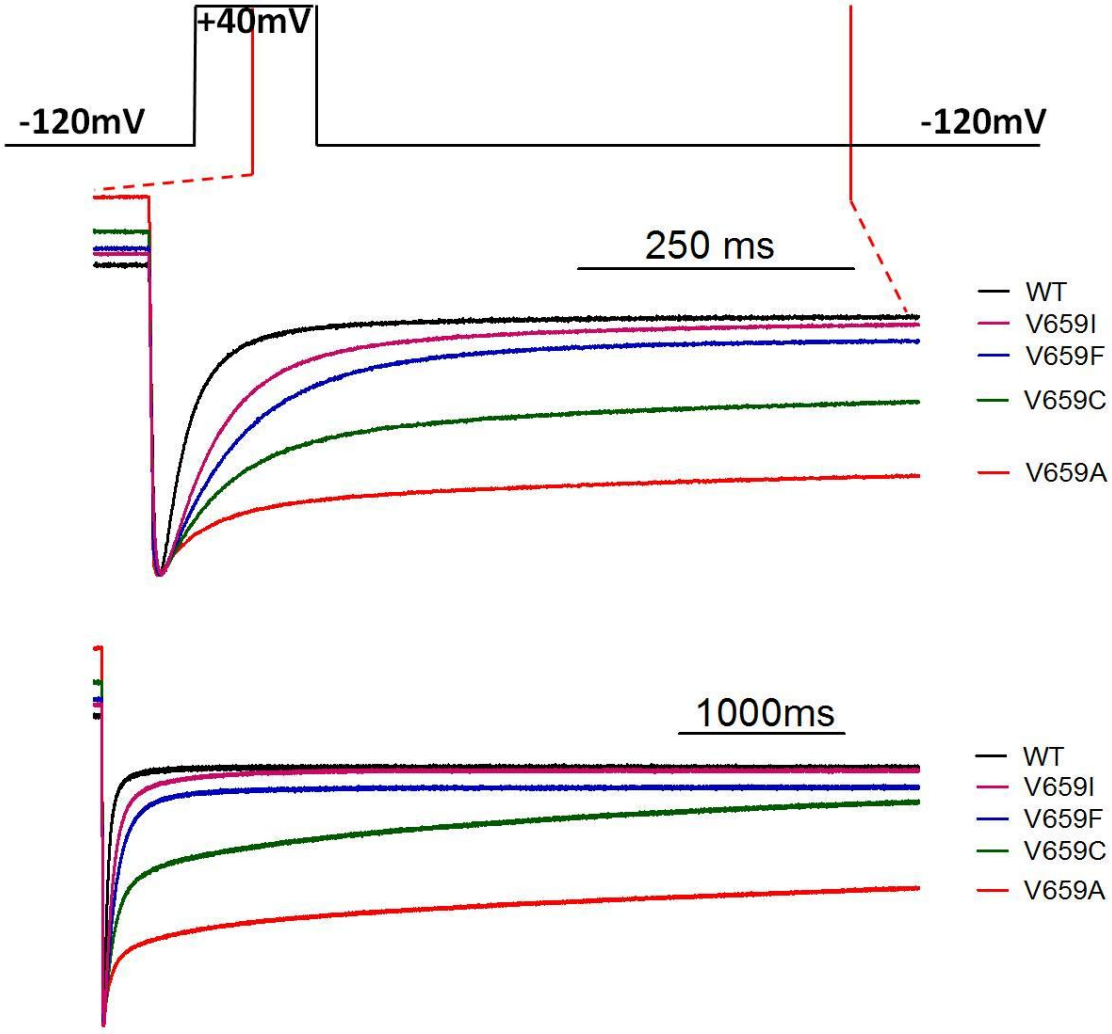

Figure 4.3. Normalised deactivation current traces at -120mV for substitutions at Val659. Membrane potential was held at -120mV, then stepped to +40mV to fully activate the channels and then stepped down to -120mV in order to measure the rate of deactivation. The last 50ms of the +40mV step and first 750ms (top) and 6 seconds (bottom) of currents are shown. Mutation of Val659 to other similar sized hydrophobic residues (Ile and Phe) had a modest affect on deactivation. Mutation to cysteine profoundly slows deactivation. However, mutation to alanine slows deactivation even more profoundly. Currents have been normilaised to the peak tail current.

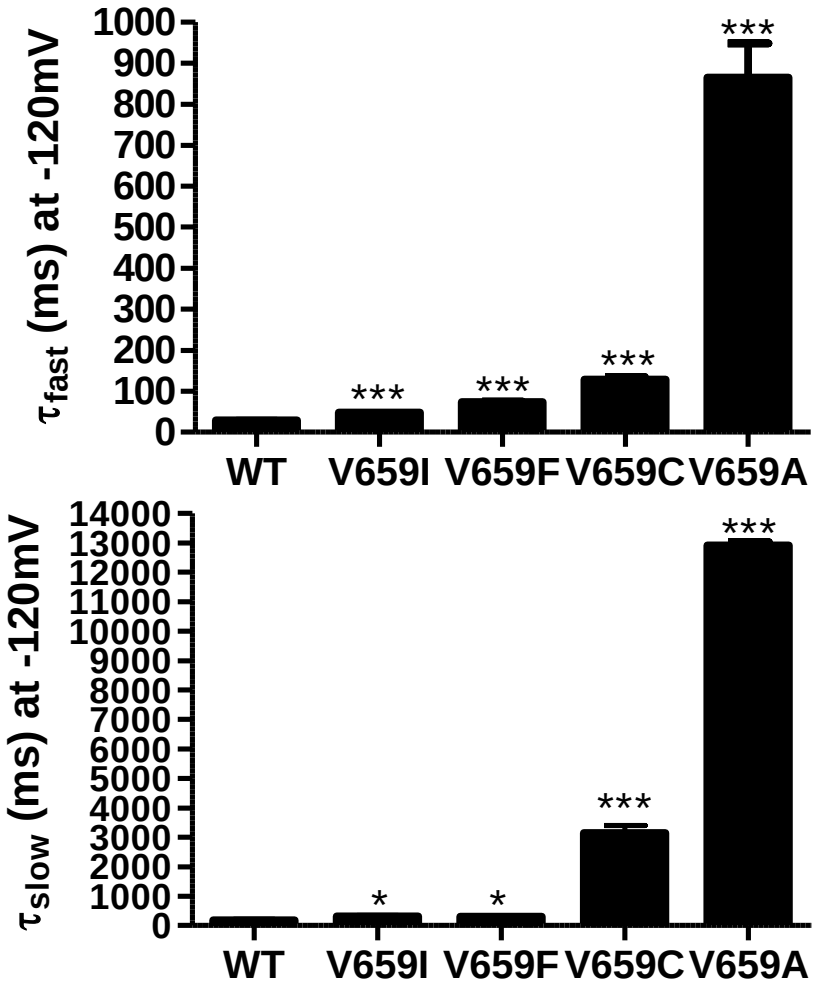

	Deactivation time constants (ms) at -120mV		n
	Slow	Fast	
WT hERG	179.5 ± 33.1	28.7 ± 2.7	6
V659I	317.4 ± 30.2	48.3 ± 2.2	8
V659F	310.2 ± 28.8	73.5 ± 4.7	6
V659C	3152 ± 250	128.4 ± 8.5	8
V659A	12904 ± 129	865 ± 83.5	4

Figure 4.4. Deactivation time constants for WT hERG, V659C, V659F, V659I and V659A. Mutation to Phe and Ile has a modest but significant affect on deactivation. Mutation to cysteine and alanine profoundly slows deactivation. Deactivation measured at -120mV. Data was fit with a double exponential fit to obtain the time constants for the fast and slow components of deactivation.

Mutation of Val659 to Gly

As mutation of Val659 to residues with progressively smaller side chains resulted in progressively slower deactivation it could be hypothesised that mutation to glycine, which has the smallest side chain of all amino acids would slow deactivation even more, however this was not the case. V659G hERG currents were unstable at negative holding potentials so a holding potential of 0mV was used and pluses from +50 down to -160mV were applied. Very little current was observed at any potential. To test if the channels were inactivated the recording solution was switched from the 'normal' 2mM external K^+ to a 96mM external K^+ solution which shifts the voltage dependence of C-type inactivation to more positive potentials.

V659G hERG currents were highly inwardly rectifying, passing little current at depolarised potentials but passing robust currents at potentials negative to -90mV. These currents continued to increase in amplitude with every more negative voltage step and showed no sign of deactivation even at potentials as negative as -160mV. Thus, the activation gate of this mutant is constitutively open (fig 4.5 B) and the only gating is by voltage dependant inactivation.

To verify that the currents observed were hERG currents, 100µM of the specific hERG blocker, cisapride, was added which resulted in complete block of the currents in both 2mM and 96mM recording solutions confirming that they were indeed hERG currents (fig 4.5 A & B).

Oocytes injected with DEPC water showed very little current when using the same voltage protocol and high external K^+ recording solution and were unaffected by cisapride (fig 4.5.C).

The mutation of Val659 to Gly resulted in a constitutively open channel that retained inactivation gating but showed no voltage dependent activation or deactivation gating, suggesting that the voltage sensing domain is no longer coupled to the activation gate.

	Control	+ 100µM Cisapride
A) V659G currents recorded in 'normal, low' 2mM external K^+ solution	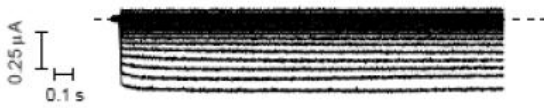	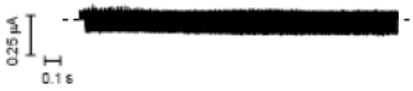
B) V659G currents recorded in 'high' 96mM external K^+ solution	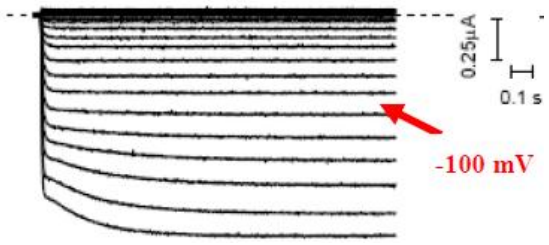	
C) Currents recorded from DEPC H_2O injected cells in 'high' 96mM external K^+ solution		

Figure 4.5. V659G hERG channels do not deactivate. V659G hERG currents were recorded by holding at 0mV and stepping from +50mV to -160mV. Dashed line indicates zero current. Currents are shown before (control, left) and after (right panels) application of 100µM cisapride. A) V659G currents recorded in 'normal' 2 mM external K^+ solution. B) V659G hERG currents recorded in 96 mM external K^+ solution. C) Currents recorded from oocytes injected with DEPC water. V659G recordings and analysis were performed by Sarah Dalibalta.

Does Val659 couple the activation gate on S6 to the S4-S5 Linker?

From the lack of voltage depentant activation and deactivation gating in the V659G hERG mutant it was hypothesised that upon repolarisation conformational changes to the voltage sensor are coupled to closure of the of the activation gate by interactions between Val659 on S6 and the S4-S5L. To verify the spatial proximity of these regions a cysteine was introduced at Val659. In this V659C channel background another cysteine was intoducted at Asp540 or at the other S4-S5L residues upto and including to Tyr545, thus creating a series of 6 double cysteine mutants (e.g. D540C:V659C through to Y545C:V659C). These double cysteine mutants were used to probe for the formation of disulfide bonds between Val659 in the activation gate to the S4-S5 linker, to determin if these amino acid posistions come into close proximity.

The voltage dependence of activation was measured using the same I-V protocol in figure 4.1. The membrane potential was held at -120mV and stepped from the holding potential to +40mV in 10mV increments for 5 seconds. The voltage was then stepped to -140mV to elicit tail currents before returning to the holding potential. There were 60 seconds between pulses to allow for the complete deactivation of the currents. The threshold for activation varied from -120mV in D540C:V659C to -60mV in Y542C:V659C with the currents reaching maximal activation by -20mV to 0mV. The shift in activation of D540C:V659C is dramatic but not entirely surprising given how exquisitely sensitive Asp540 is known to be to mutation. The voltage dependence of activation was derived by normalising the peak tail currents to maximal tail current and plotted against membrane voltage and fitting with a Boltzmann function. Figure 4.7 shows the voltage dependence of activation for the double cysteine mutants. All of the double cysteine

mutants except Y542C:V659C caused a significant shift in the voltage dependence of activation, moving it in a negative direction.

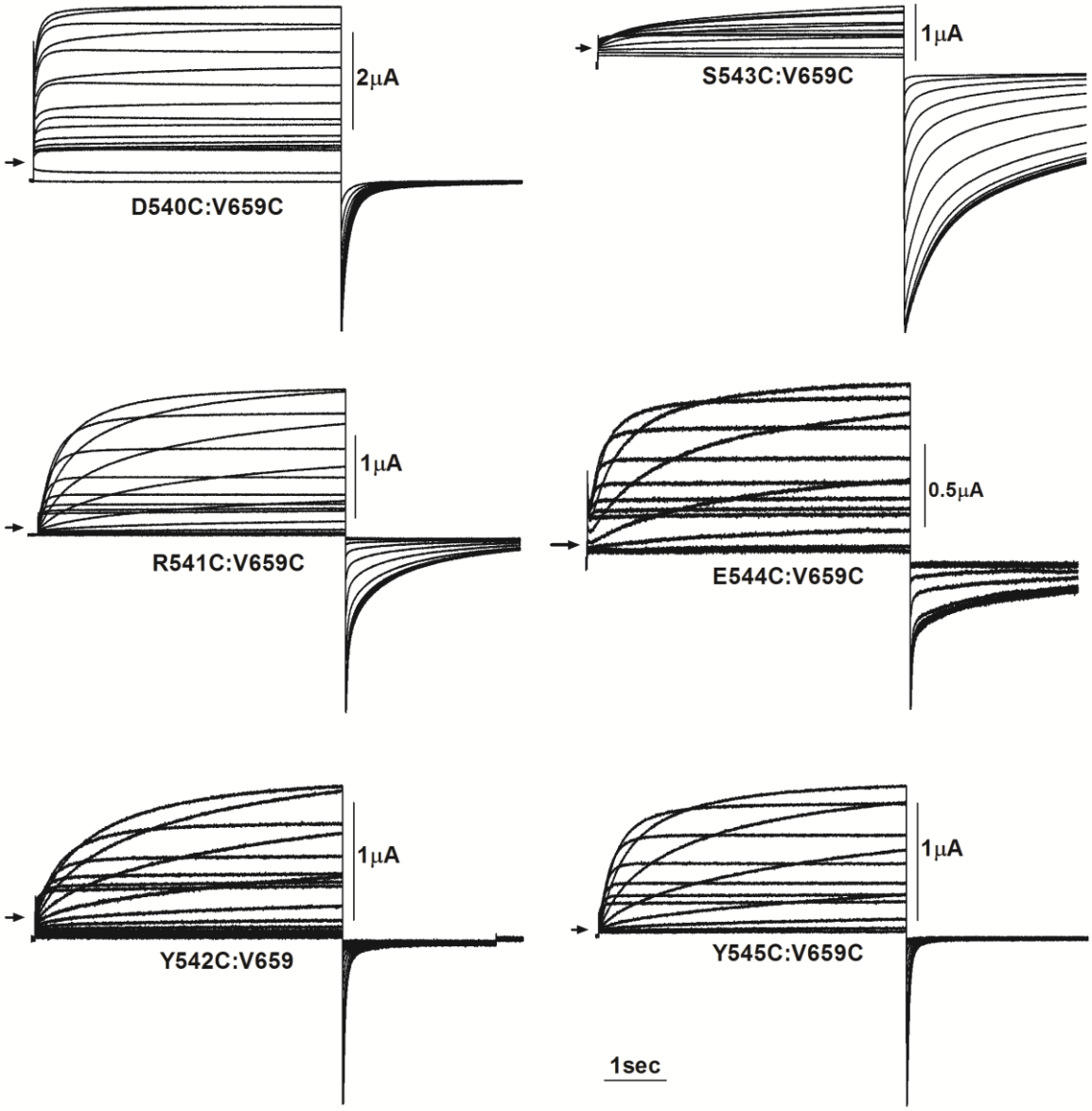

Figure 4.6. Representative I-V current traces for the S4-S5 Linker and Val659 double cysteine mutants. The currents were elicited using the voltage protocol in figure 4.1. Arrows indicate zero current level.

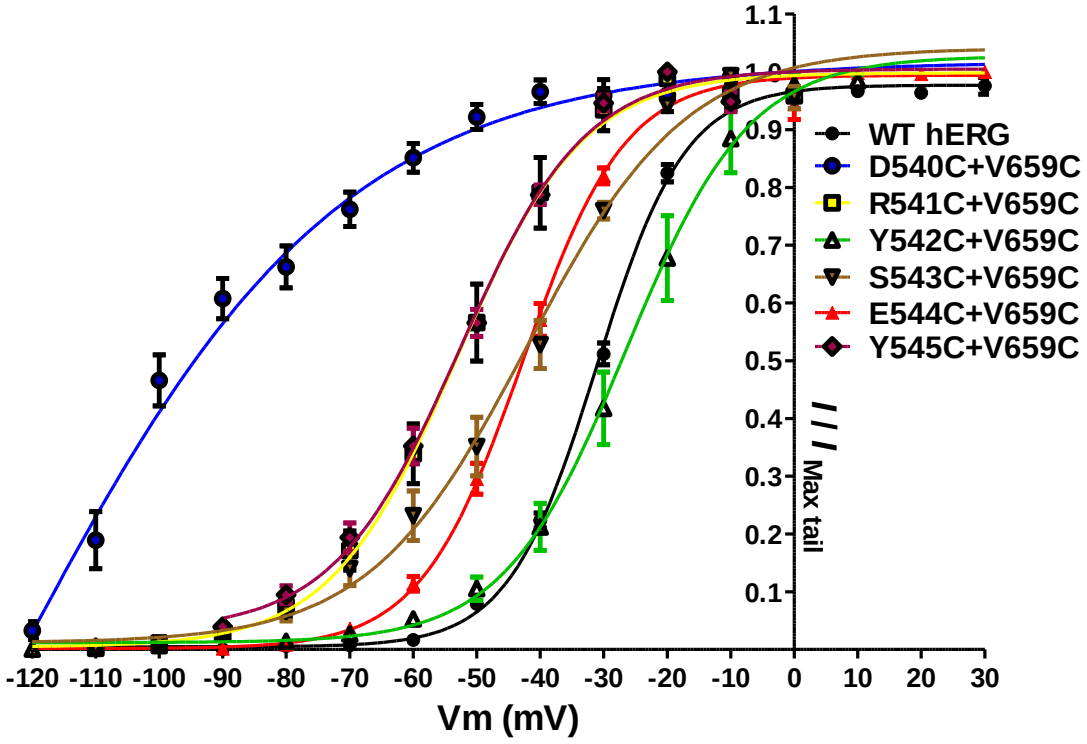

	$V_{0.5}$ of activation (mV)	Slope (mV)	n
WT	-30.7 ± 0.5	7.5 ± 0.3	9
D540C:V659C	-90.1 ± 2.4***	16.8 ± 1.8***	6
R541C:V659C	-53.2 ± 2.7***	9.8 ± 0.5**	5
Y542C:V659C	-27.3 ± 2.8	9.0 ± 0.4*	5
S543C:V659C	-44.0 ± 2.2***	11.6 ± 1.1***	4
E544C:V659C	-42.7 ± 0.9***	8.1 ± 0.4	6
Y545C:V659C	-54.0 ± 1.1***	10.3 ± 0.6***	5

Figure 4.7. Activation curve for S4-S5 linker double mutants. Mean normalised peak tail currnets were plotted as a function of test potential and fitted with a Boltzmann function to give the voltage dependence of activation. WT hERG is shown as a reference point.

Effect of $tbHO_2$ on the double cysteine mutants

Introduction of oxidising agents promotes the formation of disulfide bonds between thiol groups of cysteine side chains. For a disulpfide bond to form the distance between the side chains cannot be more than 5Å and the side chains must orientate towards each other. The formation of disulphide bonds would be expected to alter the gating of the channel. Using the same I-V protocol in figure 4.1, currents were measured under control conditions and then 2mM of the membrane permeable oxidising agent, tert-butyl hydroperoxide ($tbHO_2$), was perfused onto the oocyte while the I-V protocol was repeated over and over.

Before appling the $tbHO_2$ to the S4-S5 linker double mutants, the effects of the oxidising agent were first investigated on WT and V659C hERG. The control and $tbHO_2$ recordings were compared after ten minutes exposure to the oxidising agent. Representative current traces before and after the application of the oxidising reagent are shown in figure 4.8 and the voltage dependence of activation is shown in figure 4.9. The oxidising reagent causes a small but not statistically significant leftward shift in the $V_{0.5}$ of activation and there was also no statistically significant change in the slope of activation of WT and V659C hERG.

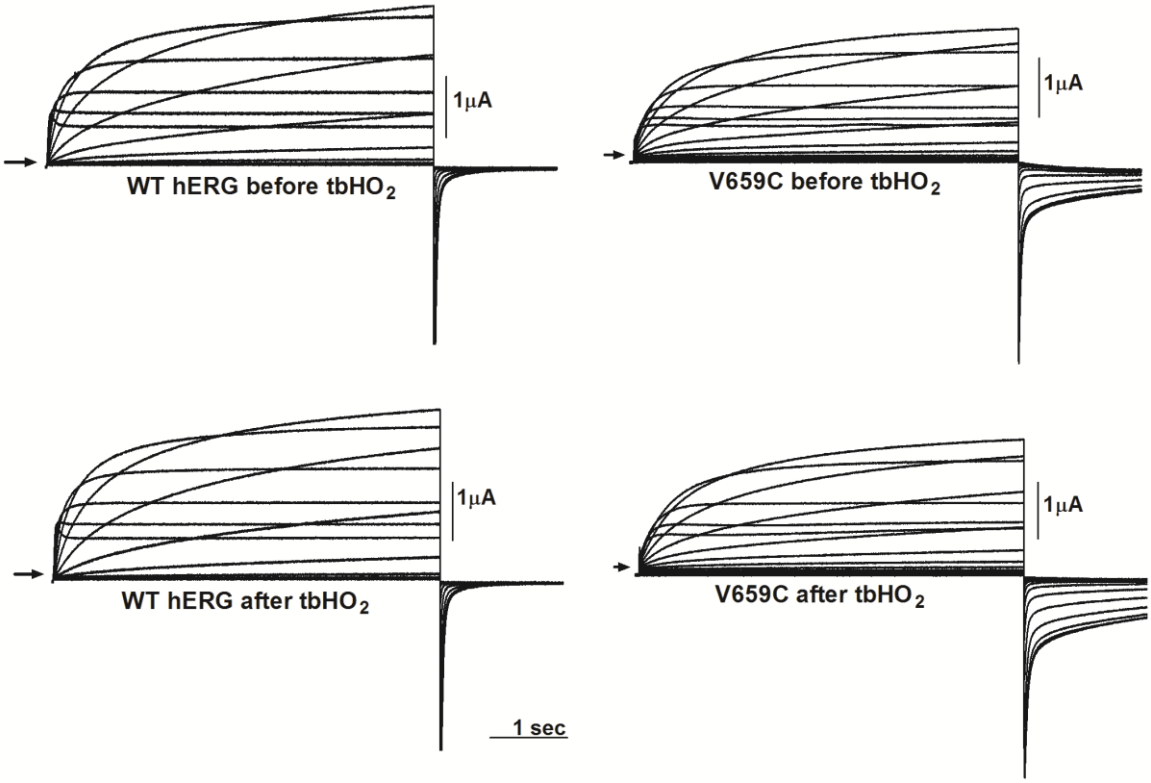

Figure 4.8. Representatives WT and V659C hERG currents before and after $tbHO_2$ application. Currents were elicited using the I-V protocol in figure 4.1 above. Current traces in control conditions (top) and after 10 minutes $tbHO_2$ (bottom). Arrows indicate zero current level.

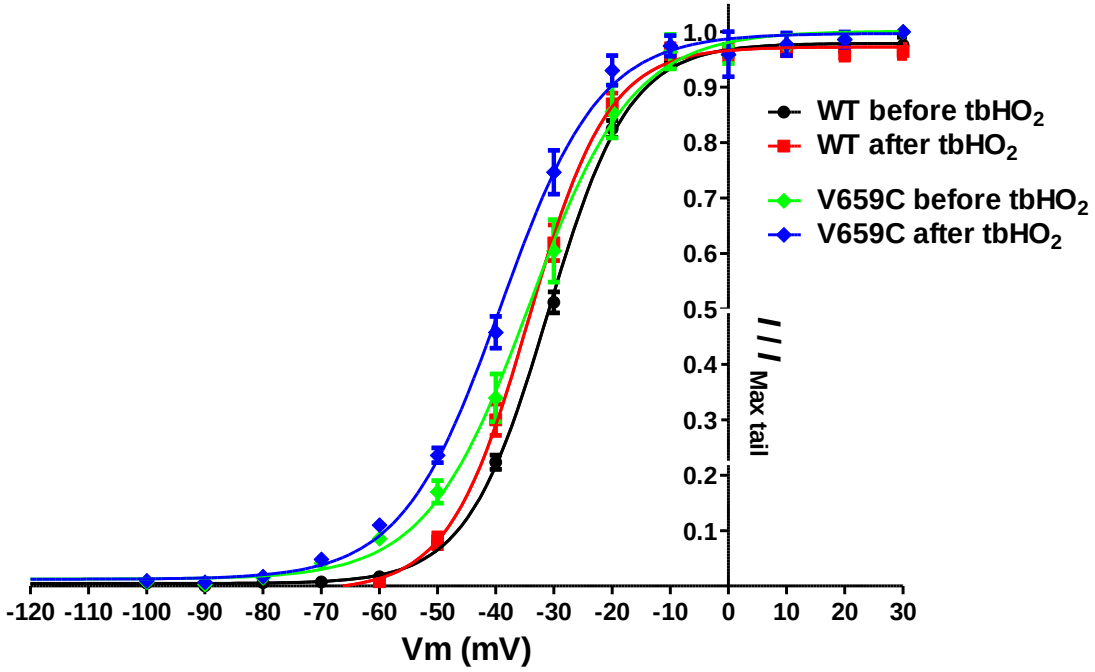

	$V_{0.5}$ of activation (mV) Before $tbHO_2$	$V_{0.5}$ of activation (mV) After $tbHO_2$	Slope (mV) Before $tbHO_2$	Slope (mV) After $tbHO_2$	n
WT	-30.7 ± 0.5	-32.3 ± 1.0	7.5 ± 0.3	7.0 ± 0.3	9
V659C	-34.4 ± 1.8	-39.1 ± 1.1	8.9 ± 0.9	8.8 ± 0.7	4

Figure 4.9. The effect of $tbHO_2$ on the voltage dependence of activation in WT and V659C hERG. Peak tail currents were normalised to maximum current, plotted against voltage and fitted with a Boltzmann function.

Using the same protocol as before, taking a control I-V and then running it repeatedly in the presences of the oxidising reagent the possible cross linking of Val659 to the S4-S5 linker was investigated. The application of $tbHO_2$ had little effect on D540C:V659C, R541C:V659C, Y542C:V659C and S543C:V549C. However, E544C:V659C hERG showed a pronounced change after the addition of the $tbHO_2$, and Y545C:V659C hERG also showed a small influence of $tbHO_2$. A representative I-V current trace of E544C:V659C is shown in figure 4.10 and representative current traces of the double cysteine mutants either side of E544C:V659C in the S4-S5 linker (S543C:V659C and Y545C:V659C) are shown in figure 4.11. The control trace of E544C:V659C (figure 4.10, top) exhibits the normally expected slow voltage dependent outward current followed by the slow decay of the inward tail current on stepping down to -140mV. After running the I-V protocol while applying the $tbHO_2$ there was a loss of the voltage dependant outward current and the slow decay of the inward tail current was no longer present. After the addition of the oxidising reagent there is an increase of holding current and an instantaneous current develops immediately after the step from the holding potential to the test potential. This instantaneous current is not a leak current because it can be seen to decrease exponentially during the test pulse, consistent with the onset of inactivation (figure 4.15, middle panel, right side). The effect of $tbHO_2$ on Y545C:V659C is not obvious from inspection on the current traces but can been seen from more detailed analysis of the recordings.

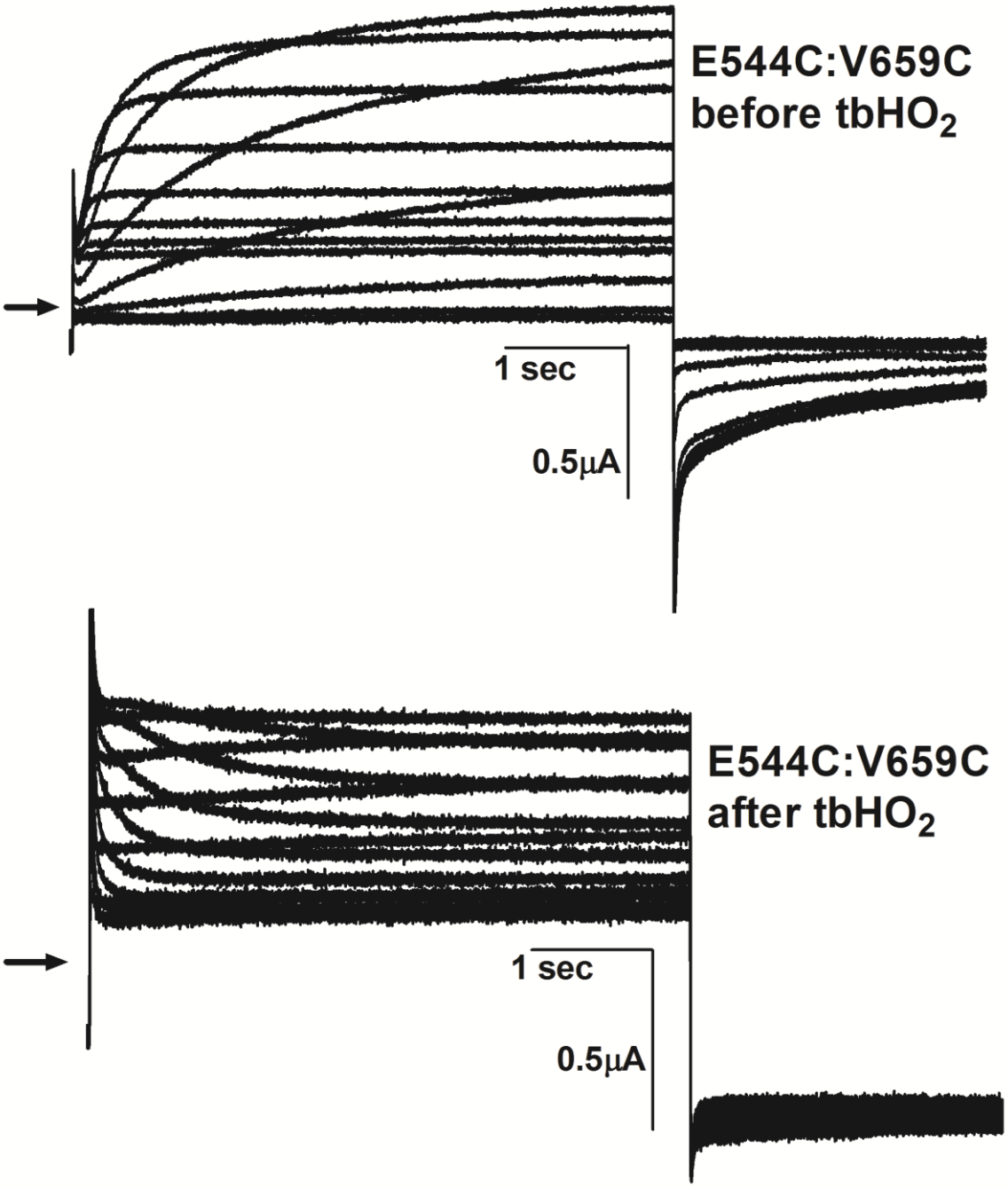

Figure 4.10. Representative current traces of E544C:V659C hERG before and after tbHO2 application. The currents were elicited using the I-V protocol in figure 4.1. The protocol was run repetitively, first without $tbHO_2$ (top) and then in the presence of the oxidising agent (bottom). The bottom current trace is after approximately 10 minutes exposure to the $tbHO_2$. Arrows indicate zero current level.

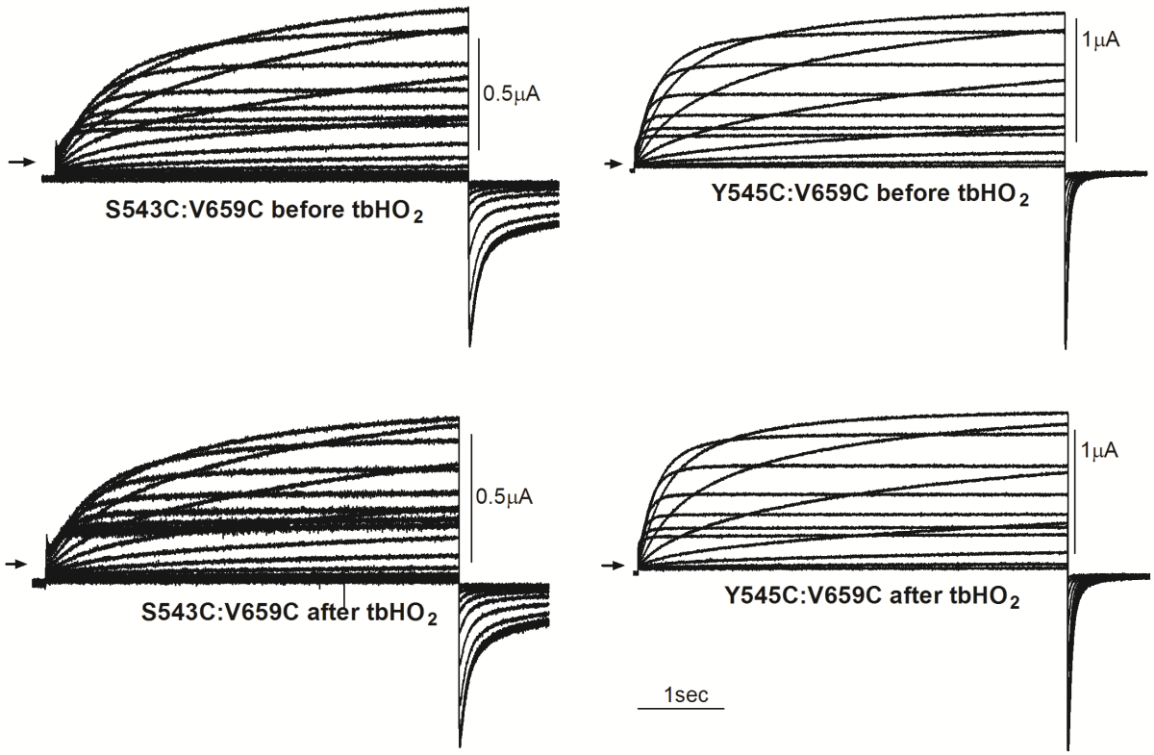

Figure 4.11. Representative current traces of S543C:V659C and Y545C:V659C hERG before and after $tbHO_2$ application. The currents were elicited using the I-V protocol in figure 4.1. The protocol was run repetitively, first without $tbHO_2$ (top) and then in the presence of the oxidising agent (bottom). The bottom current trace is after approximately 10 minutes exposure to the $tbHO_2$. Arrows indicate zero current level.

Figure 4.12 show the activation curves of all 6 of the cysteine double mutants before and after the addition of the oxidising reagent. There is no effect of the oxidising reagent on D540C:V659C, R541C:V659C, Y542C:V659C and S543C:V659C. In the double mutant E544C:V659C there was a pronounced effect of the $tbHO_2$. After the oxidising agent had been applied there was a constitutive conductance at negative membrane potentials where the channel had no conductance during the control I-V. This conductance was not due to a shift in the voltage dependence of activation. In the control I-V there was little or no conductance at -90mV, -80mV and -70mV. However after the application of the $tbHO_2$ there was a large conductance at the same voltages. The $V_{0.5}$ of activation was significantly shifted 6mV more negatively, while the slope was not significantly altered and the channel still reaches maximum activation around -20mV. The constitutive current suggests the channel may have been locked in the open state as a result of disulphide bond formation after the addition of the oxidizing agent.

The before and after activation curves for Y545C:V659C also show an effect of the oxidising reagent (figure 4.12) but these effects are less dramatic than in E544C:V659C. In control solution the activation threshold is around -80mv with the current reaching maximum activation around -20mV. After the $tbHO_2$ has been perfused onto the cell there is a background constitutive conductance at voltages (-90mV and -80mV) where there was little or no conductance in the control. The slope of the curve becomes linear between -90mV and -40mV and the slope is much shallower, reaching maximum activation around 0mV.

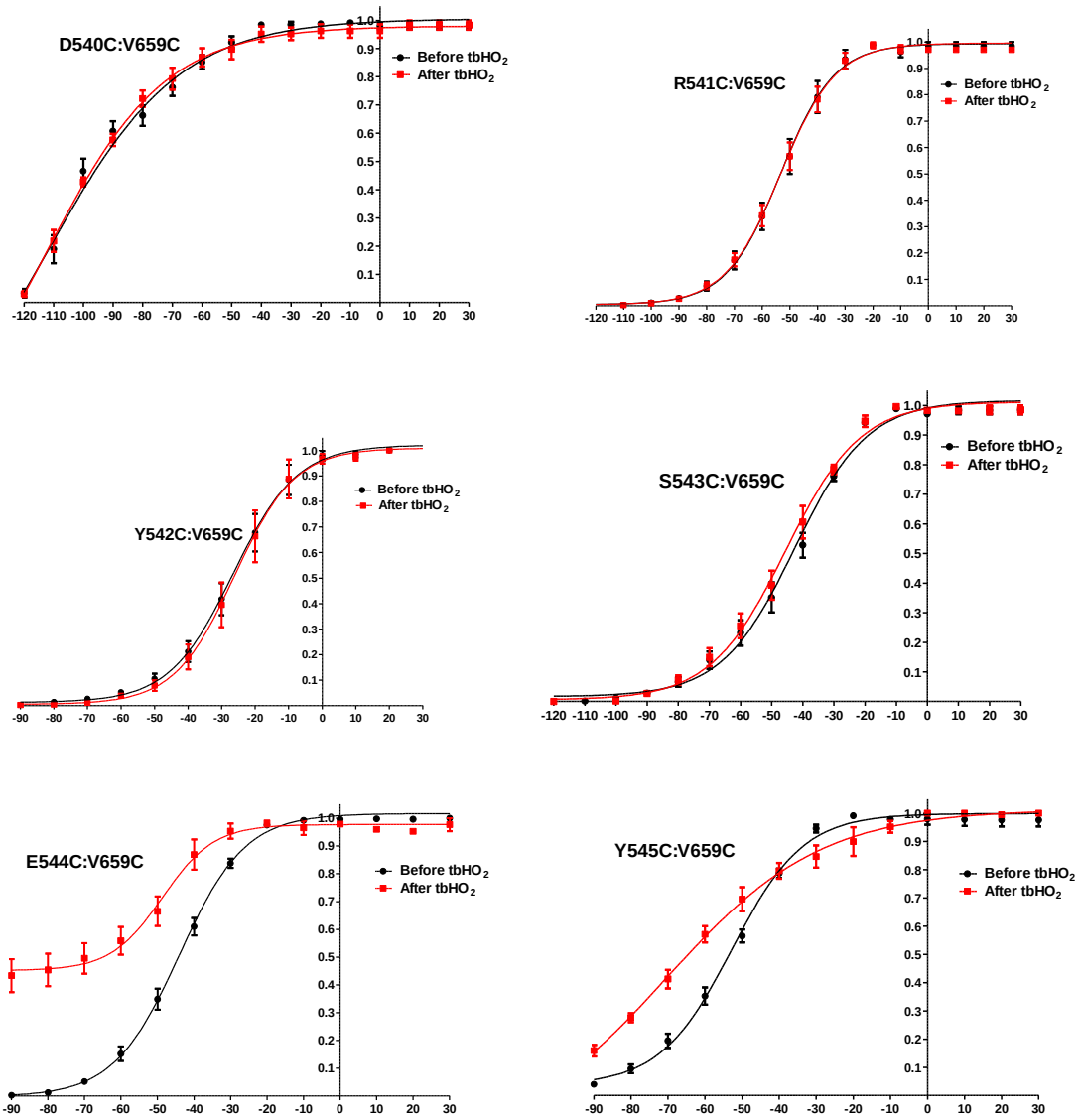

	$V_{0.5}$ of activation (mV) Before $tbHO_2$	$V_{0.5}$ of activation (mV) After $tbHO_2$	Slope (mV) Before $tbHO_2$	Slope (mV) After $tbHO_2$	n
D540C:V659C	-90.1 ± 2.4	-92.2 ± 0.8	16.8 ± 1.8	16.1 ± 1.4	6
R541C:V659C	-53.2 ± 2.7	-53.5 ± 2.1	9.8 ± 0.5	9.8 ± 0.5	5
Y542C:V659C	-27.3 ± 2.8	-26.8 ± 3.2	9.0 ± 0.4	8.9 ± 1.2	5
S543C:V659C	-44.0 ± 2.2	-45.4 ± 1.7	11.6 ± 1.1	11.4 ± 0.9	4
E544C:V659C	-42.7 ± 0.9	-48.7 ± 2.1**	8.1 ± 0.4	7.1 ± 1.6	6
Y545C:V659C	-54.0 ± 1.1	-63.5 ± 1.4***	10.3 ± 0.6	17.4 ± 1.5**	5

Figure 4.12. Activation curves for S4-S5 linker mutants before and after the addition of $tbHO_2$. Mean normalised peak tail currents plotted as a function of test potential then fitted with a Boltzmann function to give the voltage dependence of activation.

In addition to measuring the effects of the $tbHO_2$ on the activation curves the effect of $tbHO_2$ was also studied on the amplitude of the tail currents. In the WT channel the tail current was reduced by 18.8 ± 4.1%. Of all the mutants under investigation only Y545C:V659C hERG had a statistically different response in tail current reduction to the application of the $tbHO_2$ compared to WT hERG, with all of the other mutants showing roughly the same small reduction in tail current. However, even though the Y545C:V659C hERG tail current was different from the WT hERG it was essentially unaffected by the $tbHO_2$ showing only a 3.6 ± 7.9% increase. The single mutants V659C and E544C were included as controls and so is NTK:V659C:E544C hERG which is part of another experiment described below.

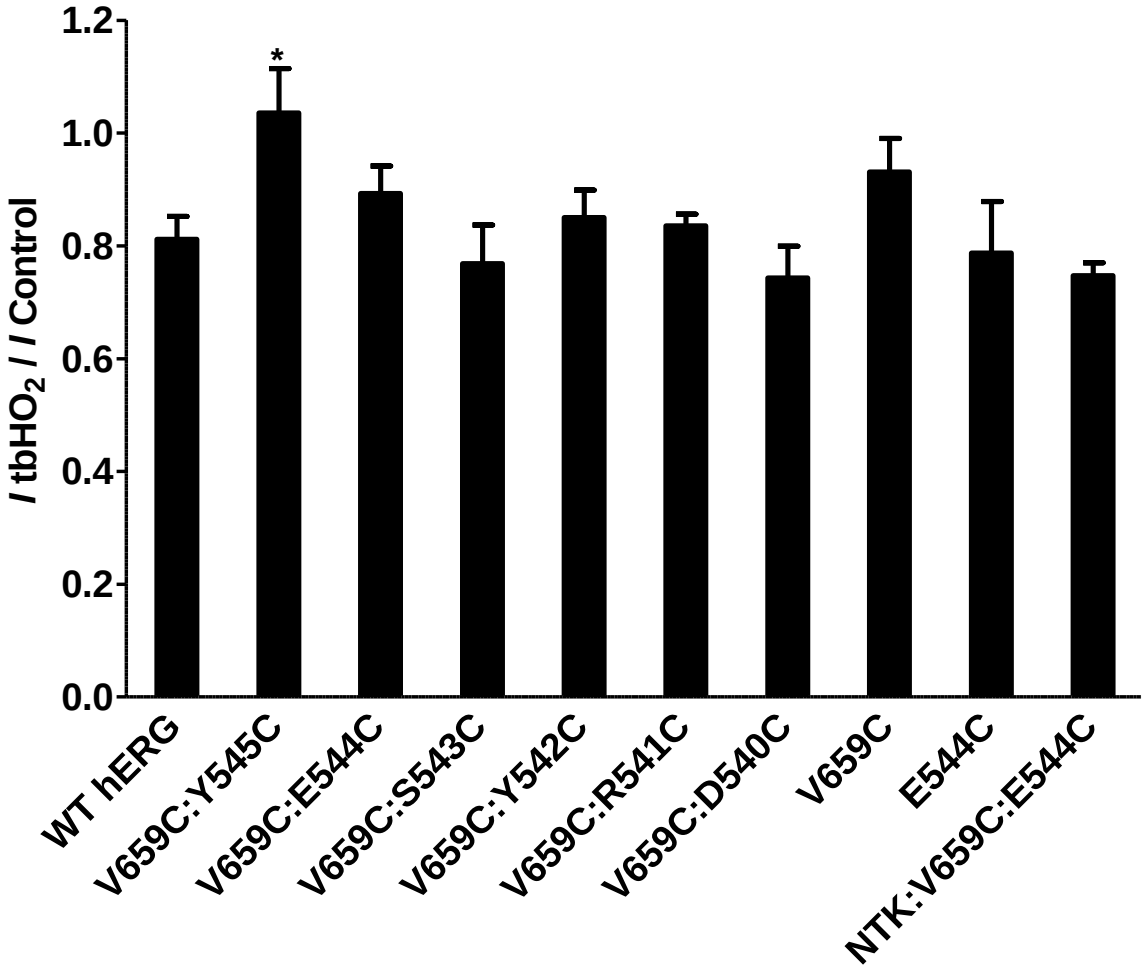

	% Current remaining from control	n
WT	81.2 ± 4.1	9
D540C:V659C	74.3 ± 5.7	6
R541C:V659C	83.5 ± 2.1	5
Y542C:V659C	85.0 ± 4.9	5
S543C:V659C	76.8 ± 6.8	4
E544C:V659C	89.3 ± 4.9	6
Y545C:V659C	103.6 ± 7.9*	5
V659C	93.1 ± 5.9	4
E544C	78.7 ± 9.1	5
NTK:V659C:E544C	74.7 ± 2.3	5

Figure 4.13. Effect of the addition of $tbHO_2$ on peak tail. Peak tail current after the addition of the oxidising agent was divided by the peak tail current from control. Tail current amplitude measured 10 minutes after exposure to $tbHO_2$. Tail currents were measured at -140mV.

On examination of the current trace in figure 4.10 it can be seen that an instantaneous current develops after the addition of the oxidising reagent. Using the same I-V protocol as before the level of instantaneous current was measured 5 ms after the step from the holding potential to the test potentials. The red arrows in the current trace in figures 4.14 and 4.15 indicate the time point 5 ms after the step from the holding potential to the test potential. It can be seen from the current traces in figure 4.14 and 4.15 that measuring the current 5 ms after the voltage step is long enough for the capacitance transient to decay but not so long that current activation or inactivation has yet occurred.

Figure 4.15 shows the instantaneous current in E544C:V659C hERG before and after the oxidising reagent had been applied. There was no instantaneous current in the control recording however there was an increase in the instantaneous current measured 5 ms after the step from the holding potential to the test potential after the $tbHO_2$ had been applied. As hERG currents activate slowly any ionic current flowing early after the voltage step has to be through channels that were already in the open state before the voltage was changed.

Current traces for the S4-S5 linker cys mutants either side of E544C are shown in figure 4.15. S543C:V659C hERG showed no change after the addition of the oxidising agent but Y545C:V659C hERG did show a small increase in instantaneous current.

Current traces are shown for WT hERG and the single mutants, E544C and V659C in figure 4.16. As expected, no instantaneous current was detected with $tbHO_2$ application,

reinforcing the evidence that the effect is specific to the double mutant and is the result of the two cysteines cross linking to lock channels in the open state.

The instantaneous current was plotted against membrane potential to give the representative instantaneous I-V graph for each of the 6 double cysteine mutants shown in figure 4.17. There was no effect on D540C:V659C, R541C:V659C, Y542C:V659C and S543C:V549C. E544C:V659C showed a progressive increase in instantaneous current that reaches saturation after about 5 runs of the I-V protocol. The first, control, run of the I-V protocol is show in red. Y545C:V659C also shows an increase in the instantaneous current albeit smaller than E544C:V659C.

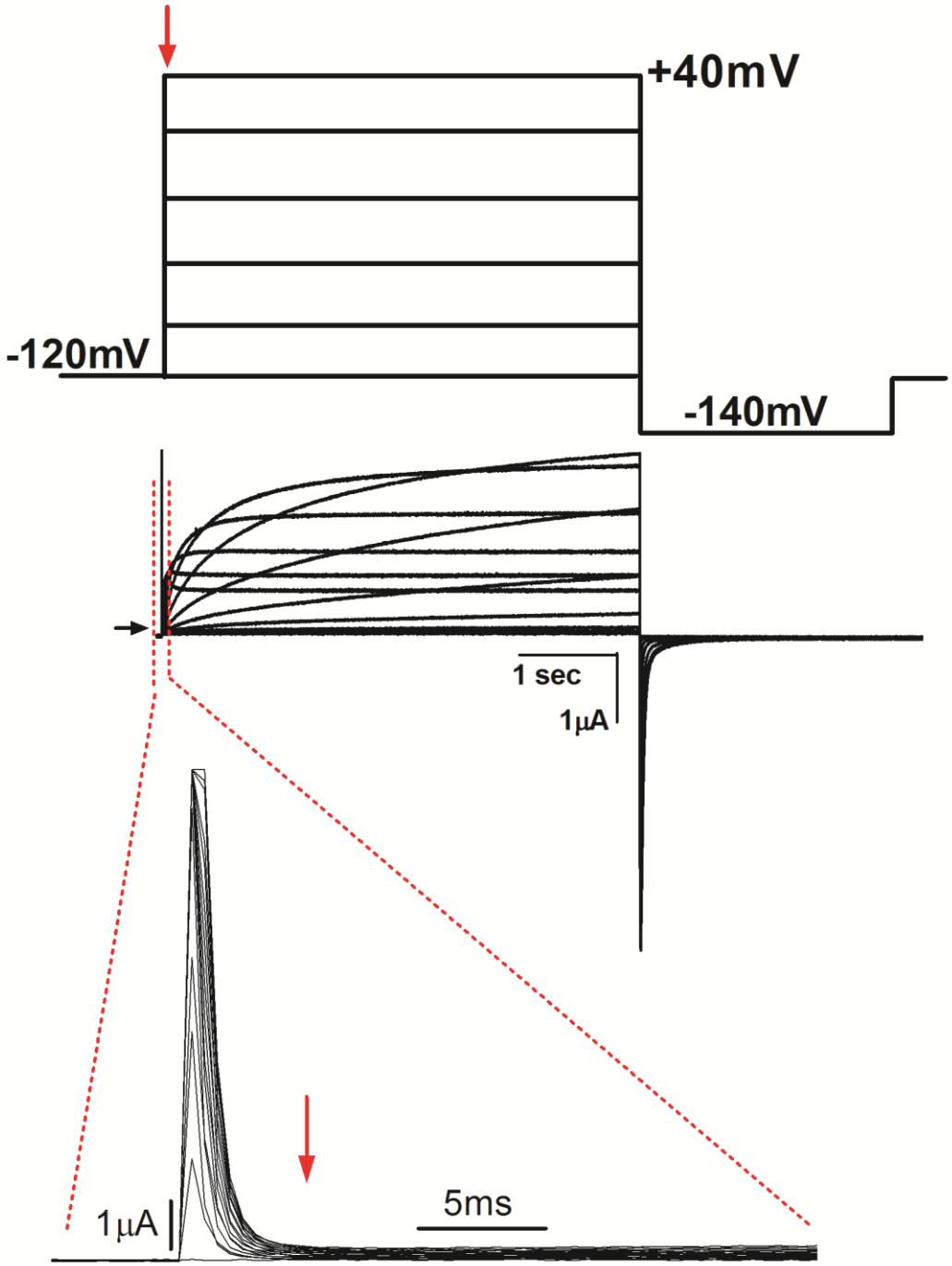

Figure 4.14. Instantaneous current was measured 5 ms after the change in voltage. The voltage protocol used is shown on top and is the same as used previously. The red arrow above the protocol indicates the point at which the instantaneous current is measured. The family of current elicited for WT hERG is shown in the middle panel under control conditions. The bottom trace shows 5ms before and 25 ms after the step from the holding potential to the test potential in much higher temporal resolution. The red arrow is placed 5 ms after the change in voltage. The capacitance transient has not been edited out and has decayed to a low baseline level within 5 ms. Note in the bottom panel that in control solution the current has not had sufficient time to activate at the 5 ms time point.

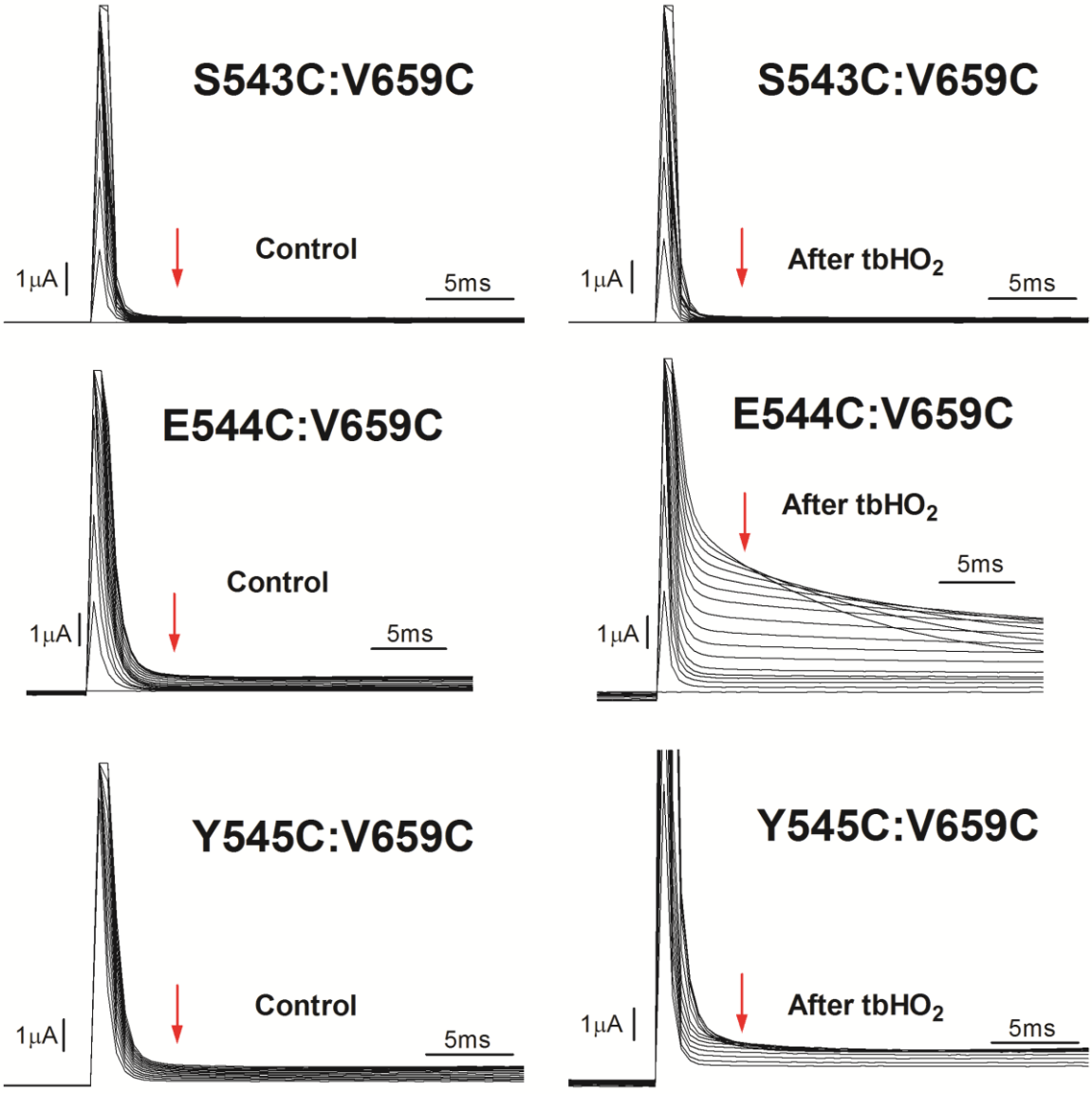

Figure 4.15. The effect of $tbHO_2$ on instantaneous current in S543C:V659C, E544C:V659C and Y545C:V659C hERG. Representative current traces at the beginning of the test pulse. Instantaneous current was quantified 5 ms (red arrow) from the start of the voltage pulses, after the decay of the capacitance transient. The control currents (before $tbHO_2$) are on the left and currents 10 minutes after $tbHO_2$ are on the right. In S543C:V659C hERG (top) there was no effect of the oxidising agent. In E544C:V659C hERG (middle) there was little current in control (left middle), but after $tbHO_2$ there was a significant current immediately after the change in voltage. This instantaneous current decayed with time due to inactivation (right, middle). Y545C:V659C hERG (bottom) shows a small instantaneous current that developed after the addition of the oxidising agent but this was small relative to changes for E544C:V659C hERG.

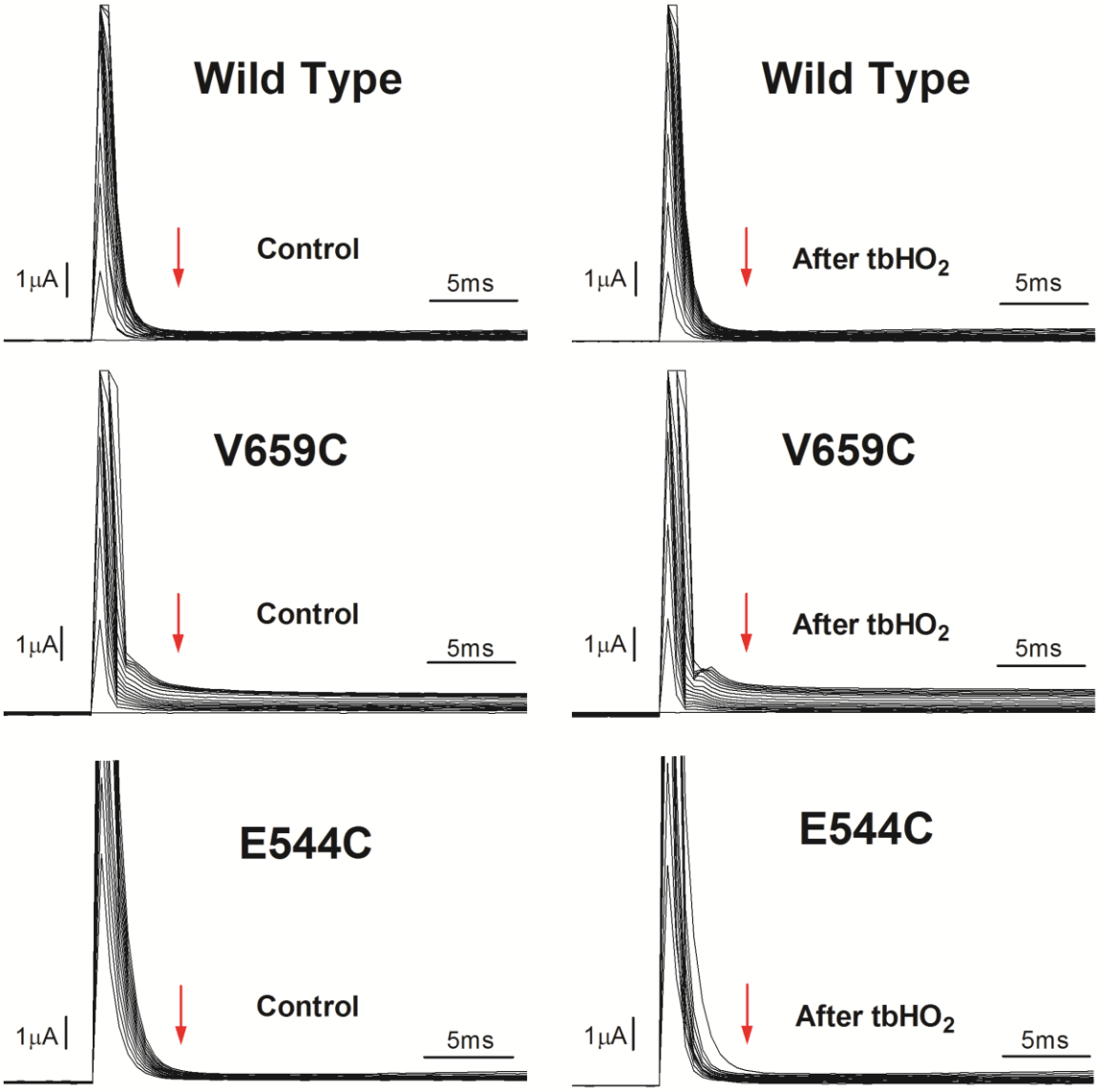

Figure 4.16. The effect of $tbHO_2$ on instantaneous current in WT hERG and E544C and V659C hERG single mutants. Instantaneous current was quantified 5 ms (red arrow) from the start of the voltage pulses, after the decay of the capacitance transient. The application of $tbHO_2$ had no effect on the instantaneous current in all three cases.

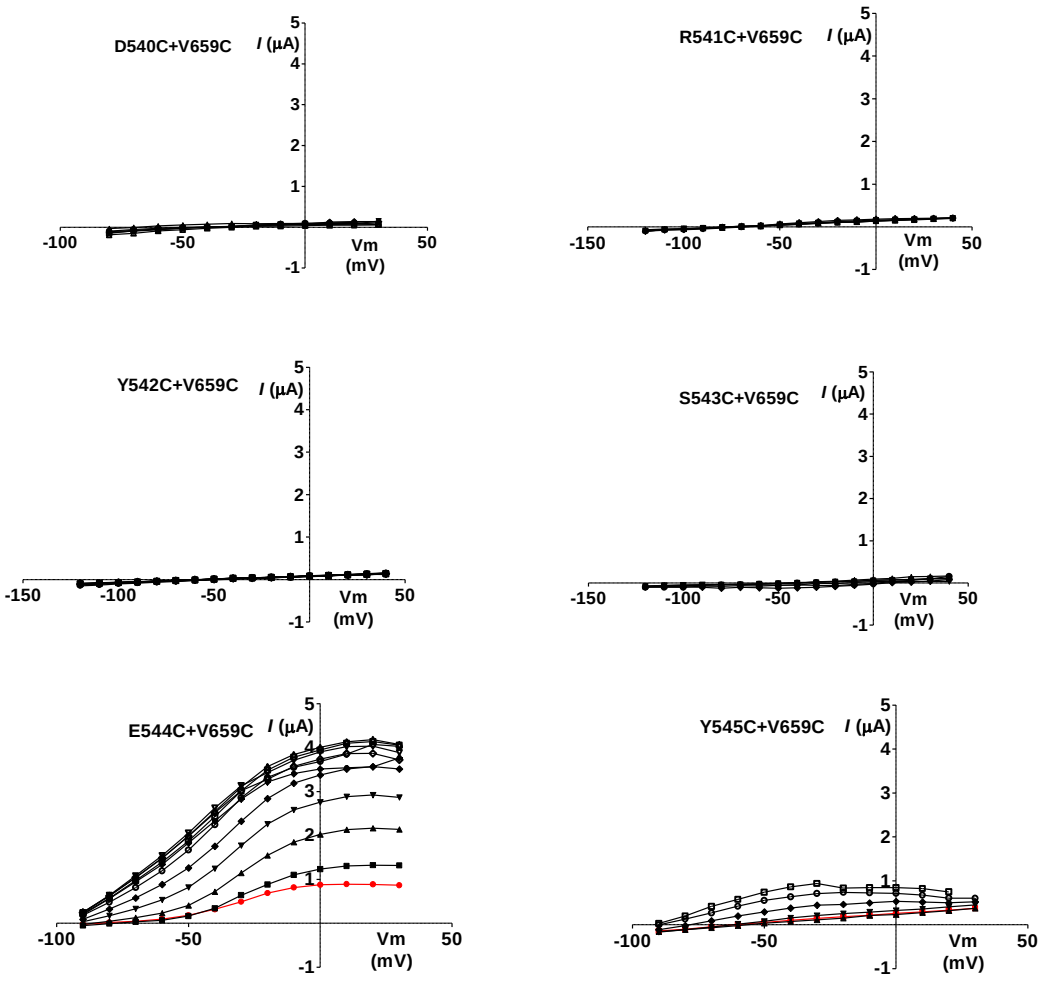

Figure 4.17. Representative instantaneous current-voltage relationships. Each symbol represents current measured at 5 ms time point and plotted against test potential. Symbols linked by a solid line are from the family of current traces during one run of the I-V protocol. The I-V protocol was repeated up to ten times on the same cell. There is a progressive increase in instantaneous current over time following $tbHO_2$ application. The $tbHO_2$ had no affect on D540C:V659C through to S543C:V659C (top 4 I-V's) but it did have an effect on E544C:V659C and to a lesser extent also on Y545C:V659C. Highlighted in red is the first, control, run of the I-V protocol.

Could endogenous cysteines in the N-terminus be interacting with the cysteines at positions 659 or 544?

It has been proposed in the past that the N-terminus may exert its effects on deactivation gating by interacting with some part of the voltage sensor or S4-S5 linker. In order to investigate if any endogenous cysteine residues in the N-terminus could be interacting with either E544C or V659C in the double mutant, the formation of disulphide bonds was investigated after deleting the N-terminus in E544C:V659C hERG. The voltage dependence of activation was measured using the same I-V protocol as used before. Figure 4.19 shows the voltage dependence of activation. NTK:E544C:V659C hERG had significant shift in the voltage dependence of activation, moving it in a negative direction. Before the oxidising reagent was applied NTK:E544C:V659C hERG threshold for activation was -60mV and the current reached maximum activation by -10mV. After the $tbHO_2$ had been applied the threshold for activation was -80mV with the current reaching maximum activation about 0 to +10mV. The slope of the activation curve was significantly shallower after the application of $tbHO_2$.

As a control, the effect of $tbHO_2$ was assessed on the single cysteine mutant E544C, having already been characterised in the other single mutant V659C and also on WT hERG. Figure 4.19 also shows the activation curve for E544C hERG before and after $tbHO_2$. The threshold for activation for E544C hERG before and after the application of $tbHO_2$ was between -60mV to -50mV with the currents reaching maximal activation by 0mV to +10mV. A representative current trace of E544C hERG is shown alongside the current trace of NTK:E544C:V659C hERG (fig 4.18).

Representative instantaneous current I-V graphs of NTK:E544C:V659C and E544C hERG are shown in figure 4.20 along with the graphs of WT and V659C hERG. The lack of effect on WT and on the two single mutants E544C and V659C show that the affect $tbHO_2$ has to be specific to the double cysteine mutant and is suggestive of cross linking between the two residues. The double mutant E544C:V659C with the N-terminus removed (NTK:E544C:V659C) still displayed the increase in instantaneous current (fig 4.20). These data show that the effect of the $tbHO_2$ is likely to be the result of in interaction between E544C and V659C and not other endogenous cysteine residue. Truncation of the C-terminus, where other endogenous cysteine residues are located, was not possible as these channels were not functional.

Figure 4.21 shows a bar graph with the mean increase in instantaneous current at +20mV after 10 minutes of the $tbHO_2$ application. The current measured 5 ms after the step from the holding potential to the +20mV test potential after 10 minutes of $tbHO_2$ application was divided by the current 5 ms after the voltage step to +20mV from the control I-V protocol. E544C:V659C hERG instantaneous current increased 850.4 ± 211.7 %, Y545C:V659C current increased 189.0 ± 23.3 % and NTK:E544C:V659C current increased 343.4 ± 52.4 %. Those 3 mutants all had a statistically significant increase in current compared to WT hERG (fig 4.21). The rest of the mutants were insensitive to $tbHO_2$.

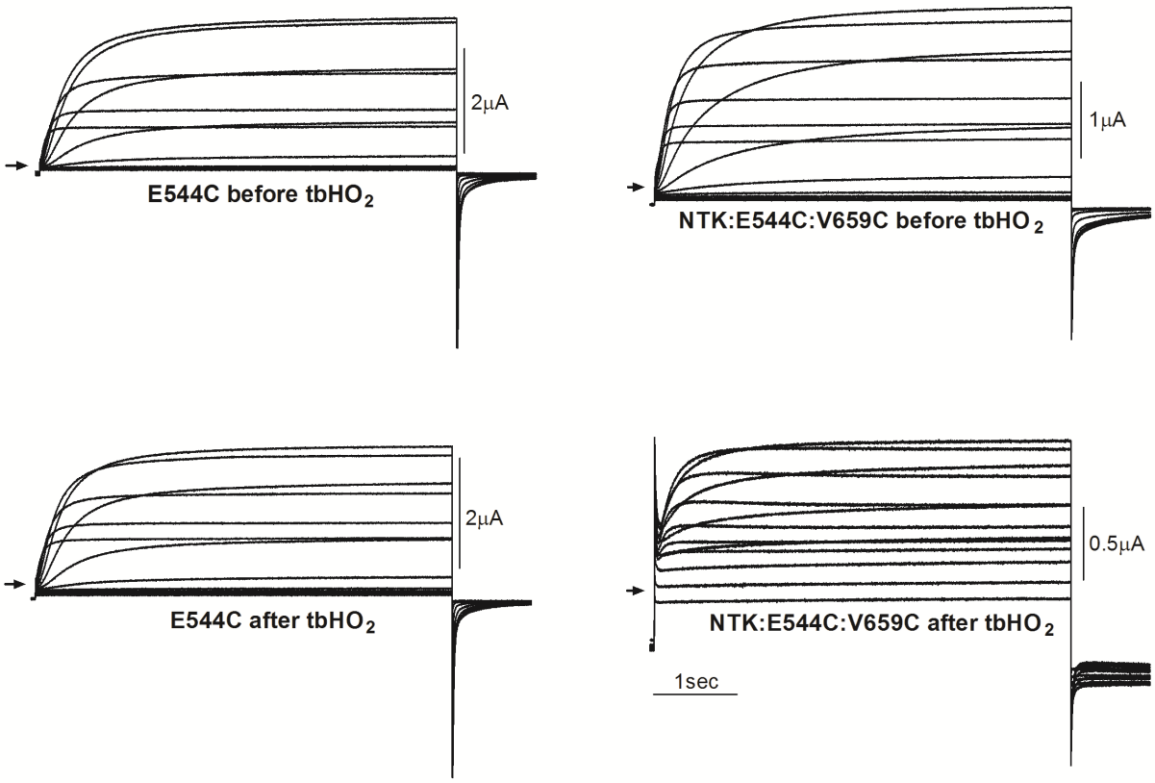

Figure 4.18 Representative current traces for E544C and NTK:E544C:V659C before and after $tbHO_2$. The currents were elicited using the previously described I-V voltage protocol. NTK:E544C:V659C hERG current before (top right) and after the addtion of $tbHO_2$ (bottom right). There is a reduction of the outward time and voltage dependent current. An instantaneous current develops after the addition of the oxidising agent. The tail currents are also affected similarly to E544C:V659C hERG. Note the difference in the current scale bar between top and bottom figures.

E544C currents before (top left) and after the addtion of $tbHO_2$ (bottom left). The oxidising agent has no effect in the currents.

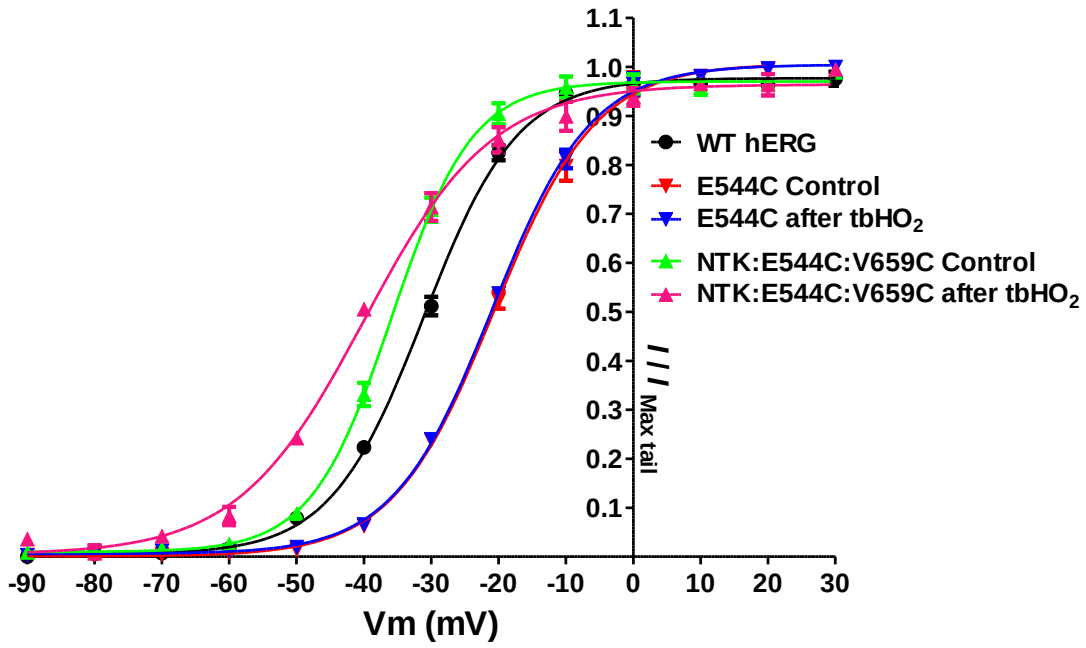

	$V_{0.5}$ of activation (mV) Before $tbHO_2$	$V_{0.5}$ of activation (mV) After $tbHO_2$	Slope (mV) Before $tbHO_2$	Slope (mV) After $tbHO_2$	n
WT hERG*	-30.7 ± 0.5	-32.3 ± 1.0	7.5 ± 0.3	7.0 ± 0.3	9
E544C	-20.7 ± 0.7	-21.0 ± 0.3	7.5 ± 0.4	7.4 ± 0.4	5
NTK E544C:V659C	-34.4 ± 0.7	-38.9 ± 0.8*	6.6 ± 0.3	10.7 ± 0.8***	5

*the after $tbHO_2$ activation curve for WT hERG is not shown in this figure but numbers are included here for information.

Figure 4.19. Activation curves for E544C and NTK:E544C:V659C before and after $tbHO_2$.

Mean normalised peak tail currents were plotted as a function of test potential and fitted with a Boltzmann function to give the voltage dependence of activation. WT hERG is shown as a reference point. $tbHO_2$ was applied for 10 minutes.

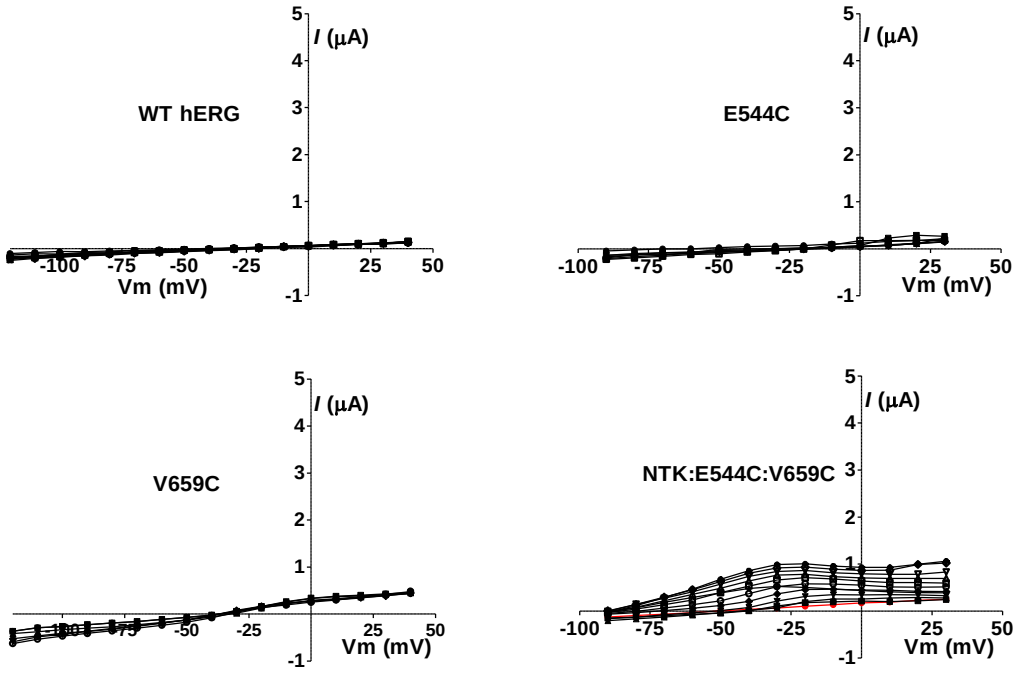

Figure 4.20. Instantaneous current-voltage relationships. The triple mutant NTK:V659:E544C is shown alongside WT and the single mutants V659C and E544C. The addition of $tbHO_2$ had a similar effect on the instantaneous I-V of NTK:E544C:V659C as in the double mutant V659C:E544C. The first 'control' I-V is highlighted red and there is an increase over time.

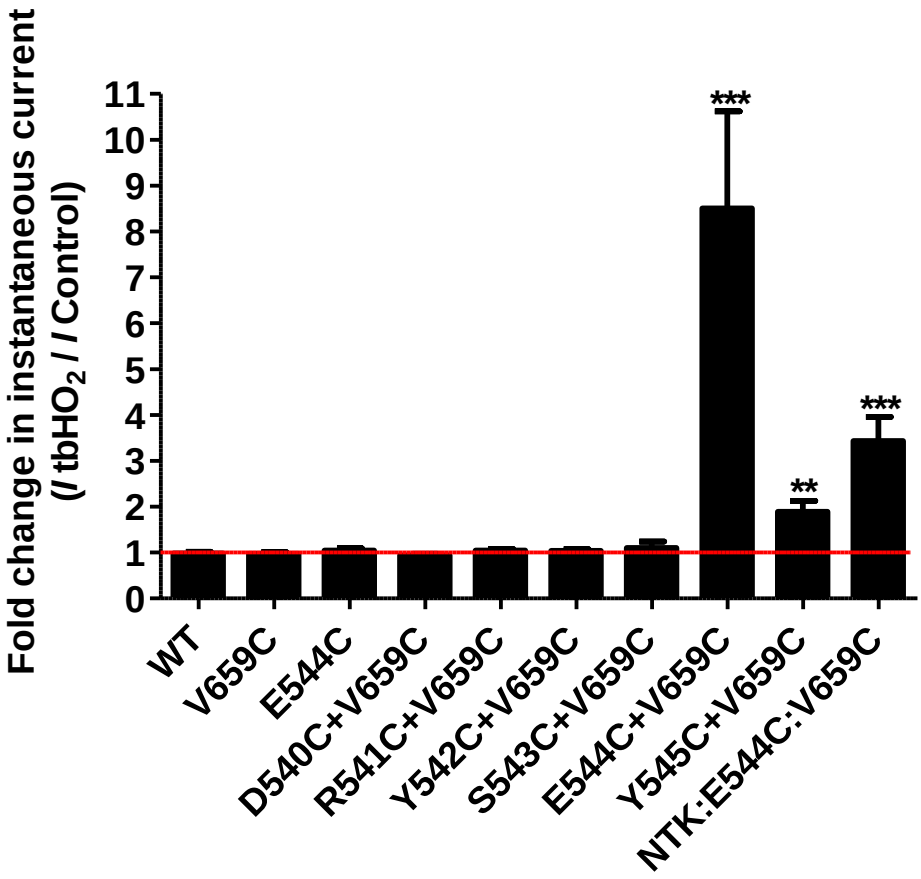

	% current of control	n
WT	97.8 ± 3.9	9
V659C	97.6 ± 2.9	4
E544C	104.4 ± 5.3	5
D540C:V659C	93.6 ± 3.5	6
R541C:V659C	104.4 ± 3.4	5
Y542C:V659C	103.5 ± 3.7	5
S543C:V659C	109.8 ± 14.4	4
E544C:V659C	850.4 ± 211.7 ***	6
Y545C:V659C	189.0 ± 23.3 **	5
NTK:V659C:E544C	343.4 ± 52.4 ***	5

Figure 4.21. Bar chart showing mean fold increase in instantaneous current at +20mV after 10 mins $tbHO_2$ in WT, V659C, E544C, S4-S5 Linker cysteine double mutants and NTK:E544C:V659C. E544C:V659C, Y545C:V659C and NTK:E544C:V659C were significantly different compared to WT. A value of 1 = no change.

Affect of DTT on the formation of disulphide bonds

Having confirmed that the increase in instantaneous current is largely confined to the double mutant E544C:V659C hERG, with a small effect on Y545C:V659C hERG, it was then necessary to confirm that the $tbHO_2$ was promoting the formation of disulphide bonds between the cysteine residue at 659 and the cysteine at positions 544 and 545.

Figure 4.22A shows recordings from an oocyte expressing E544C:V659C hERG in response to 5 second pulses to +20mV before stepping down to -140mV, to elicit inward tail currents. Panel B of figure 4.22 shows a close up view of the same currents 40 ms after the voltage step to +20mV. The membrane potential was repetitively stepped to +20mV to ensure the current had stabilised before applying the $tbHO_2$ and 10 overlapping traces in panel B show that the current was stable before the oxidising agent was applied. Panel C shows the increase in instantaneous current when the cell was repetitively stepped to +20mV in the presence of $tbHO_2$. The instantaneous current was measured at 5 ms as before and the 5 ms time point is shown by the red arrow as before.

While oxidising agents like $tbHO_2$ promote the formation of disulphide bonds between cysteines, reducing agents inhibit their formation. Oocytes expressing E544C:V549C hERG or Y545C:V659C hERG were bathed in recording solution supplemented with a reducing reagent, 20mM Dithiothreitol (DTT), for 30 minutes before electrophysiological recordings were performed.

Figure 4.23 shows the mean increase in instantaneous current measured 5 ms after stepping to +20mV in E544C:V659C hERG (top) and Y545C:V659C hERG (bottom) over time. The black traces are cells that have not been bathed in recording solution supplemented with DTT before electrophysiological were performed. In these cells there

is a steady increase in instantaneous current over time. Cells that had been bathed in recording solution supplemented with DTT (red traces) showed little effect from the application of $tbHO_2$.

It can be seen in figure 4.23 that cells which had been bathed in DTT did not display the increase in instantaneous current upon application of 0.5mM $tbHO_2$. This suggests that the oxidising agent is acting to promote the formation of disulphide bonds between the cysteines at position 659 and the S4-S5 linker, rather than having some other nonspecific pharmacological action.

The $tbHO_2$ should be promoting the formation of disulphide bonds which are covalent bonds. This means that formation of these bonds and the increase in instantaneous current should not be reversible on switching back to a recording solution without the oxidising agent. Using the same steady pulsing to +20mV protocol a control recoding was made, the cell was then perfused with $tbHO_2$ and the instantaneous current increased as before. After 7 minutes the solution was switched back to the control solution. Figure 4.24 shows that the affect of the oxidising agent was not reversible on switching from the $tbHO_2$ back to the control solution.

Overall, these results provide strong evidence that the oxidising agent is acting to form disulphide bonds, which is inhibited by the reducing agent, and the $tbHO_2$ is not having some pharmacological action on its own.

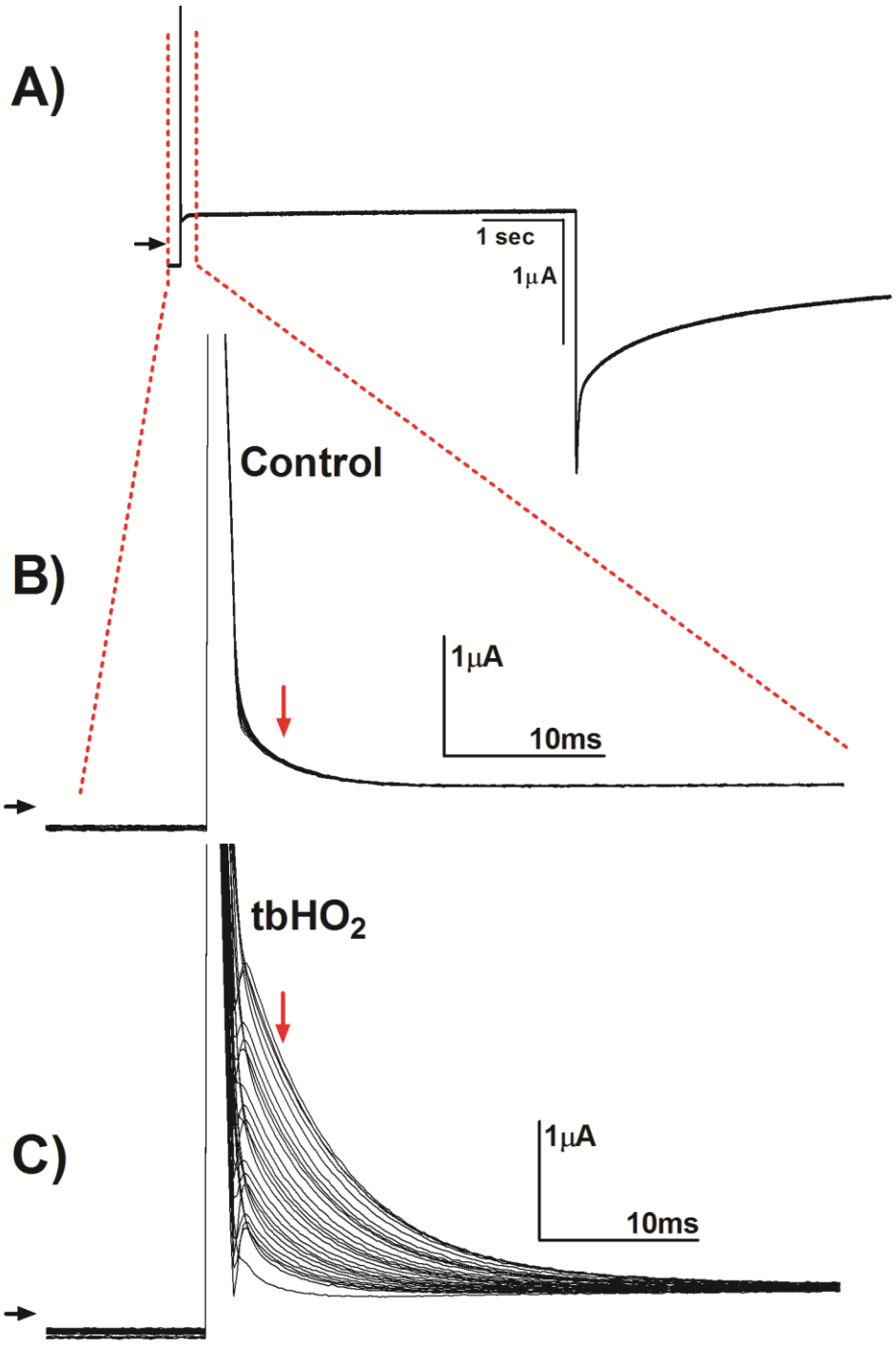

Figure 4.22. Representative current trace of E544C:V659C hERG in an untreated oocyte. The membrane potential was held at -120mV and stepped to +20mV for 5 seconds and then stepped down to -140mV for 5 seconds. In all traces the capacitance transient has not been edited out. A) Macro-view of the current in control conditions. B) Close up view of 10ms of the holding potential and first 40ms of the step to +20mV. The cell was pulsed repetitively until the current was stable. Shown are 10 sweeps which overlap because the currents are stable. C) Same close up view as in *B* but with the addition of 0.5mM $tbHO_2$. The instantaneous current increased with every new sweep of the protocol. The instantaneous current was measured 5 ms after the change in voltage as indicated by the red arrow. Cell not pre-treated with DTT.

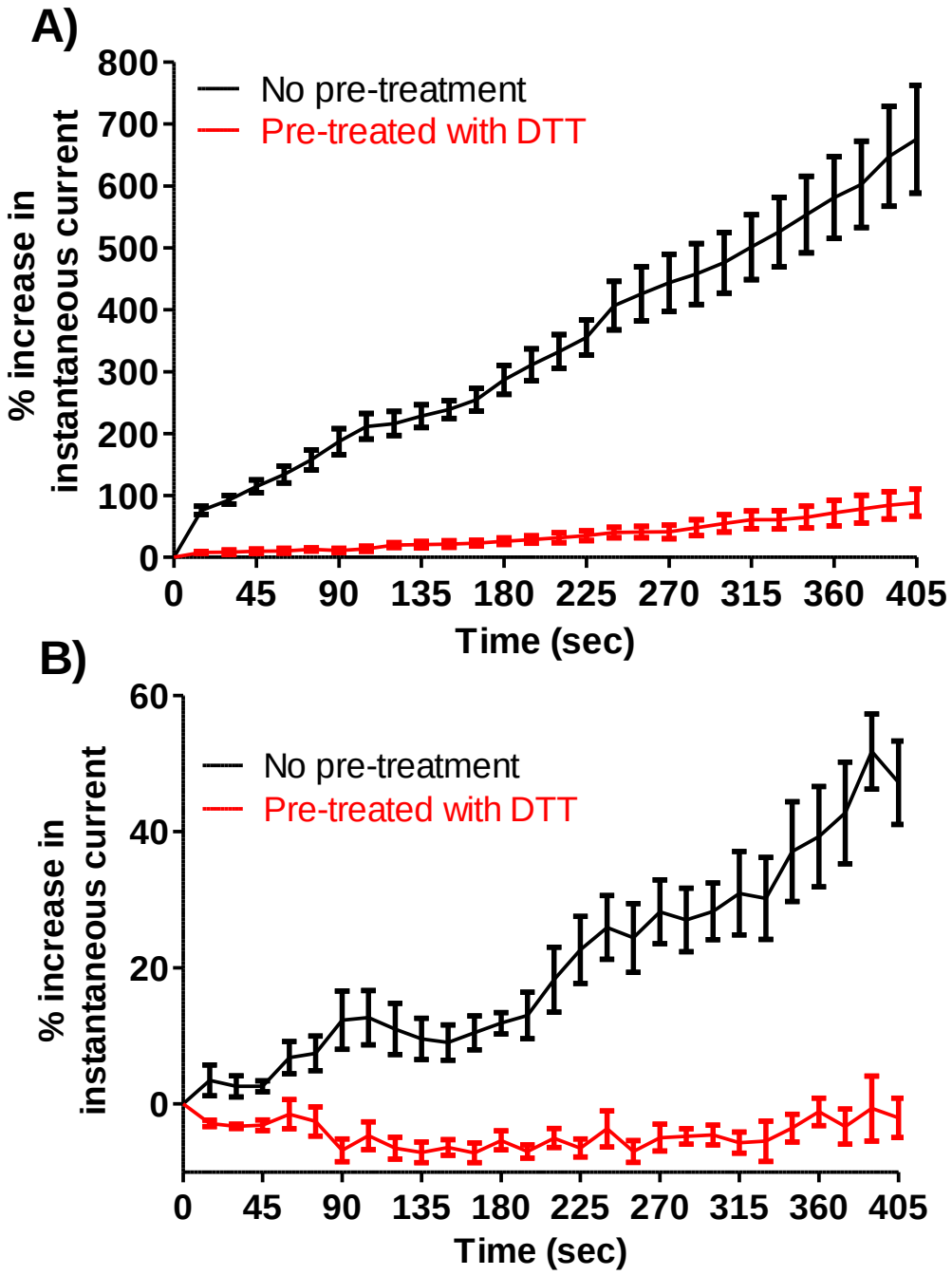

Figure 4.23. Pre-treatment with DTT stopped the increase in instantaneous current. The membrane potential was repetitively pulsed to +20 mV, first in control solution and then with $tbHO_2$. The instantaneous current was measured 5 ms after stepping to +20 mV. One group of cells were incubated in recording solution with 20mM DTT for 30 minutes before recording and they showed little effect when currents are recorded in the presence of $tbHO_2$. A) E544C:V659C hERG, B) Y545C:V659C hERG. Percentage increase in current calculated by $(I_{tbHO2}/I_{con} - 1)x100$. (E544C:V659C, No pre-treatment n=9, treated with DTT n=5) (Y545C:V659C, No pre-treatment n=5, treated with DTT n=5).

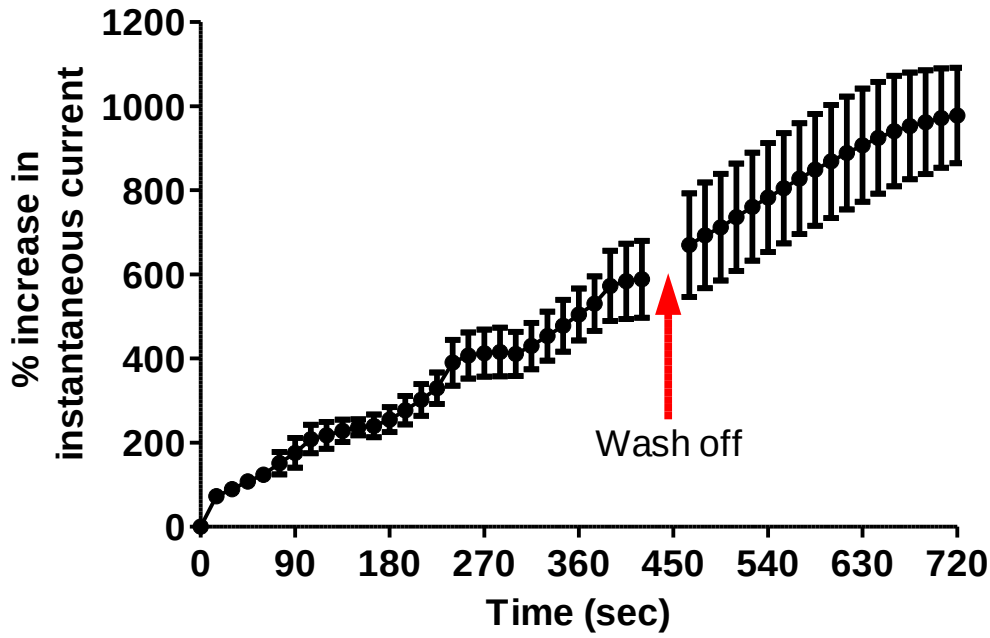

Figure 4.24. Increase in instantaneous current in E544C:V659C hERG with repetitive pulsing to +20mV. The effect of the increase in instantaneous current did not reverse on switching back to control solution. The membrane potential was repetitively pulsed to +20mV, first in control solution and then with 0.5mM $tbHO_2$. After 7 minutes the recoding solution was switched back to the control solution. The instantaneous current was measured 5ms after stepping to +20mV. (n=8)

State dependence of the interaction between Val659 and the S4-S5 Linker

Having shown there was an interaction between Val659 and the S4-S5 linker we next investigated if the interactions between 659Cys and 544Cys or 545Cys occurred while the channel was in the open or closed state. To explore if the interaction takes place in the closed state a voltage protocol was designed that minimised the time the channel spent in the open state. The membrane potential was held at -120mV and stepped to +20mV for only 100 ms to measure current amplitudes and then stepped back down to the holding potential. The instantaneous current was measured 5 ms after the step to +20mV. Two measurements of the instantaneous current were taken in control solution and then the membrane potential was held at -120mv for 5 minutes while $tbHO_2$ was applied. After 5 minutes the membrane potential was then stepped back to +20mV for 100 ms and the instantaneous current was measured again, figure 4.25.

To assess the possible open state interaction the membrane potential was again held at -120mV then stepped to +20mV for 1 second. Two control measurements were taken then the membrane potential was maintained at +40mV to maximally activate the channels while $tbHO_2$ was applied for 5 minutes. The membrane potential was then stepped down to -140mV for 10 seconds to deactivate the current and the instantaneous current subsequently measured with a depolarisation to +20mV.

The bar graph in figure 4.26 shows that for E544C:V659C hERG the instantaneous current increased 178.2 ± 5.2 % in the open state but only 14.1 ± 5.6 % in the closed state and for Y545C:V659C hERG the instantaneous current increased 117.8 ± 11.6 % in the open state and only 0.9 ± 1.1 % in the closed state. These data suggest that the interaction between 659Cys and 544Cys or 545Cys occurred in the open state.

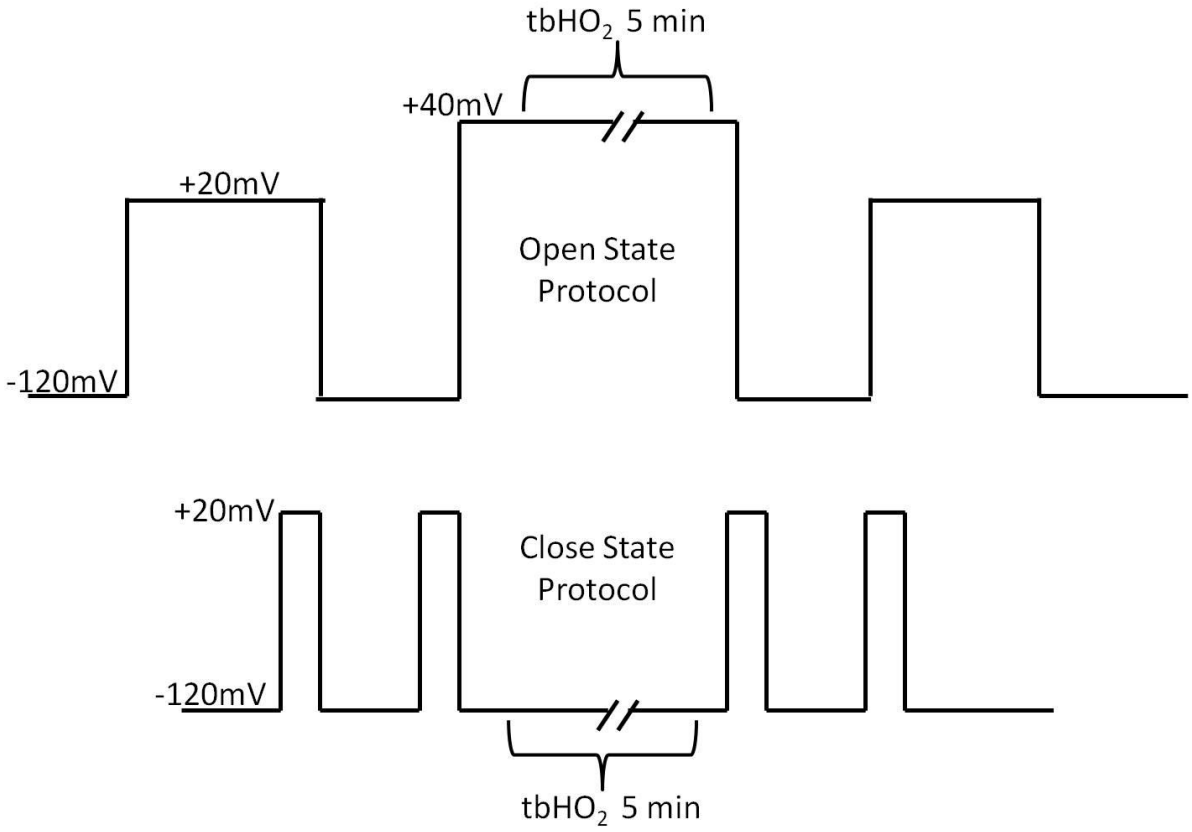

*protocols not drawn to scale

Figure 4.25. Voltage protocols used to assess the state dependence of the interaction between E544C & V659C and also Y545C & V659C.

To assess the possible open state interaction the membrane potential was held at -120mV then stepped to +20mV for 1 second. Two control measurements were taken then the channel was held in the open state at +40mV while $tbHO_2$ was applied for 5 minutes. The membrane potential was then stepped down to -140 for 15 seconds to deactivate the current so it could then be activated and the instantaneous current measured.

To assess a possible closed state interaction the membrane potential was stepped from a holding potential of -120mV to +20mV for 100ms. Two control measurements were taken then the channel was held closed at -120mv for 5 minutes while $tbHO_2$ was applied. The membrane potential was then stepped back to +20mV and the instantaneous current was measured again.

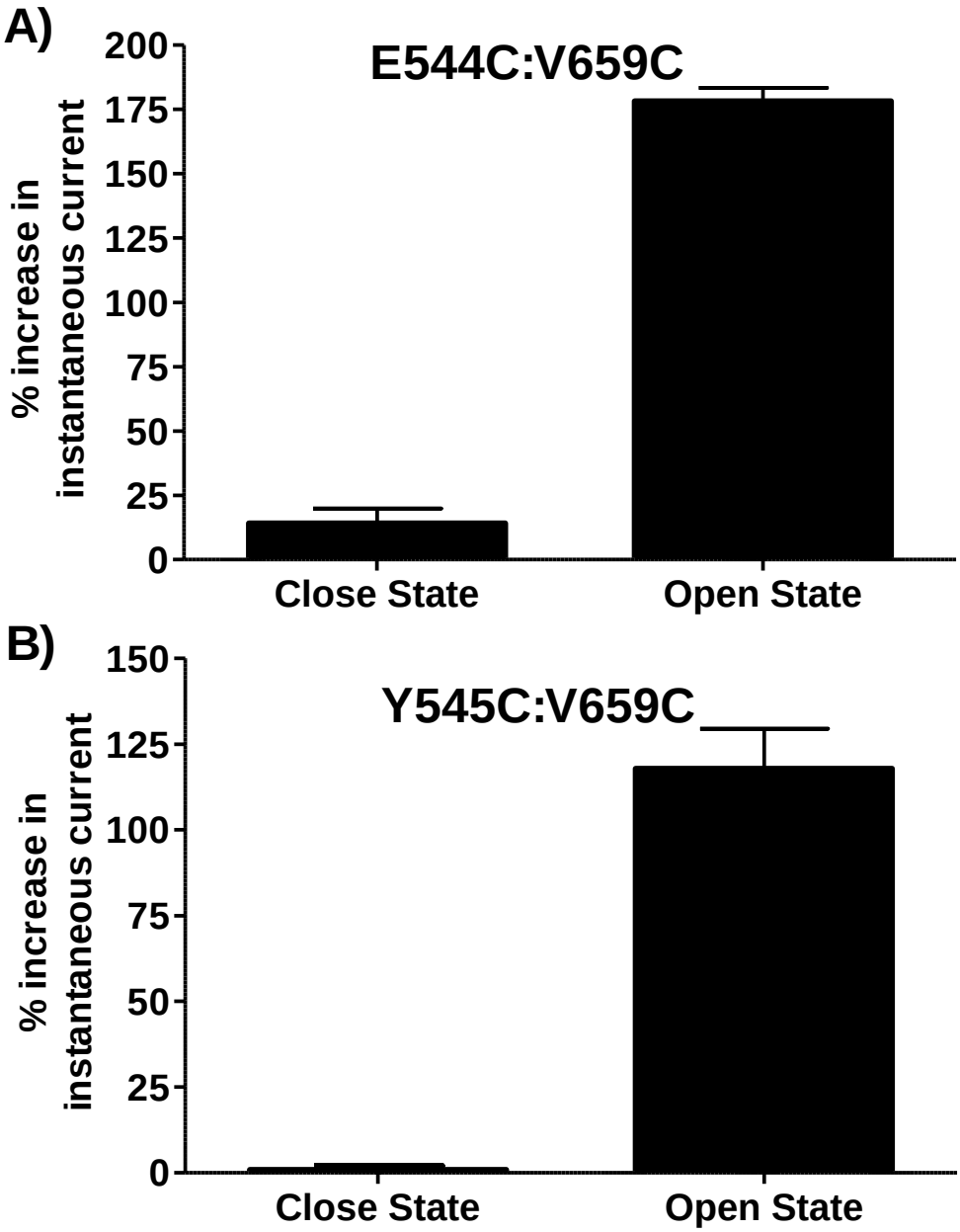

	% increase in instantaneous current	
	Close State	**Open State**
E544C:V659C	14.1 ± 5.6	178.2 ± 5.2
Y545C:V659C	0.9 ± 1.1	117.8 ± 11.6

Figure 4.26. Interaction between S4-S5 linker and Val659 occurs in the open state. The state dependence of the interaction was investigated using the voltage protocols in figure 4.25. The interaction between E544C & V659C (A) and also Y545C & V659C (B) occurs in the open state. (E544C:V659C - close state n=6, open state n=4) (Y545C:V659C - close state n=5, open state n=5).

Discussion

Val659 is crucial for the normal deactivation gating in hERG. V659A was identified during a study into drug binding to deactivate very slowly (Mitcheson et al, 2000a). In order to investigate the role of Val659 in normal deactivation gating it was mutated to a series of other residues. When Val was mutated to Ile and Phe there was a small slowing of deactivation. The mutation of Val659 to Cys which has a smaller side chain than Val causes a marked slowing of deactivation. The mutation of Val659 to Ala, which has a smaller side chain than Cys, resulted in a channel with even slower deactivation kinetics than V659C. Mutation to glycine which has the smallest side chain of all amino acids resulted in a channel that lacks voltage dependant activation or deactivation gating but retained inactivation gating, suggesting that the activation gate is no longer coupled to the voltage sensing domain. These results suggest a correlation between side chain volume at 659 and coupling with the voltage sensing domain. Two different mechanisms may explain slower deactivation seen in the Ile and Phe mutants versus the Cys, Ala and Gly mutants. The small slowing of deactivation seen in V659I and V659F may be due to the slightly larger side chains of Ile and Phe sterically hindering the tight packing of the S4-S5 linker against S6. However, as the size of the side chain is reduced to Cys then Ala and then Gly the rate of deactivation becomes progressively slower as the pore becomes uncoupled from the S4-S5 linker. Importantly, these mutants demonstrate that the pore of hERG channels is stable in the open state and that electromechanical coupling to the voltage sensor is required for channel closure rather than channel opening.

To probe if Val659 couples the activation gate to the voltage sensor a series of double cysteine mutants were engineered. They show that V659C forms disulphide bonds with

E544C and Y545C in the S4-S5 linker in the channel open state. Although the disulphide bond formation was favoured between E544C and V659C and more so than between Y545C and V659C, it is likely that the main interaction in the WT channel would be a hydrophobic interaction between Tyr545 and Val659. The nature of a hydrophobic interaction between tyrosine and valine is more logical than an interaction between glutamic acid and valine. Tyrosine is hydrophobic and naturally wants to be in the interior of the protein whereas glutamic acid is hydrophilic in nature so is more likely to be located facing the cytoplasm of the cell rather than face toward the inside of the channel protein. The reason for V659C having the main interaction with E544C rather and Y545C is that the introduction of 2 cysteine residues, one in the helix of S6 and one in the helix of the S4-S5 linker could alter the orientation of these residues so as to promote the interaction at 544 more than at 545. Disulphide bonds can only be formed over a very short distance (5Å) and the side chains of the two cysteines must be facing each other in the correct orientation so if the introduction of the cysteines causes even a slight reorientation of either helix then it could favour the formation of one interaction over another. A limitation of the cross-linking approach is that it only provides evidence that side chains come into close proximity and does not prove a direct interaction.

The increases in instantaneous current I-V (figure 4.17) in E544C:V659C was gradual and increases with every new sweep of the I-V protocol. This increase does not continue indefinitely as current reaches a saturation point where there is no more increase in the instantaneous current. The size of the instantaneous current indicates that a high proportion of the channels cross-link to stabilise the open state and that cross-linking is not a rare event.

The results presented here indicate that the channel is locked in an open state through an open state interaction between residues 659 and 544/545. What is unclear is what is happening to S4 in terms of whether it is still moving across the membrane in response to changes in voltage. An obvious follow up experiment would be to measure if the gating current is reduced in the double mutant E544C:V659C after the addition of $tbHO_2$. A reduction in gating charge would suggest that the voltage sensor has been immobilised.

The results presented here sit well in the existing body of published hERG literature. It has previously been established that Asp540 at the other end of the S4-S5 linker couples to Arg665, in S6, in the closed state (Ferrer et al, 2006). Presented here are data that show Val659 in S6, which is two turns of a helix away from Arg665, couples to Tyr545 in the S4-S5 linker, which is two turns of a helix away from Asp540, and this occurs preferentially in the open state. The data advances the notion that electromechanical coupling, in hERG at least, is a dynamic process in which the S4-S5 linker forms one discrete interaction with the activation gate that stabilises the closed state (D540 with R665) and conformational changes in the voltage sensor lead to another discrete interaction (V659 with Y545) that occurs in the open state and is required to mediate channel deactivation.

The increased instantaneous current observed in NTK:E544C:V659C was not as large as in E544C:V659C. As proposed in the first results chapter, the N-terminus interacts with the cNBD in the C-terminus and this interaction causes a rearrangement which is transduced via the C-linker to the activation gate and modulates deactivation. Val659 is located in the region of the activation gate. Removing the N-terminus means that there is no interaction with the cNBD and thus no resulting modulation of the activation gate,

this could result in Val659 no longer being in an optimal position to interact with the S4-S5 linker so upon the application of the oxidising agent a smaller proportion of the channel present in the membrane form disulphide bonds and thus there was a smaller increase in the instantaneous current. In other words, the eag domain has an allosteric effect that favours electromechanical coupling between the activation gate and the voltage sensor.

In the state dependence experiments there was an increase in instantaneous current of around 200% whereas in experiments where $tbHO_2$ was applied during repetitive pulsing there was a larger increase. In the state dependence experiments the membrane potential was held constant at +40mV for 5 minutes, whereas in the DTT and wash-off experiments the membrane potential was repetitively pulsed to +20mV and so cycled through open, closed and inactivated states. It seems feasible that at +40mV the channel is not optimally positioned to form disulphide bonds. Another explanation is there may be a frequency dependence to the interaction and the cycling in and out of the open state facilitates the formation of disulphide bonds or that the disulphide bond is formed during a pre-open state. Further experiments are required to investigate the voltage and/or frequency dependence of this interaction.

Before the structure of Kv 1.2 showed that the S4-S5 linker formed a cuff around the lower half of S6 (Long et al, 2005) there was already some mutagenesis evidence to suggest that this might be the sight of coupling of voltage sensor movement to channel gating. Chen et al, 2001 showed that the S4-S5 linker mutation Y331S in HCN2 channels that also contained a mutation in S4 that prevented channel opening (R318Q) resulted

in a constitutively open channel. They went on to show that Arg339 in the S4-S5 linker forms a salt bridge with Asp443 in the C-linker, just below S6 (Decher et al, 2004). Other work from the same lab proposed a charge interaction between the S4-S5 linker and the lower part of S6 that accounted for the strange properties of the D540K hERG mutant that can open with membrane hyperpolarisations as well as depolarisations (Tristani-Firouzi et al, 2002).

In experiments by Lu et al, 2001 and 2002 they created a chimera between Shaker and KcsA. The S5, selectivity filter and S6 of KcsA was transplanted into Shaker. This construct only gave rise to functional currents if the lower portion of S6 remained that of the Shaker channel and not KcsA. Further experiments by Labro et al, 2008 transferred the S4-S5 linker of Kv2.1 into the Kv1.5 channel but this construct did not yield functional currents. The construct could be rescued by also transferring the lower end of S6 from the Kv2.1 channel into Kv1.5.

In addition to the crystal structure of Kv1.2 showing the S4-S5 linker lying across the activation gate the recently solved crystal structure of NavAb (Payandeh et al, 2011) also shows the S4-S5 linker crossing the S6 around the activation gate suggesting that this is a conserved mechanism for coupling movement of the voltage sensor to gating in all voltage gated ion channels.

The structural information together with functional mutagenesis data provide strong evidence that coupling of the S4-S5 linker to the lower part of S6 underlies gating in voltage gated ion channels.

Chapter 5

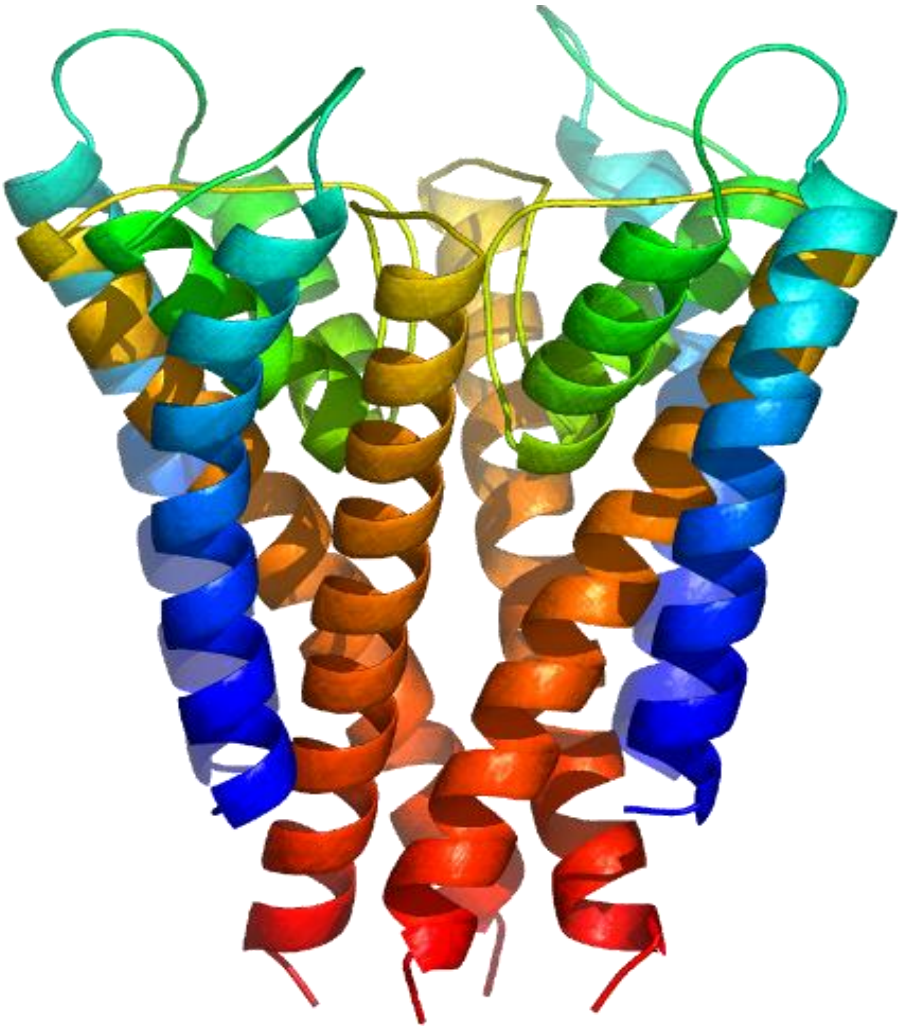

Insights into hERG channel pharmacology from studies on derivatives of E-4031

Introduction

Since the discovery in the mid 1990's that hERG is the pore forming subunit that conducts the I_{Kr} current of the cardiac action potential it has been the focus of intensive study. A large part of this research has focused on the pharmacology of hERG as a number of structurally diverse drug molecules can block hERG, reduce I_{Kr} and lead to arrhythmias. The main reasons that so many different drugs block hERG with high affinity is that the inner cavity of hERG is lined by aromatic and polar residues and it is thought to be larger than most other Kv channels due to the lack of a Pro-X-Pro motif.

For over a decade now the drug trapping hypothesis has been at the centre of why so many drugs can block hERG (Mitcheson et al, 2000b). Drug trapping occurs when the intracellular activation gate closes behind drugs that have entered the inner cavity (figure 5.1). It provided a mechanism for why recovery from block of hERG blockers was slow. A further implication was that it influenced drug potency by generating a high concentration of drug at the receptor. Direct evidence of drug trapping came from studying a hERG mutant with very unusual activation properties. The activation gate normally opens on depolarisation of the membrane. However, the mutant D540K hERG has the unusual property of also opening upon hyperpolarisation of the membrane (Mitcheson et al, 2000b). In D540K hERG experiments, when the membrane potential was depolarised to 0mV to open the activation gate, the channel was blocked by the drug. The drug was then trapped by closure of the activation gate on repolarisation to -90mV in the same way as with the WT hERG channel. The membrane potential was then hyperpolarised to -160mV and unlike the WT hERG channel it recovered from block as the drugs left the inner cavity because the activation gate has been opened.

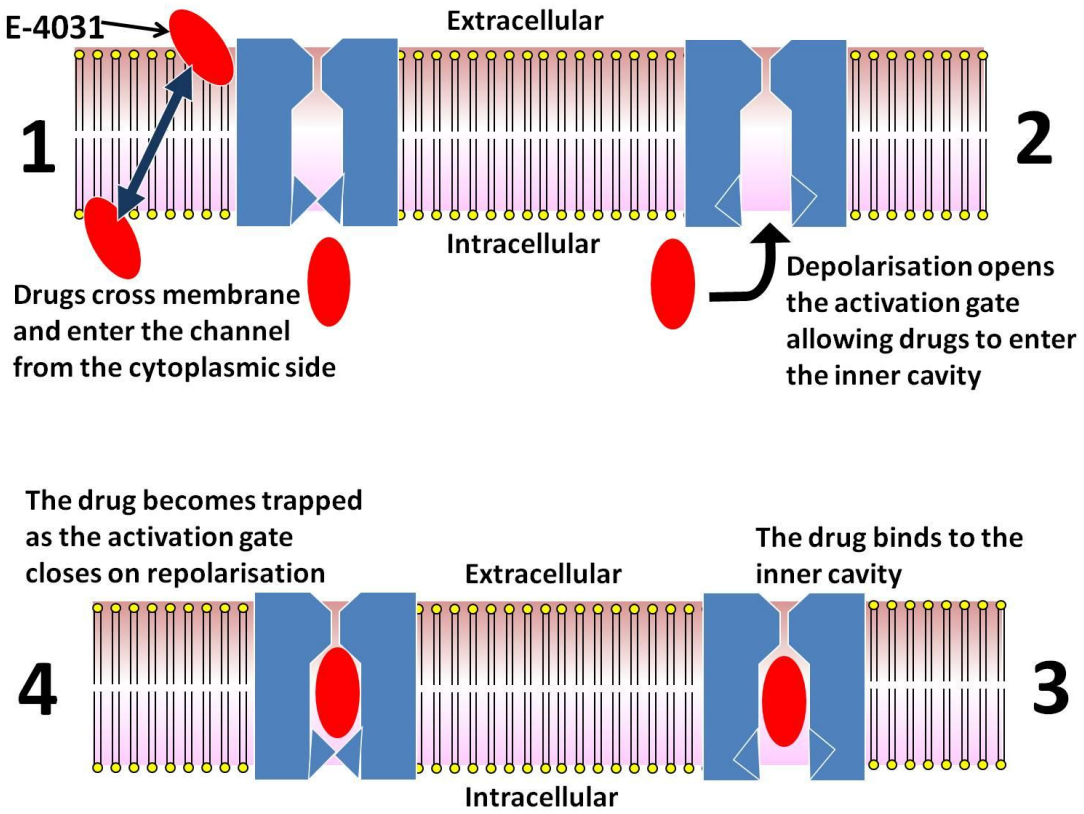

Figure 5.1. Drug bind to the inner cavity and are trapped on closure of the activation gate. 1) Drugs need to cross the cell membrane in order to reach the binding site in the inner cavity. 2) When the cell is depolarised the activation gate opens. 3) The drug enters into the inner cavity. 4) When the cell repolarises the drugs are trapped behind the activation gate.

Inactivation gating is known to be important for drug binding to hERG. hERG channels share the same drug binding residues in the inner cavity as EAG channels, however EAG channels are far less sensitive to block than hERG. A crucial difference may be the lack of inactivation in EAG channels. hERG channels exhibit C-type inactivation. Like C-type inactivation in other K_v channels this is thought to be a constriction of the selectivity filter to make it impermeable to K^+. However, the onset and recovery from inactivation is significantly faster and more voltage dependant than other Kv channels (Spector et al, 1996b; Smith et al, 1996). Mutations to EAG channels that introduce C-type inactivation

increase sensitivity to drug block (Ficker et al, 2001). Conversely, mutations that remove C-type inactivation in hERG (e.g. G628C:S631C) exhibit decreased sensitivity to drug block (Ficker et al, 1998). It is thought that inactivation in hERG causes a repositioning of inner cavity residues from a position where they are not optimally arranged to bind drug to one where there are (Chen et al, 2002). Work on Shaker has shown that during inactivation not only is there a rearrangement of amino acids around the outer mouth of the channel but there is also a rearrangement of residues in the inner cavity that alter the affinity of the channel for inhibitors such as TEA (Panyi & Deutsch, 2007).

E-4031 is a well characterised, potent hERG channel blocker. E-4031 binds to the inner cavity residues and exhibits slow recovery from block when the activation gate closes. In order to investigate the importance of trapping for drug potency we had two series of derivatives of E-4031 made that got progressively longer. The aim of developing the derivatives of E-4031 was twofold. One was to use them as a "molecular ruler" to measure the size of the inner cavity. Our hypotheses were that compounds that were too long to fit in the inner cavity would exhibit foot in the door type block rather than drug trapping. This could then be used to produce information about the size of the inner cavity. Secondly, to investigate if making drugs longer could be a means to reduce potency.

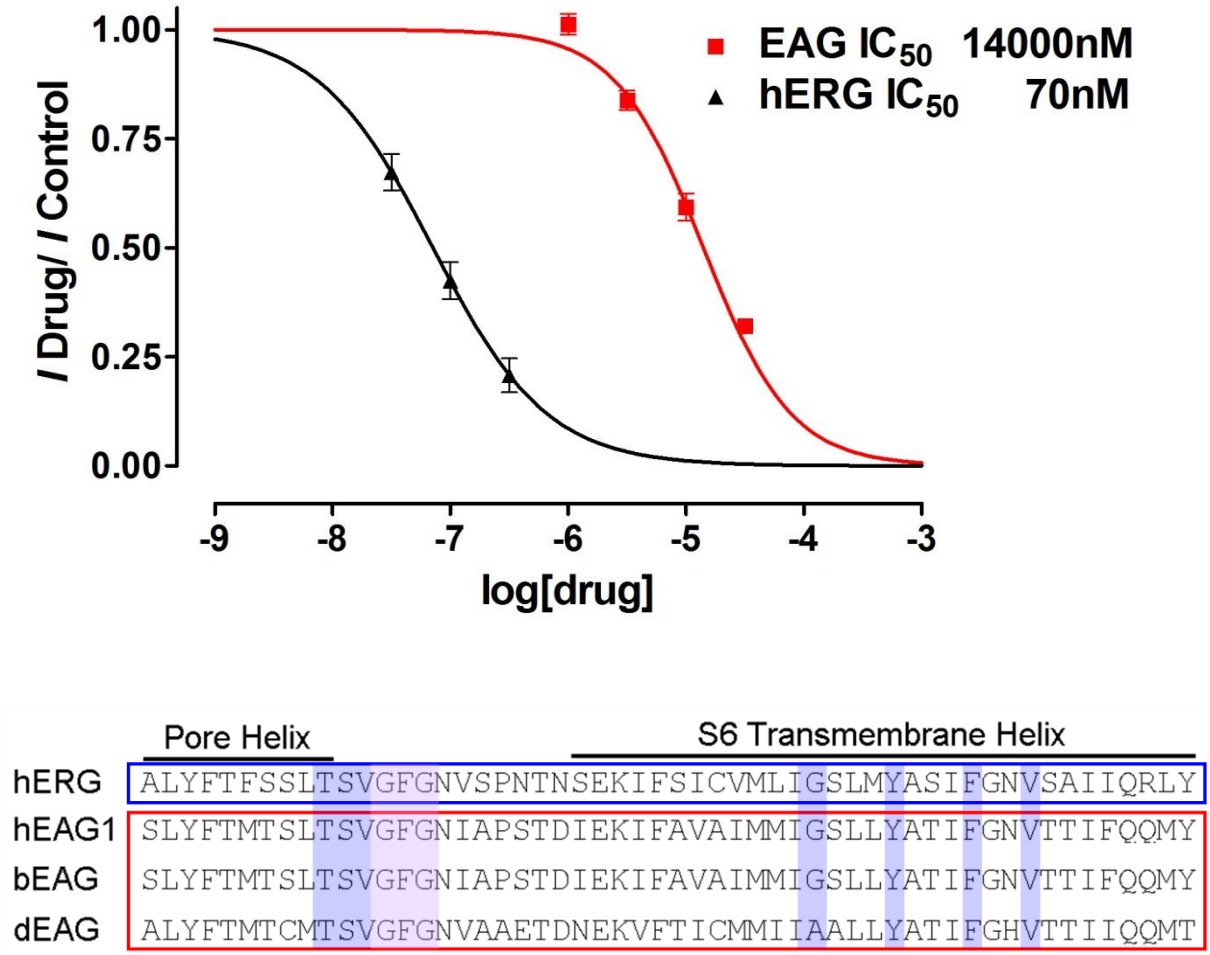

Figure 5.2. EAG is far less sensitive to block than hERG even though the key drug binding residues are conserved. The top panel shows the IC_{50} of Cisapride (a well known hERG blocker) on WT hERG and WT EAG. Cisapride is far less potent on EAG than hERG. The bottom panel is a sequence alignment of the selectively filter and S6 of hERG and EAG channels. The key aromatic residues Tyr and Phe in the middle of S6 are conserved. Also conserved are the residues at the base of the pore helix that are important in drug binding.

Results

Structure of E-4031 derivates

Derivatives of E-4031 were custom made by Chemical Synthesis Services Ltd and provided courtesy of Novartis Institute for Biomedical Research, Horsham, UK. The length of the derivatives was increased in two different ways. Either the length of the 'linker' between the piperidine and phenyl ring was changed or the length of the alkyl chain on the phenyl ring at the 'tail' of the molecule was increased (fig 5.3). The nomenclature used to describe the derivatives is L*x*T*x*, where L*x* refers to the number of carbons on the linker and T*x* refers to the number of carbons on the tail (e.g. L6T0 has 6 carbons in the linker and 0 in the tail). Due to difficulties in the chemical synthesis in lengthening E-4031 derivatives it was necessary to make two modifications to the compound. The methanesulphonamide group was substituted for a chlorine atom and the pyridine group was substituted for a phenyl group. Other high potency hERG channel blockers, such as clofilium and sertindole, have the chlorine atom in the same position so the chlorine atom substitution was envisaged to have a negligible impact on the potency. It was not known what the effect of removing the nitrogen from the pyridine would have.

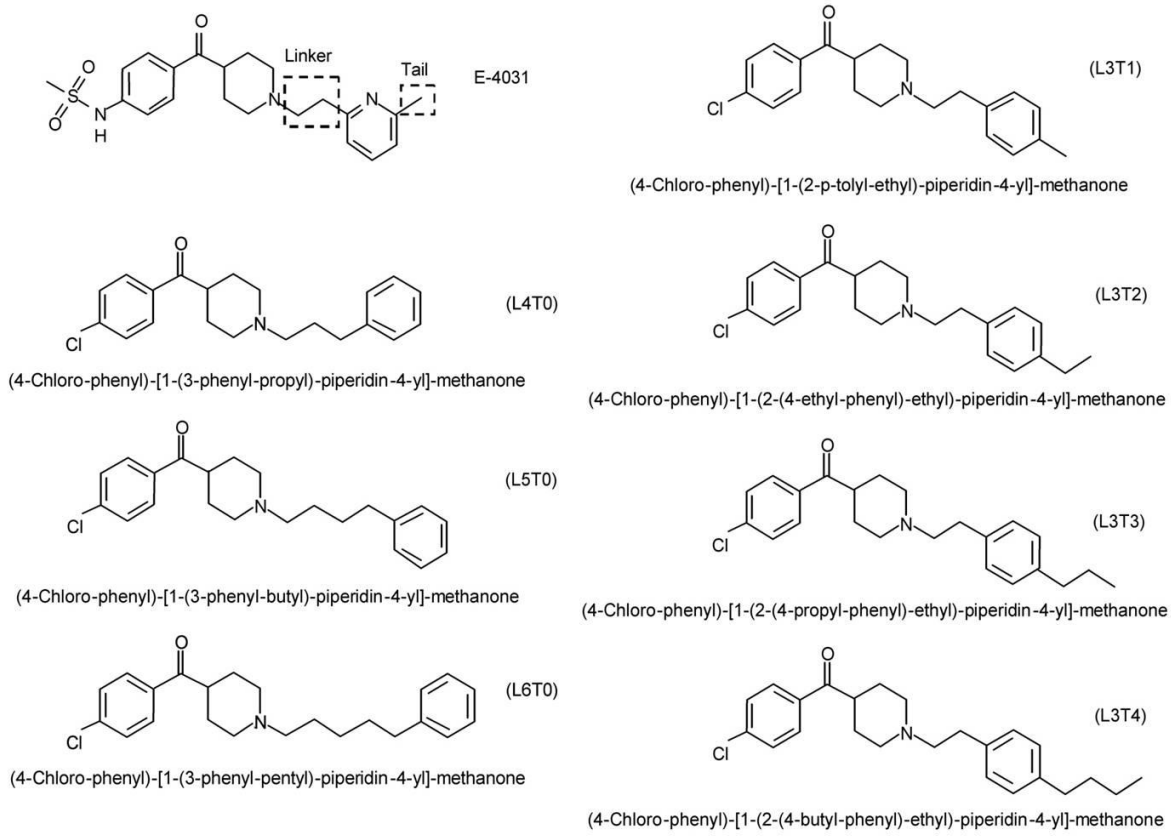

Figure 5.3. Chemical structures of E-4031 and derivatives.

E-4031 (top left) was increased in length by adding carbons to either the linker (left hand column) or tail (right hand column) of the molecule. The positions of the linker and tail regions are highlighted in the E-4031 structure (top left).

Concentration response experiments

In order to establish the potency of these new derivatives, increasing concentrations of the compounds were applied and the corresponding level of block measured. The following open state voltage protocol was used to assess drug block of hERG; the membrane potential was held at -90mV and stepped to 0mV which opens the channel, after 5 second the membrane potential was stepped down to -70mV for 400ms to elicit tail currents before returning to the holding potential (fig 5.4). This pulsing protocol was run repeatedly with only 600ms spent at the holding potential between sweeps. This was done to maintain channels in the open state for the majority of the time. A control value was measured in the absence of drug before repeating the protocol with increasing concentrations of drug. The drug solution was applied to the cell for three minutes at each concentration before recording started to allow the drug to equilibrate across the oocyte membrane. Leak current was measured after each drug concentration had been applied, by pulsing from the holding potential to -70mV. The peak tail current (after steady state current inhibition) was measured, leak current subtracted, and normalised to the peak tail current from the control. The resulting concentration-response relationships were fitted with a Hill function to obtain the IC_{50} value and the Hill slope. Figure 5.4 shows the progressive decrease in tail current amplitude with increasing concentrations of drug. Higher concentrations of E-4031 were required to achieve the same level of block as the derivatives hence the derivatives are more potent than the parent compound. The voltage protocol is shown underneath the current trances. Concentration-response curves for all E-4031 derivatives are shown in figure 5.5. Because of the log scale the pIC_{50} ± SEM is shown with the equivalent nano-molar concentration given alongside. Statistics were performed on the pIC50's.

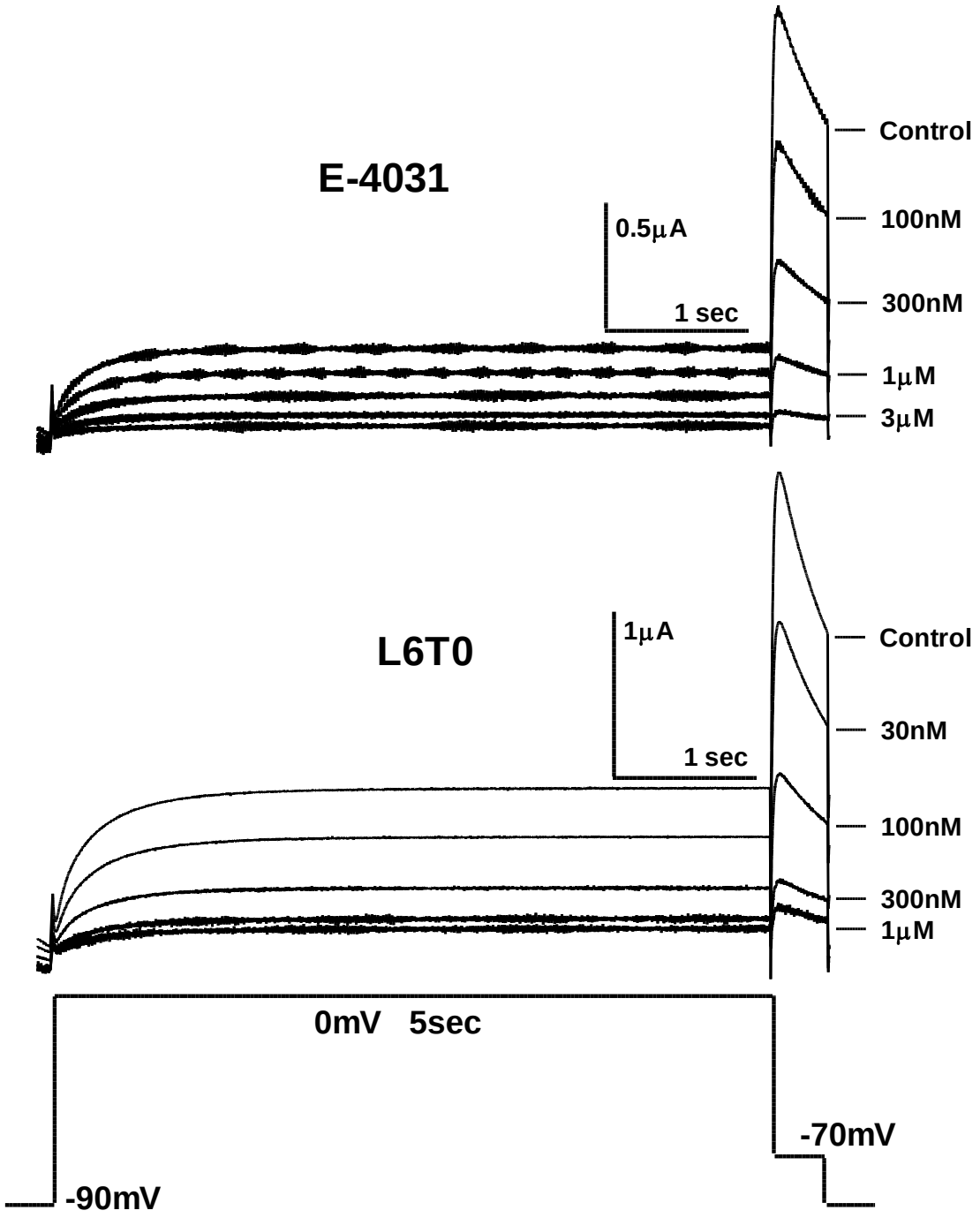

Figure 5.4. Representative current traces of WT hERG in control solution and after reaching steady-state block with the indicated concentrations of blockers. (E-4031 (top), L6T0 (middle) and voltage protocol (bottom)). Block was achieved by repetitively stepping to 0mV. The hERG current amplitude was reduced in a concentration dependant manor. Higher concentrations of E-4031 were required to achieve the same level of block as L6T0.

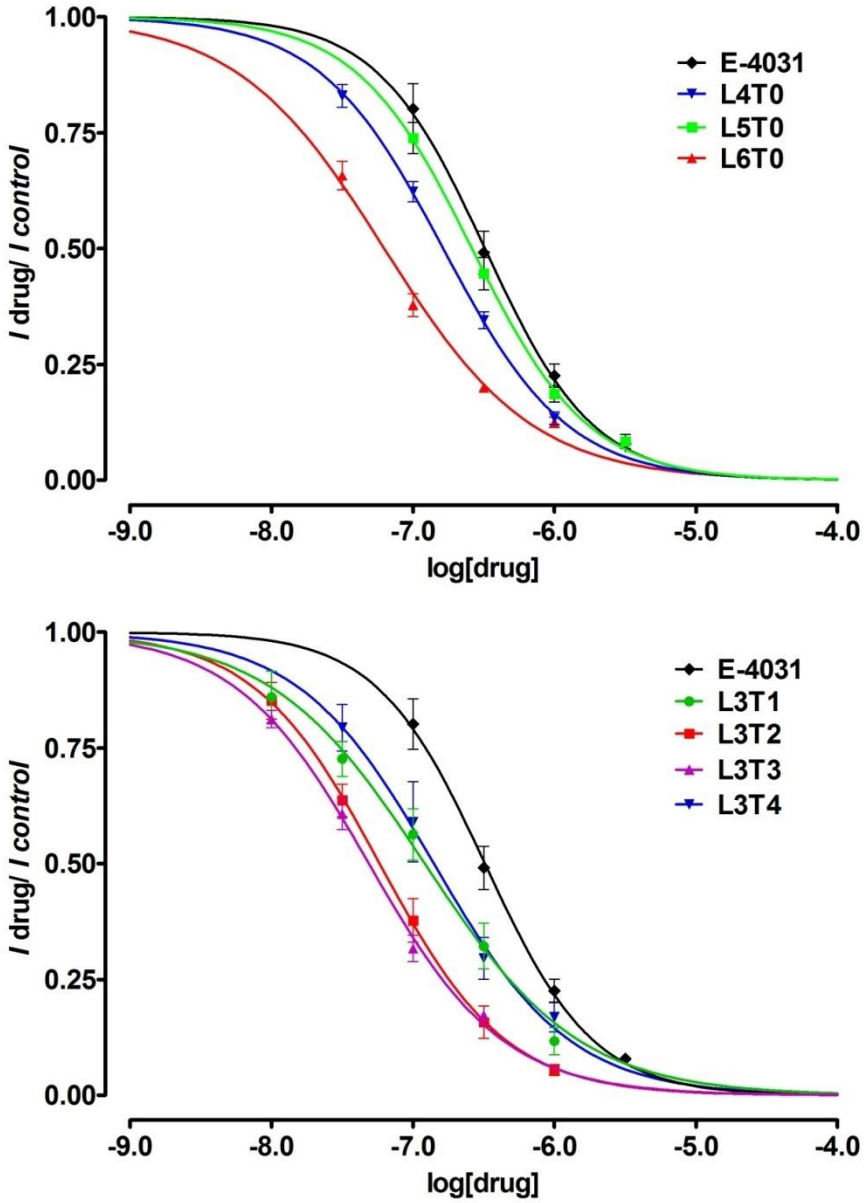

	IC_{50} (nM) & (pIC_{50} ± SEM)	Slope	n
E-4031	322.1 (-6.49 ± 0.05)	-1.14 ± 0.15	6
L4T0	162.5 (-6.79 ± 0.02)**	-0.99 ± 0.05	7
L5T0	261.2 (-6.58 ± 0.03)	-1.06 ± 0.08	9
L6T0	62.6 (-7.20 ± 0.03)***	-0.83 ± 0.06**	8
L3T1	121.3 (-6.92 ± 0.06)***	-0.80 ± 0.10**	7
L3T2	58.2 (-7.24 ± 0.04)***	-0.98 ± 0.09	7
L3T3	48.7 (-7.31 ± 0.03)***	-0.92 ± 0.06	10
L3T4	140.6 (-6.85 ± 0.07)**	-0.91 ± 0.14	5

Figure 5.5. Concentration-response curve for drugs that increase the linker (top) and drugs that increase the tail (bottom) & E-4031 on Wt hERG. The mean peak tail currents at each concentration was normalised to control and fit with a Hill function. The derivatives are potent inhibitors of WT hERG. IC_{50} concentrations in nM with pIC_{50} ± SEM in brackets. Statistics performed on pIC_{50}.

Not only were the derivates more potent than E-4031 but they also had a faster on set of block. Figure 5.6 shows the peak tail current plotted against time in the presence of increasing concentrations of drug. At each concentration the derivates reach steady-state block faster than E-4031. For the rest of the chapter the focus will be on the longest compounds, L6T0 and L3T4 as they displayed the fastest recovery from block.

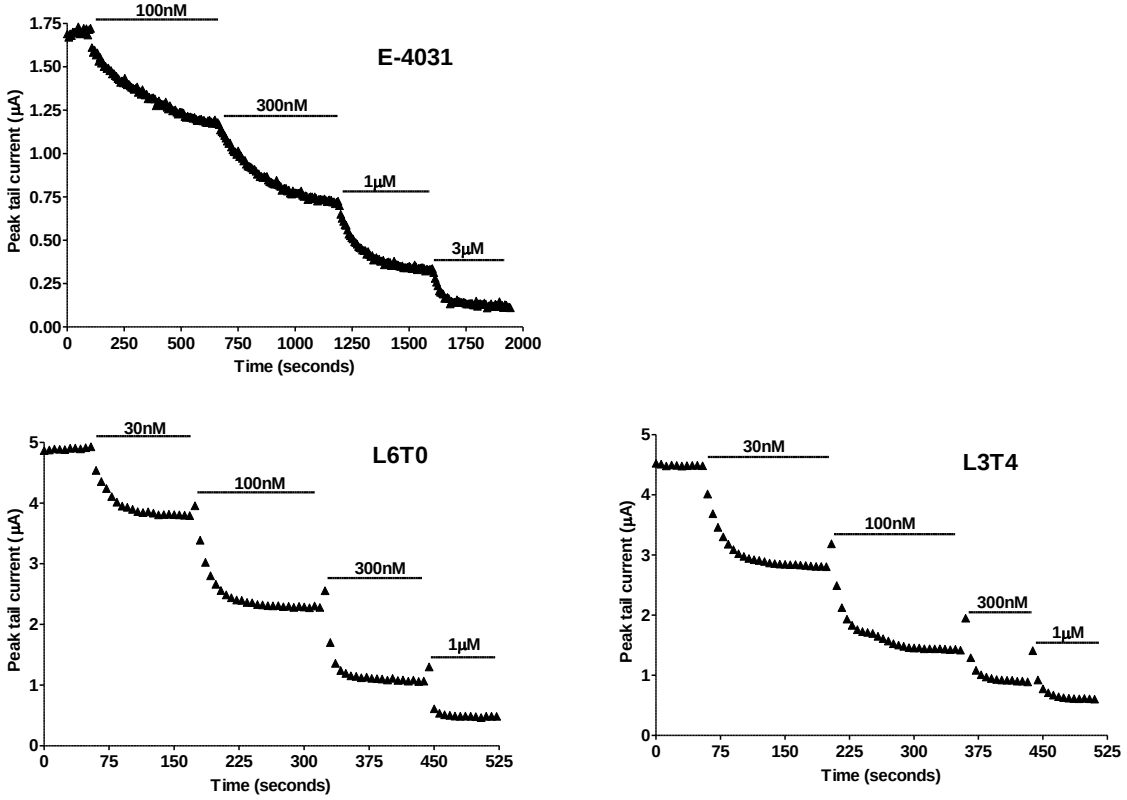

Figure 5.6. Onset of steady state block is faster with the derivatives than with E-4031. Representative plots of peak tail currents against time. The tail current amplitudes decrease with an exponential time course which is faster at higher concentrations. Note the difference in the scale of the x axis (time) in L6T0 and L3T4 compared to E-4031. The 3 minute pauses in pulsing while the next concentration of drug was being applied are not shown.

Pharmacology of mutants that perturbed inactivation

As mentioned in the introduction, alterations to inactivation gating are known to have major effects on the pharmacology of hERG. Recovery from block was studied in G628C:S631C hERG which completely removes inactivation (Spector et al, 1996b) and in S631C hERG which 'enhances' inactivation by increasing the rate of onset and recovery (Fan et al, 1999). These residues are located around the outer mouth of the selectivity filter. Removing inactivation gating has been shown to drastically reduce the potency of some drugs acting on hERG and it is the same here with respect to E-4031. Representative current traces for G628C:S631C hERG in figure 5.7 show the progressive decrease in current with increasing concentrations of E-4031. The G628C:S631C hERG tail currents at -70mV are small in amplitude, relative to currents at 0mV. This is because there is no inactivation at 0mV and no recovery from inactivation at -70mV. The reversal potential for this hERG mutant is also close to -70mV so there is little driving force for K^+ efflux. The tail currents seen in WT hERG are due to the rapid recovery from inactivation and the slow deactivation. The WT current was measured at the peak of the tail current. As the tail currents in G628C:S631C hERG were so small the current was measured at the end of the 5 second step to 0mV.

The concentration-response relationship for E-4031, L6T0 and L3T4 for inhibition of G628C:S631C hERG are shown in figure 5.8. As expected, E-4031 was significantly less potent against G628C:S631C hERG compared to WT hERG because there is no inactivation in this mutant. L6T0 and L3T4 were also significantly less potent on G628C:S631C hERG however, the shift in potency for L6T0 and L3T4 was much less that the shift in potency for E-4031 (fig 5.8)

.

After studying the G628C:S631C hERG mutation which abolishes inactivation gating, I then investigated a mutation, S631C, which has the 'opposite' effect on inactivation gating and enhances it by increasing the rate of onset and recovery from of inactivation. Ser631 is in the equivalent position as Thr449 is in Shaker and is located at the outer mouth of the channel.

The inhibition curves for L6T0 and L3T4 lie to the left of these drugs on the wild type channel and show an increase in potency which is consistent with enhanced inactivation gating. The pIC_{50}'s of these drugs on S631C hERG compared to WT hERG were significantly different. The S631C mutation had no effect on the potency of E-4031 compared to WT hERG (fig 5.8).

In addition to investigating mutations that alter inactivation gating, mutations that alter deactivation gating were also studied. V659A is known to dramatically slow the rate of deactivation (see chapter 4). The membrane potential was repetitively stepped to 0mV for 5 seconds as before but because the deactivation is so slow the holding potential was -120mV and the tail currents were measured at -140mV. E-4031 was a significantly less potent inhibitor of V659A hERG than WT hERG, as were the two derivatives L6T0 and L3T4. The shift in pIC_{50} was greater for E-4031 than for L6T0 and L3T4 (fig 5.8).

The potency of these 3 compounds had previously been studied on NTK hERG which deactivates very quickly. All the inhibition curves for these drugs lay to the left of wild type indicating an increased potency but the change in IC_{50} was not significant.

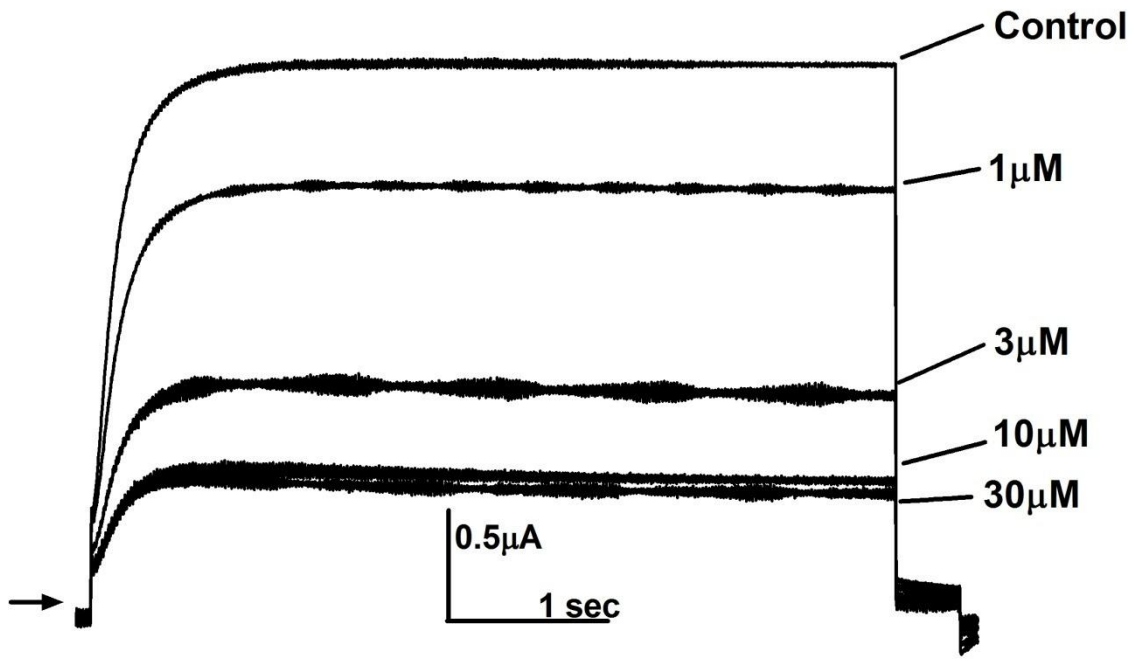

Figure 5.7. Representative current traces of G628C:S631C hERG in control solution and after reaching steady-state block with the indicated concentrations of E-4031. Block was achieved by repetitively stepping to 0mV, the same as for WT hERG. The current amplitude is reduced in a concentration dependant manor. Higher concentrations of E-4031 are required to achieve the same level of block as seen in WT hERG. Note the absence of tail currents.

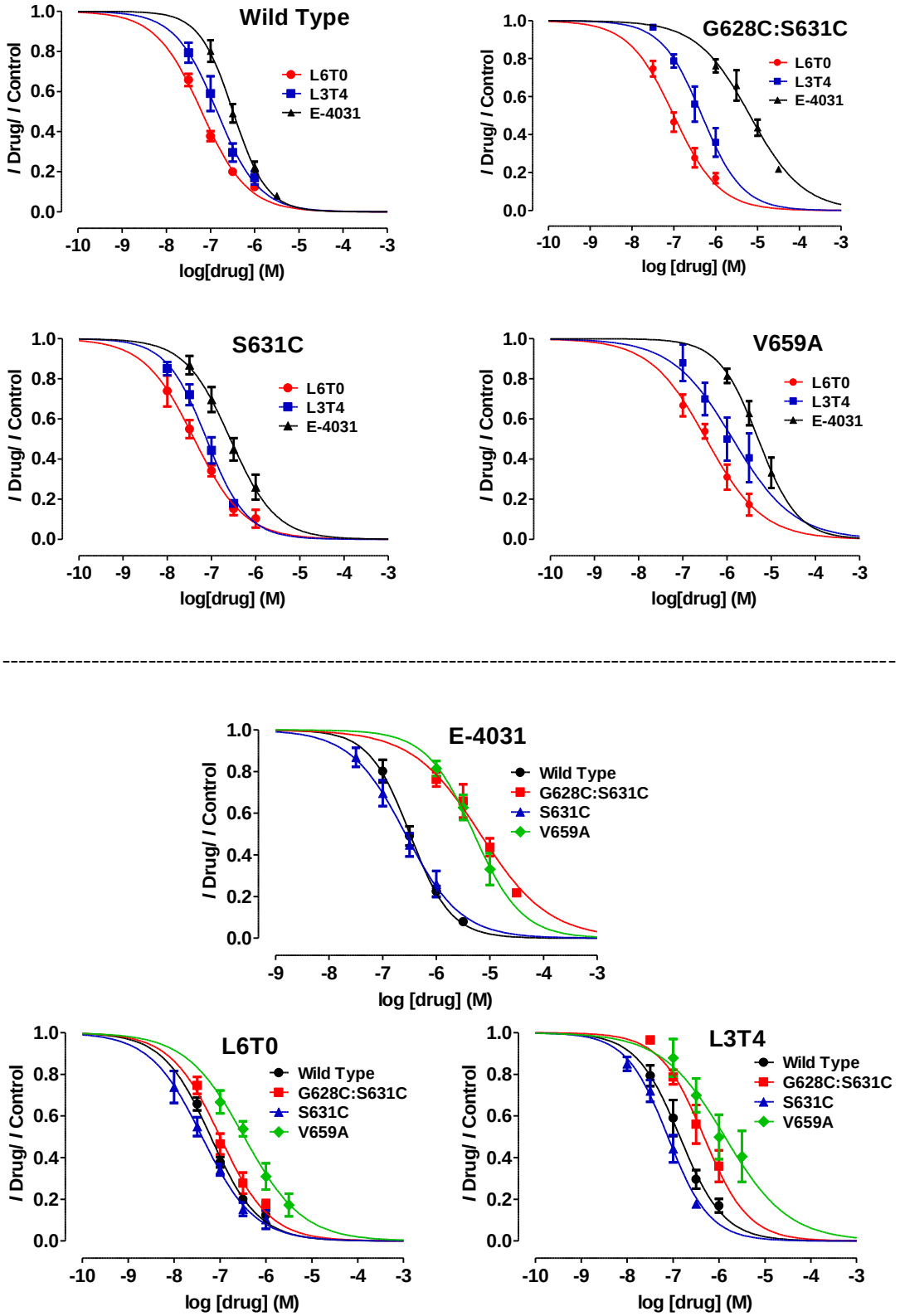

Figure 5.8. Concentration-response curves for E-4031, L6T0 & L3T4 on WT, G628C:S631C, S631C and V659A hERG. The top panel is arranged by WT or mutant hERG channel. The bottom panel is arranged by compounds. IC_{50}'s and Hill slope's are summarised in the table overleaf.

Summary of pIC_{50}'s and Hill slopes

	E-4031		L6T0		L3T4	
	IC_{50}	Hill slope	IC_{50}	Hill slope	IC_{50}	Hill slope
WT	-6.49 ± 0.05	-1.14 ± 0.15	-7.20±0.03	-0.83 ± 0.06	-6.85±0.07	-0.91 ± 0.14
G628C:S631C	-5.18 ± 0.08	-0.68 ± 0.11	-6.99±0.06	-0.80 ± 0.10	-6.33±0.08	-0.90 ± 0.17
S631C	-6.57 ± 0.07	-0.84 ± 0.13	-7.39±0.05	-0.76 ± 0.09	-7.11±0.06	-0.95 ± 0.13
V659A	-5.30 ± 0.07	-0.97 ± 0.19	-6.48±0.08	-0.68 ± 0.11	-5.87±0.17	-0.63 ± 0.20

pIC50's and Hill slopes.

Summary of equivalent nano-molar IC_{50}'s and Hill slopes

	E-4031		L6T0		L3T4	
	IC_{50}	Hill slope	IC_{50}	Hill slope	IC_{50}	Hill slope
WT	322.4	-1.14 ± 0.15	62.5	-0.83 ± 0.06	140.3	-0.91 ± 0.14
G628C:S631C	6600	-0.68 ± 0.11	100.7	-0.80 ± 0.10	469.2	-0.90 ± 0.17
S631C	266.9	-0.84 ± 0.13	40.5	-0.76 ± 0.09	77.3	-0.95 ± 0.13
V659A	5058	-0.97 ± 0.19	334.9	-0.68 ± 0.11	1342	-0.63 ± 0.20

All concentrations in nM.

Figure 5.8. Concentration-response curves for E-4031, L6T0 & L3T4 on WT, G628C:S631C, S631C and V659A hERG. The mean peak tail currents at each concentration were normalised to control and fit with a Hill function. (n = 4 - 8)

E-4031 was significantly less potent on G628C:S631C and V659A hERG but unchanged at S631C compared to WT.

L6T0 was significantly less potent on G628C:S631C and V659A hERG. However it was more potent at S631C hERG compared to WT.

L3T4 was significantly less potent on G628C:S631C and V659A hERG. However it was more potent at S631C hERG compared to WT.

Recovery from block

Wild Type hERG recovery from block

Taking a closer look at the onset of steady state block (from figure 5.6 above, now enlarged in figure 5.10 below) it can be seen there is an increase in the level of current from the end of one pulsing set at one drug concentration and the start of another set of pulsing at a higher concentration. Thus, the currents are showing recovery from inhibition and this is happening in the continued presence of drug and while the channels are closed by holding membrane potential at -90mV. All derivatives showed recovery from inhibition, only L3T4 is shown to illustrate the point. In contrast to the derivates, hERG currents did not show signs of recovery from inhibition by E-4031.

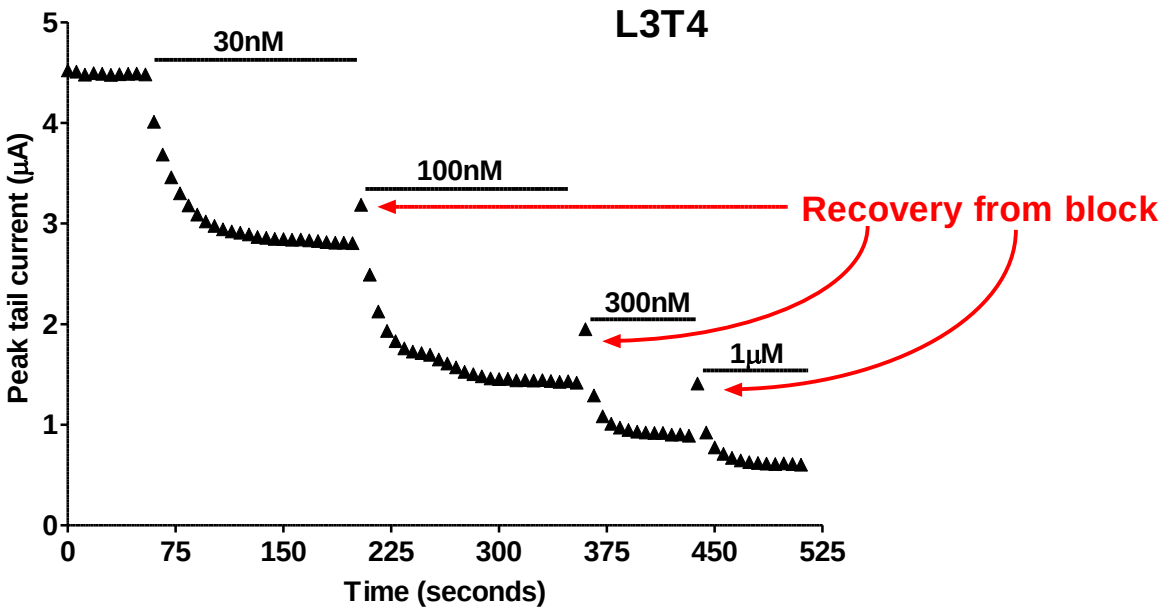

Figure 5.10. Current recovers in-between pulsing in continued application of drug. Representative plots of peak tail currents against time. The amplitude of tail current increase from when recording was stopped after reaching steady state block at one concentration and the start of recording at the next concentration even thought the channel had been held at -90mV and the hERG's activation gate is closed.

The recovery from inhibition seen with the derivatives indicates they may not be trapped in the inner cavity. Recovery from block in these type of experiments was unexpected, particularly as the E-4031 derivatives were more potent than E-4031. It was therefore quantified more systematically.

In order to assess the recovery from block it was therefore first necessary to block the channels. The follow voltage protocols were used in the following order. The 'steady pulsing' to 0mV as used for the concentration response experiments were run in control solution until the currents were stable. The recovery from block protocol (described below and in fig 5.11) was run in control solution to obtain the current levels to use as comparison for after the channels had been blocked. The recovery from block protocol was run 3 times, once at each holding potential, -120mV, -90mV and -60mV. The current was then inhibited by repetitively by stepping to 0mV as above but this time in the presence of drug, then the recovery from block protocol was run again in the continued presence of drug. As some recovery from inhibition is seen it was then necessary to re-block the channels by pulsing the cell to 0mV again before running the recovery from block protocol at a different holding potential. A 10 times IC_{50} concentration was used to inhibit the current and after the current was inhibited for the first time the drug solution was continuously perfused onto the cell during the experiments. The recovery from block was assessed by taking the peak tail currents in the presence of drug and normalising to the control current and plotting against time (fig 5.12).

The voltage protocol used to evaluate recovery from inhibition is shown in fig 5.11 and also shown in fig 5.11 are the currents elicited using the protocol. The holding potential

was the variable in these set of experiments and was set at either -120mV, -90mV or -60mV. At -120mV and -90mV the channels have a very low open probability whereas -60mV is around the threshold for activation. From the holding potential the cell was stepped to +40mV for 50ms, just long enough to activate the channel so there would be tail currents when stepping down to -70mV for 50ms. The cell was returned to the holding potential and there was ten seconds between pulses (fig 5.11). The cell was held in the closed state for the vast majority of the time and was only in the open-inactivated state for 50ms while at +40mV and prior to deactivation upon repolarisation.

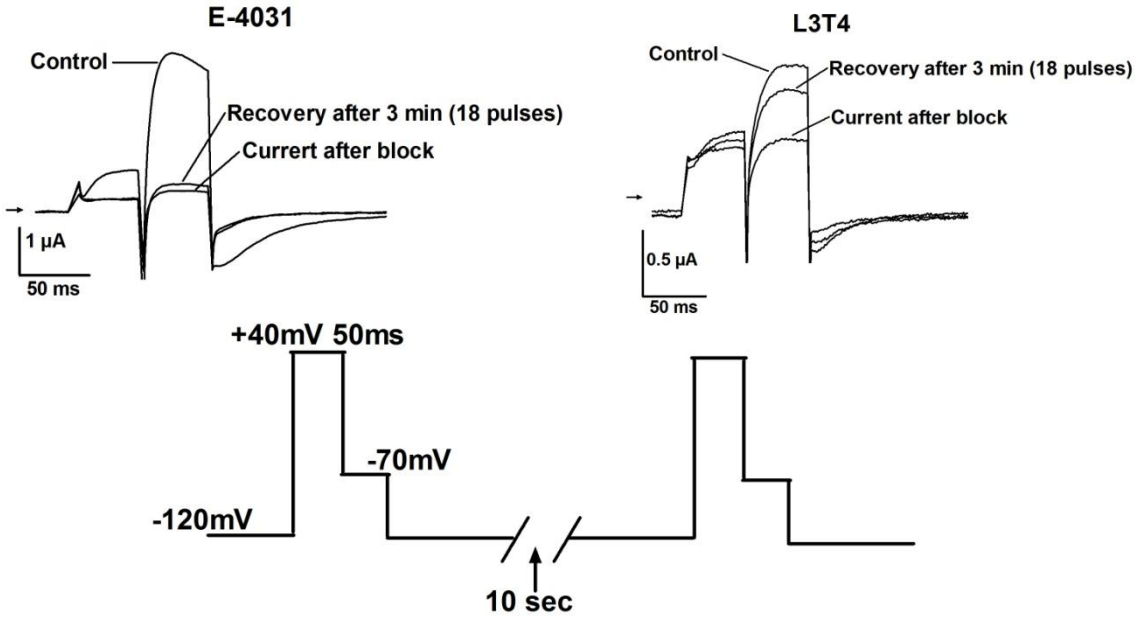

Figure 5.11. Differential recovery from inhibition of WT hERG from E-4031 and L3T4. Representative WT hERG currents in control conditions and with 10 x IC_{50} concentration of drug. Currents were first inhibited by repetitively stepping to 0mV, as in fig 5.4, before running the recovery from block protocol (bottom panel). Currents elicited by short 50ms pulses to +40mV followed by repolarisation to -70mV are shown in the absence of drug (control), in the first pulse following steady state inhibition and 3 minutes after steady state block.

Figure 5.12 shows the level of current over time using the recovery from block voltage protocol. Plotted is the normalised mean peak tail current observed on stepping down to -70mV after the 50ms step to +40mV. Data from WT hERG currents after block with E-4031 are shown in the top panel of figure 5.12. When the cell was held at -120mV and -90mV between stepping to +40mV the currents display little recovery from inhibition as seen by the lack of increase of current over time. This is consistent with the drug trapping hypothesis in that when the channel is held closed at -90mV and -120mV the level of block remains high. However, when the cell is held at -60mV, which is around the threshold of channel activation, between pulses there is a gradual increase in the level of tail current over time, which is indicative of recovery from block.

In contrast to the results seen for E-4031, L6T0 and L3T4 display a large degree of recovery from inhibition at -120mV and -90mV (middle and bottom panels in figure 5.12). There is the most recovery at -120mV with slightly less recovery while holding the cell at -90mV between pulsing. The recovery from inhibition is much less at -60mV for L3T4 and L6T0.

Figure 5.13A shows the recovery from inhibition of E-4031, L6T0 and L3T4 at the -120mV holding potential. There is no increase in tail current over time when the current is inhibited by E-4031 but there is an increase in current levels with every passing sweep of the recovery for block voltage protocol with the E-4031 derivatives, which reaches a steady state level after ~100 seconds. Panel B of figure 5.13 shows the voltage dependence of recovery from inhibition of E-4031 and the derivates. E-4031 does not recover when the membrane potential is held at -120mV or -90mV between sweeps of the voltage protocol but does start to recover when the membrane is held at -60mV between sweeps of the voltage protocol. The derivatives of E-4031 have the opposite

voltage dependence than E-4031 itself. The current after inhibition by L6T0 and L3T4 recovers close to its control level at -120mV, with just slightly less recovery observed at a holding potential of -90mV and the least recovery is seen when the membrane potential was held at -60mV between sweeps of the recovery from block voltage protocol.

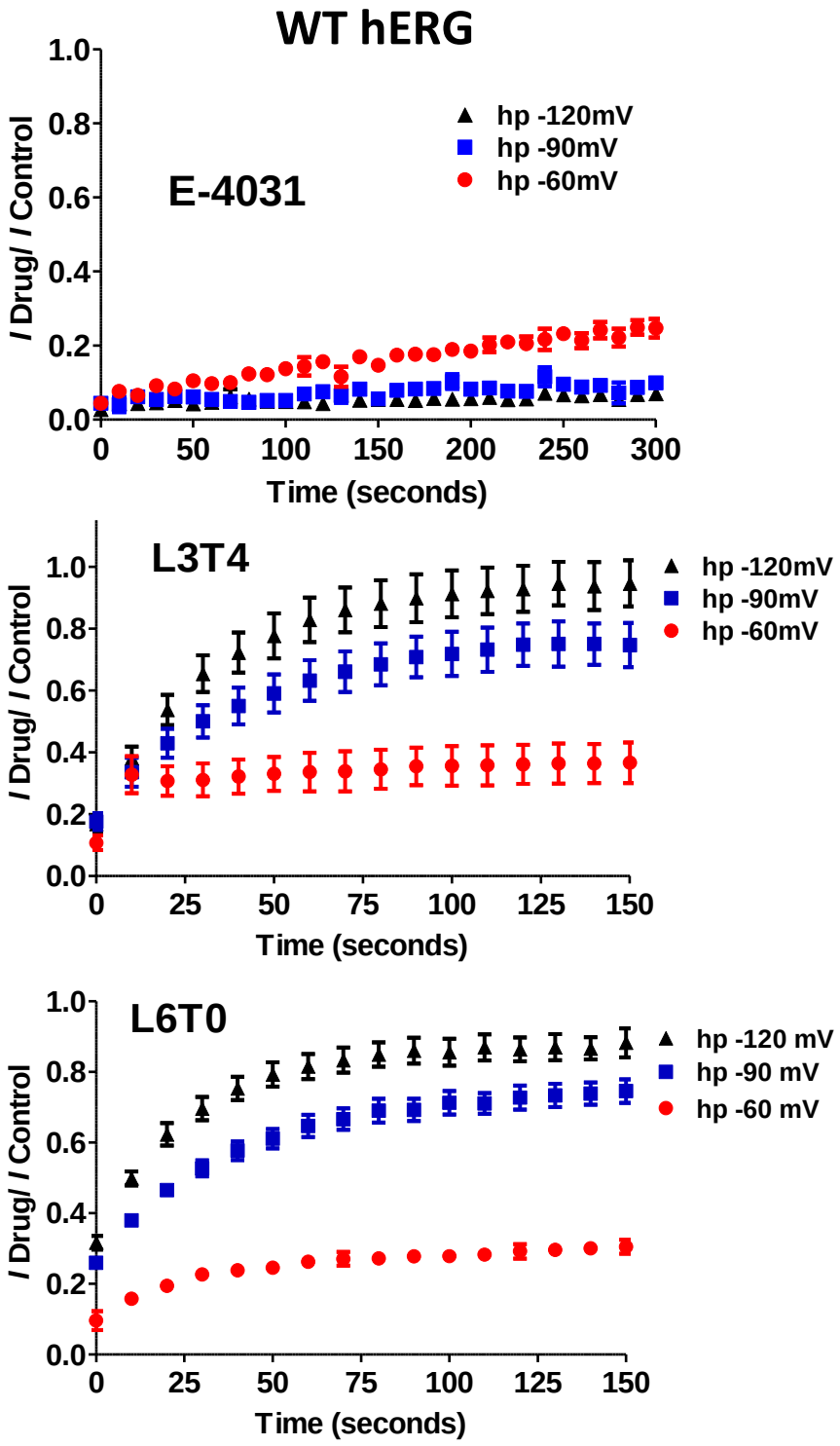

Figure 5.12. Recovery from inhibition of WT hERG over time and at varying holding potentials for E-4031, L3T4 and L6T0. Peak tail current was normalised to peak tail current from control recording and plotted against time. When holding the channels closed at -120mV and -90mV there is no recovery from block as indicated by a consistent level of current inhibition. At a holding potential of -60mV there is a gradual increase in the tail current indicative of recovery from block. (hp = holding potential).

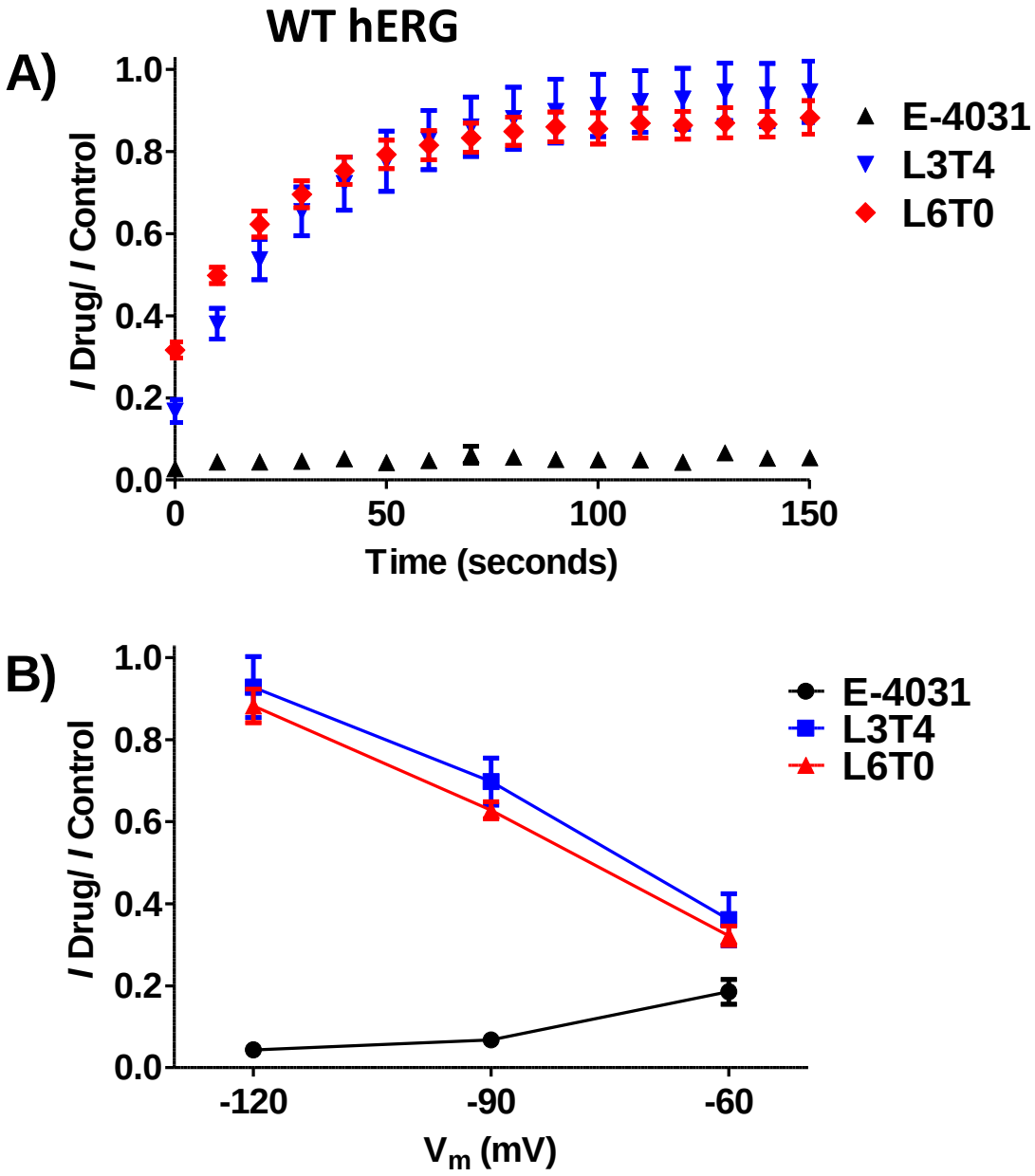

Figure 5.13. Rate and voltage dependence of recovery from inhibition of WT hERG with E-4031, L6T0 and L3T4 at -120mV holding potential. A) The rate of recovery for E-4031, L6T0 and L3T4 at -120mV holding potential from the protocol in figure 5.11 . Recovery in E-4031 is almost nonexistent at a holding potential of -120mV, whereas L6T0 and L3T4 show close to complete recovery. B) The voltage dependence of recovery from block. E-4031 show little recovery at holding potentials of -120mV and -90mV but starts to recover when the cell is held at -60mV between pulses.

Percentage recovery after 3 minutes (~18 sweeps of voltage protocol)			
	E-4031	**L6T0**	**L3T4**
-120mV	4.4 ± 0.5	88.3 ± 4.4	92.9 ± 7.4
-90mV	6.8 ± 0.1	62.8 ± 2.1	69.8 ± 5.8
-60mV	18.5 ± 3.1	32.2 ± 2.0	36.1 ± 6.4

Effects of inactivation perturbing mutants on recovery from block

G628C:S631C hERG

The G628C:S631C hERG mutant was used to investigate the effect of removing inactivation on recovery from inhibition. As this mutant has very small tail currents the point used to measure the current was at the end of the step to +40mV. Although this mutant had a significantly shifted E-4031 IC_{50} compared to WT hERG, the recovery current inhibition by E-4031 (10 x IC_{50} concentrations were used) was the same as in WT hERG. There was little recovery at from inhibition at -120mV and at -90mV and a small amount of recovery at -60mV (fig 5.14). The G628C:S631C hERG mutant did not have any significant effect on the IC_{50}'s of L6T0 and L3T4, there was much faster recovery from inhibition in this mutant than in WT hERG (fig 5.14 & 5.16). Recovery reached steady state after 4 sweeps (~30 seconds) for the G628C:S631C hERG mutant. WT and G628C:S631C hERG shared the same voltage dependant recovery from inhibition, both derivates recovery close to control levels at -120mV, slightly less at a holding potential of -90mV but less so at -60mV whereas E-4031 hardly recovers at the two more negative holding potentials and starts to show recovery at -60mV (fig 5.14).

S631C hERG

Recovery from inhibition from the S631C hERG mutant was also faster than recovery from inhibition from WT hERG (fig 5.15 & 5.16). There was near complete recovery when the holding potential between sweeps was -120mV and slightly less recovery when held at -90mV. At a holding potential of -60mV the derivatives recovery was about the same amount as E-4031. All three drugs shared the same voltage dependant

recovery from S631C current inhibition as WT hERG, both derivates recovery close to control levels at -120mV and -90mV but less so at -60mV whereas E-4031 hardly recovers at the two more negative holding potentials and starts to show recovery at -60mV.

Effect of mutants that alter deactivation gating on recovery from block

It was intended that the effect of the V659A hERG, a slowly deactivating mutant, would be studied but this proved not to be feasible. The property of interest in this mutant, the slow deactivation, meant that the channel never closed in-between sweeps of the voltage protocol and there was an accumulation of current due to the channels being further activated. This problem was compounded by holding the membrane at more positive potentials (e.g. holding the membrane at -90mV and -60mV) as there was less of a force driving deactivation.

The recovery from block of a mutant that deactivates quickly has already been investigated by a past member of the lab. The recovery from block in NTK hERG is faster than the recovery seen in WT hERG.

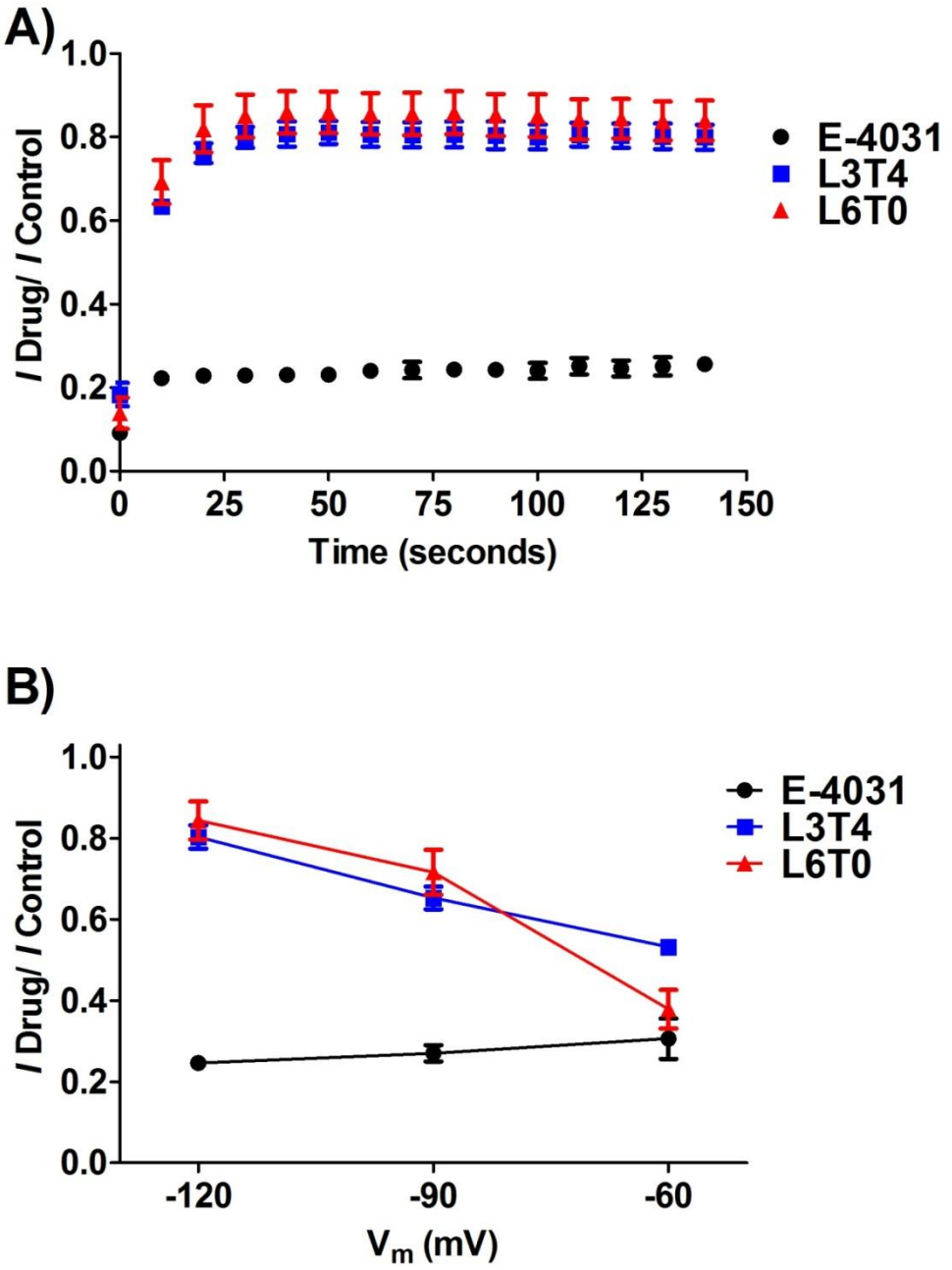

Figure 5.14 Rate and voltage dependence of recovery from inhibition of G628C:S631C hERG with E-4031, L6T0 and L3T4 at -120mV holding potential. A) The rate of recovery for E-4031, L6T0 and L3T4 at -120mV holding potential using the protocol in figure 5.x. Recovery in E-4031 is almost nonexistent at a holding potential of -120mV, whereas L6T0 and L3T4 show close to complete recovery. B) The voltage dependence of recovery from block. E-4031 show little recovery at holding potentials of -120mV and -90mV but starts to recover when the cell is held at -60mV between pulses.

Percentage recovery after 3 minutes (~18 sweeps of voltage protocol)			
	E-4031	**L6T0**	**L3T4**
-120mV	24.6 ± 1.9	84.4 ± 4.7	80.3 ± 2.9
-90mV	27.0 ± 2.0	71.6 ± 5.6	65.3 ± 2.8
-60mV	30.6 ± 5.0	37.6 ± 4.8	53.2 ± 1.4

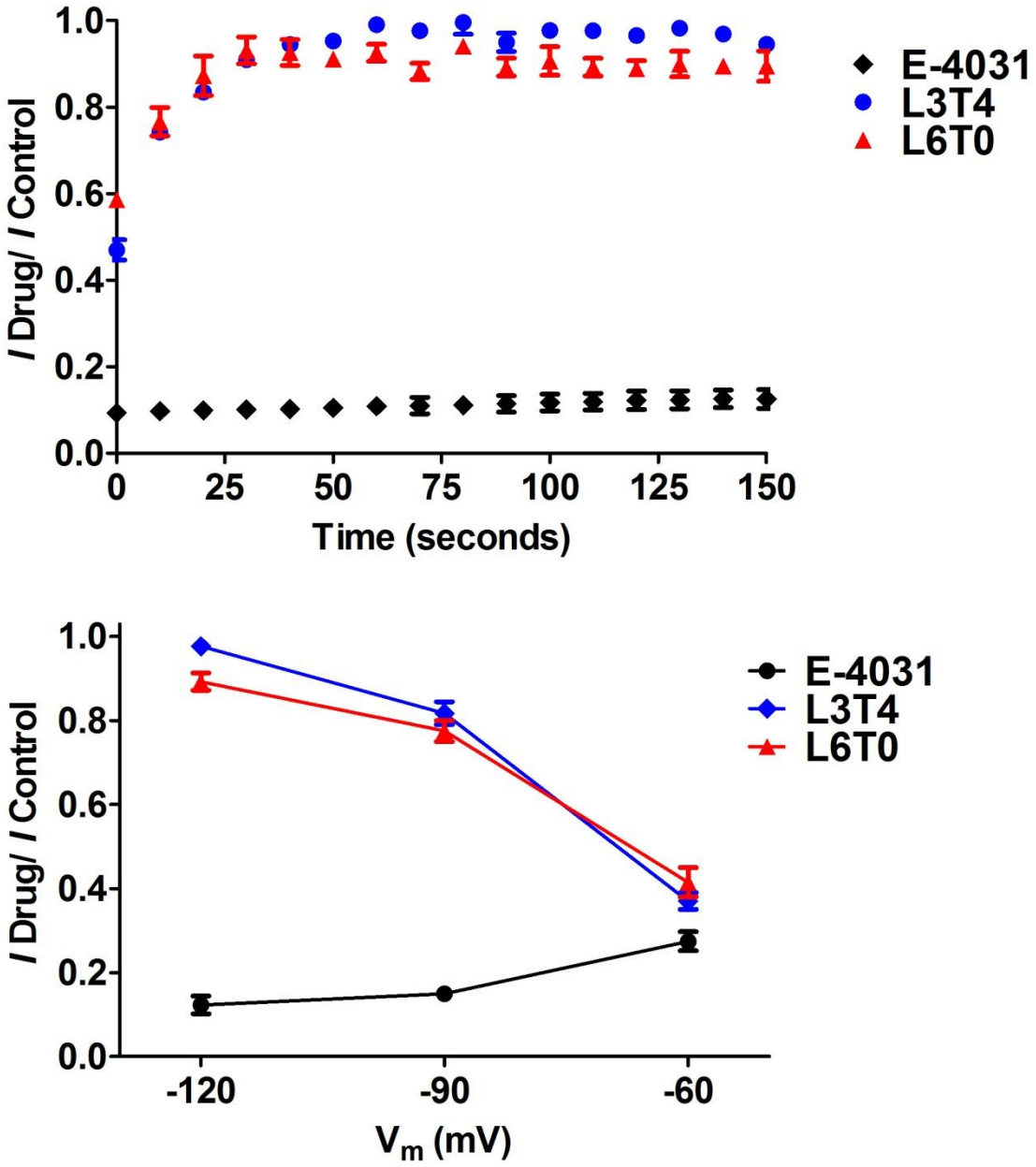

Figure 5.15 Rate and voltage dependence of recovery from inhibition of S631C hERG with E-4031, L6T0 and L3T4 at -120mV holding potential. A) The rate of recovery for E-4031, L6T0 and L3T4 at -120mV holding potential using the protocol in figure 5.x. Recovery in E-4031 is almost nonexistent at a holding potential of -120mV, whereas L6T0 and L3T4 show close to complete recovery. B) The voltage dependence of recovery from block. E-4031 show little recovery at holding potentials of -120mV and -90mV but starts to recover when the cell is held at -60mV between pulses.

Percentage recovery after 3 minutes (~18 sweeps of voltage protocol)			
	E-4031	**L6T0**	**L3T4**
-120mV	12.3 ± 2.1	89.2 ± 2.1	97.7 ± 0.8
-90mV	15.0 ± 1.6	77.5 ± 2.5	81.7 ± 2.7
-60mV	27.5 ± 2.7	41.5 ± 3.5	37.0 ± 2.0

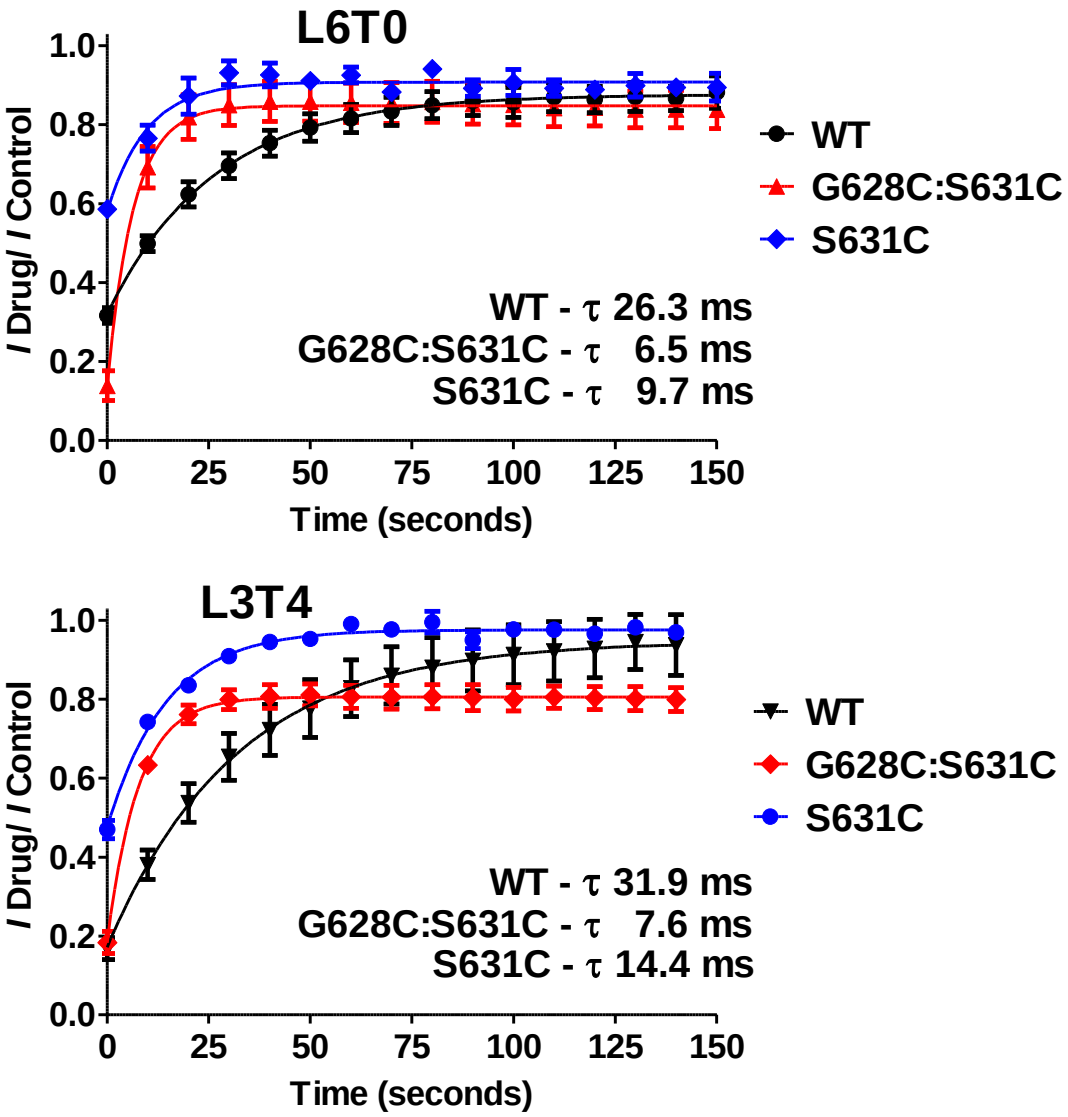

Figure 5.16. The rate of recovery in WT, G628C:S631C & S631C hERG. Recovery is faster is the non-inactivating mutant than WT, still faster than WT in S631C mutant and slowest in WT. Holding potential was -120mV.

Investigation of closed state block

The E-4031 derivatives appear to be able to escape the closed channel resulting in recovery from block. This raised the question, if they could recover from block while the channel was closed could they also enter the channel to cause block while the channel was closed? To assess this the following envelop of tails protocol was used; the membrane potential was held at -120mV and stepped to +70mV to briefly activate the current before stepping down to -140mV to measure the tail currents. To begin with the step to +70mV was for only 10ms and then with each new sweep of the voltage protocol the duration of the step to +70mV was increased in 20ms increments so that the duration of the +70mV pulse went 10ms, 30ms, 50ms etc up to a maximum duration of 250ms. The tails were measured at -140mV for two reasons. One, the negative potential means that the current deactivates rapidly so the channel is spending the maximum amount of time in the closed state. Two, because at the shorter pulse durations hERG current will have achieved only a small amount of activation, choosing a potential further away from the reversal potential ensured there was sufficient driving force to more easily detect and measure current amplitudes. The protocol was first performed in recording solution without drug and then with a 10 times IC_{50} concentration of drug that was washed onto the oocyte for 10 minutes before applying any depolarisations to allow ample time for the compounds to equilibrate across the membrane. Figure 5.17 shows that with the shortest duration pulse to +70mV there was no tonic block. The current after 10 minutes of drug application was the same amplitude as the control current. However, inhibition of WT hERG current increased with increasing channel open time as expected for an open channel blocker. The E-4031 derivates can thus not gain access to their binding site from the closed state and exhibit open state block only.

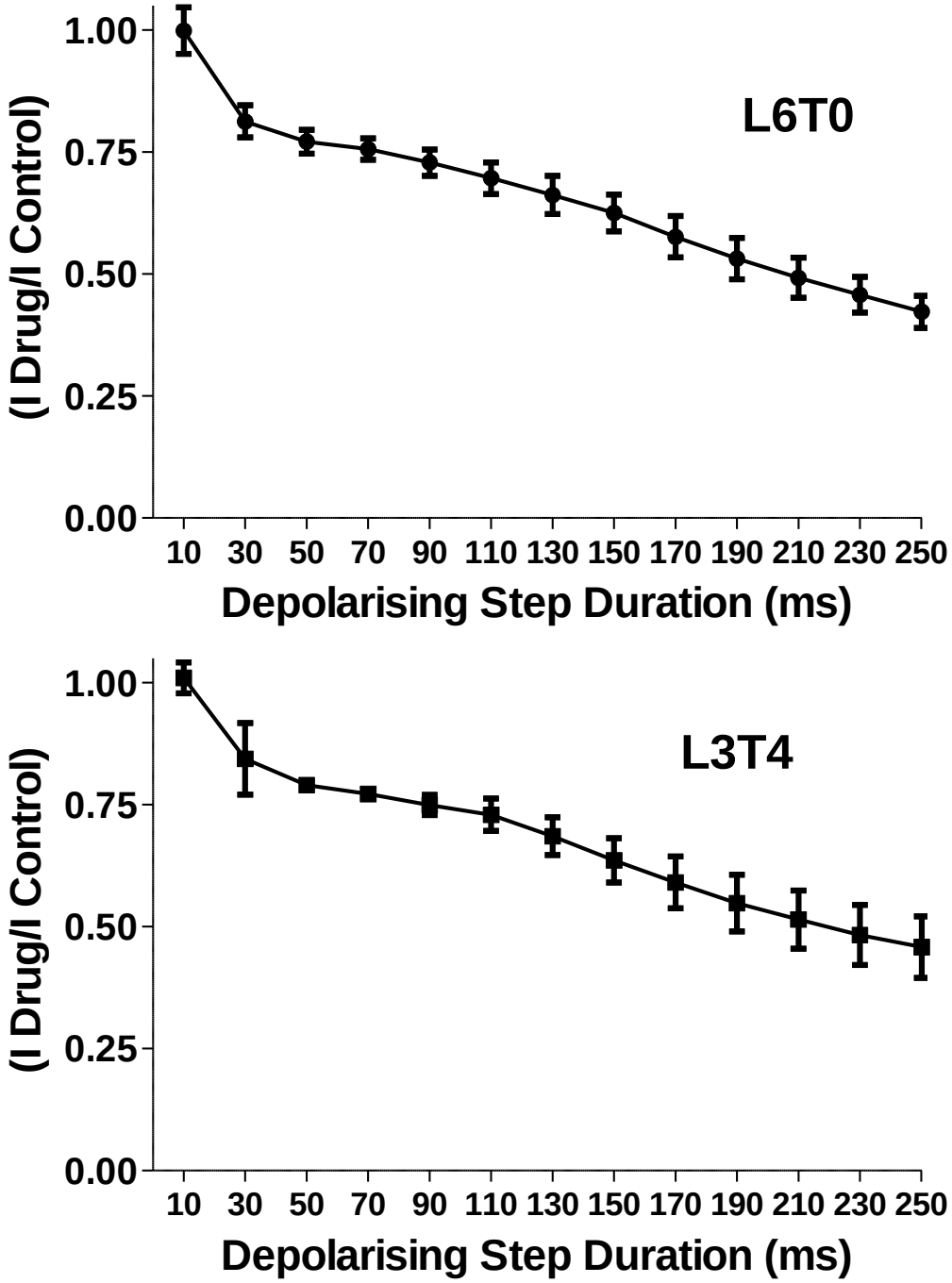

Figure 5.17. Current inhibition increases with increasing pulse duration. Mean peak tail current amplitudes are plotted against depolarising duration. The tail currents were normalised to current amplitude in control solution. The channel was held -120mV and stepped to +70mV to briefly activate the channel before stepping down to -140mV to measure the tail currents. To begin with the channel was stepped to +70mV for 10ms and then to +70mV in 20ms increments with each pulse up to a channel open time of 250ms. There is no evidence of tonic block and the level of block increases with increasing channel open time.

The term 'foot in the door' block has been used to describe a type of channel block where there is an apparent slowing of deactivation gating. In this type of block it is thought that the drug molecule is too large to be trapped in the inner cavity of a channel, it protrudes out of the inner cavity and hinders the activation gate from closing and is seen as a slowing of current deactivation. Mike Chang, a former PhD student in the lab, explored the possibility that the derivatives exhibit foot in the door type block. Shown in figure 5.18 is a representative current trace of tail currents in control solution or in the presence of 10 times IC_{50} concentration of L3T4. The current in the presence of drug has been scaled up so that the time course of deactivation can be compared. There was no sign that L3T4 causes a slowing of deactivation. In fact deactivation is slightly faster in the presence of the blocker, indicating that L3T4 does not demonstrate a foot in the door type block. Similar effects were seen with other E-4031 derivatives.

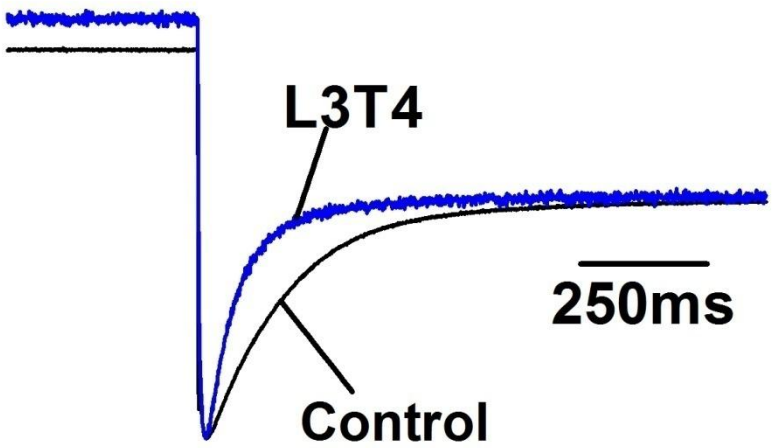

Figure 5.18. L3T4 does not show 'foot in the door' block. Peak tail currents have been normalised to the same amplitude to compare the rate of deactivation. The cell was stepped from -90mV to 0mV for 30 seconds to block the channel. The cell was then stepped down to -120mV to deactivate the current. One long pulse to 0mV was used rather than repetitively stepping to 0mV to avoid multiple activation/deactivation cycles. The last 250ms of the 0mV step and 1 second of the -120mV step are shown. The rate of deactivation at -120mV is slightly faster in the presence of drug. Data for this figure was generated by Mike Chang.

Site of drug binding

Until now it has been presumed that the derivatives have been binding to a site on S6 in the inner cavity in a manner similar to E-4031. In order to confirm that this was the case L6T0 and L3T4 were tested against mutations of inner cavity residues that are known to be key for drug binding, Y652A and F656A in the middle of S6. A concentration 10 times the IC_{50} for inhibition of wild type hERG was applied in all experiments. The cell was repeatedly stepped to 0mV for 5 seconds and then stepped down to -70mV to evoke tail currents in the same way as the concentration response experiments at the beginning of this chapter.

The peak tail current after the application of drug was normalised to the peak tail current in control and is shown in figure 5.19. When L6T0 is applied to WT hERG the tail current is reduced 85.4% and when L3T4 is applied to WT hERG the tail current is reduced by 87.3% (black columns, figure 5.19). In contrast to this the same concentrations of L6T0 and L3T4 only reduced the tail currents of F656A hERG by 3.4% and 4.3% respectively (red columns, figure 5.19). The level of block seen in Y652A hERG was in-between that seen in WT hERG and F656A hERG. L6T0 inhibited Y652A hERG 38.8% and L3T4 reduced the tail currents in Y652A hERG by 67.0% (blue column, figure 5.19). These results indicate that mutating inner cavity residues reduced the potency of these compounds and that they do indeed bind within the inner cavity of hERG.

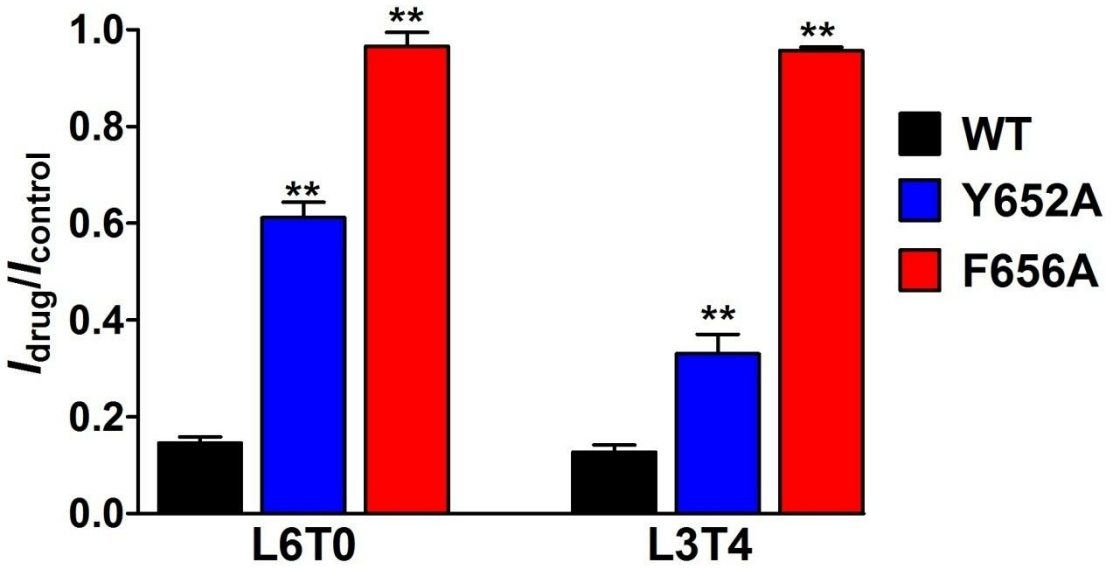

	WT	Y652A	F656A
L6T0	14.6 ± 0.01	62.1 ± 0.03	96.6 ± 0.02
L3T4	12.7 ± 0.01	33.0 ± 0.04	95.7 ± 0.01

% current remaining form control after block with 10 times WT IC_{50} concentration.

Figure 5.19. L6T0 and L3T4 have reduced potency in mutants where the aromatic drug binding residues have been mutated to alanine. A 10x times IC_{50} concentration of drug was used to block hERG current. WT hERG current is blocked but F656A is insensitive to block and Y652A has a profile between the two. Data for this figure was generated by Rachael Hardman.

Discussion

The aim of developing the derivatives of E-4031 was twofold. One was to use the derivatives as a 'molecular ruler' to measure the size of the inner cavity. The rational was to increase molecule length. It was expected that small molecules would be trapped, whereas the larger molecules would exhibit foot in the door recovery from inhibition. And two, to investigate if molecules that are no longer trapped reduce the potency of the drug.

The two aromatic residues on S6, Tyr652 and Phe656, are known to be important for the binding of many drugs and this is also true of the derivatives of E-4031. Because the derivatives can recover from block so quickly at potentials where the channel is closed it may have been possible that they were binding somewhere else on the channel, perhaps on the outer mouth of the selectively filter. However, the site of interaction is the same as E-4031, binding to the aromatic residues on S6. WT hERG current was reduced by 85% on application of L3T4 and L6T0 whereas F656A hERG current was virtually unchanged. There was more of a variable effect of Y652A on drug binding. Y652A currents were reduced as much L6T0 compared to L3T4. This variability in Y652A has been reported before with the blocker propafenone (Witchel et al, 2004).

All of the derivatives, apart from L5T0, were more potent than E-4031. There does not appear to be any clear correlation between the length of the linker or tail and potency. However, there are only three linker and four tail molecules so perhaps more compounds in each series would enable a pattern to be discerned.

It is well established that E-4031 is trapped inside the inner cavity of hERG when the channel closes. The lack of recovery at holding potentials of -120mV and -90mV is consistent with trapping. The slow recovery seen at -60mV is likely due to the increase in channel open probability allowing E-4031 to gradually exit the inner cavity. L6T0 and L3T4's binding appears to be highly state selective for the open state of the channel. The drugs have a fast onset (fig 5.10) and also appear to unbind very rapidly and are able to exit the channel before it can close at -120mV and -90mV. At -60mV the increased open probability of the channel may allow for the derivatives to re-block the channel so it appears like there is less recovery. The derivatives unbind at negative potentials without causing any slowing of deactivation associated with foot in the door block.

Experiments by Mike Chang (not included here) show that the shortest of all the derivatives also recovers from block and is not trapped the same as the longest ones, even though it is smaller in size than E-4031. Clearly the extra length of the derivatives is not the reason for the rapid recovery from block.

Block of hERG by the derivatives of E-4031 is highly state dependant. The channels have a high affinity for the open state of the channel but not the closed state. The onset of block was faster and the channels are able to recover from block which is not seen with E-4031. Mutations that effect inactivation were used here to gain more insight to the binding of the derivatives. Removing inactivation gating is known to reduce the potency of some blockers. G628C:S631C hERG removes inactivation and there is a corresponding large rightward shift in E-4031 potency. However, there is less of a shift in the derivatives, particularly in L6T0 which is not much less potent at G628C:S631C than WT hERG. S631C hERG enhances inactivation and has an increased sensitivity to block by the

E-4031 derivatives but not E-4031. Thus, the amount of inactivation appears to influence compound potency.

Both of the inactivation mutants exhibited faster recovery form block than WT hERG for both L6T0 and L3T4 but there was no change in the rate of recovery of E-4031. Although G628C:S631C hERG shifted the potency of E-4031 a 10 times concentration of blocker was used for all drugs in all experiments so this circumvents the differences in IC_{50}'s seen between the different compounds and mutants. It is strange that G628C:S631C hERG and S631C hERG have the 'opposite' effects on inactivation gating but they both increase the rate of recovery from inhibition. The mutation G628C:S631C hERG shifts the IC_{50} of E-4031 rightward whereas S631C hERG does not but both mutants have the same effect on the recovery from inhibition of L6T0 and L3T4 and increase the rate of recovery compared to WT hERG. It seems odd that two mutations that have 'opposite' effects on inactivation gating have similar effects on the rate of recovery from inhibition. But this only seems strange if we think of these mutations purely in terms of their effect on the selectivity filter and don't consider what other changes these mutations might induce in other parts of the channel.

Eduardo Perozo laboratory has been doing some very interesting structural and functional studies on potassium channel C-type inactivation. They have shown that there is 'cross talk' between inactivation gating at the selectivity filter and a corresponding reorientation of residues on S6 during inactivation (Cuello et al, 2010). This could account for why some mutations around the selectivity filter, and nowhere near the drug binding residues on S6, can result in a decreased affinity for some drugs and the increase rate of recovery from inhibition seen here. Work by Mike Chang and Rachael Hardman showed that NTK hERG also recovers from inhibition faster than WT

hERG. While NTK hERG is often thought of as very quickly deactivating mutant, which it is, it also has a very positively shifted $V_{0.5}$ of inactivation. The effect of the fast recovery from inhibition in NTK hERG could be due to altered inactivation properties rather than any effect on the rate of deactivation.

With the E-4031 derivatives able to recovery from block, seemingly being able to escape a closed channel, we decided to investigate if there was any sign of closed state block. Block of hERG with E-4031 and the derivatives was open state dependant. The channel was held closed with a membrane potential of -120mV for 10 minutes while a 10 times IC_{50} concentration of drug was washed on to the cell. The cell was then depolarised to +70mV for 10ms. This voltage protocol was repeated several times with the depolarising step increasing in duration each time by 20ms up to a maximum of 250ms. Block of the channel with L6T0 and L3T4 increase with an increase in channel open time which is consistent with these drugs having open state block and not being able to block the channel before the activation gate has opened.

Although drug trapping is very important for many drugs that block hERG it is clearly not an absolute requirement that drugs are trapped to achieve high potency block as the derivatives shown here block with high affinity and are not trapped.

Chapter 6

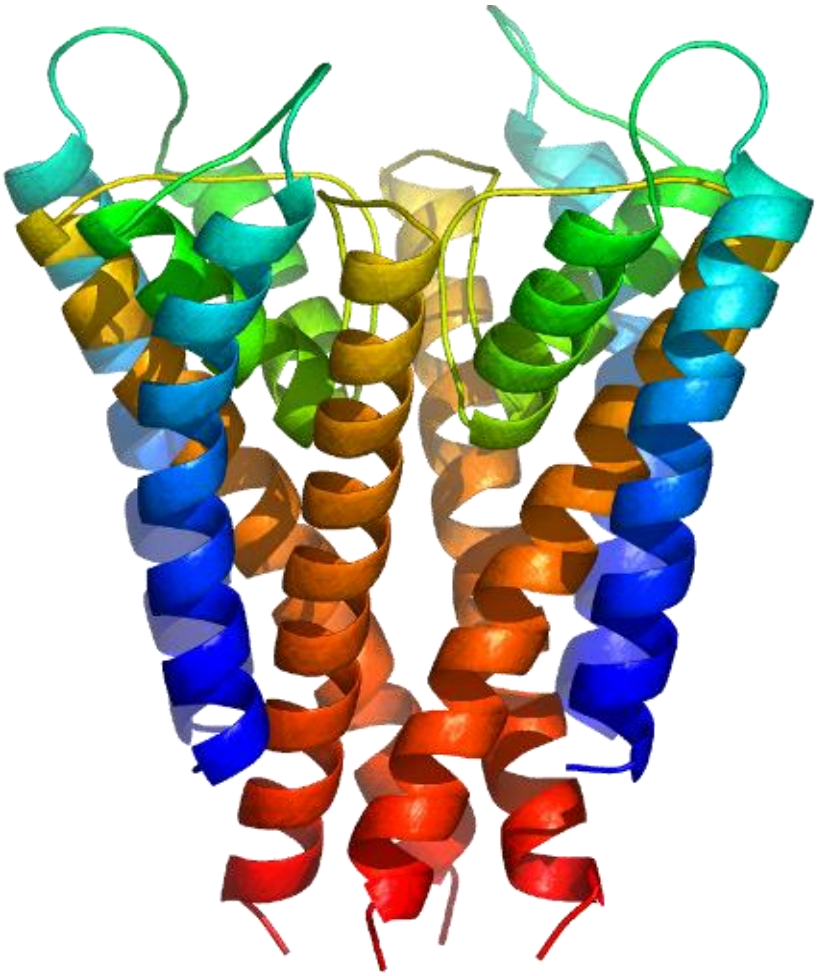

Summary & Future Directions

The work presented in this thesis has explored hERG deactivation gating from two different angles, one was the role the NT 1-26 region has in regulating the slow deactivation seen in hERG and the other was to investigate the molecular basis for the slow deactivation of the V659A mutant. Also presented in this thesis is an investigation into drug binding with a series of E-4031 derivatives and potential new insights into the nature of the deactivation gate. The aim of this final chapter is to summarise the findings of the thesis and discuss possible future directions of hERG research.

Role of the N-terminus in deactivation gating

The hERG potassium channel deactivates slowly. This slow deactivation is critical for is normal role in the cardiac action potential. The N-terminus in hERG is approximately 355 residues long. Within the N-terminus residues 1 – 135 are well conserved among the EAG family of potassium channels and thus residues 1 – 135 are termed the EAG domain. Within the EAG domain residues 26 – 135 form a PAS domain. The first crystal structure of a eukaryotic potassium channel from Rod MacKinnon's laboratory was of the hERG PAS domain. It has been known for some time that the intracellular N-terminus has a very important role in the slow deactivation process and removing the N-terminus yields a mutant termed NTK hERG, which deactivates about 10 fold faster than WT hERG and a number of naturally occurring mutations associated with LQTS are located in the EAG domain. The effect of accelerated deactivation seen when the ~355 residues of the N-terminus are removed can be reproduced when only the first 16 residues of the N-terminus are deleted. In the study by MacKinnon's group the structure of the NT 1-26 region was not resolved. Here we present the structure of the NT 1-26

region for the first time along with mutagenesis experiments to determine the molecular basis of the ability of this region to slow deactivation.

The NT 1-26 region was found to contain two distinct parts; residues 1-10 were disordered and residues 11-24 formed an amphipathic α-helix. One face of NT 1-26 was basic and the other face was neutral/hydrophobic. The basic residues are critical for normal slow deactivation. Mutating Arg4 and Arg5 to alanine results in a mutant with deactivation kinetics very similar to that of NTK hERG. Mutations to the other basic residues also accelerated deactivation to rates similar to NTK hERG. The influence of the basic residues on slowing deactivation was limited to NT 1-26 and did not extend to Arg27 and Lys28 in the PAS domain. As well as increasing the speed of deactivation, when the N-terminus is truncated or when certain substitutions are made there is also a substantial shift in the voltage dependence of inactivation gating.

The structure of the NT 1-26 amphipathic helix is important for normal deactivation gating. Introducing a proline at position 18 accelerates deactivation whereas substituting a proline at position 16 on the opposite face of the helix has the opposite effect on deactivation gating. Prolines kink or break α-helices. Disrupting the helix at position 18 seems to prevent the NT 1-26 domain from binding to its receptor and stabilising the open state, whereas at position 16 the change in structure favours stabilisation of the open state.

Previous studies have suggested that the EAG domain acts to slow deactivation by binding to a receptor site somewhere on the channel (Morais-Cabral et al, 1998; Wang et al, 2000). Given the importance of the basic residues in NT 1-26 in deactivation we

looked of areas of acidic residues that the basic residues might be interacting with. One area stood out, the cNBD on the intracellular C-terminus.

A number of charge neutralisation and charge reversal mutants of some of the acidic residues were constructed to investigate the impact on deactivation gating. All of the mutants under investigation increased the rate of deactivation – although it should be pointed out that the effects were modest compared to NT1-26 mutations. This data supports the idea of a charge interaction between the NT 1-26 region and the cNBD.

I believe that the large intracellular N and C-termini will be one of the main focuses of future hERG, and EAG family, research. hERG is one of the largest known potassium channels and the intracellular domains comprise about 75% of the channel. Much of the focus of past research has been around the areas of voltage sensing, transducing movements of the voltage senor into activation of the channel and on ion selectivity and conduction. This research is all in the membrane spanning portion of the channel and we now have good explanations to the questions around those areas. The PAS domain accounts for about one third of the N-terminus and it is not known what the rest of the N-terminus does. Other parts of the N-terminus may be important in gating either directly or through protein/protein interactions that modulate gating. The C-terminus is larger than the N-terminus and is around 500 residues long. Very little is known about how this domain contributes to channel function.

The nature of the interaction of the N-terminus and C-terminus and how this interaction slows deactivation will remain the focus of ongoing research for some time to come. It remains unclear where the site on the cNBD is located, and if it is perhaps elsewhere on

the C-terminus that NT 1-26 interacts with. It is also not known how many of the 4 N-termini that comprise a tetrameric hERG channel are required to slow deactivation. Another question that remains unanswered is whether the N-terminus from one subunit interacts with the C-terminus on that subunit or if it interacts with the C-terminus of another subunit. Solving the structure of the NT 1-26 has given new insights into hERG deactivation gating. The molecular dynamic simulation data was based on the HCN2 cNBD solved by Zagotta et al, 2003. Zagotta's group have just published the cNBD from a member of the EAG family (Kv 12.1) (Brelidze et al, 2012). A structure of the cNBD of hERG would provide more insight into its role in regulating deactivation gating. A structure of both N and C-termini together would provide even better insights into deactivation gating.

The slow activation and deactivation seen in hERG is associated with slow gating currents (Piper et al, 2003). It would be interesting to measure the gating currents in NTK hERG that deactivates very quickly to see if there has been an increase in the rate of the gating currents associated with deactivation. Further to this, it would also be interesting to measure the gating currents of some of the mutants such as R4A:R5A that increase the rate of deactivation to see if there is an increased rate of the gating currents.

Coupling of the voltage sensor domain to the pore domain

How changes in voltage across the plasma membrane are transduced into gating of the pore have been at the forefront of biophysics research for a long time. Crystallographic

studies by MacKinnon and colleagues have provided great insights to the structures of K^+ channel. Long et al, 2005 showed that the S4-S5 linker, a short helical structure that runs perpendicular to the membrane and links the primary voltage sensor in S4 to S5, lies in close proximity to the C-terminal portion of S6. The S4-S5 linker forms a 'cuff' around S6 and what is thought to be the location of the activation gate.

Val659 is crucial for the normal deactivation gating in hERG and is located in the region in the lower part of S6 thought to form the activation gate. In order to investigate the role of Val659 in normal deactivation gating it was mutated to a series of other residues. When Val was mutated to Ile and Phe there was a small slowing of deactivation. The mutation of Val659 to Cys which has a smaller side chain than Val causes a marked slowing of deactivation. The mutation of Val659 to Ala, which has a smaller side chain than Cys, resulted in a channel with even slower deactivation kinetics than V659C. Mutation to glycine which has the smallest side chain of all amino acids resulted in a channel that lacks voltage dependant activation or deactivation gating but retains inactivation gating, suggesting that the activation gate is no longer coupled to the voltage sensing domain – although interestingly inactivation gating is preserved.

To probe if Val659 couples the activation gate to the S4-S5 linker a series of double cysteine mutants were engineered to see if residues came close enough to form disulphide bonds. Results showed that V659C interacts with E544C and Y545C in the S4-S5 linker – and this occurs preferentially when the channel is in the open state. The increases in instantaneous current I-V in E544C:V659C were gradual and increased with every new sweep of the I-V protocol. This increase does not continue indefinitely as current reaches a saturation point, the effect of the oxidising agent does not reverse and is inhibited by pre-treating the cells with the reducing agent DTT.

The results presented here indicate that the channel is locked in an open state through an open state interaction between residues 659 and 544/545. What is unclear is what is happening to S4 in terms of whether it is still moving across the membrane in response to changes in voltage. An obvious follow up experiment would be to measure if the gating charge is reduced in the double mutant E544C:V659C after the addition of $tbHO_2$. A reduction in gating charge would suggest that the voltage sensor has been immobilised.

The results presented here sit well in the existing body of published hERG literature. It has previously been established that Asp540 in the S4-S5 linker couples to Leu666/ Arg665, in S6, in the closed state. Presented here are data that show V659 in the S6, which is two turns of a helix away from Arg665, couples to Glu544 and/or Tyr545 in the S4-S5 linker, which is two turns of a helix away from Asp540, in the open state. The data advances the notion that electromechanical coupling, in hERG at least, is a dynamic process in which the S4-S5 linker forms one discrete interaction with the activation gate in the closed state (D540 with R665) and upon moving into the open state forms another discrete interaction (V659 with Y545) to mediate channel deactivation.

Pharmacology

The aim of developing the derivatives of E-4031 was twofold. One was to use the derivatives as a 'molecular ruler' to measure the size of the inner cavity. The rational was to increase molecule length. It was expected that small molecules would be trapped, whereas the larger molecules would exhibit foot in the door recovery from inhibition. And two, to investigate if molecules that are no longer trapped reduce the

potency of the drug. The derivatives of E-4031 were more potent than E-4031 and increasing the length of the compounds did not reduce their potency. The derivatives displayed rapid recovery from block suggesting that while trapping is important for many drugs that block hERG it is not an absolute requirement for high affinity block.

The pharmacology of hERG is very complex and incredibly interesting. A vast number of structurally diverse drugs block the channel and can lead to Long QT syndrome. Adding to the complexity of hERG channel block is the role that inactivation gating plays. The role of inactivation gating and high affinity drug binding is one of the most intriguing features of hERG. The key aromatic drug binding residues as well as the important drug binding residues at the base of the selectivity filter are conserved in the EAG (Kv10.1) channel but this channel has a considerably lower affinity for blockers. Inactivation gating, which is present in hERG and absent in EAG channels, is thought to cause a rearrangement of the residues on S6 in such a way they are facing into the inner cavity and thus able to bind drugs in hERG but not in EAG. It may be possible to probe the inner cavity residues using the substituted cysteine accessibility method (SCAM) and from the rate of the reaction of MTS reagents with cysteine residues deduce their orientation with respect to the inner cavity.

Mutagenesis experiments have been have been a mainstay of structure/function studies for many years and will continue to be a useful tool in the future. However, the over the past 10 years crystal structures (and also NMR studies) have been pushing the field along at a terrific pace. While mutagenesis studies have enabled great insights into the molecular basis of drug binding to hERG, I believe we are now reaching a point where they have limited value to provide new insights. One area where mutagenesis studies could provide new information is by constructing concatamers to investigate how many

of aromatic residues and those at the base of the selectivity filter are required to achieve high affinity binding and shed light on how many of the four subunits are involved in drug interactions.

A crystal structure of hERG with a drug bound could potentially provide more of an insight than the majority of past mutagenesis studies combined. Given the large size of hERG the prospects of solving the structure with the current techniques soon is slight. However, with every passing year the size of the structures being solved is increasing so I believe this will happen eventually. One strategy that could be used now to solve the structure of the drug binding site with a drug bound is to create a chimera of the S6 and selectivity filter of hERG with a bacterial channel that has previously been crystallised such as KcsA.

Introduction to Appendixes

As well as the three results chapters presented here I have also worked on two other projects. These projects, while fruitful, did not reach a conclusion hence are presented briefly in appendix form rather than in the main body of the thesis.

The aim of these two appendixes are to provide a flavour of the work done so far and not to provide a detailed biophysical analysis of all of the mutants presented here or to provide a detailed description of the methodology.

Project one was the generation of stable cell lines of two hERG mutants, S624A and G648A, to be used to screen and large number of drugs against them using high throughput IonWorks Quattro Automated Patch Clamp System at Novartis Biomedical Research Institute in Horsham, Sussex.

Project two was to investigate if inactivation gating causes a rearrangement of S6 inner cavity drug binding residues in hERG and EAG channels using the substituted cysteine accessibility method.

Chapter 7 - Pharmacology of S624A and G648A hERG mutations

Introduction

The two aromatic resides on S6, Tyr652 and Phe656, are known to be key residues for drug binding to hERG. Other residues around the end of the pore helix and base of the selectively filter are also known to be important. Virtually all hERG blockers are known to be effected by mutation of the aromatic residues. However, mutation of the residues around the base of the selectively filter reduce the potency of some drugs but not others. Two such residues that we wanted to investigate were Ser624 and Gly648 hERG. Ser624 and Gly648 hERG are very important for the binding of some high affinity blockers but appear to play no role in the binding of other high affinity blockers.

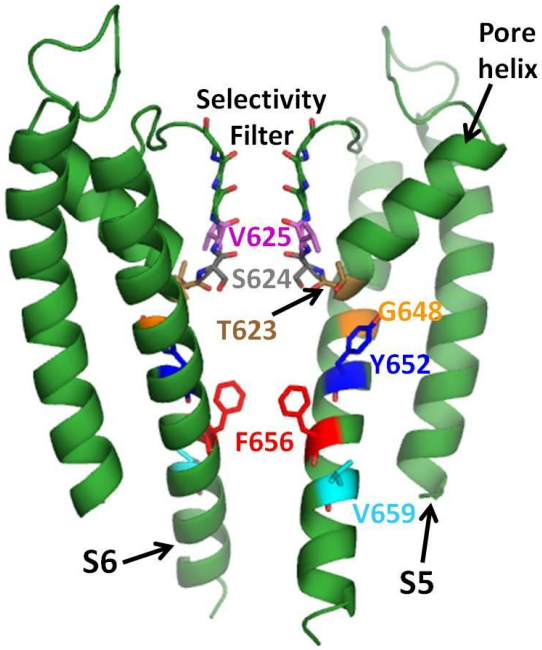

To further investigate this phenomenon we decided to screen a large number of compounds against stable cell lines of S624A and G648A hERG channel mutants using high throughput IonWorks Quattro Automated Patch Clamp System at Novartis Biomedical Research Institute in Horsham, Sussex. By screening a large number of compounds against these mutants we could identify common chemical features of the compounds that are or aren't affected by these mutations and this would aid in the design of future drugs that have reduced hERG potency. An example of the kind of features we hope to detect is shown in figure 7.1. Clofilium is a well known hERG blocker that has a chlorine attached to its phenyl ring.

Analogues of Clofilium with a nitro group increase the potency whereas amine and amide groups attached to the phenyl ring reduce the potency. By screening lots of drugs, a mixture of structurally unrelated and also a close series of structurally related compounds like in figure 7.1, we would be able to establish what are the important physiochemical features of the compounds that are required for high affinity binding to Ser624 or Gly648 and this would help in developing drugs with lower hERG affinity.

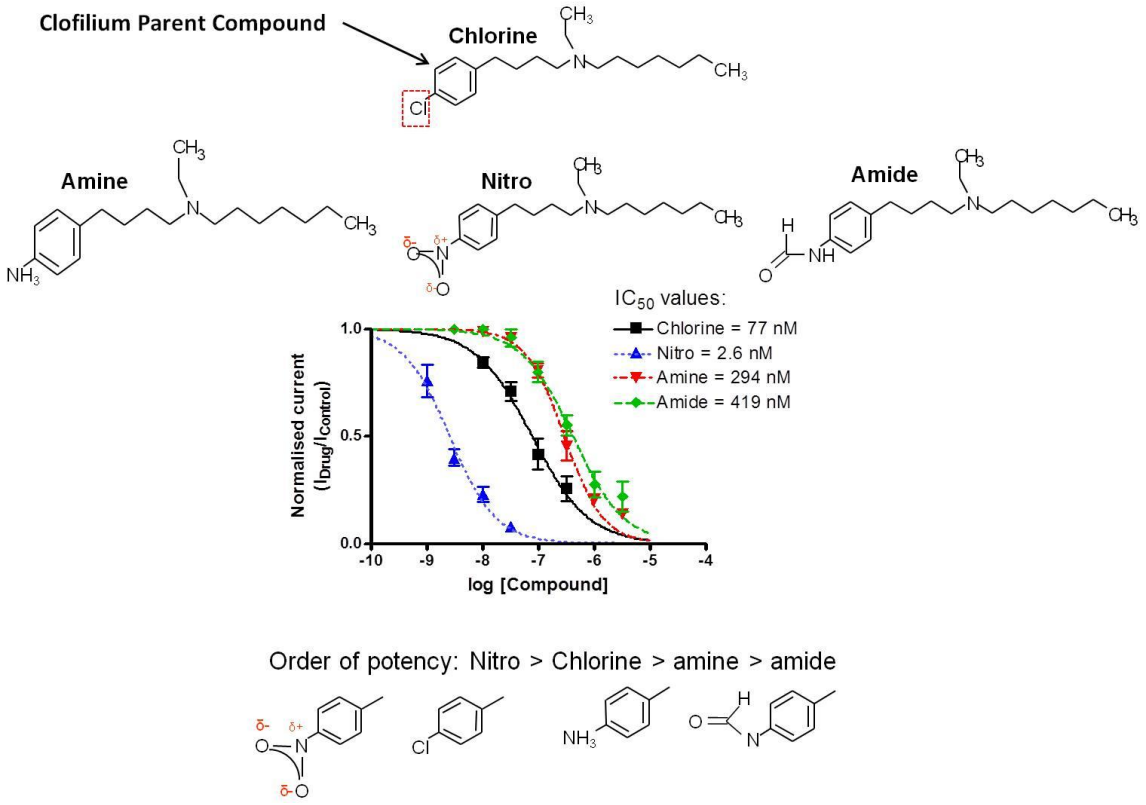

Figure 7.1. Substitution of the phenyl ring para substituent of Clofilium alters potency. The top compound is Clofilium which has a chlorine attached to the phenyl ring. The three compound underneath have had the chlorine swapped for an amine, nitro or amide group. The Clofilium with the nitro group is more potent than the original parent compound whereas the amide and amine compounds are less potent. Data from Dr Matt Perry.

Generation of stable cell lines of S624A and G648A hERG in CHO Cells.

Pervious members of the laboratory had performed experiments on S624A and G648A hERG mutants (not related to this project) therefore it was not necessary to generate these mutations. However, these constructs were in the pSP64 vector that is suitable for expression in *Xenopus* oocytes and not mammalian cell lines. The hERG sequence was cut out of the pSP64 vector by sequential digestion by restriction enzymes first with *Hin*dIII at the 5' end and then with *BamHI* (New England BioLabs, UK) at the 3' end. The hERG sequence was then ligated into pCDNA3, which is suitable for expression in mammalian cell lines such as the CHO T-Rex cells used here, using T4 DNA Ligase (New England BioLabs, UK). CHO T-Rex cells were chosen as the background to make the stable cell lines because this is the standard cell line that Novartis use on their IonWorks Quattro Automated Patch Clamp System and the cells were provided courtesy of Novartis

Before generating the stable cell lines it was necessary to confirm that these new constructs produced functional channels and to validate the transfection protocol. Transiently transfected CHO cells were tested for expression of hERG channels by recording whole cell currents using the patch clamp technique 24 to 48 hours after transfection.

The transfection protocol was as follows. Pre-transfection the cells were maintained in Ham's F-12 media supplemented with 10% FBS (fetal bovine serum) and 1% Pen/Strep (10µg/ml) (Gibco, UK). 24 hours before transfection cells were plated into a 6 well plate and grown in antibiotic free media to be 90 – 95% confluent at the time of transfection. Just prior to transfection the media was aspirated, the cells were washed with PBS and new media with no supplements was added to the wells. The S624A/G648A DNA and

Lipofectamine 2000 mix was added to the wells and left for 6 hours in the incubator. After 6 hours the media was changed for 'normal' media. The cells were then tested for expression of hERG channels using the patch clamp technique 24 to 48 hours after transfection.

Figure 7.2 shows S624A currents. The top panel shows currents recorded using a standard I-V voltage protocol. The membrane potential was held at -80mV and stepped in 10mV increments for 5 seconds up to +50mV. The tail currents were recorded at -50mV before returning to the holding potential. S624A produces robust voltage dependant currents similar to WT hERG. The bottom panel of figure 7.2 shows S624A currents from a fully activated I-V protocol similar to the one used in chapter 3 to measure the rate of deactivation. From a holding potential of -80mV the membrane potential was stepped to +50mV for 1 second to fully activate and inactivate the current. The membrane potential was then stepped down from in 10mV increments from -30mV to -140mV. Current were recorded in a 4mM external K^+ solution.

Figure 7.3 shows a representative I-V current trace of G648A hERG. This mutant is known to be highly inactivated so this mutant was recorded in a high, 96mM external K^+ solution that shifts inactivation to more negative potentials. The membrane potential was held at -80mV and stepped in 10mV increments for 5 seconds up to +40mV. The membrane potential was then stepped down to -140mV to record inward tail currents before returning to the holding potential. There are no observable outward voltage dependant currents when depolarising the cell for 5 second steps but on stepping down to -140mV there are robust voltage dependant inward tail currents, show in the expanded trace in the bottom panel.

To make the stable cells the protocol was as above but rather than patch clamping the cells after 24 hours the cells were split 1:10 and left for a futher 24 hours in the incubator then teh media was changed for media contains the same supplements as above but with the addition of 1% G418 (500µg/ml). The G418 serves as a selection medium to kill any non-transfected cells. The cells were left for 2 weeks while to allow non-transfected cells to die with the media being changed every 2 days. After 2 weeks individual cells were picked and placed into a 96 well plate. These clones were then grown up through 48, 24, 12 and 6 well plates until there were enough cells to be seeded into a T-10 flask. The cells continued to been grown until they reached 90% confluent in a large T-175 flask. The reason for growing the cells up to such a large number in a T-175 flask was that the cells were to be tested for expression of hERG channels by patch clamp on IonWorks Quattro Automated Patch Clamp System by directly patching them from frozen cell stocks. Thus the cells were grown into T-175 flasks to ensure that there would be more than the $3.5x10^6$/ml required to be able to patch them directly from frozen.

Approximately 60 clones of each of the 2 mutants were made. The cells were shipped on dry ice to Novartis. Around a quarter of the clones made were tested for hERG channel expression on the IonWorks Quattro Automated Patch Clamp System. A change in research priorities for Novartis resulted in the rest of the clones not being tested and the project was not pursued any further.

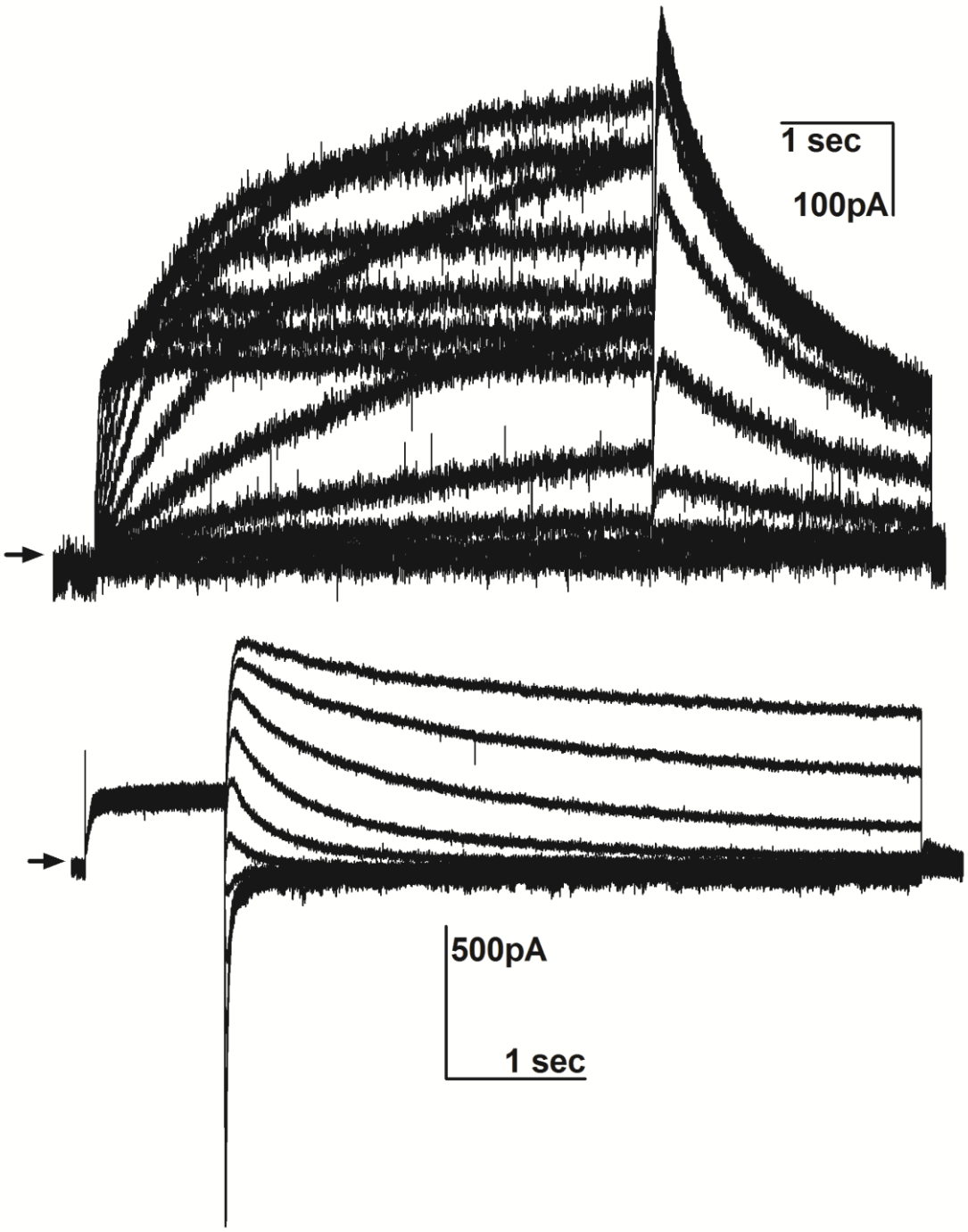

Figure 7.2 Representative current traces of S624A hERG.

The top panel shows an I-V current trace. The cells were held at -80mV and stepped in 10mV increments for 5 seconds to +50mV before stepping down to -50mV to elicit tail currents.

The bottom panel shows a current trace for a fully activated I-V. The cell was held at -80mV and stepped to +50mV for 1 second to fully activate and inactivate the channel. The cell was then stepped down to a range of potentials from -30mV to -140mV in 10mV increments for 5 seconds. Currents recorded in the whole cell configuration of the patch clamp technique.

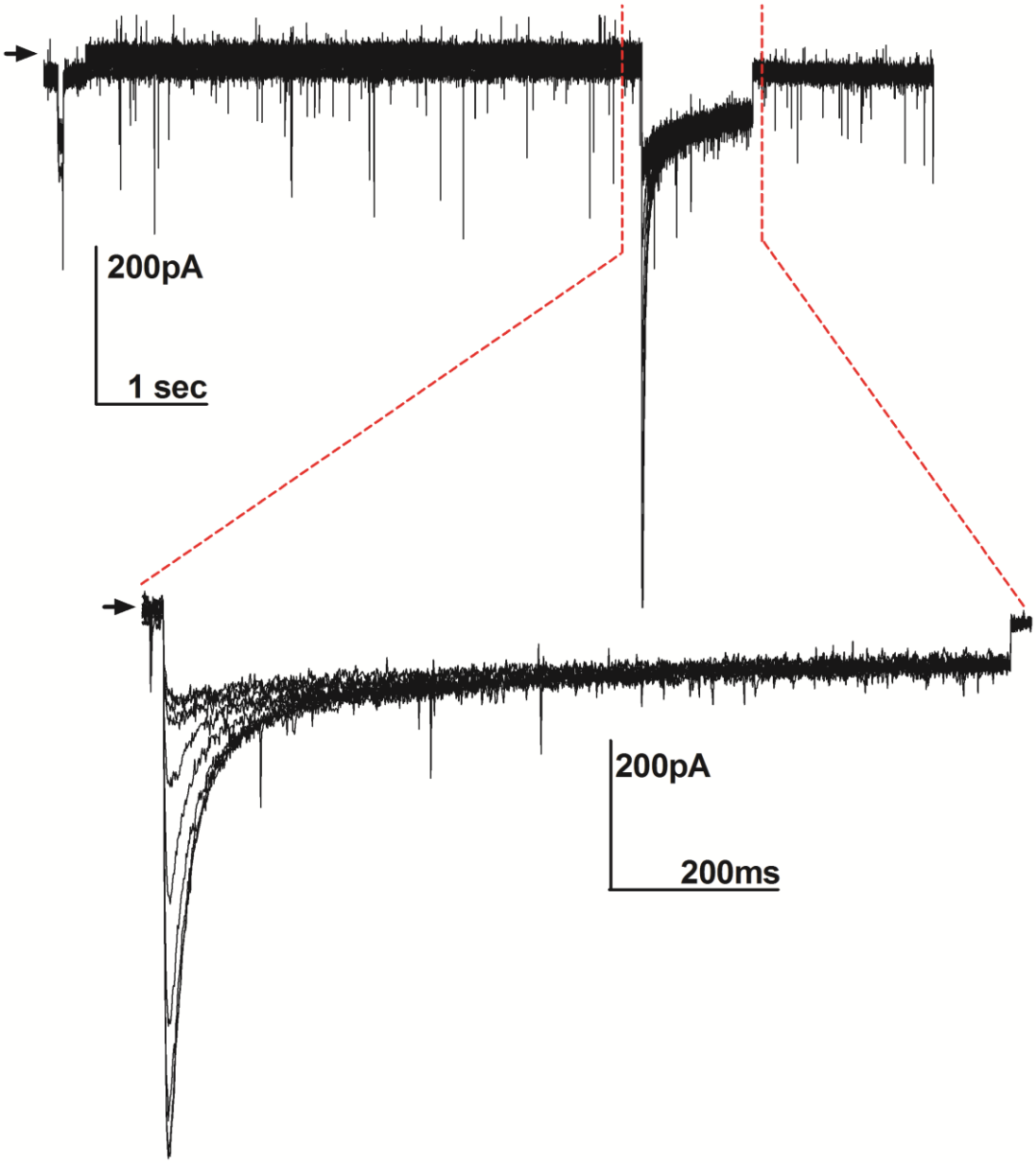

Figure 7.3 Representative I-V current trace of G648A hERG.

The top panel shows an I-V current trace. The cells were held at -80mV and stepped in 10mV increments for 5 seconds to +40mV before stepping down to -140mV to elicit tail currents. G648A is highly inactivated therefore a high 96mM K^+ solution was used to shift the $V_{0.5}$ of inactivation in a negative direction. The G648A mutant has little in the way of outward voltage dependant current on stepping to the test potentials but displays robust voltage dependant inward currents on stepping down to -140mV.

The bottom panel shows an expended view of the tail currents. The inward tail currents increase with every passing step to a new test potential.

Conclusions

The S624A and G648A hERG mutants produce robust hERG currents when transiently expressed in CHO T-Rex cells. Around a quarter of the ~120 clones generated so far have been tested for stable expression of hERG channels by patching them directly from frozen cell stocks on the IonWorks Quattro Automated Patch Clamp System at Novartis Biomedical Research Institute in Horsham, Sussex. The remaining clones remain in storage in -80^{O}C freezers in Leicester and Horsham. This project could easily be continued by another PhD student at some point in the future.

Chapter 8 - Appendix 2

What accounts for the difference in drug binding between hERG and EAG?

Introduction

hERG (Kv 11.1) and EAG (Kv 10.1) channels belong to the EAG family of potassium channels. hERG is block by many drugs with high affinity where as EAG is far less sensitive to block by the same compounds (figure 8.1, top). The molecular basis of this is not understood as the two key aromatic drug binding residues on S6 as well as the important residues around the base of the selectivity filter are present in both hERG and EAG channels (figure 8.1, bottom). A crucial difference may be the lack of inactivation in EAG channels. hERG channels exhibit C-type like inactivation. Like C-type inactivation in other K_v channels this is a constriction of the selectivity filter to make it impermeable to K^+ ions. However, the onset and recovery from inactivation is significantly faster than other Kv channels (Spector et al, 1996; Smith et al, 1996). It has been known for some time now that there is a link between inactivation gating and drug binding. Mutations to EAG channels that introduce C-type inactivation increase sensitivity to drug block (Ficker et al, 2001). Conversely, mutations that remove C-type inactivation in hERG (e.g. G628C:S631C) exhibit decreased sensitivity to drug block (Ficker et al, 1998). Experiments by Chen et al 2002, showed that if the two aromatic residues on S6 of EAG are mutated to be placed one residues lower (towards the carboxy terminus) this increases the sensitivity of EAG to block. They also showed that if the two aromatic residues on the S6 of hERG are mutated to be one position lower (again towards the carboxy terminus) this decreases the sensitivity of hERG to block. Moving the aromatic residues to the adjacent position means that they are now orientated 100^O round the S6 helix and the side chains of the aromatic residues are not facing in the same directions

as they were in the WT channel. It therefore appears that simply having the aromatic residues present on S6 is not enough for high affinity drug binding but these residues must be in the correct orientation to be able to interact with the drug molecules. It is thought that inactivation in hERG causes a repositioning of inner cavity residues from a position where they are not optimally arranged to bind drug to one where there are (Chen et al, 2002). Work on Shaker has shown that during inactivation not only is there a rearrangement of amino acids around the outer mouth of the channel but there is also a rearrangement of residues in the inner cavity (Panyi & Deutsch 2006).

We believe that inactivation gating in hERG causes a rearrangement of the inner cavity drug binding residues that results in them facing into the inner vestibule of the channel but as EAG channels lack inactivation gating they are not positioned in facing into the inner vestibule but are faced toward S5 and not optimally positioned to bind drugs.

To test this experimentally we introduced cysteine residues along the S6 of hERG and EAG channels, from Met651 to Gly657 in hERG and Leu462 to Gly469 in EAG and used the substituted cysteine accessibility mutagenesis (SCAM) method to assess the rate of modification of the cysteine residues to Methanethiosulfonate (MTS) reagents. The thiol group on the cysteine side chain will react with the thiol group on the MTS reagent and this is detectable though alterations to channel current levels or altered gating processes. The higher the rate of modification the more accessible the residue is to the MTS reagents. Thus a residue with a high rate of modification compared to its neighbouring residue is more like to be orientated towards the inner cavity of the channel.

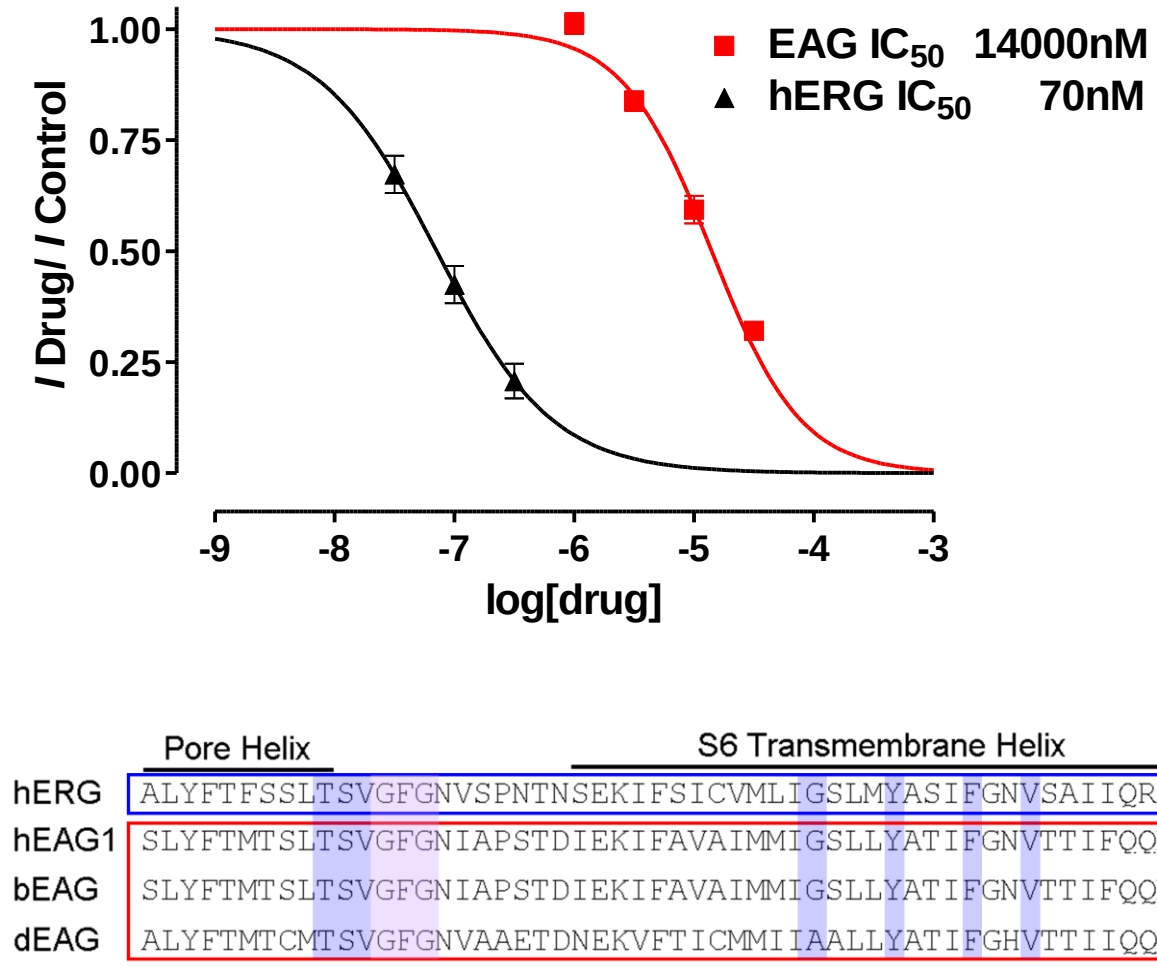

Figure 8.1. EAG is far less sensitive to block than hERG even though the key drug binding residues are conserved. The top panel shows the IC_{50} of Cisapride (a well known hERG blocker) on WT hERG and WT EAG. Cisapride is far less potent on EAG than hERG. The bottom panel is a sequence alignment of the selectively filter and S6 of hERG and EAG channels. The key aromatic residues Tyr and Phe in the middle of S6 are conserved. Also conserved are the residues at the base of the pore helix that are important in drug binding.

The aims of this chapter were to

1) Precisely measure and compare the accessibility of hERG and EAG S6 residues using substituted cysteine accessibility mutagenesis (SCAM)

2) Investigate if EAG mutations around the outer mouth of the channel that induce inactivation also have an allosteric effect on drug binding residues.

3) Probe voltage dependent differences in the hERG cavity of inactivated versus non-inactivated channels.

Results

A personal communication between Dr Mitcheson and Roland Schonherr in Germany indicated there were 5 endogenous cysteine residues in WT EAG that may react with MTS reagents and that would have to be mutated to alanine before any experiments could commence, thus the following mutations were made sequentially to remove them. The final construct with the 5 cysteines mutated to alanines was called 5A EAG.

Table 8.1. Mutations in EAG to remove endogenous cysteines

	EAG mutation	Note
1	C128A	The first 3 mutations are in the N-terminus
2	C128A:C145A	
3	C128A:C145A:C214A	
4	C128A:C145A:C214A:C532A	The last 2 mutations are in the C-terminus
5	C128A:C145A:C214A:C532A:C562A	This construct with all 5 Ala mutations is called 5A EAG

Having constructed 5A EAG it was necessary to validate that this construct produced a functional channel with gating properties similar to WT EAG. Figure 8.2 shows representative I-V current traces of WT EAG and 5A EAG. 5A EAG channels produce the similar slow activating outward voltage dependant currents as WT EAG.

Having validated that 5A EAG currents are similar to WT EAG currents using two-electrode voltage clamp I then validated if 5A EAG was affected by MTS reagents by excising inside-out patches of oocyte membrane contain 5A EAG channels using the patch clamp technique. It was necessary to use inside-out patches as the MTS reagents are not membrane permeable and in order to access the inner cavity they must have access to the intracellular side of the membrane. Patches were excised and repetitively

pulsed to +40mV from a holding potential of -80mV to activate the channel. This protocol is similar to the repetitive pulsing protocol used in chapter 5 to block hERG channel with E-4031 and the derivatives. After the current had stabilised a high concentration (1mM) MTS was bath applied while still repetitively pulsing. Figure 8.3 shows a representative current trace of 5A EAG before and after the addition of MTS reagent. The MTS reagents had no effect on the current.

Having confirmed that 5A EAG is a functional channel and that it is not affected by MTS regents I could then mutate the S6 residues from Leu462 to Gly469 to cysteine in the 5A EAG background figure 8.4. These mutations are shown in table 8.2. Also shown in table 8.2 are the cysteine mutations made at the equivalent positions in hERG which are presented later in figure 8.7. L462C, L463C and T466C EAG currents are wild type like. Y462C currents are wild type like but currents are very small. A465C, I467C and F468C EAG currents display inactivation. G469C shows slight inactivation at the most positive potentials. This inactivation is not an indented consequence of the mutation.

Table 8.2. EAG and hERG cysteine mutations in S6

EAG **(all mutations below are made in the 5A EAG background)**	**hERG**
L462C	
L463C	M651C
Y464C	Y652C
A465C	A653C
T466C	
I467C	I655C
F468C	F656C
G469C	G657C

MTS reagents are not though to affect WT hERG so no endogenous cysteines were removed and the S6 cysteine scan was made in the WT hERG background. I655C appears to be constitutively open and displays inactivation gating at the more positive membrane potentials. F656C hERG is very similar to WT hERG. M651C and A653C hERG deactivate slower than WT hERG. Y652C hERG deactivates faster than WT hERG.

In order to investigate if the introduction of mutations that induce inactivation increase the rate of modification of the inner cavity residues to MTS reagents it was therefore necessary to engineer in such mutations. The mutations that were introduced into EAG to elicit inactivation gating are shown in table 8.3. These mutations are located around the outer mouth of the channel.

Table 8.3. Mutations that introduce inactivation gating to EAG

	Mutation (all mutations below are made in the 5A EAG background)	**Note**
1	5A EAG + T432S	
2	5A EAG + T432S + A443S	
3	5A EAG+T432S+A443S+A453S	This construct is called 5A 3inact EAG and contains 8 mutations

The 5A 3inact EAG construct, which contains 8 mutations, produces a functional channel, figure 8.5. At the more positive membrane potentials there is a decrease in current as shown in the conductance-voltage relationship in figure 8.5 and 8.6 which is consistent with inactivation gating.

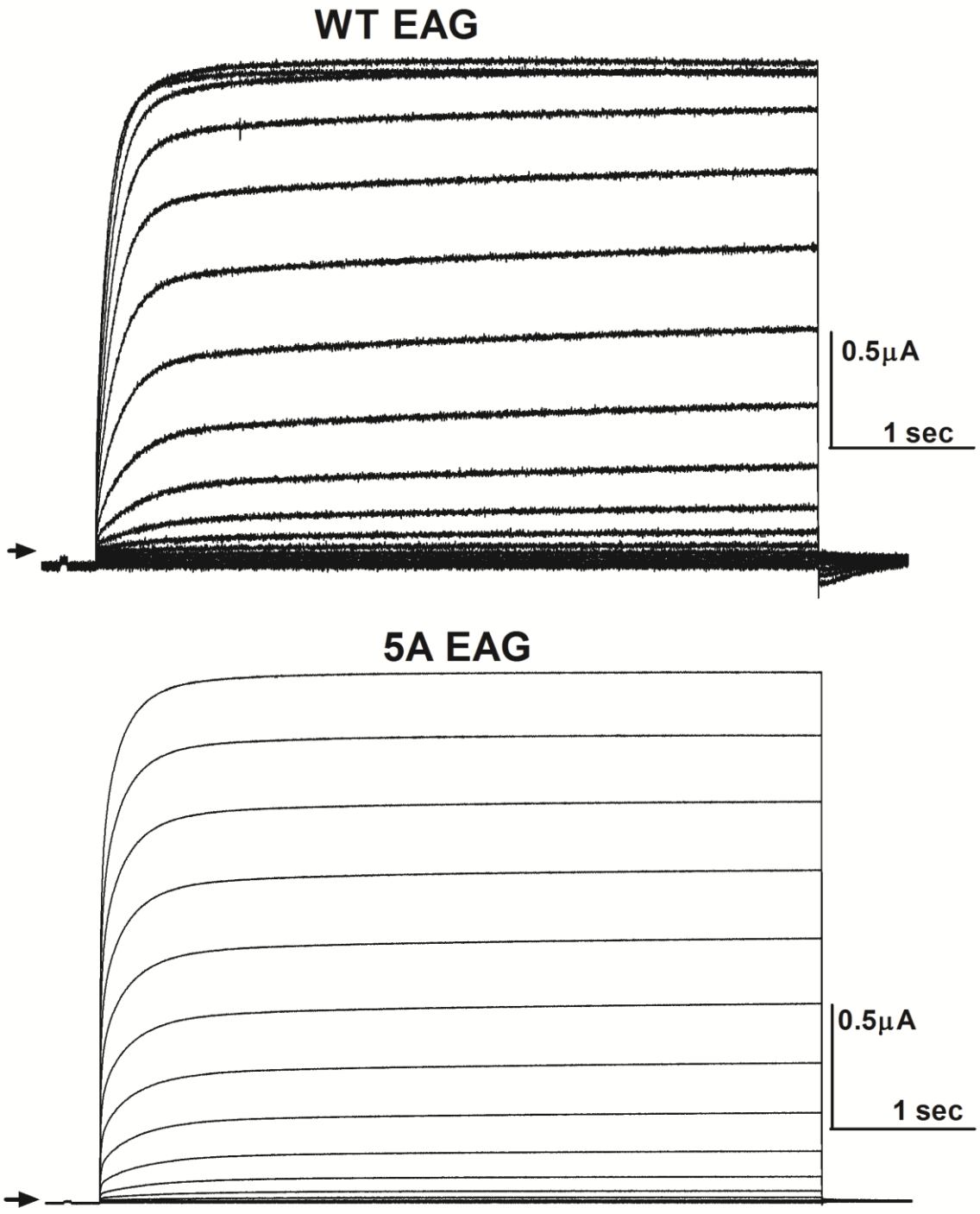

Figure 8.2 Representative I-V current traces of WT and 5A EAG. The membrane potential was held at -90mV and stepped in 10mV increments to +70mV for 5 seconds before stepping down to -70mV for 2 seconds then returned to the holding potential. WT and 5A EAG have similar current traces.

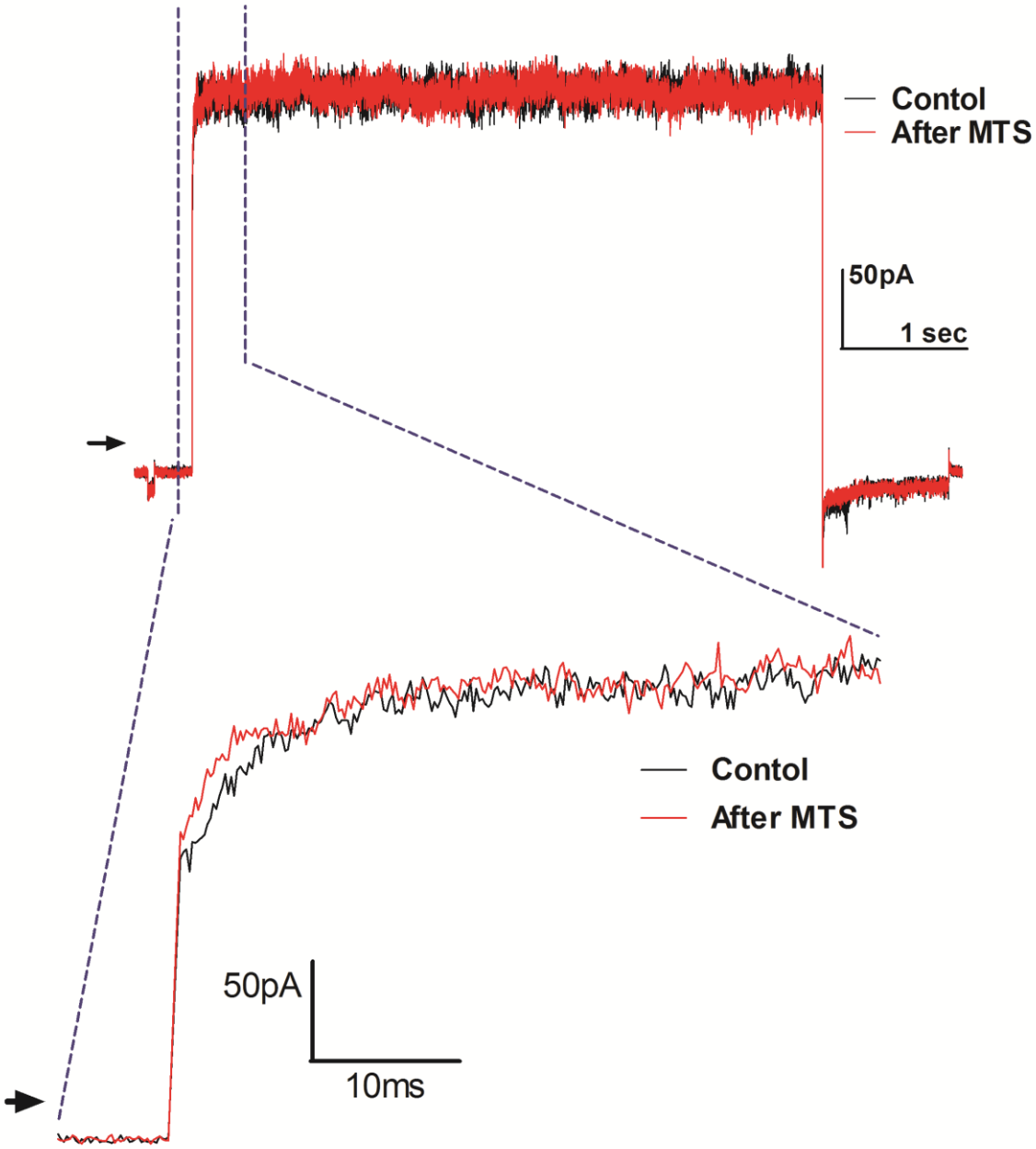

Figure 8.3 Representative current traces of 5A EAG before and after application of MTS reagents. The membrane potential was held at -80mV and stepped to +40mV for 5 seconds before stepping down to -50mV for 1 seconds and then back to the holding potential. 5A EAG expresses well and produces robust current in inside-out patches of excised oocyte membrane. These currents are not affected by MTS reagents. Current trace with MTS is around 45 seconds after application of the MTS.

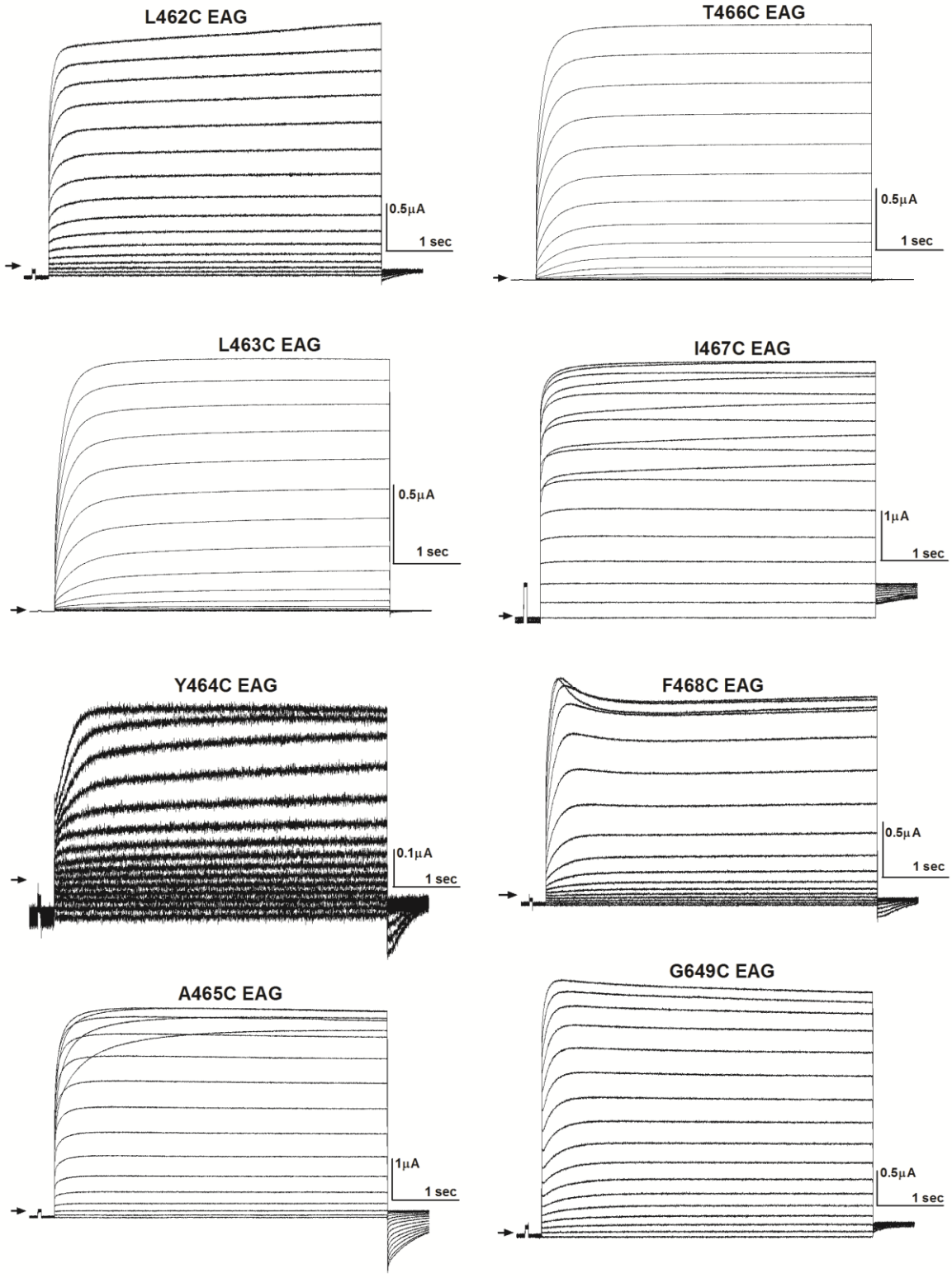

Figure 8.4. Representative I-V current traces for EAG S6 Cysteine. The membrane potential was held at -90mV and stepped in 10mV increments to +70mV for 5 seconds before stepping down to -70mV for 2 seconds then returned to the holding potential. Expression of Y464C was low.A465C, I467C and F468C show reduced current levels at the most positive potentials indicative of inactivation. All of these mutants were made in the 5A EAG mutant background.

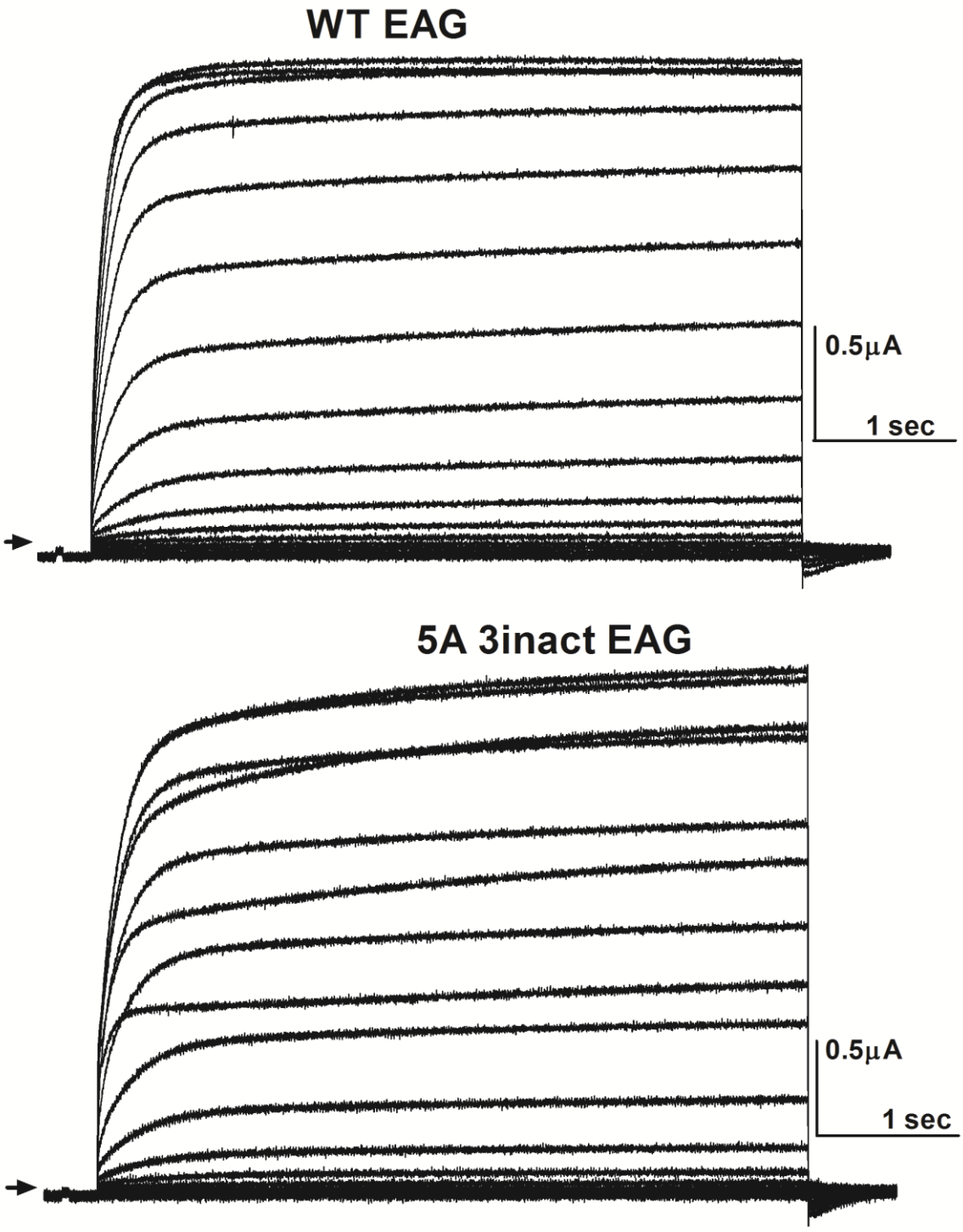

Figure 8.5. Representative I-V current traces of WT and 5A 3inact EAG. The membrane potential was held at -90mV and stepped in 10mV increments to +70mV for 5 seconds before stepping down to -70mV for 2 seconds then returned to the holding potential. 5A 3inact EAG currents reduce at more positive

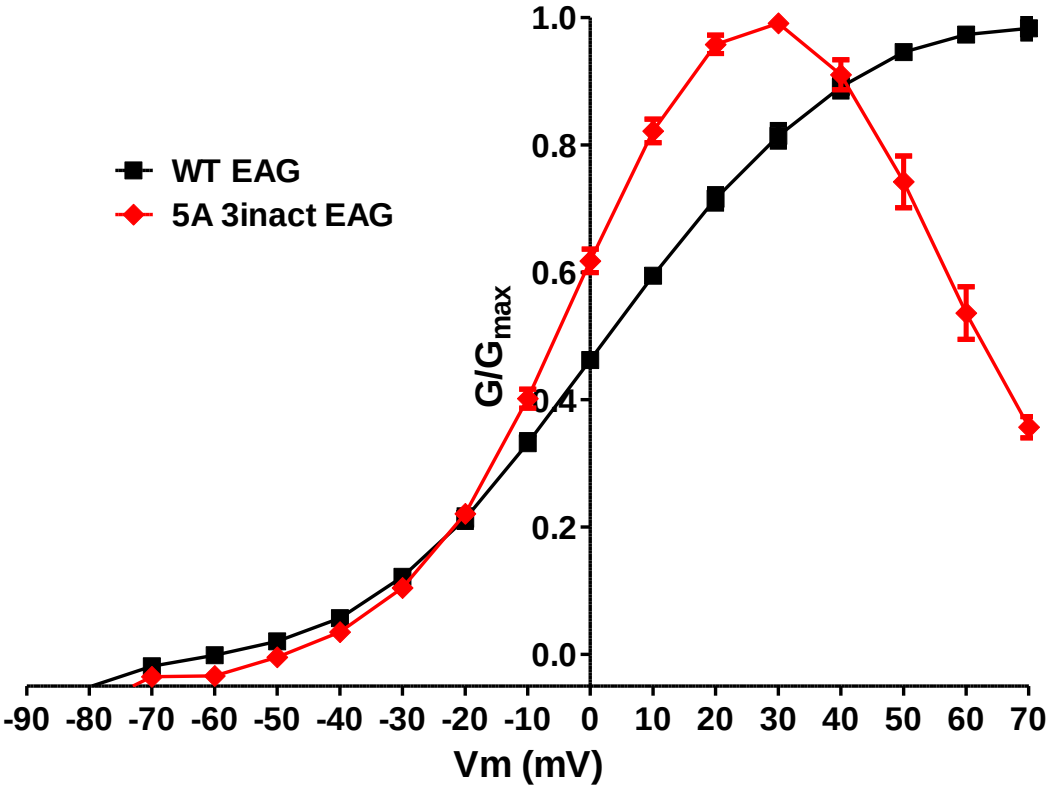

Figure 8.6. Conductance voltage relationship for WT and 5A 3inact EAG. WT EAG has a shallow G-V relationship and the channel reaches maximum conductance around +60mV. There is no reduction in conductance at positive membrane potentials in WT EAG. The G-V relationship for 5A 3inact EAG is steeper than WT EAG and reaches maximum conductance about +30mV. Positive to +30mV there is a reduction in conductance that is consistent with inactivation gating.

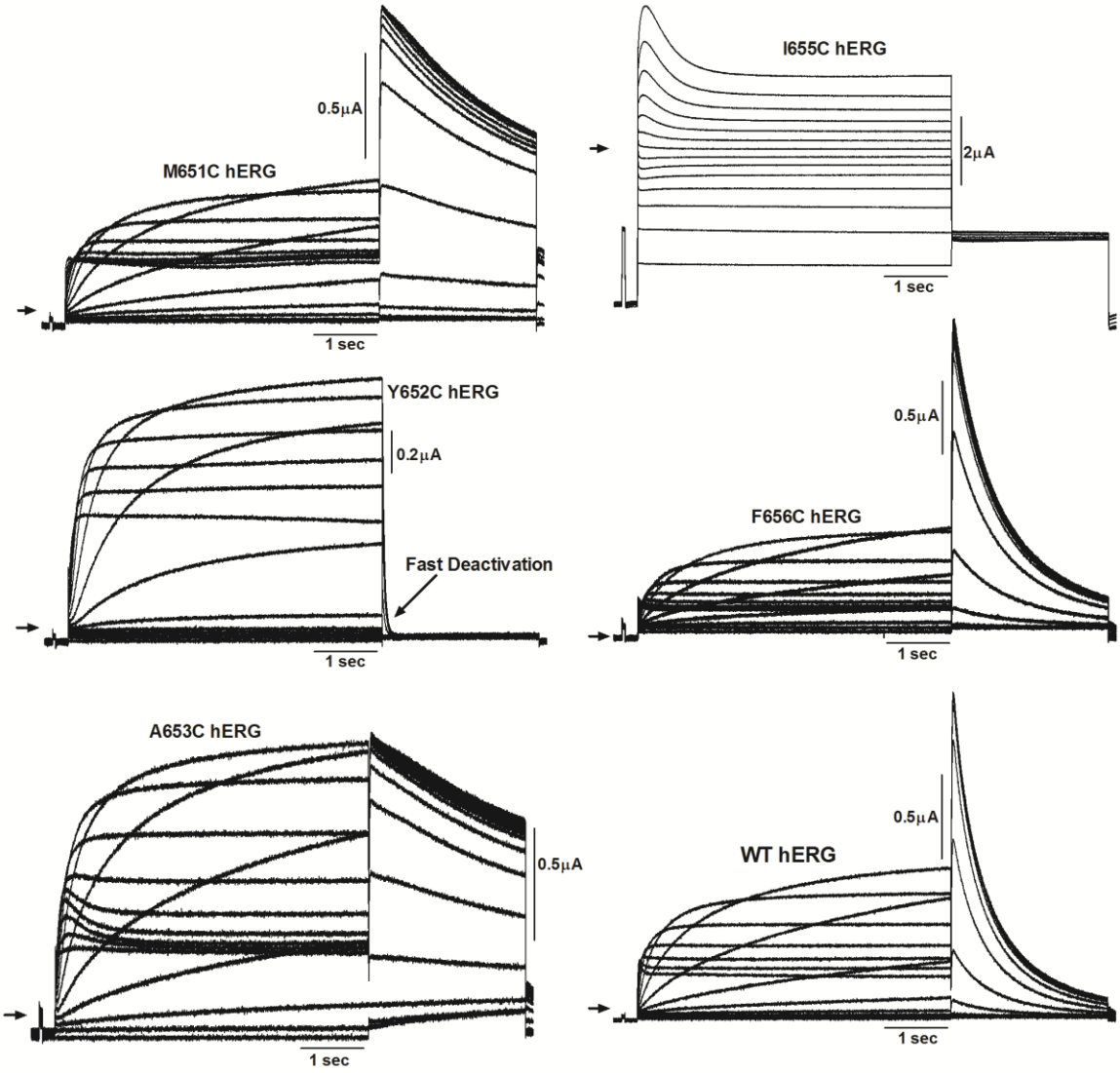

Figure 8.7. Representative I-V current traces for hERG S6 Cys mutants. The currents were elicited using the standard I-V voltage protocol as in previous chapters. The membrane potential was held at -90mV and then stepped to +50mV for 5 seconds in 10mV increments. The membrane potential was then stepped down to -70mV to elicit tail currents before returning to the holding potential. WT hERG is shown bottom right for comparison. I655C appears to be constitutively open and displays inactivation gating at the more positive membrane potentials. F656C hERG is very similar to WT hERG. M651C and A653C hERG deactivate slower than WT hERG. Y652C hERG deactivates faster than WT hERG. Arrow indicates zero current level.

Conclusions

All of the mutants made for the project so far produce functional channels, although some express poorly and some have altered gating properties. These alterations to gating are not entirely surprising, for example, it is already know that I655A hERG produces a non-functional channel (Mitcheson, 2000) so the altered gating in I655C hERG seen here is not a great revelation. The data presented provide the proof of concept that these experiments are feasible and should provide insights into the relationship between inactivation gating in hERG and EAG channels and drug binding. The 5A EAG construct produces currents similar to WT EAG and 5A EAG was not affected by MTS reagents. The S6 cysteine scan in the 5A EAG background produced functional channels.

There are 8 mutations in the cysteine scan of the EAG S6 and 6 mutations in the cysteine scan of hERG. This is so the experimental technique and hypothesis could be validated before making all the mutants required for the whole project. Further mutants that will need to be made are to put the same cysteine scan into the 5A 3inact background to enable comparison of the accessibility of the MTS reagents between the EAG channel with and without inactivation gating.

The cysteine scan in the S6 of hERG will also have to be reproduced in various inactivation mutant backgrounds such as W563A and Y542A. W563A shifts the voltage dependence of activation about -60mV with no affect on inactivation gating meaning that the channel can be almost fully activated at -80mV with little or no inactivation gating. Y542A has the opposite effect on gating, it shifts the voltage dependence of inactivation to positive potentials without effecting activation gating, and thus the channel can again be opened with little or no inactivation. I have already made and

characterised W563A and Y542A but as these mutants have previous described in published work (ref, Vandenberg paper and Xu paper) I have not presented the data here. Mutations that abolish inactivation such as S620T and G628C:S631C may also be used.

The work presented here (and also work by Mike Chang, not presented here) was used in a successful grant application to the British Heart Foundation and this work is being continued by Dr Eva Loerinczi.

References

Abbott, G.W., Sesti, F., Splawski, I., Buck, M.E., Lehmann, M.H., Timothy, K.W., Keating, M.T., Goldstein, S.A., 1999. MiRP1 forms IKr potassium channels with HERG and is associated with cardiac arrhythmia. *Cell.* **97,** 175-87.

Aggarwal, S.K. & MacKinnon, R., 1996. Contribution of the S4 segment to gating charge in the Shaker K+ channel. *Neuron.* **16,** 1169-177.

Alabi, A.A., Bahamonde, M.I., Jung, H.J., Kim, J.I., Swartz, K.J., 2007. Portability of paddle motif function and pharmacology in voltage sensors. *Nature.* **450,** 370-375.

Al-Owais, M., Bracey, K., Wray, D., 2009. Role of intracellular domains in the function of the herg potassium channel. *Eur Biophys J.* **38,** 569-576.

Armstrong, C.M., 1971. Interaction of tetraethylammonium ion derivatives with the potassium channels of giant axons. *J Gen Physiol.* **58,** 413-437.

Armstrong, C.M., 1969. Inactivation of the potassium channel conductance and related phenomena caused by quarternary ammonium ion injection in squid axons. *J Gen Physiol.* **54,** 553-575.

Armstrong, C.M., 1968. Induced inactivation of the potassium permeability of squid axon membranes. *Nature.* **219,** 1262-1263.

Armstrong, C.M. & Bezanilla, F., 1977. Inactivation of the sodium channel. II. Gating current experiments. *J Gen Physiol.* **70,** 567-590.

Aydar, E. & Palmer, C., 2001. Functional characterization of the C-terminus of the human ether-a-go-go-related gene K+ channel (HERG). *Journal of Physiology-London.* **534,** 1-14.

Barhanin, J., Lesage, F., Guillemare, E.,Fink, M., Lazdunski, M., Romey, G., 1996, KvLQT1 and IsK (mink) proteins associate to form the I_{Ks} cardiac potassium current. *Nature,* **384,** 78-80.

Barry, D.M. & Nerbonne, J.M., 1996. Myocardial potassium channels: electrophysiological and molecular diversity. *Annu Rev Physiol.* **58,** 363-94.

Bers, D.M., 2001. Excitation-Contraction Coupling and Cardiac Contractile Force. 2nd Ed.

Bers, D.M., 2002. Cardiac excitation-contraction coupling. *Nature.* **415,** 198-205.

Brelidze, T.I., Carlson, A.E., Sankaran, B., Zagotta, W.N., 2012. Structure of the carboxy-terminal region of a KCNH channel. *Nature.* **481,** 530-533.

Brelidze, T.I., Carlson, A.E., Zagotta, W.N., 2009. Absence of direct cyclic nucleotide modulation of mEAG1 and hERG1 channels revealed with fluorescence and electrophysiological methods. *J Biol Chem.* **284,** 27989-27997.

Chen, J., Mitcheson, J.S., Tristani-Firouzi, M., Lin, M., Sanguinetti, M.C., 2001. The S4-S5 linker couples voltage sensing and activation of pacemaker channels. *Proc Natl Acad Sci U S A.* **98,** 11277-11282.

Chen, J., Seebohm, G., Sanguinetti, M.C., 2002. Position of aromatic residues in the S6 domain, not inactivation, dictates cisapride sensitivity of HERG and eag potassium channels. *Proc Natl Acad Sci U S A.* **99,** 12461-12466.

Chen, J., Zou, A., Splawski, I., Keating, M.T., Sanguinetti, M.C., 1999. Long QT syndrome-associated mutations in the Per-Arnt-Sim (PAS) domain of HERG potassium channels accelerate channel deactivation. *Journal of Biological Chemistry.* **274,** 10113-8.

Choi, K.L., Aldrich, R.W., Yellen, G., 1991. Tetraethylammonium blockade distinguishes two inactivation mechanisms in voltage-activated K+ channels. *Proc Natl Acad Sci U S A.* **88,** 5092-5095.

Clayton, G.M., Altieri, S., Heginbotham, L., Unger, V.M., Morais-Cabral, J.H., 2008. Structure of the transmembrane regions of a bacterial cyclic nucleotide-regulated channel. *Proc Natl Acad Sci U S A.* **105,** 1511-1515.

Cordero-Morales, J.F., Cuello, L.G., Perozo, E., 2006. Voltage-dependent gating at the KcsA selectivity filter. *Nat Struct Mol Biol.* **13,** 319-322.

Cordero-Morales, J.F., Cuello, L.G., Zhao, Y., Jogini, V., Cortes, D.M., Roux, B., Perozo, E., 2006. Molecular determinants of gating at the potassium-channel selectivity filter. *Nat Struct Mol Biol.* **13,** 311-318.

Cordero-Morales, J.F., Jogini, V., Lewis, A., Vasquez, V., Cortes, D.M., Roux, B., Perozo, E., 2007. Molecular driving forces determining potassium channel slow inactivation. *Nat Struct Mol Biol.* **14,** 1062-1069.

Cordes, F.S., Bright, J.N., Sansom, M.S.P., 2002. Proline-induced distortions of transmembrane helices. *J Mol Biol J Mol Biol.* **323,** 951-960.

Cuello, L, G., Jogini, V., Cortes, D., Pan, A, C., Roux, B., Perozo, E., 2010. Structureal basis for the coupling between activation and inactivation gates in K+ channels. *Nature,* **466**, 272-276.

Curran, M.E., Splawski, I., Timothy, K.W., Vincent, G.M., Green, E.D., Keating, M.T., 1995. A molecular basis for cardiac arrhythmia: HERG mutations cause long QT syndrome. *Cell.* **80,** 795-803.

Decher, N., Chen, J., Sanguinetti, M.C., 2004. Voltage-dependent Gating of Hyperpolarization-activated, Cyclic Nucleotide-gated Pacemaker Channels: MOLECULAR COUPLING BETWEEN THE S4-S5 AND C-LINKERS. *J Biol Chem.* **279,** 13859-13865.

Delisle, B.P., Anson, B.D., Rajamani, S., January, C.T., 2004. Biology of cardiac arrhythmias: ion channel protein trafficking. *Circ Res.* **94,** 1418-1428.

Ding, S., Ingleby, L., Ahern, C.A., Horn, R., 2005. Investigating the putative glycine hinge in Shaker potassium channel. *J Gen Physiol.* **126,** 213-226.

Doyle, D.A., Morais Cabral, J., Pfuetzner, R.A., Kuo, A., Gulbis, J.M., Cohen, S.L., Chait, B.T., MacKinnon, R., 1998. The structure of the potassium channel: molecular basis of K+ conduction and selectivity. *Science.* **280,** 69-77.

Elliott, D.J., Neale, E.J., Aziz, Q., Dunham, J.P., Munsey, T.S., Hunter, M., Sivaprasadarao, A., 2004. Molecular mechanism of voltage sensor movements in a potassium channel. *Embo J.* **23,** 4717-4726.

Elliott, D.J.S., Dondas, N.Y., Munsey, T.S., Sivaprasadarao, A., 2009. Movement of the s4 segment in the herg potassium channel during membrane depolarization. *Molecular Membrane Biology.* **26,** 435-447.

Fan, J.S., Jiang, M., Dun, W., McDonald, T.V., Tseng, G.N., 1999. Effects of outer mouth mutations on hERG channel function: a comparison with similar mutations in the Shaker channel. *Biophysical Journal.* **76,** 3128-3140.

Fernandez, D., Ghanta, A., Kauffman, G.W., Sanguinetti, M.C., 2004. Physicochemical features of the HERG channel drug binding site. *Journal of Biological Chemistry.* **279,** 10120-10127.

Ferrer, T., Rupp, J., Piper, D.R., Tristani-Firouzi, M., 2006. The S4-S5 linker directly couples voltage sensor movement to the activation gate in the human ether-a'-go-go-related gene (hERG) K+ channel. *J Biol Chem.* **281,** 12858-12864.

Ficker, E., Jarolimek, W., Brown, A.M., 2001. Molecular determinants of inactivation and dofetilide block in ether a-go-go (EAG) channels and EAG-related K+ channels. *Molecular Pharmacology.* **60,** 1343-1348.

Ficker, E., Jarolimek, W., Kiehn, J., Baumann, A., Brown, A.M., 1998. Molecular determinants of dofetilide block of HERG K+ channels. *Circ Res.* **82,** 386-95.

Gustina, A.S. & Trudeau, M.C., 2011. hERG potassium channel gating is mediated by N- and C-terminal region interactions. *Journal of General Physiology.* **137,** 315-325.

Gustina, A.S. & Trudeau, M.C., 2009. A recombinant N-terminal domain fully restores deactivation gating in N-truncated and long QT syndrome mutant hERG potassium channels. *Proc Natl Acad Sci U S A.* **106,** 13082-13087.

Hardman, R.M., Stansfeld, P.J., Dalibalta, S., Sutcliffe, M.J., Mitcheson, J.S., 2007. Activation gating of hERG potassium channels: S6 glycines are not required as gating hinges. *Journal of Biological Chemistry.* **282,** 31972-31981.

Hedley PL; Jorgensen P; Schlamowitz S; Wangari, Romilda., 2009. The genetic basis of long QT and short QT syndromes: a mutation update. *Human Mutation* **30** (11): 1486–511.

Hille, B. Ion channels of Excitable Membranes, 3rd Ed, 2001

Holmgren, M., Smith, P.L., Yellen, G., 1997. Trapping of organic blockers by closing of voltage-dependent K+ channels: evidence for a trap door mechanism of activation gating. *J Gen Physiol.* **109,** 527-35.

Hoshi, T., Zagotta, W.N., Aldrich, R.W., 1991. Two types of inactivation in Shaker K+ channels: effects of alterations in the carboxy-terminal region. *Neuron.* **7,** 547-56.

Jespersen, T., Grunnet, M., Angelo, K., Klaerke, D.A., Olesen, S.P., 2002. Dual-function vector for protein expression in both mammalian cells and Xenopus laevis oocytes. *Biotechniques.* **32,** 536-8.

Jiang, Y., Lee, A., Chen, J., Cadene, M., Chait, B.T., MacKinnon, R., 2002a. Crystal structure and mechanism of a calcium-gated potassium channel. *Nature.* **417,** 515-522.

Jiang, Y., Lee, A., Chen, J., Cadene, M., Chait, B.T., MacKinnon, R., 2002b. The open pore conformation of potassium channels. *Nature.* **417,** 523-526.

Jiang, Y., Lee, A., Chen, J., Ruta, V., Cadene, M., Chait, B.T., MacKinnon, R., 2003. X-ray structure of a voltage-dependent K+ channel. *Nature.* **423,** 33-41.

Klement, G., Nilsson, J., Arhem, P., Elinder, F., 2008. A tyrosine substitution in the cavity wall of a k channel induces an inverted inactivation. *Biophys J.* **94,** 3014-3022.

Labro, A.J., Raes, A.L., Bellens, I., Ottschytsch, N., Snyders, D.J., 2003. Gating of shaker-type channels requires the flexibility of S6 caused by prolines. *J Biol Chem.* **278,** 50724-50731.

Labro, A.J., Raes, A.L., Grottesi, A., Hoorick, D, V,. Sansom, M, S, P., Snyders, D.J., 2008. Kv channel gating requires a compatible S4-S5 linker and bottom part of S6. *J. Gen. Physiol*, **132**, 667-680.

Labro, A.J., Raes, A.L., Snyders, D.J., 2005. Coupling of voltage sensing to channel opening reflects intrasubunit interactions in kv channels. *J Gen Physiol.* **125,** 71-80.

Larsson, H.P. & Elinder, F., 2000. A conserved glutamate is important for slow inactivation in K+ channels. *Neuron.* **27,** 573-83.

Lee, S.Y., Lee, A., Chen, J., MacKinnon, R., 2005 Structre of the KvAP voltage dependent K^+ channel and its dependence on the lipid membrane. *Proc. Natl. Acad. Sci. USA*. **102**, 15441 – 15446.

Lees-Miller, J.P., Duan, Y., Teng, G.Q., Duff, H.J., 2000. Molecular determinant of high-affinity dofetilide binding to HERG1 expressed in Xenopus oocytes: involvement of S6 sites. *Mol Pharmacol.* **57,** 367-74.

Liu, Y., Holmgren, M., Jurman, M.E., Yellen, G., 1997. Gated access to the pore of a voltage-dependent K+ channel. *Neuron.* **19,** 175-84.

Logothetis, D.E., Movahedi, S., Satler, C., Lindpaintner, K., and Nadal-Ginard, B. 1992. Incremental reductions of positive charge within the S4 region of a voltage-gated K+ channel result in corresponding decreases in gating charge. *Neuron* **8**, 531–540

Long, S.B., Campbell, E.B., Mackinnon, R., 2005a. Crystal structure of a mammalian voltage-dependent Shaker family K+ channel. *Science.* **309,** 897-903.

Long, S.B., Campbell, E.B., Mackinnon, R., 2005b. Voltage sensor of Kv1.2: structural basis of electromechanical coupling. *Science.* **309,** 903-908.

Long, S.B., Tao, X., Campbell, E.B., MacKinnon, R., 2007. Atomic structure of a voltage-dependent K+ channel in a lipid membrane-like environment. *Nature.* **450,** 376-382.

Lopez-Barneo, J., Hoshi, T., Heinemann, S.H. & Aldrich, R.W. 1993. Effects of external cations and mutations in the pore region on C-type inactivation of Shaker potassium channels. *Receptors and Channels* **1**, 61-71.

Lu, Z., Klem, A.M., Ramu, Y., 2001. Ion conduction pore is conserved among potassium channels. *Nature*, **413**, 809-813.

Lu, Z., Klem, A.M., Ramu, Y., 2002. Coupling between voltage sensors and activation gate in voltage-gated K+ channels. *J Gen Physiol.* **120,** 663-676.

MacKinnon, R., Aldrich, R.W., Lee, A.W., 1993. Functional stoichiometry of Shaker potassium channel inactivation. *Science.* **262,** 757-759.

Marban, E., 2002. Cardiac channelopathies. *Nature.* **415,** 213-218.

Mitcheson, J.S., Chen, J., Lin, M., Culberson, C., Sanguinetti, M.C., 2000a. A structural basis for drug-induced long QT syndrome. *Proc Natl Acad Sci U S A.* **97,** 12329-1233.

Mitcheson, J.S., Chen, J., Sanguinetti, M.C., 2000b. Trapping of a methanesulfonanilide by closure of the HERG potassium channel activation gate. *Journal of General Physiology.* **115,** 229-240.

Morais Cabral, J.H., Lee, A., Cohen, S.L., Chait, B.T., Li, M., Mackinnon, R., 1998. Crystal structure and functional analysis of the HERG potassium channel N terminus: a eukaryotic PAS domain. *Cell.* **95,** 649-655.

Noda, M., Shimizu, S., Tanabe, T., Takai, T., Kayano, T., Ikeda, T., Takahashi, H., Nakayama, H., Kanaoka, Y., Minamino, N., et al. 1984. Primary structure of Electrophorus electricus sodium channel deduced from cDNA sequence. *Nature* **312**, 121–127.

Panyi, G. & Deutsch, C., 2007. Probing the cavity of the slow inactivated conformation of shaker potassium channels. *J Gen Physiol.* **129,** 403-418.

Panyi, G. & Deutsch, C., 2006. Cross talk between activation and slow inactivation gates of Shaker potassium channels. *J Gen Physiol.* **128,** 547-559.

Papazian, D.M., Timpe, L.C., Jan, Y.N., Jan, L.Y., 1991. Alteration of voltage-dependence of Shaker potassium channel by mutations in the S4 sequence. *Nature.* **349,** 305-310.

Payandeh, J., Scheuer, T., Zheng, N., Catterall, W, A., 2011. The crystal structure of a voltage gated sodium channel. *Nature*, **475**, 353-359.

Perry, M., de Groot, M.J., Helliwell, R., Leishman, D., Tristani-Firouzi, M., Sanguinetti, M.C., Mitcheson, J., 2004. Structural determinants of HERG channel block by clofilium and ibutilide. *Molecular Pharmacology.* **66,** 240-249.

Perry, M., Stansfeld, P.J., Leaney, J., Wood, C., de Groot, M.J., Leishman, D., Sutcliffe, M.J., Mitcheson, J.S., 2006. Drug binding interactions in the inner cavity of HERG channels: molecular insights from structure-activity relationships of clofilium and ibutilide analogs. *Molecular Pharmacology.* **69,** 509-519.

Piper, D.R., Varghese, A., Sanguinetti, M.C., Tristani-Firouzi, M., 2003. Gating currents associated with intramembrane charge displacement in HERG potassium channels. *Proc Natl Acad Sci U S A.* **100,** 10534-10539.

Ranganathan, R., Lewis, J.H., MacKinnon, R., 1996. Spatial localization of the K+ channel selectivity filter by mutant cycle-based structure analysis. *Neuron.* **16,** 131-139.

Robertson, G.A., Jones, E.M.C. and Wang, J. (2005). Gating and Assembly of Heteromeric hERG1a/1b Channels underlying IKr in the Heart. Novartis Foundation Symposium 266:4-15.

Roden DM (2008) Cellular basis of drug induced torsades de pointes. Brit J Pharmacol, 154: 1502-1507.

Roden, D.M., Balser, J.R., George, A.L.,Jr., Anderson, M.E., 2002. Cardiac ion channels. *Annu Rev Physiol.* **64,** 431-475.

Sanguinetti, M.C., Curran, M.E., Spector, P.S., Keating, M.T., 1996. Spectrum of HERG K+-channel dysfunction in an inherited cardiac arrhythmia. *Proc Natl Acad Sci U S A.* **93,** 2208-212.

Sanguinetti, M.C., Curran, M.E., Zou, A., Shen, J., Spector, P.S., Atkinson, D.L., Keating, M.T., 1996. Coassembly of K(V)LQT1 and minK (IsK) proteins to form cardiac I(Ks) potassium channel. *Nature.* **384,** 80-3.

Sanguinetti, M.C., Jiang, C., Curran, M.E., Keating, M.T., 1995. A mechanistic link between an inherited and an acquired cardiac arrhythmia: HERG encodes the IKr potassium channel. *Cell.* **81,** 299-307.

Sanguinetti, M.C. & Jurkiewicz, N.K., 1990. Two components of cardiac delayed rectifier K+ current. Differential sensitivity to block by class III antiarrhythmic agents. *J Gen Physiol.* **96,** 195-215.

Sanguinetti, M.C. & Mitcheson, J.S., 2005. Predicting drug-hERG channel interactions that cause acquired long QT syndrome. *Trends in Pharmacological Sciences.* **26,** 119-124.

Sanguinetti, M.C. & Tristani-Firouzi, M., 2006. hERG potassium channels and cardiac arrhythmia. *Nature.* **440,** 463-469.

Sanguinetti, M.C. & Xu, Q.P., 1999. Mutations of the S4-S5 linker alter activation properties of HERG potassium channels expressed in Xenopus oocytes. *Journal of Physiology.* **514,** 667-75.

Schonherr, R. & Heinemann, S.H., 1996. Molecular determinants for activation and inactivation of HERG, a human inward rectifier potassium channel. *Journal of Physiology-London.* **493,** 635-642.

Seoh, S.A., Sigg, D., Papazian, D.M., Bezanilla, F., 1996. Voltage-sensing residues in the S2 and S4 segments of the Shaker K+ channel. *Neuron.* **16,** 1159-167.

Shealy, R.T., Murphy, A.D., Ramarathnam, R., Jakobsson, E., Subramaniam, S., 2003. Sequence-function analysis of the K+-selective family of ion channels using a comprehensive alignment and the KcsA channel structure. *Biophys J.* **84,** 2929-2942.

Shi, W., Wymore, R.S., Wang, H.S., Pan, Z., Cohen, I.S., McKinnon, D., Dixon, J.E., 1997. Identification of two nervous system-specific members of the erg potassium channel gene family. *J Neurosci.* **17,** 9423-932.

Smith, P.L., Baukrowitz, T., Yellen, G., 1996. The inward rectification mechanism of the HERG cardiac potassium channel. *Nature.* **379,** 833-86.

Smith, P.L. & Yellen, G., 2002. Fast and slow voltage sensor movements in HERG potassium channels. *Journal of General Physiology.* **119,** 275-293.

Sobolevsky, A.I., Rosconi, M.P., Gouaux, E., 2009. X-ray structure, symmetry and mechanism of an AMPA-subtype glutamate receptor. *Nature.* **462,** 745-756.

Spector, P.S., Curran, M.E., Keating, M.T., Sanguinetti, M.C., 1996a. Class III antiarrhythmic drugs block HERG, a human cardiac delayed rectifier K+ channel. Open-channel block by methanesulfonanilides. *Circulation Research.* **78,** 499-503.

Spector, P.S., Curran, M.E., Zou, A., Keating, M.T., Sanguinetti, M.C., 1996b. Fast inactivation causes rectification of the IKr channel. *Journal of General Physiology.* **107,** 611-9.

Stansfeld, P.J., Sutcliffe, M.J., Mitcheson, J.S., 2006. Molecular mechanisms for drug interactions with hERG that cause long QT syndrome. *Expert Opinion on Drug Metabolism & Toxicology.* **2,** 81-94.

Stork, D., Timin, E.N., Berjukow, S., Huber, C., Hohaus, A., Auer, M., Hering, S., 2007. State dependent dissociation of HERG channel inhibitors. *Br J Pharmacol.* **151,** 1368-1376.

Subbiah, R.N., Clarke, C.E., Smith, D.J., Zhao, J., Campbell, T.J., Vandenberg, J.I., 2004. Molecular basis of slow activation of the human ether-a-go-go related gene potassium channel. *J Physiol.* **558,** 417-431.

Subbiah, R.N., Kondo, M., Campbell, T.J., Vandenberg, J.I., 2005. Tryptophan scanning mutagenesis of the HERG K+ channel: the S4 domain is loosely packed and likely to be lipid exposed. *J Physiol.* **569,** 367-379.

Tempel, B.L., Papazian, D.M., Schwarz, T.L., Jan, Y.N., and Jan, L.Y. 1987. Sequence of a probable potassium channel component encoded at Shaker locus of Drosophila. *Science* **237**, 770–775.

Tristani-Firouzi, M., Chen, J., Sanguinetti, M.C., 2002. Interactions between S4-S5 linker and S6 transmembrane domain modulate gating of HERG K+ channels. *Journal of Biological Chemistry.* **277,** 18994-19000.

Trudeau, M.C., Warmke, J.W., Ganetzky, B., Robertson, G.A., 1995. HERG, a human inward rectifier in the voltage-gated potassium channel family. *Science.* **269,** 92-95.

Vassilev, P. M., Scheuer, T., Catterall, W, A., 1988. Identification of an intracellular peptide domain segment involved in sodium channel inactivation. *Proc. Natl. Acad. Sci. USA*. **86**, 8147-8151.

Vieira-Pires, R.S & Morais-Cabral, J.H., 2010, 3_{10} helices in channels and other membrane proteins. *JGen Physiol*. **136**, 585-592.

Wang, J., Myers, C.D., Robertson, G.A., 2000. Dynamic control of deactivation gating by a soluble amino-terminal domain in HERG K(+) channels. *J Gen Physiol.* **115,** 749-58.

Wang, J., Trudeau, M.C., Zappia, A.M., Robertson, G.A., 1998. Regulation of deactivation by an amino terminal domain in human ether-a-go-go-related gene potassium channels. *J Gen Physiol.* **112,** 637-47.

Warmke, J.W. & Ganetzky, B., 1994. A family of potassium channel genes related to eag in Drosophila and mammals. *Proc Natl Acad Sci U S A.* **91,** 3438-342.

Weerapura, M., Nattel, S., Chartier, D., Caballero, R., Hebert, T.E., 2002. A comparison of currents carried by HERG, with and without coexpression of MiRP1, and the native rapid delayed rectifier current. Is MiRP1 the missing link? *Journal of Physiology-London.* **540,** 15-27.

West, J.W., Patton, T., Scheuer, Y., Wang, A.L., Goldin, Catterall, W, A., 1991. A cluster of hydrophobic amino acid residues required for fast Na+ channel inactivation. *Proc. Natl. Acad. Sci. USA*. **89**, 10910-10914.

Witchel, H.J., Dempsey, C.E., Sessions, R.B., Perry, M., Milnes, J.T., Hancox, J.C., Mitcheson, J.S., 2004. The low-potency, voltage-dependent HERG blocker propafenone--molecular determinants and drug trapping. *Molecular Pharmacology.* **66,** 1201-1212.

Yellen, G., 2002. The voltage-gated potassium channels and their relatives. *Nature.* **419,** 35-42.

Yellen, G., 1998. The moving parts of voltage-gated ion channels. *Q Rev Biophys.* **31,** 239-95.

Zagotta, W.N., Hoshi, T., Aldrich, R.W., 1990. Restoration of inactivation in mutants of Shaker potassium channels by peptide derived from ShB. *Science,* **250**, 568 – 571.

Zagotta, W.N., Olivier, N.B., Black, K.D., Young, E.C., Olson, R., Gouaux, E., 2003. Structural basis for modulation and agonist specificity of HCN pacemaker channels. *Nature.* **425,** 200-205.